Chenopodium quinoa, a model plant for investigating the crosstalk of abiotic and biotic stress tolerance mechanisms

Floren Villanueva Scrafton

Worcester College

University of Oxford

A thesis submitted for the degree of Doctor of Philosophy

(Interdisciplinary Biosciences, Department of Biology)

Michaelmas 2023



Covid-19 statement

The impact of Covid-19 on my thesis can be described in two parts: firstly, a discrete impact of time loss on my progress completing the PhD, specifically delaying the obtainment of three of four major 'omics' datasets of my thesis, and secondly, the ongoing impact on my personal life through two big family losses to the disease itself, which have resulted in significant hardship and reduced prioritisation for the thesis following the upheaval in our family.

Due to Covid-19, we were forced to leave the lab and abandon our plants and experiment plans which caused large disruptions to the flow of work. My thesis was planned to be 90% lab-based experimental due to the high amount of 'groundwork' needed to establish the novel plant species *Chenopodium quinoa* as a research system in Oxford for studying disease, immunity and the combinatorial impact of salt on these mechanisms. This was also due to hands-on experimental work aligning better with my skills, interests, career aspirations and learning style. Whilst there would be an opportunity for computer-based bioinformatic analyses, I was yet to generate these datasets by the time the lockdown was enforced, in fact, the processing of samples for all my omics studies (two RNA-seq experiments and two Plant RNA Interactome Capture RBPome experiments) were abandoned just as the pandemic was starting. This meant I had to balance re-doing these experiments as well as other outstanding ones with trying to learn new and challenging bioinformatic skills to process the datasets yielded from them and managing the sudden mental load and distracting circumstances of covid-related factors detailed in the next paragraph. This was incredibly difficult for me as it meant I didn't have the focus needed for computational analysis which heavily delayed the obtainment of results, the interpretation of them and the possibility for working off leads generated (discussed therefore as future work in this thesis). The exclusion from the lab started in the middle of March 2020 and lasted until early July 2020 when doors reopened again, however, we then had to work on a part-time rota system for the following 6-months, which continued to slow the rate of experimental progression.

The biggest impact on my PhD progress however was the loss of my father who contracted Covid-19 in May 2020 whilst visiting us in England. The timing was especially heart-breaking

as he had come over from Bolivia to England for the first time in seven years to support my older brother Amaru who had suddenly been diagnosed with stage four brain cancer 6-months prior in November 2019. This caused intense grief, distractions and further logistical implications which all meant I spent time away from the thesis and struggled with my mental health and focus. Consequently, I then flew out to Bolivia when the borders reopened at the end of 2020 to be with and support my little sister and her mother, my dad's partner and my beloved Bolivian step-mum Maria. Unfortunately, Maria caught covid whilst I was out there and so I spent the whole of January 2021 supporting, looking after my little sister and coordinating solutions desperately with my family across both countries to raise money, to locate and then personally transport medicines including oxygen tanks to her bedside because private hospitals were too expensive and public ones were full and understaffed. Maria, aged 42, devastatingly passed away at the end of January 2021 leaving my little sister Aruza without any parents and so we suddenly needed to find a means to care for her. I have barely had any time to grieve the losses of my dad and Maria as my family and I went straight into mission mode concerned for Aruza's upbringing and for our dear older brother Amaru who we were supporting the best we could to make his last years of life as enjoyable as possible, but who we then lost to cancer last September 2022.

These three major family losses which were either directly due to, or complicated further by, covid-19 affect me every day and the stress of trying to keep going with my PhD along with additional financial implications has led to issues with my own mental and physical health, manifesting as chronic insomnia, chronic tonsillitis and low mood, collectively a sign of mental and physical burn out for which I've had to take sick-leave for intermittently. Therefore, even despite being granted the maximum allowance of 6-months of Covid-19 extension along with securing additional 3-months of funding from the British Society of Plant Pathology (BSPP) to support the completion of my PhD, Covid-19 has had an irreversible impact on my life and with it the quality and timeliness of my PhD completion.

Abstract

Chenopodium quinoa (quinoa) is a highly nutritious and naturally stress tolerant crop originating from the Andes. Thanks to the germplasm conservation efforts of Andean smallholder farmers, quinoa's immense genetic diversity has facilitated the crop's adaptation to over 120 countries. As quinoa cultivation expands to non-traditional environments the crop will encounter novel pathogens (biotic stresses), yet quinoa's immune mechanisms are not well characterised, nor is their knowledge of how the crop responds to combinations of environmental (abiotic) and biotic stresses. Because several abiotic stress signalling mechanisms are also known to be involved in plant immunity, it was hypothesised that immune mechanisms and plant-pathogen interactions in a halophytic crop such as quinoa may be distinct to glycophytic species such as Arabidopsis. Immune elicitors (pathogen-associated molecular patterns; PAMPs) and the model pathogen *Pseudomonas syringae* were used to study immunity and infection processes in the commercial European quinoa cultivar Atlas. Several canonical PAMP-Triggered Immunity (PTI) responses were observed in quinoa but were often induced to lower intensities or at delayed time-points compared to Arabidopsis. However, collectively, quinoa's PTI was sufficient to inhibit the growth of the type III secretion system deficient strain *P. syringae* pv. tomato DC3000 *hrpA*-. *P. syringae* strains belonging to diverse pathovars produced a range of disease outcomes where isolates from related species sugar beet and spinach were found to be pathogenic. Salt stress assays were used to characterise the salt tolerance of Atlas and guide the establishment of a saline hydroponics growth system to evaluate how immune responses and disease susceptibility to *P. syringae* varied in a high vs low salt-acclimated phenotype. Atlas demonstrated high salt tolerance by hyperaccumulating salt in its leaves which then became significantly more disease resistant to *P. syringae*. The combinatorial stress of salt x bacterial PAMP flg22 produced different transcriptional responses to individually applied stresses, where redox homeostasis appears critical to quinoa's defences. In future work, this combinatorial stress system could be used to screen a wider panel of native Andean and European quinoa varieties of varying abiotic and biotic stress tolerances, as well as testing the salt-acclimation strategy against other field pathogens of quinoa. Together, this could identify core stress tolerance genes of agronomic value for improving yield security of crops in a range of environments.

Acknowledgements

This PhD project has meant considerably more to me than I ever expected. In part this is due to it serving as a footing from which to realise applied science and career opportunities, but also because it has allowed me to develop my personal connections with Bolivia. The completion of a PhD itself wouldn't have been possible without my close network of friends, family and my sport as unrivalled escapes and sources of joy and empowerment. I also wouldn't have been able to complete this thesis to a depth and standard I am happy with without the guidance and encouragement of my supervisor Prof Gail Preston.

I'd like to firstly thank Gail and her Oxford Interdisciplinary Bioscience DTP programme for the opportunity to realise research on quinoa at Oxford. This PhD project and Gail's support for my determination to make impact beyond it allowed me to explore a fascinating plant and to tangibly connect with its wider social impact. Gail, through her supervision and research group created an excellent, inclusive and equitable environment to develop a PhD in. Thank you Gail for supporting me in many different ways: from before even arriving to Oxford with research contacts for future potential collaborations with Bolivia and Chile; for supporting my ambitious aspirations for making it to the Olympics for Bolivia whilst completing a PhD; for helping with grant applications so we could develop collaborative follow-on projects; for supporting my personal goal of bringing two Bolivian quinoa researchers Nancy and Marcelo over to experience Oxford/the UK; and lastly, for always making time for me with fruitful and inspiring scientific discussions and for reviewing my v0.001 thesis drafts.

There are three important people I'd like to especially thank for the drive, determination and inspiration to complete a PhD in the first place and who I am dedicating this body of work to. This thesis therefore is for, and because of, my mum, Diana, dad Adrian, and older brother Amaru.

Firstly, I'd like to thank my mum Diana for doing whatever you possibly could to make this marathon more manageable and rewarding for me, reminding me to occasionally slow down (enough) to reflect on the process and to celebrate progress, whilst at the same time always encouraging me to keep going at my ambitious sporting, academic and 'whatever's next' goals. You gave me the confidence to be bold and inquisitive, to push the boat out and follow my interests/heart/instincts no matter how much harder these goals and aspirations might be or became, you trusted I'd rise up and find a way to make things work. Thank you for instilling in me the desire to search for new grounds, an enjoyment of problem solving, to be grateful for other peoples' help and new opportunities, and to just work really hard – all very much needed to complete this thesis!

Secondly, I thank my dad, Adrian, who would be the proudest person to know his half-British, half-Bolivian “Vicuña” “Chaski” daughter’s “book on quinoa” is finally in press. I’ll never forget every visit I got to see you in La Paz between 2013-2019. To connect with yours, and increasingly now my own country Bolivia, a world that I wouldn’t have known without you and with it, the quinoa crop that I couldn’t have become so enthused by. Remember the two-up quinoa journalist tag-team we became during August 2014? You accompanied me to explore the local socio-economic and scientific impact the quinoa boom was having on the Bolivian people of the Altiplano. The local empowerment we saw happening first-hand through our native ‘grano de oro’ has been etched at the front of my mind ever since. I wish I could have become a Dr of Quinua Research with you still around to see it, just so you could salute to it loudly with your original hand-crafted recycled Pututu horn and beautiful kena flutes.

The last closely personal acknowledgement and dedication goes to my older brother Amaru. I can’t keep my face dry trying to write about the impact you’ve had on me and how much you continue to inspire me for completing a PhD on quinoa (at your almer mater). From checking my early applications to attend Oxford UNIQ and Eton summer schools, or to Birmingham Uni for my undergrad and then Oxford for the PhD, to inspiring me to see my dual heritage as a rich opportunity for experiencing and perceiving new things. For encouraging me through a particularly difficult period of my life as a lost 18-year-old and giving me the confidence to give a journalism internship a go which led me to writing an article with photo assays about local Bolivian culture and food for the Bolivian Express magazine in 2013. You told me then about this new craze for a healthy Bolivian food product that could interest me because of my sports passion; I perhaps never would have developed a deep curiosity for quinoa had it not been for your initial suggestion and the experience to independently research it. You balanced a PhD in Sociology on the Bolivian class structure alongside many important other projects and jobs, and then finished writing it to become Dr Amaru Villanueva Rance despite the intense physical challenges faced through sudden illness. I have missed you so much these last 12 months and you’re one of three main people I wanted to celebrate its completion with. Thank you, Bro, for being my academic/life idol and for being the most inspiring and supportive older brother to me.

Thank you to the rest of my family: my beautiful, supportive, creative and resilient sisters Nina and Aruza, mil gracias Nina por tus consejos sabios esta última semana, to my twin brother Mauro “weevil-aww-weevil” for making me laugh, bounce back and feel proud of being here, to Maria, Julio, Hattie and especially to Dr Susanna Rance and Prof Laura Rodrigues for both inspiring and encouraging me as badass Latin America-focused female academics. Laura, that 3-week work experience placement with you at the London School of Hygiene and Tropical Medicine summer of 2016 inspired me to do a

PhD: seeing you hold your own in a room full of male academics and how a PhD led you to bridging socially impactful research between Brazil-UK through your incredible work on the Zika epidemic.

Thank you to all my friends: in Oxford especially Ellen, your sisterhood and shared but independently developed love for quinoa and sustainable development was incredibly motivating, to Eddy, Tom, Liam and Kaitie, to my Yamasaki chicas from UoB, and my Bristol girls who have been rooting for me from afar. You centred me every time and built me back up whenever insomnia, imposter syndrome, grief, illness or injuries temporarily got me down. Thank you to my eclectic and widespread sports family, my running, triathlon and cycling teammates in Oxford, Bristol, Birmingham, Spain and Bolivia, and a special mention to my former Oxford athletics coach Kyle Bennett for your friendship, mentorship, belief and tonnes of hype. Lastly, I am so grateful to Ali and other friends who put me up in London countless times over the last three years at short notice; you enabled me to spend as much time as possible with my brother Amaru during his cancer treatment and final stages at St Joseph's Hospice.

Oxford

Thank you to Dr MBP Marcel Bach-Pages for your guidance and friendship in and out the lab and for the inspiration to be as organised, HTP and clever as you. You always made time for me and helped me to think strategically about my research story. You cracked me up so much, brought me GF snacks and were always there at the end of the phone line for whatever, especially when I needed to laugh.

To my labmates Will and Lauren, aka my favourite postdocs, thank you for making the lab environment exceptional. I've loved exploring the world of spin-out/starts up with you. Lauren, you inspired me massively for putting research into practise and fostering connections with everyone from farmers to academics, to those in industry, and to Alpacas (Beans and Quinoa #TeamABQ). Thanks to my lovely labmates Julianna, Morgan, Ashleigh, Rose, Brett and Dave (#TeamRBP), Alison and Caroll (Mis Piticas) and adopted labmate Zoe (for making me a flower print office-based siesta pillow) for the best vibes, discussions, all-round support (solidarity?) and snacks (especially you Morgan #craven #Racoons).

To Renier's Plant Chemetics sister lab, with special mentions to Emma, Pierre & Phillipe for your early tips on lab skills, results discussions and critical feedback on protocols.

To the DTC Admin Team 2017 – 23 for your incredible support, generosity, friendliness and patience.

To Mischka Byworth at Worcester College for your invaluable support helping me to manage the load of difficult family news, illness and the PhD, and to John Bloomer this last year for your belief and encouragement which re-built my confidence and helped me to put everything into perspective.

Specific research acknowledgements

- Prof Andrew Smith and Prof Renier van der Hoorn for your support as secondary supervisors. Your injections of wisdom and new angles for interpreting results or follow-on work through specialist insights on salt tolerance and plant immunity were extremely helpful and inspiring. Thank you, Andrew, for your discussions and guidance on the experimental design of my early salt tolerance screening assays in Atlas and later for your tips on establishing the osmotic point assay.

- Dr Stephen Jones of the British Quinoa Company for gifting me Atlas seed to begin my research with and for your longstanding comms adding insights on applied, locally relevant quinoa farming.

- Ing Marcelo Gonzales Torrico, Ing Nancy Huanca Alanoca and Dr Carla Colque-Little in Bolivia for unique contextual quinoa insights and support for two of my applied projects in quinoa.
- Dr Tin Hang, Henry (Mackay group, Oxford), for getting me started on RNA-seq analysis, creating an analysis strategy and solving many of my 'computationally challenged' queries.
- Chloe Harper and Jasmine Dodd, for your amazing work on the comparative *P. syringae* project: the bioinformatic effector/phytotoxin/Pfam analyses on my sequenced strain genomes.
- Morgan Wade, for undertaking your DTP rotation project in quinoa with me which enabled additional *P. syringae* infection assays to be completed and for your insightful discussions.
- Dr Wael Kamel and Dr Alfredo Castello (University of Glasgow) for RBP bioinformatic and statistical analyses and helpful discussions on quinoa RBPome data interpretation.
- Dr Farnusch Kashchani and Dr Sabrina Ninck (ACE, University of Essen) for RBP Mass spectroscopy.
- Dr Nattapong Sanguankiattichai ("Teeee"), for all your assistance with R script builds and R de-bugging and for just explaining things like no other. A true MVP of both Preston/Chemetics labs.
- Ellen Williams for your BSPP Biotic Threats to Quinoa Review and Bolivia fieldwork collaboration!
- Prof Steve Kelly, for preparing specific OrthoFinder comparative species analyses for quinoa.
- Dr Niloufer Irani, the microscopy wizard who taught me the ways, and resonated and then escalated my excitement for researching with the novel quinoa plant.
- Dr Tom Hughes for help with histology work and Prof Hugh Dickson for help with the SEM.
- Lastly, many thanks to our lab group technicians, especially Sarah Rodgers "the lab's secret weapon" (van der Hoorn ~2018) for making our Chemetics/Preston research space a fantastic place to work in. Thanks to Úrsula for watering my soil grown quinoa plants whenever I couldn't. To technicians Caroline and Patty, and to Patty and Maria also for tu sentido de communidad Latina en la facultad, alegrándome y sacándome risas con cada encuentro.

Statement of originality

I carried out the work in this thesis at the Department of Plant Sciences (now the Department of Biology) at the University of Oxford under the supervision of Prof. Gail Preston. My research was funded by the Biotechnology and Biological Sciences Research Council (BBSRC). I declare that no part of this thesis has been submitted in support of another degree, diploma or other qualification at the University of Oxford or any other university. Except where otherwise stated, the work in this thesis is my own work.

Contents

Chapter 1: General Introduction..... 13

1.1. Supporting food security through expanding the cultivation of new nutritious crops..... 13

1.2. *Chenopodium quinoa*; a promising crop for food security and new opportunity for researching combinatorial stress responses in plants 15

1.2.1. Quinoa's origin, social importance, botany and nutrition 15
1.2.2. Quinoa; a naturally stress tolerant plant with valuable agronomic traits for marginal climates 20
1.2.3. The impact of salt stress on agriculture 22
1.2.4. Common salt tolerance mechanisms of plants and specialised adaptations of halophytes 24

1.3. Disease in quinoa..... 28

1.3.1. Common field diseases and native biotic threats 28
1.3.2. Bacterial pathogens of quinoa 33

1.4. Leaf-based pathosystems with the model bacterial species *Pseudomonas syringae* 35

1.5. Plant Immunity..... 37

1.5.1 Current understanding of the plant immune system 37
1.5.2. The impact of environmental adaptations on plant immunity 38

1.6. Combinatorial stresses and the challenge for agriculture 39

1.6.1. Combinatorial stress responses and interactions between abiotic and biotic stress signalling pathways..... 40
1.6.2. The role of ABA in abiotic – biotic stress interactions 42

1.7. Rationale, Aims and Chapter Objectives 44

Chapter 2: Exploring PAMP-Triggered Immunity in the halophytic crop Chenopodium quinoa; similarities and differences to the model species Arabidopsis thaliana..... 47

2.1. Introduction 47

2.1.1. A PAMP-Triggered Immunity model for perception and signal transduction..... 47
2.1.2. Use of transcriptomics and proteomics for elucidating PTI response genes 51
2.1.3. Translating our understanding of PTI from model species to crops 52
2.1.4. Aims and rationale 53

2.2. Results 54

2.2.1. Establishing a series of biochemical PTI assays in quinoa using artificial PAMPs 54

2.2.1.1. MAPK activation in response to PAMPs is conserved in quinoa but orchestrated by different MAPK enzymes to Arabidopsis 54
2.2.1.2. Quinoa produces ROS bursts in response to diverse PAMPs but at a delayed time and reduced intensity relative to Arabidopsis 56
2.2.1.3. PAMP-induced peroxidase upregulation in quinoa is subtle and delayed relative to Arabidopsis 60
2.2.1.4. Quinoa deposits callose papillae at the cell wall in response to flg22 62
2.2.2. Profiling an early transcriptomic response of quinoa to flg22 treatment 63
2.2.2.1. Global functional enrichment analyses reveal more differences than similarities between the two hour flg22-induced transcriptomes of Arabidopsis and quinoa 66
2.2.2.2. De-novo analysis of the DEGs annotated with enriched GO and KEGG terms reveal putative flg22-responsive candidate genes in quinoa 75
2.2.3. Profiling an early proteomic response of quinoa to flg22 treatment 83
2.2.3.1. The novel Plant RNA Interactome Capture method reveals preliminary background and flg22-induced quinoa RBPomes 83
2.2.3.2. Comparison of the quinoa flg22-RBPome to the Arabidopsis flg22-RBPome reveals little overlap (and could not be used to retrieve additional putative flg22-responsive RBPs) 89

2.3. Discussion 92
2.3.1. Quinoa's PTI responses show a mix of expected, unexpected and novel results relative to Arabidopsis 93
2.3.2. Oxidoreductase activity plays an important role in quinoa's biotic stress response 96

2.4. Conclusion 97

2.5. Methods 99

Chapter 3: Establishing saline phenotypes in the European Quinoa variety Atlas 103

3.1. Introduction 103
3.1.1. Land salinization and food security solutions with halophytic crops 103
3.1.2. Salt stress adaptations 104
3.1.3. Salt tolerance mechanisms in quinoa 105
3.1.4. Salt stress administration 107
3.1.5. Aims and rationale 108

3.2. Results 109
3.2.1. Evaluating the salt tolerance of the European-bred quinoa cultivar Atlas 109
3.2.2. In-vitro salt-supplemented growth systems are amenable for evaluating the early growth responses of Atlas 111
3.2.3. Longer term salt exposure from two-week-old plants reveals a halophilic phenotype in Atlas grown under 100 mM NaCl 112
3.2.4. Quinoa plants accumulate high concentrations of salt in their leaves in response to salt irrigation 112
3.2.5. Establishing a hydroponics system in quinoa for improved control of salt exposure and saline phenotype development 113
3.2.6. Ultrastructural analyses reveal unique constitutive and salt-induced phenotypes in quinoa 116
3.2.7. Transcriptional analysis of the 200 mM NaCl foliar phenotype in Atlas reveals a typical halophytic expression profile 119

3.3. Discussion 122
3.3.1. Salt treatment of *C. quinoa* cv. Atlas produces halophilic and halophytic phenotypes at the macroscopic to ultrastructural and biochemical Levels 122
3.3.2. Global functional analysis of the salt induced DEGs provides a snapshot of the halophytic mechanisms underpinning the saline foliar phenotype of Atlas 125

3.4. Conclusion 127

3.5. Methods 128

Chapter 4: Establishing a pathosystem in quinoa with Pseudomonas syringae 130

4.1. Introduction 130

4.1.1. *P. syringae* pathosystems 130

4.1.2. *P. syringae* biology, diversity and its crop host and environmental niches 130

4.1.3. Virulence factors 131

4.1.4. The influence of external environment and leaf microenvironment on pathogenesis 132

4.1.5. Aims and rationale 133

4.2. Results 134

4.2.1. Infection assays 134

4.2.1.1. P. syringae pathovars from distinct phylogroups can infect quinoa and cause differential symptoms in a type III secretion system dependent manner 134

4.2.1.2. Sugar beet P. syringae pathogen pv. aptata NCPPB3539 is especially virulent on quinoa 135

4.2.1.3. The PG1 pathovar isolated from spinach causes more severe disease symptoms than other PG1 pathovars isolated from tomato and brassicas 137

4.2.1.4. PG3 strains cannot grow in quinoa whilst PG4 rice pathogen pv. oryzae 1_6 causes pronounced chlorosis 139

4.2.1.5. The alpine snow-isolated, low effector carrying P. syringae strain CC1557 is highly virulent on quinoa 139

4.2.2. Sequencing the complete genomes of model pathogen strain isolates of *P. syringae* pv. *aptata* and pv. *spinaciae* 140

4.2.3. Comparative genomic analyses of *P. syringae* pathovars reveals key differences and similarities in effector and phytotoxin repertoires 141

4.2.4. Salt-adapted quinoa plants are significantly more resistant to infection by *P. syringae* pv. *aptata* NCPPB3539 143

4.2.5. Saline quinoa leaves have a higher apoplastic fluid osmolality and extracts inhibit the *in vitro* growth of *P. syringae* 147

4.2.6. Salt x pathogen *in vitro* stress studies reveal differential salt tolerance of model strains 149

4.2.7. Pv. *aptata* strains contain an expanded number of genes encoding proteins containing Na^+ Transporter domains relative to PG1 pathovar pv. *spinaciae* and pv. DC3000 and PG2 pathovar pv. B728a 152

4.2.8. Salt inhibits virulence gene expression 153

4.3. Discussion 155

4.3.1. The bacterial species *Pseudomonas syringae* is an amenable model pathogen for investigating disease and resistance processes in *Chenopodium quinoa* 156

4.3.2. Limitations of the *C. quinoa – P. syringae* pathosystem 158

4.3.3. Abiotic stress tolerance and host-relatedness to quinoa influences the virulence potential of *P. syringae* isolates on quinoa 161

4.3.4. Salt accumulation in quinoa leaves creates an inhibitory microenvironment which could be exploited as a defence strategy against apoplast-colonising pathogens 163

4.4. Conclusion 164

4.5. Methods 165

Chapter 5: The influence of quinoa's halophytic adaptations on PAMP Triggered Immunity 169

5.1. Introduction 169

5.1.1. Plant responses to combinatorial or sequential stresses 169

5.1.2. Combinatorial stress experimental systems: theories and practicalities 170
5.1.3. Aims and rationale 173

5.2. Results 175
5.2.1. Upstream and downstream PTI responses MAPK activation and callose deposition are conserved in high salt-acclimated quinoa 175
5.2.2. High concentrations of flg22 cannot elicit an observable ROS signal in the leaves of high salt quinoa 177
5.2.2.1. Excess NaCl is not responsible for inhibiting the chemiluminescence signal of the ROS assay 184
5.2.2.2. Endogenous antioxidants of saline quinoa leaf tissue can suppress the measurable PAMP-triggered oxidative burst 186
5.2.3. A novel combinatorial abiotic x biotic transcriptomic dataset in quinoa allows an exploration of how quinoa's salt-acclimation interacts with PTI 191
5.2.3.1. Global functional and gene-level comparisons of the low salt vs high salt PTI responses reveal strikingly opposing mechanisms in quinoa 195
5.2.3.2. Further inter single stress and single vs combinatorial stress treatment comparisons shed light on core stress response functions and candidate genes in quinoa 204
5.2.3.3. Peroxidase genes are differentially regulated in quinoa's response to single and combined stresses 206

5.3. Discussion 207
5.3.1. The salt-acclimated phenotype of quinoa significantly affects flg22-inducible PTI responses 208
5.3.2. Endogenous antioxidants may play an important role in the PTI of naturally stress resilient plants 209
5.3.3. A combinatorial abiotic x biotic stress RNA-seq experiment elucidates candidate genes responsible for a salt-primed enhanced disease resistance in quinoa 210

5.4. Conclusion 219

5.5. Methods 220

Chapter 6.0: General Discussion 225

6.1. Quinoa, a model system for evaluating combinatorial stress responses of plants 227
6.1.1 Limitations of this quinoa research system 233

6.2. The halophytic salt-acclimation of quinoa interacts with basal PTI responses, challenging the robustness of canonical PTI under changing environments 237

6.3. Could the salt acclimation of quinoa be used as a disease mitigation strategy? 243
6.3.1. Could salt acclimation crosstalk principles be extended to other crops? 247

6.4. Conclusion 248

References 250

Supplementary Material 297

Chapter 1: General Introduction

1.1. Supporting food security through expanding the cultivation of new nutritious crops

Two agronomic methods for increasing food production and food security for a growing population include: expanding agriculture to new under-utilised lands, and the adaptation of new nutritious crop species into pre-existing agricultural systems. For these efforts to be successful, consideration must be given to the combinatorial effect that local abiotic and biotic stresses impose on crops as they adapt to new environments. Novel crop-pathogen interactions that arise can result in significant yield losses if the environmental conditions become conducive to disease development and/or when newly adapted crops lack adequate immunity to combat a pathogen's virulence mechanisms (McDonald & Stukenbrock, 2016; Velásquez et al., 2018). This concept is often depicted by disease triangles, where the vertices represent key factors that govern plant fitness and the success of agricultural systems (McNew, 1960). An example of a how a disease triangle framework can be used to support the successful adaptation of the Andean 'superfood' quinoa crop to new lands is shown in Fig.1. The question marks on the vertices of the 'new agricultural system' of quinoa in Shropshire (UK) denote three key unknowns: quinoa's plant immunity (I) and its new local environmental/abiotic (E) and pathogen/biotic stresses (P). The next two questions then develop from this by asking how robust quinoa's immunity is under specific abiotic (E) or biotic stresses (P), and finally, when under the combination of these stresses to mimic more realistic challenges in the field. By understanding these important unknowns, new field stress mitigation strategies or new improved cultivars can be developed to improve the productivity of new crops and therefore the food security of new agricultural systems. When doing this for a novel plant species and/or under novel combinations of stress, a fundamental science opportunity also arises for furthering our understanding of the evolution of and interaction between plant abiotic and biotic defences. Indeed, these interactions or 'nodes of crosstalk' could represent the plant's core stress tolerance mechanisms which could be the basis for engineering multi-stress tolerance traits in crops.

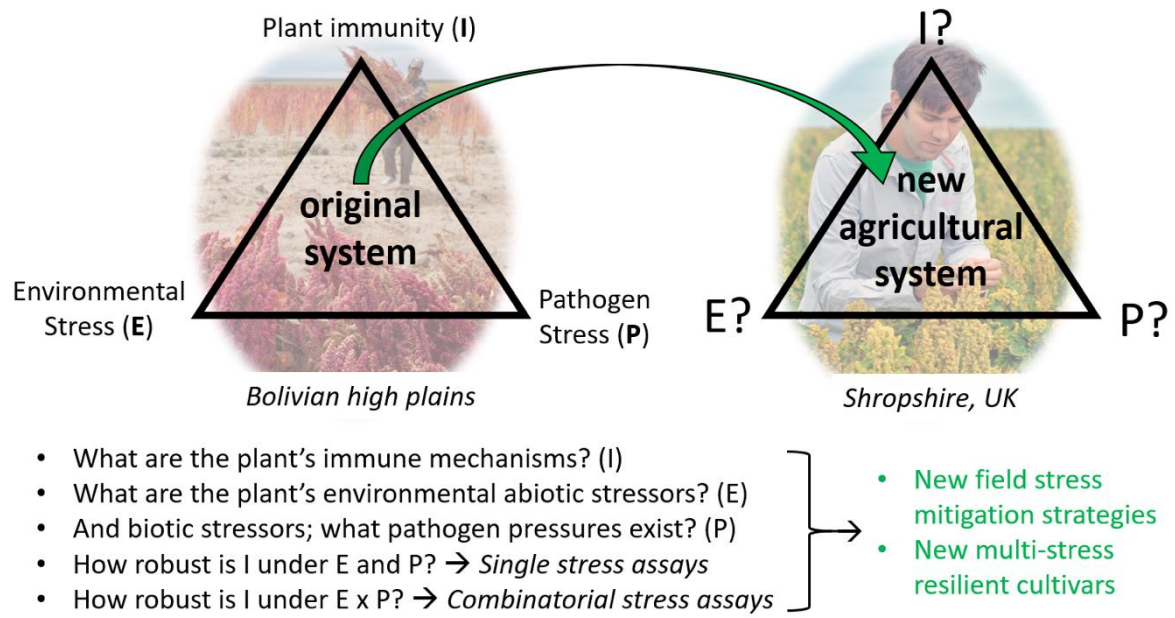


Fig.1. A research framework to support the expansion of crops from their sites of origin to new agricultural systems. Disease triangles can be drawn up to guide the fundamental research questions needed to address applied science goals such as achieving improved yields of novel crops in new countries. In this example, the disease triangle is drawn for quinoa being expanded beyond its site of origin in the Bolivian Altiplano to fields in Shropshire (UK) where The British Quinoa Company first established the crop in 2012 using European-bred cultivars developed by Wageningen University. Quinoa's abiotic stress tolerance and plant immunity have evolved to thrive in native climates and soils but today are being tested by novel stresses in the UK and other new environments. Therefore, to secure higher yields of quinoa production, these pressures must first be understood in order to guide the design of relevant model research systems for identifying crucial molecular (gene-level) insights underpinning the stress biology of the plant. This then allows stress susceptibilities to be managed via mitigation strategies and eventually for tolerance traits to be improved through breeding programmes (i.e., applied science goal outputs from fundamental science inputs). The vertices of the triangle represent key components underpinning yield security: an understanding of the plant's basal immunity (I), along with prominent environmental (E) and pathogen (P) stresses is needed to then query the robustness of (I) under these stresses, including simultaneous or sequential combinations of them (E x P).

1.2. *Chenopodium quinoa*; a promising crop for food security and new opportunity for researching combinatorial stress responses in plants

1.2.1. Quinoa's origin, social importance, botany and nutrition

Chenopodium quinoa (quinoa) is an annual, self-fertile allotetraploid (4x = 2n = 36) 'pseudocereal' crop of the Amaranthaceae family originating from the Andes. Quinoa was domesticated twice in the Andean highland and coastal regions (Jarvis et al., 2017) some 7000 years ago where it has since maintained important local nutritional and cultural significance. Even through the Spanish colonisation period where many traditional agricultural practices were supressed or replaced, the work of resilient smallholder farmers successfully maintained a high genetic diversity of quinoa, which is now proving to be of growing global value for food security. Quinoa's exceptional nutritional completeness as a plant-based food source inspired NASA to include it in their Controlled Ecological Life Support System (CELSS) (Schlick, 1993), and later, along with an appreciation of quinoa's rich genetic resource the crop was recognised by the United Nations who declared 2013 as the 'International Year of Quinoa'. This helped boost international awareness and curiosity for quinoa and stimulated an economic boom for the crop. Today, prices have fallen considerably since the quinoa boom because many more countries (120+) outside of quinoa's native regions successfully grow it, aided by better technology and locally adapted or improved quinoa varieties (Alandia et al., 2020). Whilst this has caused serious economic problems for local Andean farmers (McDonell 2018; Scrafton and Williams unpublished), the result is beneficial for more people globally and highlights the critical need to improve benefit sharing and continued recognition of the food's countries of origin whilst also achieving wider goals of global food security.

The Amaranthaceae family is highly diverse, containing a heterogenous mix of over 2500 species, including pseudocereal and vegetable crops, succulents, herbs, carnivorous plants and carnations (Morales-Briones et al., 2021). Amaranthaceae crops are unified by their high nutrition and remarkable stress-resilience traits which reflects their widespread adaptations to extreme environments. Quinoa's three most recognised and economically important crop relatives are *Spinacia oleracea* (spinach), *Amaranthus* spp. (amaranth) and *Beta vulgaris*

(sugar beet), while the ancestral diploid species *Chenopodium pallidicaule* (Cañahua) is another key stress resilient pseudocereal of particular importance to the Andean Altiplano (high plains) communities (Jarvis et al., 2017). Important to note is quinoa, unlike *Amaranthus* spp. and model halophytes such as *M. crystallinum* is a C3 and not a C4 photosynthesising plant, which is in common with most staple crops like wheat, rice, potato and beans and therefore might offer easier translation of stress buffering mechanisms for maintaining efficient photosynthesis (García-Parra et al., 2020; Raines, 2011). The evolutionary relationship between these species, along with other Amaranthaceae species are shown in Fig.2, adapted from Morales-Briones et al. (2021). Additional *Chenopodium* species of increasing interest are *C. fornasum* (Djulis), *C. berlandieri* (Huauzontle) and *C. album* (Bathua) which are important traditional nutritional sources in Taiwan, Mexico and India respectively (Jarvis et al., 2022; Jellen et al., 2019; Poonia & Upadhayay, 2015).

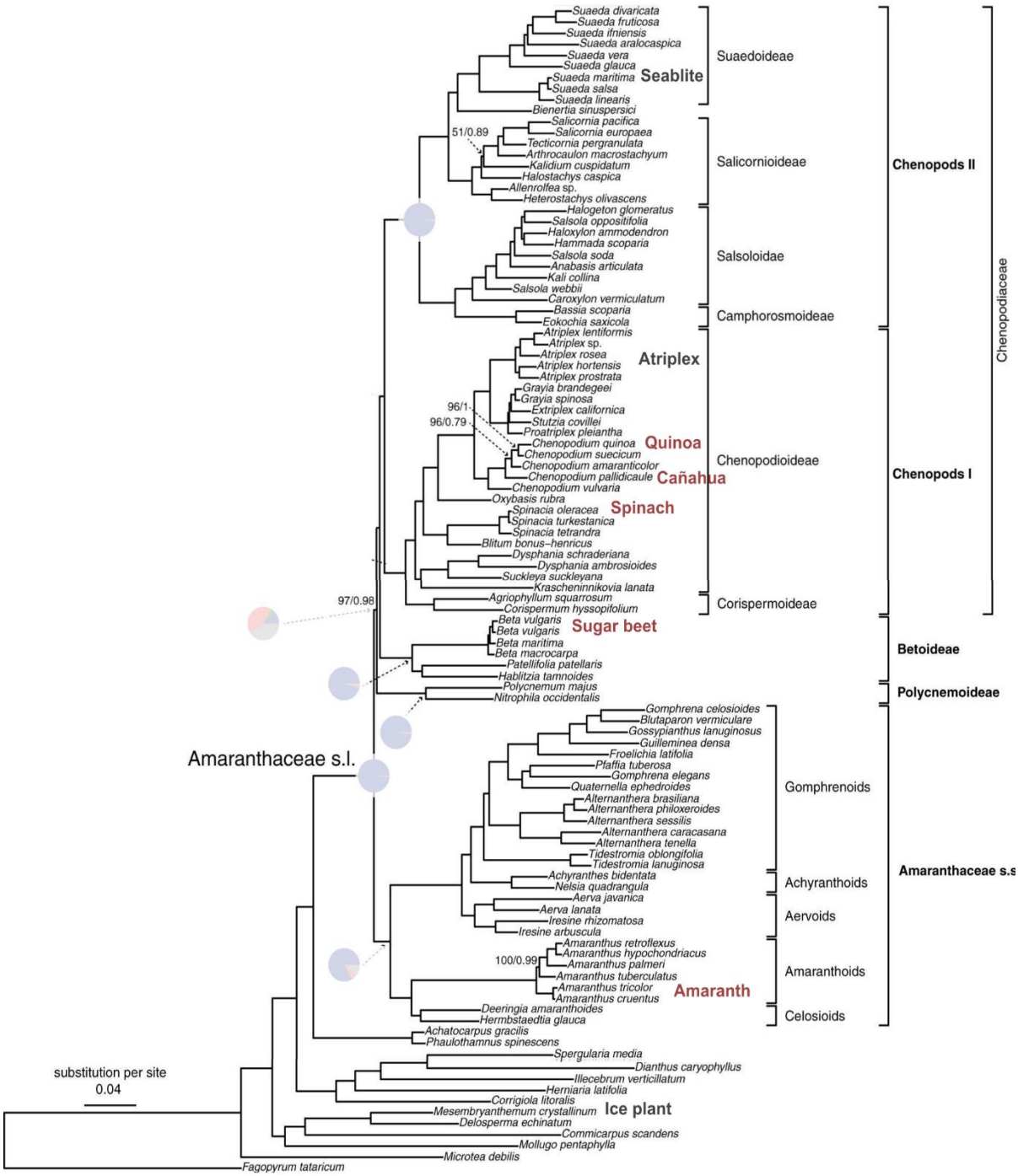


Fig.2. Phylogenetic tree of representative species from the Amaranthaceae family. The maximum likelihood phylogeny of Amaranthaceae s.l. was created "using 92 ingroup species (88 transcriptomes and four genomes) representing 53 genera (out of ca. 181) of all 13 currently recognized subfamilies and 16 out of 17 tribes of Amaranthaceae s.l.". Key crops are highlighted in red, and key salt tolerance model species are highlighted in black. Figure adapted from Morales-Briones et al. (2021).

The success of quinoa's adaptation to over 120 countries can be attributed to its exceptional environmental stress resilience and phenotypic plasticity, and to its rich genetic diversity, where the quinoa germplasm boasts over 14,500 accessions in South America alone (88% of the total available worldwide) (Bazile et al., 2016; Rojas et al., 2015). Quinoa ecotypes are adapted to five climatically distinct environments: sea level, valleys, Las Yungas (subtropics), Salares (salt flats; see Fig.3.) and the Altiplano (Ruiz et al., 2016) covering an altitudinal gradient of 4500 m, wind speeds upwards of 60 kph, temperatures from -12 to 35 degrees and nutrient poor, highly saline soils proximal to the Uyuni salt flats (Barrientos-Perez et al., 2023; Jacobsen, 2003). In Bolivia alone, germplasm banks across regions ('departamentos') conserve over 6500 accessions. The central INIAF National Germplasm Bank has characterised 3000 of these at the morphological level for superior abiotic hardiness or disease resistance (Rojas et al., 2015) but molecular level studies are still outstanding. Additionally, they hold several locally eaten Amaranthaceae crop wild relatives *Amaranthus caudatus (*Kiwicha) and wild black seed producing plants called 'Ajara', which describes seed from *C. album*, *C. petiolare* and *C. hircinum* (Nancy Huanca Alanoca, personal comms 2023), extending the pool of putative agronomic genes of interest. To help realise the potential of quinoa for global food security, genetic understanding of key agronomic traits (stress adaptive mechanisms and nutrition) is needed. Therefore, high-quality complete reference genomes were sequenced in 2017 (Jarvis et al., 2017; Zou et al., 2017) with subsequent improvements made through various re-sequencing projects (Tester et al., personal comms 2023) and the mitochondrial and chloroplast genomes of quinoa were sequenced in 2019 (Maughan et al., 2019; Gao 2021).

Quinoa is called a superfood because it provides a complete protein (all nine essential amino acids) and a balanced macronutrient complement of carbohydrate, fats, fibre and key minerals including, zinc and iron, vitamins and antioxidants, as well as being gluten-free (Villacrés et al., 2022). Both the seeds and leaves can be eaten, the stalks are used for animal fodder and traditionally the saponins from the outer seed coat were used as natural shampoo (Bonifacio/various, personal comms 2014). In 1993, a NASA technical paper claimed: *"While no single food can supply all the essential life sustaining nutrients, quinoa comes as close as any other in the plant or animal kingdom"* and studies since have investigated quinoa as a

'functional food' (having disease-preventing and/or health-promoting benefits in addition to their nutritive value; Turr and Bibiloni 2016). A wide array of quinoa food derivates from the seed have been developed including beverages such as beer, milk and vodka, puffed snacks, bread and pastries, and specific nutritional supplements for both the young and older ages (OrganicCrops website, accessed August 2023; Scrafton and Preston market research observations in the UK, Europe and Bolivia 2014-2023). Seed extracts such as quinoa protein and starch isolates have also been explored for use in the food industry for their unique quality and physicochemical properties respectively (Li and Zhu, 2017) and secondary metabolites such as phenolic compounds, saponins and coloured pigments betalains (especially from Taiwanese "red quinoa" *C. formosanum*) have been explored for uses in cosmetics, pharmaceuticals and as a natural food colourant respectively (Tsai et al., 2011).



Fig.3. Typical quinoa field from an experimental site in Salinas de Garci Mendoza, Bolivia, owned by Oruro Technical University (UTO). The site is located 10 km from the edge of the Salar de Uyuni salt flats, coordinates: 19.64°S, 67.68°W, elevation: 3,743m with soils comprising 90% sand and 10% silt and low levels (3.6%) of organic matter. Plants shown are 8-week-old native quinoa varieties, spaced at low density, typical of the southern altiplano region. Photo and data are from field experiments run as part of Ellen William's MBiol and my BSPP Junior Fellowship project 2021 with UTO collaborators.

1.2.2. Quinoa; a naturally stress tolerant plant with valuable agronomic traits for marginal climates

Plant species which have endured intense combinations of environmental stress in their native environments, or species which are suddenly introduced to non-native conditions through agricultural expansion, could be relevant candidates for investigating combinatorial stress responses. What genetically encoded or transiently induced adaptive mechanisms exist? Quinoa is an example of both scenarios: the crop has evolved tolerance mechanisms to prosper in the arid, salty and exposed high plains of Bolivia where temperatures, wind speed and light intensity fluctuate between extreme margins, and today, the stability of quinoa's abiotic and (comparably uncharacterised) biotic defences are being tested in field settings increasingly distanced from its native conditions (Jacobsen, 2017). Several excellent reviews have characterised the abiotic stress tolerance of quinoa (Hinojosa et al., 2018; Grenfell-Shaw & Tester, 2021), however the focus of this thesis is the specific interaction between quinoa's salt adaptations and plant immunity and thus only factors related to salt stress, disease and plant immunity will be covered in subsequent subsections.

Major limiting factors for expanding quinoa cultivation to new areas continue to be day length insensitivity, heat tolerance and resistance to biotic stresses such as diseases, pests and weed pressure (Schmöckel 2017; Gomez-Pando et al., 2015; Tester, World Quinoa Congress, personal comms 2023). Additional key priority areas for breeding programmes include early vigour, dwarfing, low branching, yield and trait stability, larger grains of higher yield and quality and mechanisation compatibility at the level of sowing and harvesting (Tester, World Quinoa Congress, personal comms 2023). Some of these traits are already being addressed by the European breeding company RADICLE which *"invests in novel crops to reduce the world's over-dependency on major staple crops."* RADICLE, with long-standing support from Wageningen University has released several elite quinoa varieties (including cv. Atlas used in this thesis) for European day-lengths and climates (Fig.4).

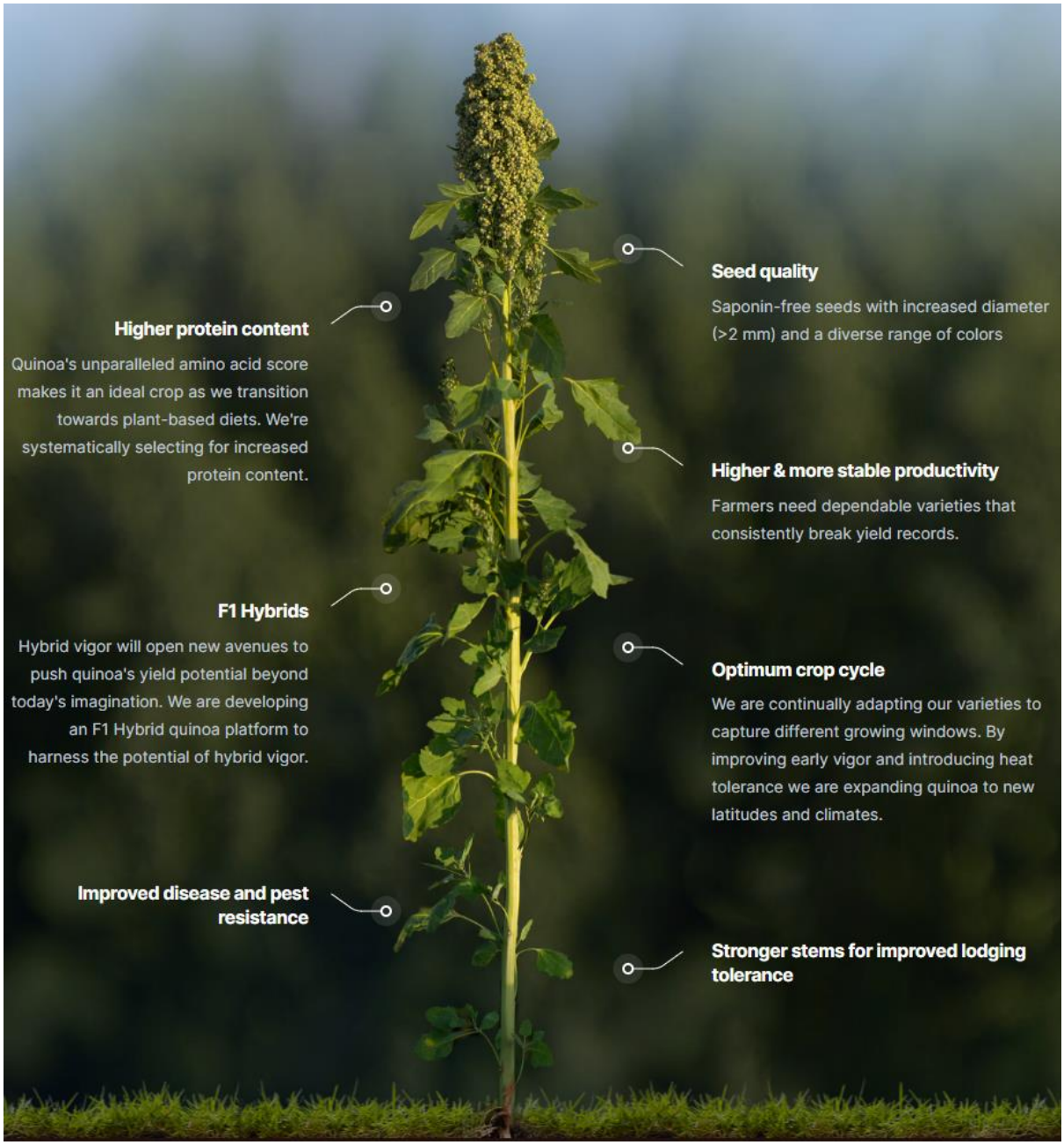


Fig.4. The quinoa plant and key agronomic traits being developed currently by RADICLE's breeding programme. Outstanding objectives such as improved disease and pest resistance are also shown. (Image from Radicle Crops website August 2023).

1.2.3. The impact of salt stress on agriculture

A major abiotic stress affecting crop productivity is soil salinity, which affects approximately 7-10% of the earth's land surface and 23-33% of arable lands. (Shahid et al., 2018; Chele et al., 2021). The socio-economic impact is large, not only is the food-supply chain affected but also employment and yearly economic losses in Europe alone already exceed half a billion euros (Ruto et al., 2020) (Fig.5.).

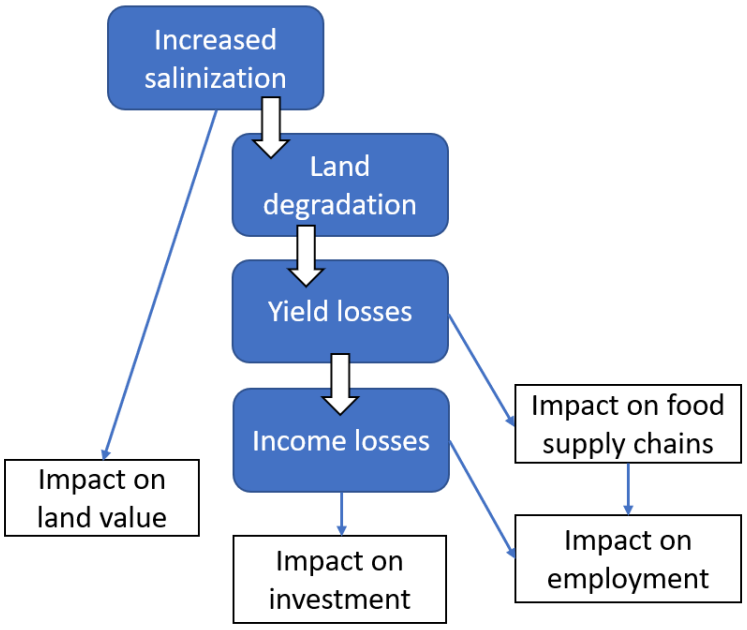


Fig. 5. Framework for assessing multiple impacts of salinization on land and society. Adapted figure from Ruto et al. (2020).

The process of soil salinization is due to the excessive accumulation of salts through either natural 'primary salinisation' such as deposition of oceanic salts through rainfall, the physical or chemical weathering of rocks or encroachment of saline water from natural sources (Hassani et al., 2021), or anthropogenic 'secondary salinisation' processes such as irresponsible irrigation or land drainage management (Rengasamy, 2006). Climate change drives salinization through several levels, predominantly via primary mechanisms, where drylands (which occupy ~45% of the Earth surface) in South America, southern and western Australia, Mexico, southwest United States, and South Africa have been predicted as salinization hotspots whilst rising temperatures and increasing food demands will force the expansion of irrigated arable lands demanding careful crop choices and land management (Hassani et al., 2021).

Salt-affected soils are classified as saline, saline-sodic or sodic soils, where sodium is the dominant cation of soluble salts such as sodium chloride (NaCl), sodium sulfate (Na_2SO_4) and sodium carbonate (Na_2CO_3) responsible for reduced crop yields (Osman, 2018). The measure of soil salinity is given by the electrical conductivity of the saturation extract (ECe) and generally, a concentration of soluble salts giving an ECe of 2 - 4 dS/m, which is equivalent to ~20 - 40 mM NaCl is considered high enough to adversely limit the growth of most glycophytic crop plants (Osman, 2018; Munns & Tester 2008). Quinoa has been shown to withstand NaCl ECes up to 15-20 dS/m (Wilson et al., 2002; Adolf et al., 2013) and for the cv. Andean Hybrid, Wilson et al. (2002) evaluated the effect of other salt types $MgSO_4$, Na_2SO_4, NaCl, and $CaCl_2$ at 3 – 19 dS/m and found no significant reduction in plant height and fresh weight. The extent of salt-induced growth inhibition is governed by the species effectiveness (and type of strategy) of salt stress adaptation, which will be discussed further below.

The major worry for future global food security is that the staple crops wheat, rice and maize, which make up two-thirds of the world's energy intake are all salt sensitive crops and therefore at risk of yield insecurity. Munns and Tester 2008 illustrated the diversity in salt tolerance of key crops and plants (Fig.6) where rice was the most salt sensitive and barley the most salt tolerant of the cereals. Quinoa would follow a similar trend to the halophyte saltbush species *Atriplex* spp., increasing dry biomass at 100 mM before a steady decline reaching null growth beyond 500 mM NaCl. Indeed, certain quinoa cultivars can complete their lifecycle even when irrigated with sea water ~500 mM NaCl (Ruiz et al., 2016).

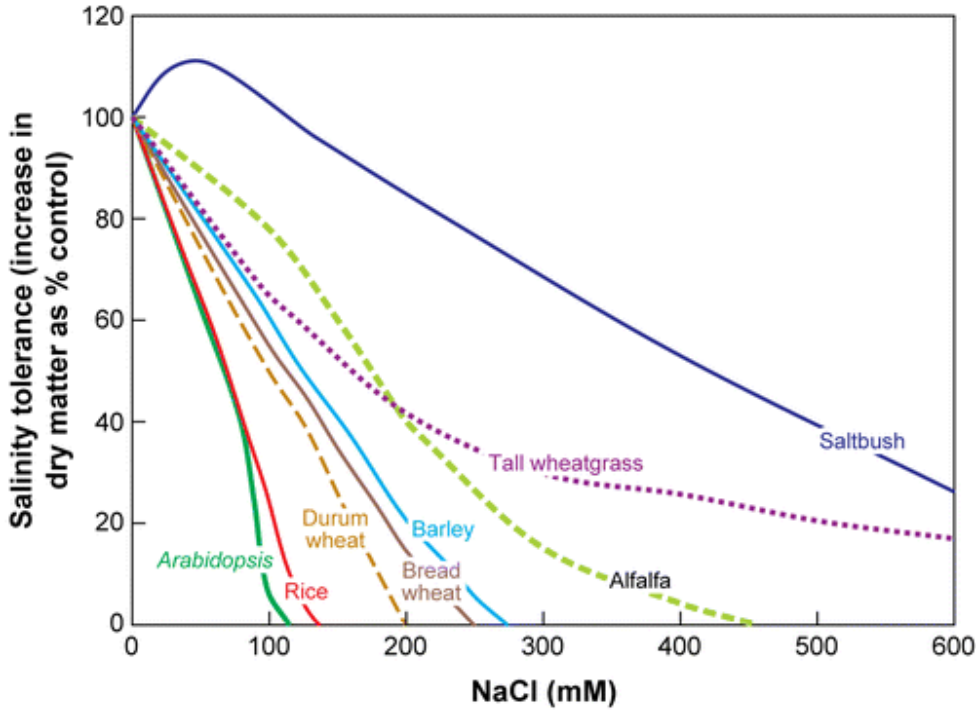


Fig. 6. Effect of salinity on biomass of various key crops and plant species. Munns & Tester 2008.

1.2.4. Common salt tolerance mechanisms of plants and specialised adaptations of halophytes

Salinity imposes two types of stress owing to the ionic and osmotic potential of salt ions. An osmotic gradient is created between plant root cells and surrounding soil where water is drawn to reach osmotic equilibrium. When the external concentration is higher water moves back out of plant cells causing aerial tissues to become dehydrated (loss of cell volume and turgor) until the plant can osmotically adjust through mobilising or synthesising compatible solutes to maintain turgor. Ionic toxicity occurs through excessive salt concentration in plant tissues, specifically in the cytosol, where Na^+ and Cl^- can denature cytosolic enzymes or disrupt core cellular signalling necessitating the need for efficient compartmentalisation in vacuoles (Flowers et al., 2015). These two components are perceived and managed by plants in different ways, which is also dependent on plant phenological age and the relative age differences of leaves (Munns & Tester 2008; Rankenberg et al., 2021; El-Iklil et al., 2000). For example, salt accumulates particularly in the older leaves of plants which have ceased expansion and therefore offer no further means for diluting the salt concentration, but which can then be shed (Munns & Tester 2008). If the rate at which older leaves are dying is greater

than the production of new leaves however, then whole plant level growth is reduced so that its photosynthetic capacity (and the availability of carbohydrate energy sources) can meet the demands of expanding tissues. This highlights the value of growth measurements (such as the lowest concentration causing 50% inhibition, LD_{50}) in assessing the degree of salt stress experienced by a particular species, where appropriate concentrations must be established on an interspecies and intraspecies (genotype to genotype) basis considering the differing dependence on types of and efficiencies within salt tolerance mechanisms.

Stress tolerance in plants is thus a complex trait with important sub-traits such as ion homeostasis, osmotic balance and reactive oxygen species (ROS) regulation (Munns and Tester, 2008; Ruiz et al., 2016; Zou et al., 2017). This makes engineering salt-tolerance into non-salt tolerant crops challenging. Salt tolerance genes which underpin these traits are categorised by function: controlling rate of salt uptake, translocation, and compartmentalisation; adjusting ionic and osmotic balance and regulating developmental processes, especially at the leaf-organ-level (a salt-dependent slow growth phenotype) or increased leaf turgor (Munns, 2005; Flowers et al., 2015).

Halophyte species have many inherent specialised salt tolerance traits, and a detailed description of quinoa's salt tolerance mechanisms (including the role of ion transporters, antioxidants, phytohormones and other upregulated genes identified through transcriptome studies) is provided in Chapter 3. One of the most striking features present in 50% of halophytic species including quinoa, ice plant (*Mesembryanthemum crystallinum)* and *Atriplex hortensis* however is the presence of epidermal bladder cells (EBCs). EBCs cover leaves, petioles and stems (Shabala & Mackay, 2011) and recent omics and electrophysiology studies have revealed details of their functions (Kiani-Pouya et al., 2017; Bohm et al., 2018; Moog et al., 2022; Shen et al., 2022). Example images of quinoa's EBCs are provided in Fig.7.

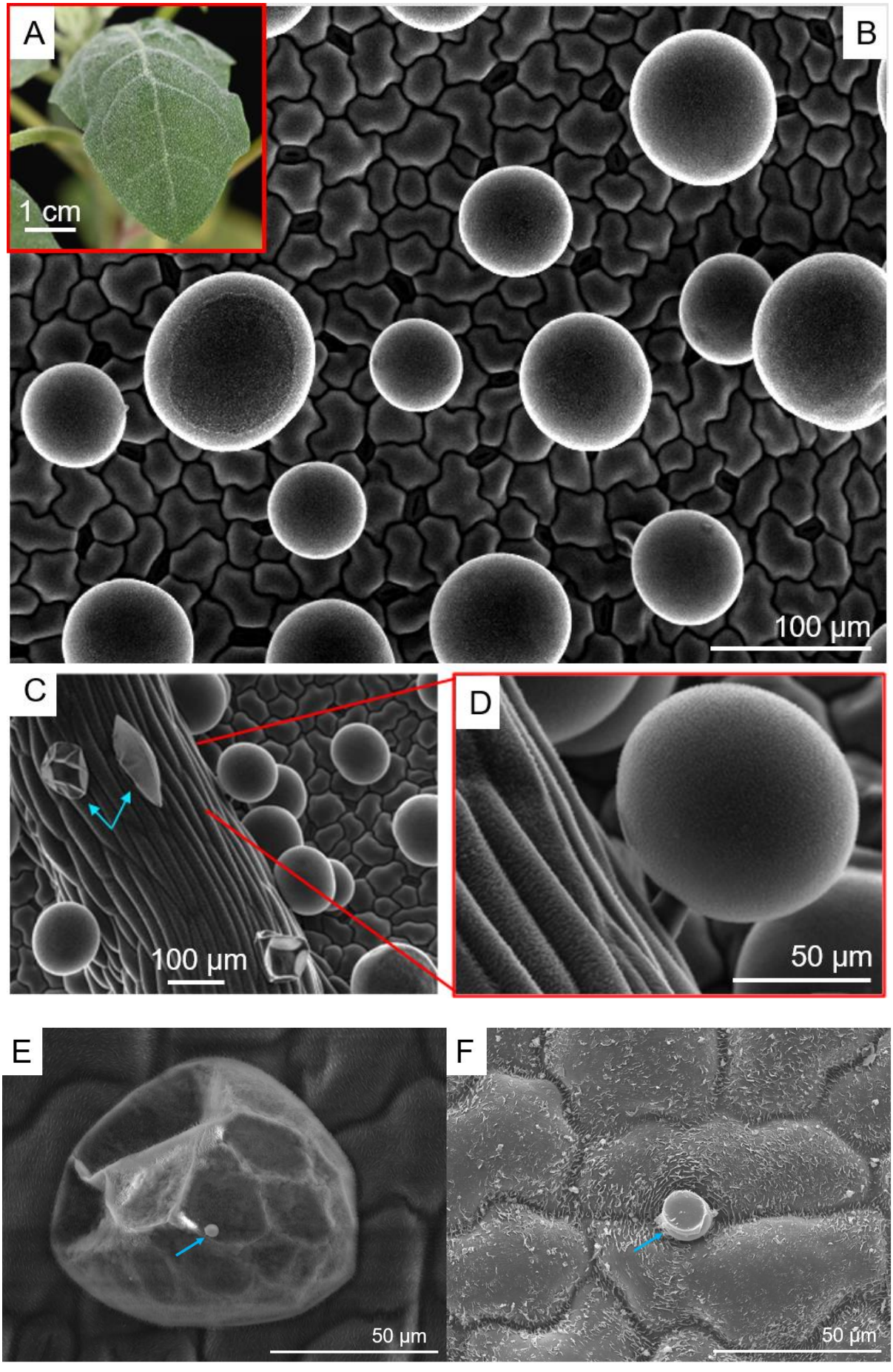

A
1 cm
B
100 µm
C
100 µm
D
50 µm
E
50 µm
F
50 µm

Fig. 7. Quinoa epidermal bladder cells and stalk cells. EBCs are large enough to see with the naked eye (A) and observed to greater details on the abaxial side of quinoa leaves (B, C, D, E & F) using scanning electron microscopy (SEM) with (A-D, F) or without (E) a surface shield enhancer (SSE) solution. B) 250 x magnification shot of the leaf lamina showing spacings of EBCs relative to stomata and epidermal pavement cells. C) x100 magnification showing midrib vein and collapsed EBCs (blue arrows). D) x500 magnification zoomed in on an EBC and stalk cell. E) 1100x magnification showing a collapsed EBC due to the effect of the SEM vacuum on unprotected leaf tissue (no SSE) which allows the stalk cell to be visualised (blue arrow), observed more clearly in F (110x magnification). All leaves (except in E) were protected by dipping into a sodium-based SSE solution (Takaku et al., 2013), blotted dry on filter paper to remove excess solution and mounted on the SEM. The SEM's electrobeam upon contact with the SSE solution forms a NanoSuit enabling EBCs to be preserved in their natural state for the duration of the imaging. Experimental conditions were optimised, and photos taken with Dr Niloufer Irani, with thanks to Prof. Hugh Dickinson for SEM training.

The large size of EBCs relative to the leaf lamina is visualised in Fig.7 where inside the EBCs are specialised central and enlarged vacuoles approximated to have a volume up to 1000x greater than mesophyll cells (Shabala et al., 2014; Bazihizina et al., 2022). When quinoa is grown under saline conditions, EBCs sequester inorganic and organic osmolytes into the vacuole, which is accompanied by water uptake which produces the turgid form (Böhm et al., 2018). As important to EBCs in salt adaptation is the EBC-anchoring stalk cell, which acts as both an ion (Na^+, Cl^- and K^+) and solute (sugars and metabolites) *"selectivity filter and flux controller"* (Bazihizina et al., 2022) ensuring bladder expansion, turgidity and physical support for maximal solute storage capacity. The stalk cell is specialised for solute transport due to the high number of active ion channels, sugar transporters and a large respiratory and metabolic capacity owing to densely packed mitochondria and Golgi complexes at the apical end (EBC-facing). High amounts of open (eu)chromatin in the nucleus of stalk cells relative to EBCs or epidermal cells suggests a highly active state of gene expression to support these features underpinning EBC-directed solute flow, and Bazihizina et al. (2022) conclude that this energetically and structurally polarised organisation is typical of a transfer cell.

1.3. Disease in quinoa

1.3.1. Common field diseases and native biotic threats

Conversely to quinoa's remarkable abiotic tolerance, quinoa is notably susceptible to biotic stresses. However, until recently, assessments of quinoa's biotic stress tolerance were largely limited to field studies and were largely descriptive. The major field disease of quinoa is downy mildew caused by the biotrophic oomycete *Peronospora variabilis Gaüm* which can cause up to 99% of crop loss in susceptible lines (Bonifacio et al., 2001; Danielsen et al., 1999). Fungal diseases include brown stalk rot caused by *Phoma exigua var. Foveata*, grey mould by *Botrytis cinerea,* leaf spot caused by *Ascochyta hyalospora* and yellow blotch disease caused by *Alternaria* spp. (Danielsen et al., 2003; Li et al., 2017; Colque-Little et al., 2021; Colque-Little et al., 2023). In Bolivia, other foliar biotic stresses include pests such as 'la polilla de quinua' (*Eurysacca quinoae*) and moth larvae (*Helicoverpa quinoa*). Locally in quinoa fields in the UK, a major problem is weed pressure from *C. album*, or other plants, as no herbicides are currently licensed for quinoa. 'Damping off' has also been found to limit seed germination, however the causative agent has not been determined (Stephen Jones, British Quinoa Company, personal comms 2023). Downy mildew and (suspected) viral infections are mild biotic threats to UK-grown quinoa where photosynthetic efficiency of the plant appears to be reduced due to significant blotching or speckled yellowing of the leaves which does not stop seed production but may reduce the crop's yield (Fig.8).

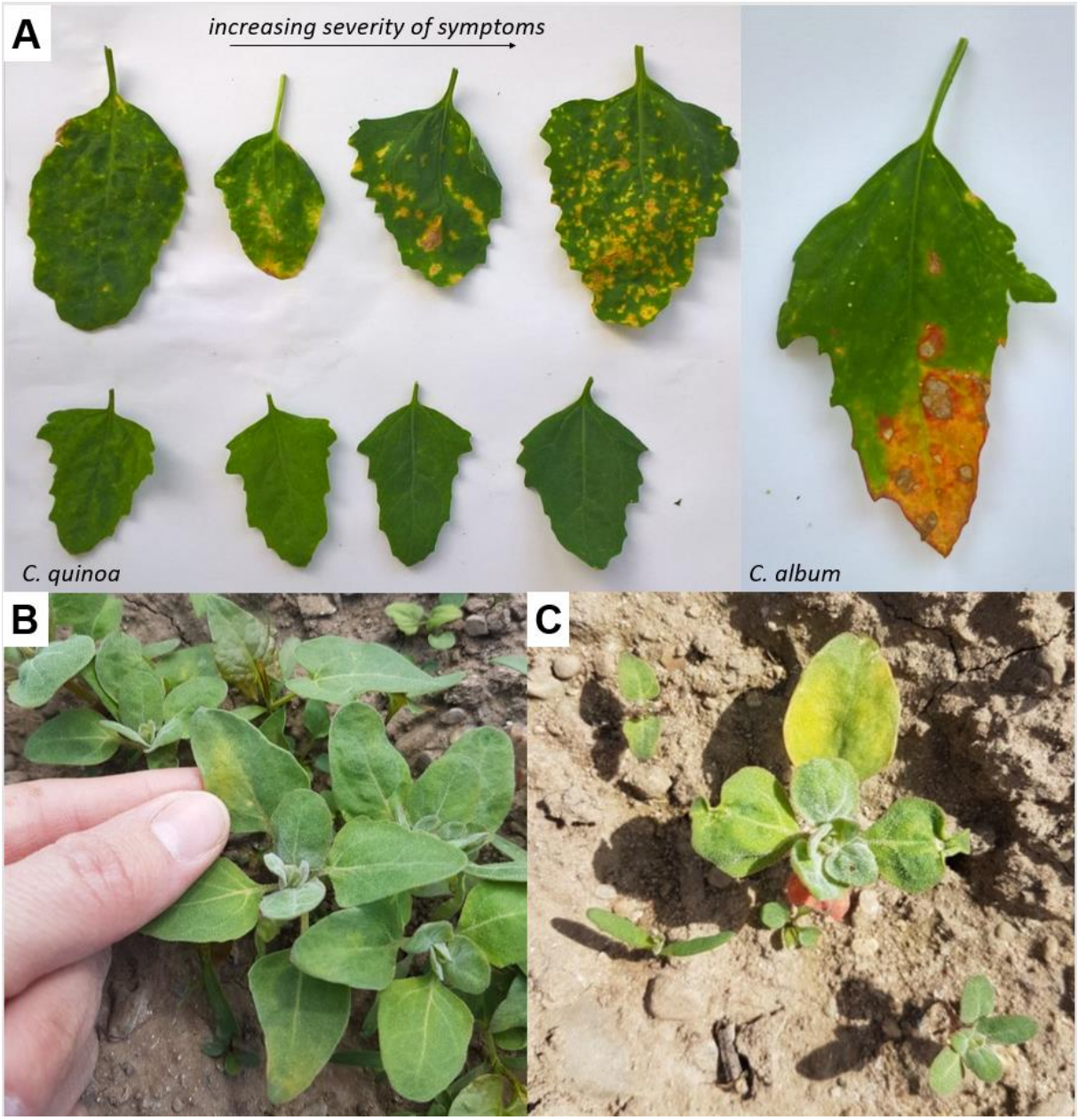


Fig.8. Diseased leaves from quinoa cv. Atlas growing in British Quinoa Company fields in Shropshire, July 2019. Healthy and diseased *C. quinoa and C. album* leaf examples (A) and young plants growing in the same field that year displaying symptoms that are characteristic of fungal or oomycete diseases such as downy mildew (B & C). More details in Supplementary Material.

The use of quinoa in scientific research prior to its growing interest as a food crop has been as a laboratory tool, a 'universal' plant virus host (Nerva et al., 2019). DEFRA viral expert Adrian Fox (2021 personal comms) comments that quinoa is *"part of a standard range of test plants for bioassay testing, virus isolation and propagation. The consequence of this is that there is an extensive list of viruses which we know will infect quinoa but relatively little is*

known about the relative risk of these to the plant, especially outside of its native environment." Examples of quinoa as an alternate virus crop host under laboratory conditions for quinoa include: Beet soil-borne virus, tomato black ring virus, strawberry mild yellow edge-associated protexvirus, citrus tristeza virus, Cucumber mosaic virus and Tobacco mosaic virus with (Crutzen et al., 2009; Hasiów-Jaroszewska and Zarzyńska-Nowak 2022; Lamprecht and Jelkmann, 1997; Garcia et al., 1991; Bamunusinghe et al., 2013; Guo and Wong, 2018; Williams BSPP report unpublished) and known cases of viral diseases of field grown quinoa crops were caused by tospoviruses (Chou et al.,.2017). Mitovirus 1 has also been found in the seed of multiple European commercial varieties but was interestingly absent from native Bolivian and Peruvian accessions (Nerva et al., 2019).

Most studies of *P. variabilis* downy mildew (DM) infections in quinoa have focused on screening quinoa cultivars for resistance in agricultural fields (Danielsen et al., 2000; Danielsen et al., 2004; Kumar et al., 2006; Gabriel et al., 2012) and countries of origin of quinoa such as Bolivia have documented morphological disease symptoms and annotated the passport data for key local accessions in their germplasm banks showing that quantitative differences in susceptibility likely exist. Recently, Colque-Little and collaborators performed a large comparative study to assess precisely the genotypic basis for the variability of downy mildew tolerances observed within quinoa collections. Using 132 South American genotypes, largely from the INIAF Bolivian National germplasm bank, three Danish-bred cultivars and the weedy relative *Chenopodium album*, plants were infected with a Danish field isolate of *P. variabilis* (originally isolated from *C. album*) under greenhouse conditions. The severity of infection was found to range widely from 5% in control species *C. album* and 11% (cv. Puno) to 83% (INIAF accession G9) and to strongly correlate ($R = 0.91$, $P < 0.001$) with pathogen sporulation, which ranged from 0.2 % in Puno to 83.6 % in cultivar 21. The results from Colque-Little et al., 2021 using the Danish isolate reflected resistance trends seen for cultivars Kurmi and Maniqueña Real infected by a Bolivian isolate in another study (Rollano-Peñaloza et al., 2022). Some levels of correlation were also found with the INIAF germplasm passport data which were performed using local races under natural conditions which together suggests that DM tolerance is not just race-specific but rather depends on quantitative resistance.

Indeed, Colque-Little et al., 2021 effectively used genome-wide association mapping to confirm that the basis for DM resistance observed in the wide panel was polygenic by identifying seven potential contributing loci, which again supports previous findings. Interestingly, quinoa ecotypes from the Andean Valley (2500–3500 m altitude) where humidity is higher and thus also DM disease pressure (due to a more favourable environment for the pathogen; specific details to follow) were found to be among the most tolerant accessions. Conversely, five accessions from the arid southern Altiplano of Bolivia were found to be the most susceptible. This suggests that ecotypes adapted to these regions may not have experienced such evolutionary disease pressure needed to evolve more robust DM resistance mechanisms, but it is interesting to speculate whether alternate stress tolerance strategies are engaged by these ecotypes when grown in their native localities.

Environmental factors as well as genetic factors therefore play a key role in disease incidence and disease severity of pathogens. As expected, quinoa plants grown in the southern Altiplano of Bolivia around the arid, highly saline and exposed salt flats suffer less from biotic threats (Gonzales Torrico, 2017 and Bonifacio 2018, personal comms; Scrafton & Williams unpublished). During a British Society of Plant Pathology Junior Fellowship project 2021-22 disease symptoms were found affecting only the leaves of the lower third portion of plants from two out of seven tested cultivars (Kurmi and Kellu) grown in major quinoa regions on the central and southern Altiplano (Scrafton & Williams unpublished) (Fig.3 & Supplementary Figure 1). In these regions, unlike in the warmer temperate regions of the aforementioned Andean Valleys, DM does not appear to affect the upper portions of the plant and importantly does not appear to directly limit seed production. Additionally to the direct inhibitory effects of harsh environmental conditions on the pathogen, these observations could also be due to enhanced disease tolerance mechanisms of the plants conferred through immune-specific priming effects of abiotic stresses, or through abiotic stress tolerance associated phenotypes such as salt-acclimation. For example, an antimicrobial leaf microenvironment could be created through the accumulation of salts or stress-induced antimicrobials such as phenolic compounds (Lelario et al., 2018; Al-Qabba et al., 2020; Kumar et al., 2021). High humidity (>80%) and cooler-temperate conditions, which are prevalent in the Andean valleys and

across many areas of Europe are opt for oomycete, fungal and bacterial diseases of quinoa (Danielsen et al., 2003; Li et al., 2017; Gomez-Pando et al., 2019).

Lastly, disease phenotyping in quinoa can be complicated due to complex multispecies associations as well as basal differences in leaf colour pigmentation, which produce a range of discolorations and so Colque-Little and collaborators have since standardised foliar disease scoring in quinoa for *P. variabilis* and other diseases (Stanschewski et al., 2021) (Fig.9).

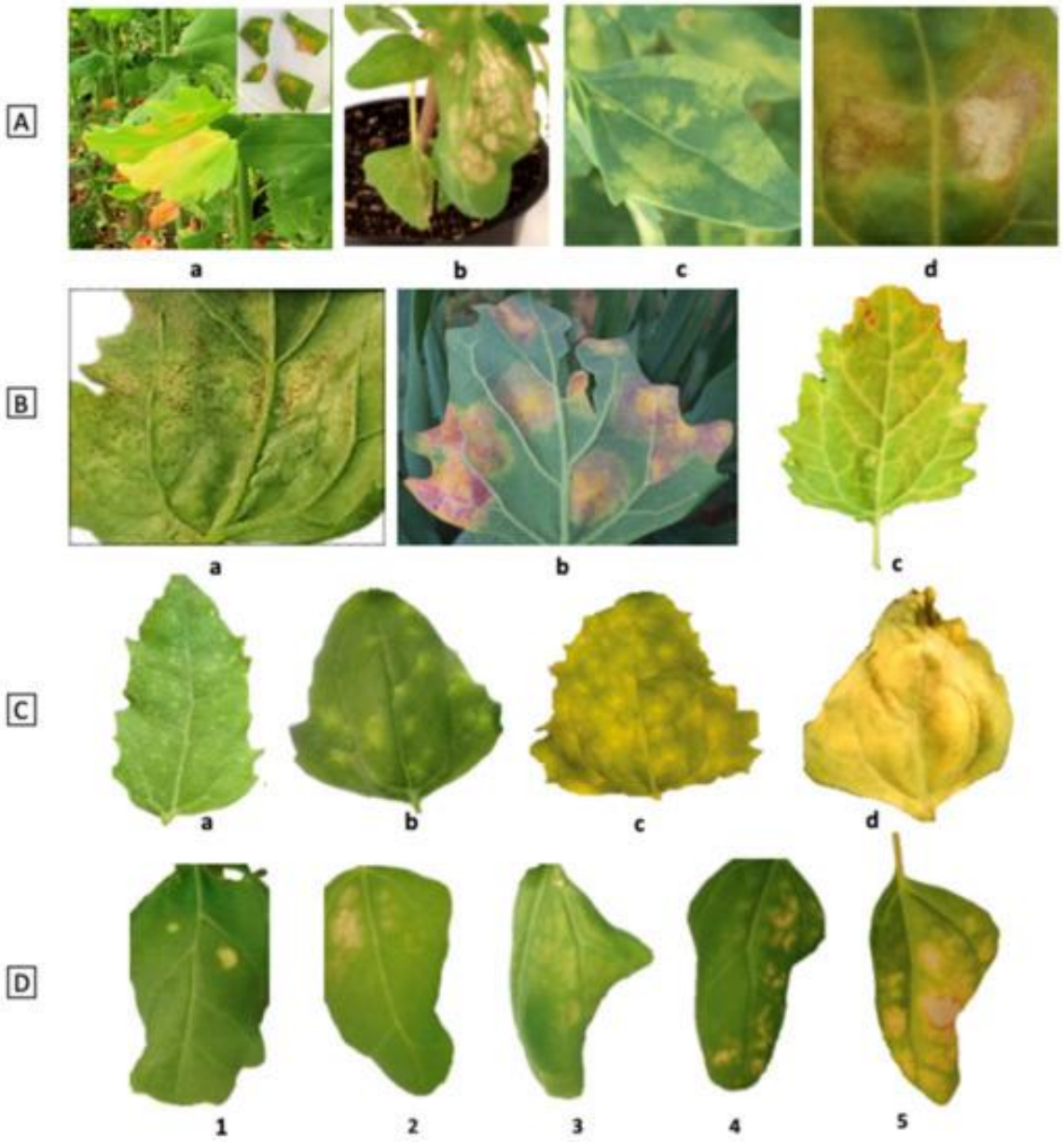


Fig.9. Phenotyping guide for foliar disease of quinoa by Colque-Little 2021: Lesions on leaf surface: "(**a**) pale or yellow chlorotic lesions with or without a halo and occasional pink-orange discoloration caused by leaf pathogens, (**b**) bronze irregular lesions caused by *Alternaria* sp., (**c**) diffuse chlorotic

spots caused by *P. variabilis* and (**d**) concentric and chlorotic halo under artificial inoculation with Alternaria sp. (**B**) Sporulation on lower side leaf surface with (**a**) black dots showing downy mildew sporangia, (**b**) dark gray-violaceous sporulation caused by *P. variabilis* and (**c**) vein discoloration, general chlorosis and pink-orange spots caused by *Fusarium* sp. (**C**) Lesion type on upper surfaces and amount of disease ranging from (**a**) dots, (**b**) dots expanding, (**c**) diffuse, and (**d**) extensive. (**D**) Severity phenotyping scale used for assessing the percentage of the leaf area affected where 1 = 0–10%, 2 = 11–25%, 3 = 26–50%, 4 = 51–70% and 5 = 71–100%. Leaf examples given represent different degrees of severity during the infection of *Alternaria* spp."

1.3.2. Bacterial pathogens of quinoa

Information regarding bacterial pathogens of quinoa has been the least documented in the literature (Williams BSPP report unpublished) but the economically important sugar beet pathogen *P. syringae* pv. *aptata* was shown to cause aggressive disease symptoms in quinoa by Maraite et al. (2013), who also showed that *P. syringae* pv. *atrofaciens* was able to infect quinoa. In 2021, Fonseca-Guerra et al. reported the first natural infection and isolation of *P. syringae* from quinoa grown in Colombian fields in the subtropical municipality of Tunja. Under laboratory settings the researchers re-infected quinoa plants with the isolated strains and observed canonical bacterial leaf spots around the needle prick inoculation point three - five days post inoculation and 50 % of infected leaves of each trial were symptomatic (Fig.10) and *P. syringae* was identified as the causal agent. Tunja's subtropical highland climate is most similar to the 'Cfb' climate descriptor in the Köppen Geiger classification system, where 'C' denotes a temperate climate, 'f' = no true dry season and 'b' = warm summers (Climate-Data.org). The temperate and year-round humid climate of Tunja would favour the epidemiology of *P. syringae* (Baltrus et al., 2017) and it would be interesting to know exactly when the bacterial leaf spot disease was first observed, the corresponding climate conditions at the time and the developmental stage of the quinoa plants. For example, it is suggested that the month of January in Tunja has the lowest precipitation rate and April the highest (Climate-Data.org) and knowing how these periods correlate with the quinoa crop cycle could be significant for developing mitigation strategies; how would disease susceptibility to *P. syringae* vary between the vegetative to early flowering and panicle development stages which would likely span across this variable seasonal period?

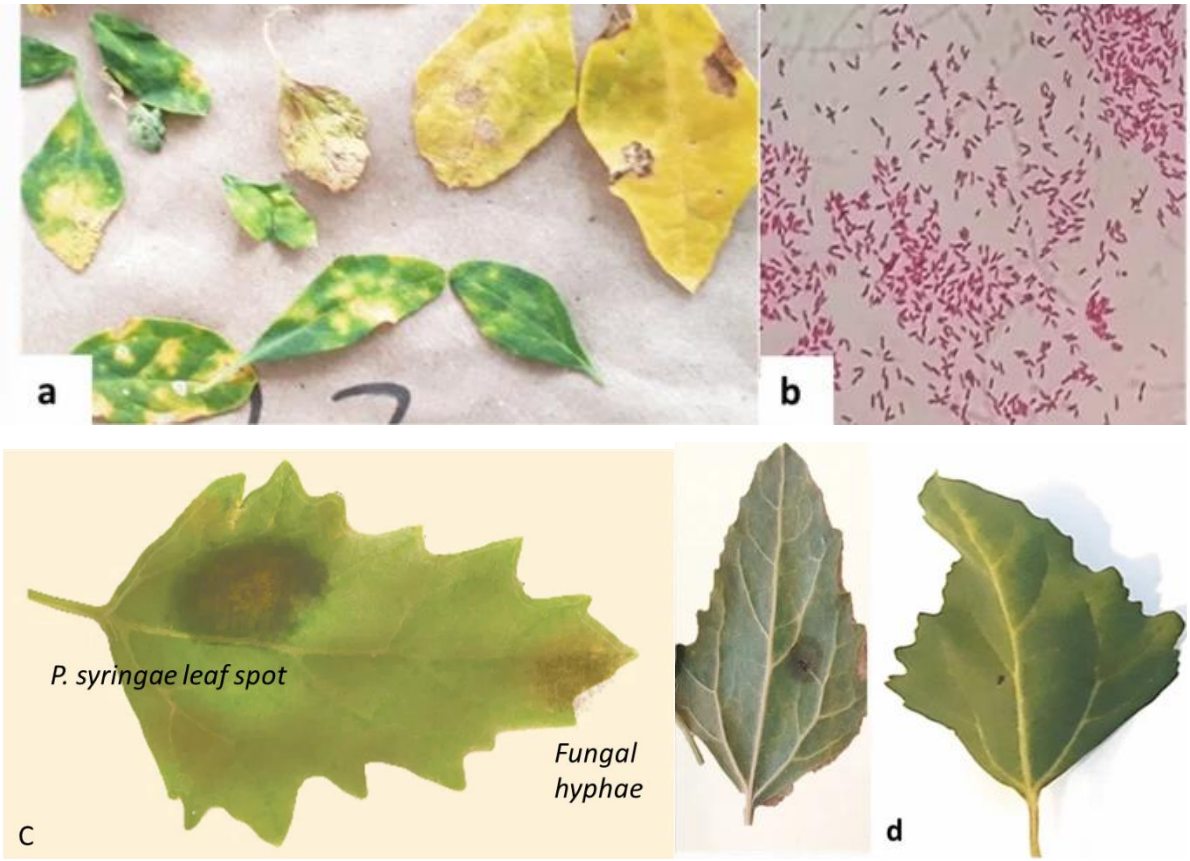


Fig.10. Bacterial leaf spot on *C. quinoa* leaf. A Symptomatic leaves from which the pathogen was isolated; **B** Gram-negative *P. syringae* cells ×100 magnification; **C** inoculated leaves with pathogen specific annotations (adaptions to the figure); D control leaf. (Fonseca-Guerra et al., 2021).

In addition to pathogenic bacteria, several researchers believe quinoa harbours beneficial endophytic bacteria as part of their seed, root and leaf microbiome which promote environmental stress tolerance and could additionally confer resistance to additional bacterial pathogens (Urcelay et al., 2011; Ortuño Castro et al., 2014; Colque-Little et al., 2021; Gonzales Torrico, personal comms 2021; Badran et al., 2023). Recently, Badran et al. (2023) published results from trialling the disease protective role of four bacterial endophytes (*Pseudomonas taiwanensis*, *Bacillus velezensis*, *Bacillus subtilis,* and *Pseudomonas putida)* of quinoa roots, stems and leaves, against controlled *P. syringae* infection. They found that disease resistance improved and related it to an enhanced nutrient use efficiency of plants pre-treated with the endophytes.

1.4. Leaf-based pathosystems with the model bacterial species *Pseudomonas syringae*

Just as Arabidopsis has been a pivotal model plant for furthering our core understanding of plant immunity, the ubiquitous bacterial pathogen *P. syringae* is widely regarded as a prototype pathogen, taking the top spot in Mansfield's et al. (2012) list of 'Top 10 plant pathogenic bacteria in molecular plant pathology'. This is due to its natural ubiquity, extensive phylogeny and because its amenability to genetic manipulation allows pathogenicity and virulence mechanisms to be studied in a wide range of plant backgrounds (Arnold and Preston, 2019). For example, *P. syringae*-based pathosystems in model plants such as *Arabidopsis* and *Nicotiana benthamiana* and in crops such as bean (*Phaseolus vulgaris*) and tomato (*Solanum lycopersicum*) have revealed key molecular interactions underpinning pathogenesis or disease resistance outcomes between bacteria and plant host cells (Preston, 2000). This makes *P. syringae* a key laboratory tool with direct field relevance considering the vast number of crop species affected globally by host-specialised pathovars. These include strains that infect closely related crops to quinoa such as sugar beet and spinach: pv. *aptata* and pv. *spinaciae*. Furthermore, Maraite et al. (2013) and Nikolić et al. (2018) have already shown how *P. syringae* pv. *aptata* has a wide and diverse host range, and virulence (Nikolić et al., 2023), which could be problematic for quinoa as cultivation expands to affected areas such as Southeastern Europe (Nikolić et al., 2018). Key molecular components of the interaction between *P. syringae* pathovars with their hosts or non-host species are illustrated in Fig.11. The virulence factors include phytotoxins such as syringomycin or coronatine (a structural and functional mimic of the plant hormone jasmonoyl isoleucine JA-Ile; Zhao et al., 2003), phytohormones (e.g., Indole-3-acetic acid), plant host protein inhibitors such as galactosyrin and type three effectors (T3Es) which are injected via a Type III secretion system (T3SS) (Preston, 2000; McClerklin et al., 2018). Virulence factors alter plant immune responses or manipulate host physiology (Lindeberg et al., 2012). Specific T3E-deficient or T3SS virulence mutant backgrounds can be produced within a *P. syringae* pathosystem, especially important where robust (targeted) genetic modification systems on the plant side are unavailable, which was the case for quinoa upon starting this project and which continue to be challenging today (López-Marqués et al., 2020).

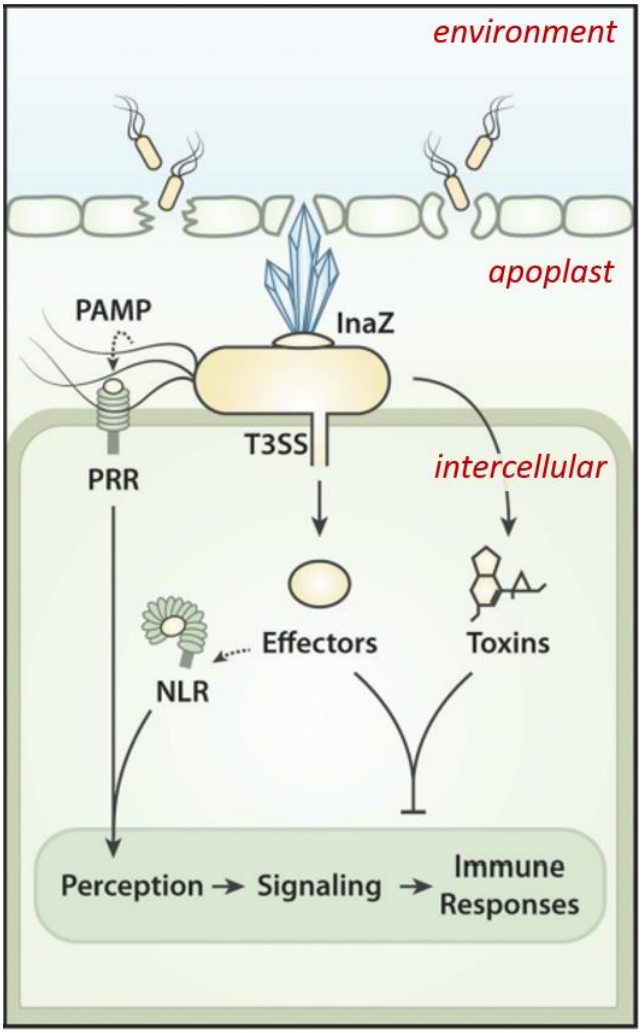


Fig.11. *P. syringae* - host interactions, figure copied with minor additions from Arnold and Preston, 2019. *P. syringae* enter the plant apoplast through openings in the cell wall (stomata or gaps due to wounding) where they release a range of virulence factors to suppress host immune signalling and responses before their invasion is recognised (via PRRs for PAMPs and NLRs for effectors) and resistance mechanisms are established. Further host immune responses are given in Fig.12.

The major pathogens of quinoa are foliar (Bonifacio et al., 2001) hence establishing a leaf-based infection system will be critical. Furthermore, considering how *P. syringae* colonise the plant apoplast, the extracellular space, a quinoa – *P. syringae* pathosystem could also provide a novel opportunity for evaluating how quinoa's halophytic microenvironment impacts the pathogenesis of this important pathogen. Further details on *P. syringae* biology, epidemiology and virulence strategies are provided in Chapter 4.

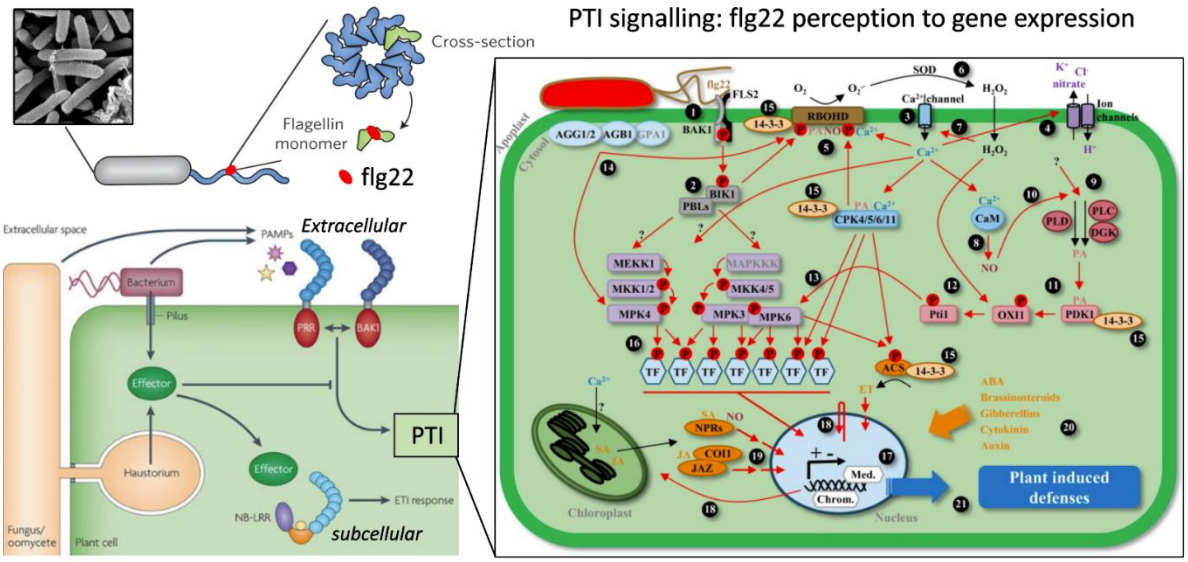
1.5. Plant Immunity

1.5.1 Current understanding of the plant immune system

Plants have evolved a highly intricate immune system to perceive, respond to and overcome pest and pathogen attacks (Iriti and Vitalini, 2021). Plant pathogens also evolve to evade plant immunity and consequently the host and pathogen engage in an 'arms race'. This phenomenon can be observed at the molecular level on the pathogen's side via discrete changes in amino acid sequence or sugar structures (glycan polymorphism) of immunogenic peptides (PAMPs) or of their effector proteins, or in maintaining the efficacy of specific inhibitors to crucial host enzymes, or on the plant's side through changes to their pathogen perception components, such as PAMP recognition receptor proteins (e.g. PRRs) or apoplastic proteases such as beta galactosidase 1 (BGAL1) or papains (Buscaill et al., 2019; Godson and van der Hoorn, 2021). It is understood therefore that the local environment and its typical pathogen pressures drive the evolution of specific immune mechanisms in plants (Burdon and Thrall, 2009). This has important consequences for disease mitigation strategies especially when crops move to new locations or climate change facilitates the incidence of new pathogens: how robust are a plant's immune defences?

Plant innate immunity has traditionally been classified into two branches with analogy to a "two-tiered surveillance system": PAMP (Pathogen-Associated Molecular Patterns) triggered immunity (PTI) and effector triggered immunity (ETI) (Jones and Dangl, 2006) (Fig.11). Central to the immune networks (with fundamental similarities to the immune system of animals) are receptors, a relay system and response components (Fig.12) which together achieve resilience, tunability and balance to discern pathogens of varying threats, as well as combinatorial stresses (where immune components interact with abiotic stress defences) (Kanyuka and Rudd, 2019). Within each branch there are canonical immune features which, depending on the plant species and local environment, may have roles of varying importance. Several key molecular signatures of PTI along with a composite plant immunity summary figure adapted from various studies are shown in Fig.12.

The plethora of immune signatures provide multiple molecular and biochemical points to study from perception (receptors), upstream and downstream signalling (relay system) to changes in gene expression for stress specific or non-specific gene products (response components) using laboratory protocols and bioinformatic analyses.



Gordon Vrdoljak, Dodds & Rathjen 2010, Bigeard et al., 2015, Fliegmann & Felix 2016

Fig.12. Overview of plant immunity. Plant immunity can be interrogated using artificial immune elicitors such as the PAMP flg22, an immunogenic peptide which is cleaved by extracellular plant proteases from flagellin monomers of invading bacterias' flagella (top left of figure) or by inoculating with disease inducing (or virulence defective; not shown) pathogens such as bacteria or fungi/oomycetes. Pathogen recognition by surface extracellular receptors activates multiple protein kinases and NADPH oxidases including respiratory burst oxidase homolog D (RBOHD), which produces ROS such as superoxide (O_2•), which can be dismuted into hydrogen peroxide (H_2O_2) which triggers further intracellular PTI signalling. Transcription factors (TFs) are activated and induce the expression of key immunity genes. Composite figure compiled and adapted from Dodds & Rathjen (2010), Bigeard et al. (2015), Fliegmann & Felix (2016) and the *P. syringae* SEM image is from Gordon Vrdoljak.

1.5.2. The impact of environmental adaptations on plant immunity

There are however unique immune features which certain plant species have evolved in response to niche environmental pressures. If we revisit the disease triangle in Fig.1, we can see how the factors representing the individual vertices can interact over long evolutionary

timescales, as well as in discrete instances for a crop growing in one season. If the abiotic environmental pressures are more detrimental to the plant than local biotic pressures, the tolerances evolved to these stresses over time, such as the halophytic adaptations of quinoa, could produce novel immune strategies. One example of an abiotic-stress tolerant species evolving a unique immune strategy is *Noccaea caerulescens,* termed the 'elemental defence': when grown in heavy-metal contaminated soils, *N. caerulescens* has evolved to sequester extraordinarily high amounts of zinc for storage in its leaves which then confers resistance to biotic predators (Fones et al., 2013). However, consequential and unique trade-offs occurred in the evolution of this trait at the level of ROS immune signalling. A molecular explanation was provided by Fones et al. (2013) who hypothesised that metal accumulation in leaves increased the ROS and thus also the ROS-quenching antioxidant status of cells, invalidating the dispensability of ROS to signal for biotic stresses such as infection by *P. syringae*.

Few studies have considered the potential for pathogen-buffering effects also occurring through the hyper localisation of salt in tissues of salt-tolerant plants. The idea that 'freely available' inorganic elements can be sequestered and utilised by the plant for improving survival chances has also been ascribed for chloride ions as 'cheap osmotica' when nutrient and light conditions are unfavourable; this is thought to spare the use of catabolically more useful anions, nitrate and malate (Wege et al., 2017). Considering also how molecular characterisation of quinoa's immune system has not been done a unique opportunity arises for studying both. Quinoa may be fundamentally different from glycophytic species in its biotic stress mechanisms due to its halophytic nature; constitutively or transiently produced salt-related molecular mechanisms could positively or negatively influence the way the plant responds to pathogens.

1.6. Combinatorial stresses and the challenge for agriculture

Crops growing in fields are subjected to multiple simultaneous or successive abiotic and biotic stresses yet achieving both stress tolerance and high yields of crops requires significant energy investment from the plant (Huot et al., 2014). To optimise energy partitioning for growth under changing and stressful environments, plants exhibit many kinds of temporal and spatial trade-offs at the molecular to phenotypic level, prioritising certain development

or stress signalling pathways over others (Koornneef and Pieterse, 2008; Huot et al., 2014; Berens et al., 2019; Nobori and Tsuda, 2019). It is logical to speculate that these trade-offs are orchestrated at points of interaction which could be harnessed as modules for achieving higher yielding multi-stress tolerant crops. This project aims to establish a research system in the naturally abiotic stress resilient crop quinoa to explore combinatorial stress responses and elucidate potential points of interaction between the plant's abiotic and biotic stress signalling pathways.

1.6.1. Combinatorial stress responses and interactions between abiotic and biotic stress signalling pathways

As plants are sessile organisms, stress signalling interactions (sometimes referred to as 'crosstalk') enables the plant to integrate and react to combinations of environmental stresses with mechanistic prioritisation (Nobori and Tsuda, 2019). Highly orchestrated 'perceive and respond' signalling frameworks ensure the plant acts efficiently (quickly and energetically-resourcefully) to combat the most significant external stresses. This entails the transient 'shutting down' or postponement of less-critical energy-demanding pathways. Interactions exist between shared components in 'distinct' signalling pathways ('nodes'). These nodes can be induced by different cues (stress signals) and the response is transduced via coordination of agonistic or antagonistic interactions along either signalling pathways (Fujita et al., 2006) (Fig. 13). Interactions between stress signalling pathways can also occur at the phenotypic level, the final stress response outcome, for example, a stress response to drought and cold which closes stomata can also inhibit natural modes of pathogen invasion, or the production of stress-associated secondary metabolites (e.g., phenolic-based phytoalexins and phytoanticipins) may be inhibitory to pathogens (Agurla et al., 2018; Peng at al., 2022; Kumar et al., 2021). These are examples of how stress response interactions could be harnessed to benefit abiotic and biotic (combinatorial) stress resilience in the field.

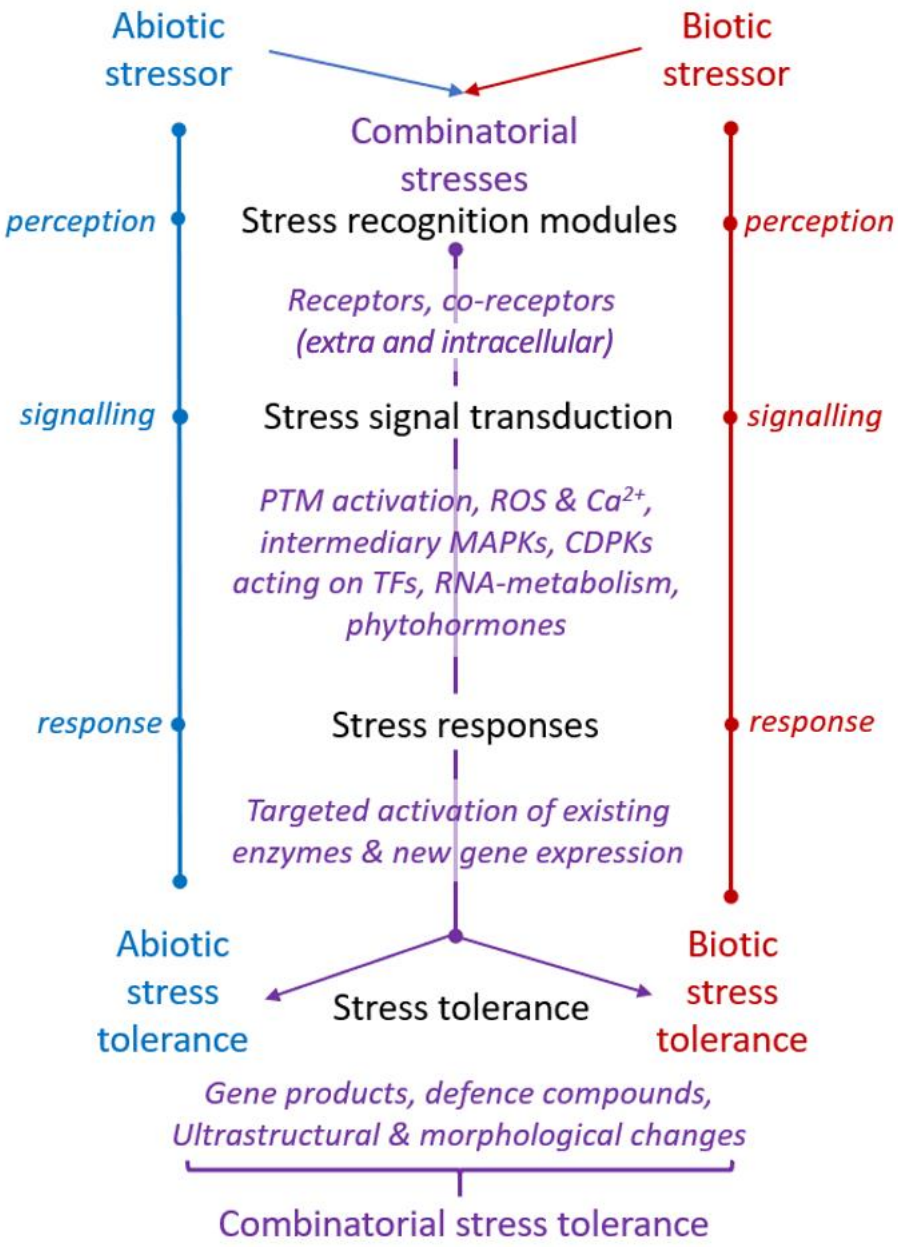


Fig. 13. A conceptual framework for combinatorial stress signalling and stress response outcomes. Abiotic and biotic stress signalling pathways (shown as blue and red-coloured axes) converge at nodes (small circles) to create a third central axis (purple) for managing combinatorial stress responses. Interactions can occur at many stages along the signal perception-signalling-response pathways and through components of varying chemical nature: from ions such as calcium, to small molecules such as hormones or ROS (hydrogen peroxide, superoxide, nitric oxide), to proteins such kinase enzymes (MAPK or CDPK phosphorylation propagators) or transcription factors (TFs) (ERFs or WRKYs) and final gene products, defence metabolites (antioxidants and antimicrobial compounds), structural or morphological changes such as cell wall strengthening or stomata closure (Zhu et al., 2002; Tuteja and Sopory 2008; Mittler et al., 2011).

Plant immunity and biotic stress signalling however have typically been shown to be suppressed by abiotic stresses such as salt stress and drought or by the exogenous application of the phytohormone abscisic acid (ABA) in glycophytic species such as Arabidopsis, tobacco, tomato and soybean (Mohr and Cahill, 2003; Rezzonico et al., 1998; McDonald and Cahill, 1999; Audenaert et al., 2002).

1.6.2. The role of ABA in abiotic – biotic stress interactions

ABA is a key regulator of responses to abiotic stresses in plants. ABA genes (for biosynthesis, transport and perception) are expanded in the quinoa genome and play an important role in the regulation of the plant's salt and drought tolerance (Jacobsen et al., 2009; Zou et al., 2017; Morales et al., 2017). Recent discoveries regarding ABA perception and signalling in quinoa were reviewed by Pizzio (2022) where ABA signalling components such as ABA-receptors PYLs were found to be overrepresented in quinoa roots and EBCs, along with ABA synthesis (NCEDs and SDRs) and transport genes (Xiao-Lin et al., 2022; Zou et al., 2017). Studies have produced transgenic crops with improved abiotic stress tolerance by overexpressing equivalent genes for ABA signalling: ABA synthesis (NCED1) or receptor genes (PYR/PYL), which enhanced drought and salt or drought and cold tolerance respectively (Seki et al., 2002; Rabbani et al., 2003; Gonzalez-Guzman et al., 2014; Tian et al., 2015; Aswath et al., 2005; Zhang et al., 2009). This illustrates the potential for achieving combinatorial abiotic stress tolerance via ABA transgenes which converge to regulate the signalling pathways of various abiotic stresses. This interaction can occur at the level of MAPK signalling cascades (Fig.12 & Fig.13), which are triggered by various environmental stresses of abiotic and biotic nature (Manaa et al., 2023) where ABA has been shown to affect the transcriptional regulation, protein accumulation, and stability of various MAPK signalling components, and also at the point of hormone regulation, which has been the focus of more studies.

Examples of abiotic – biotic stress signalling interactions at the level of plant hormones include the antagonistic interaction between ABA and ethylene (ET) when regulating stomata aperture: ET delays stomata closure by inhibiting the ABA signalling pathway (Tanaka et al., 2005), while ABA can also inhibit ET biosynthesis by repressing the rate limiting enzyme (ACS5) through the inhibitory actions of ABA-induced ET response factor 11 ERF11 and LONG

HYPOCOTYL5 (HY5) transcription factors (Li et al., 2011). ABA-induced stomatal closure can limit early pathogen (e.g., *P. syringae*) colonization (pre-invasive PTI) which the pathogen may block through the phytotoxin JA-Ile mimic coronatine (Zhao et al., 2003), yet once in the apoplast, post-invasion strategies may involve several ABA-promoting T3Es including HopAM1, HopAB2 and AvrE. These post-invasion T3Es manipulate host ABA signalling either through increasing ABA-sensitivity or through inducing ABA synthesis to create a more favourable osmotic pressure/aqueous environment in the apoplast (Goel at al., 2007; Mur et al., 2007; Hu et al., 2022). This shows a precise spatio-temporal importance of ABA in the host-pathogen interaction with contrasting roles pre- and post-invasion.

ABA has also been shown to have antagonistic actions on jasmonic acid (JA) and salicylic acid (SA), two other important hormones for plant immunity which mediate defence responses to a wide array of pathogens (Tamaoki et al., 2013; Gupta et al., 2020). Exogenous ABA treatment could suppress both basal and JA responsive defence gene induction which has been validated through ABA-synthesis mutants resulting in the upregulation of JA genes (Anderson et al., 2004). ABA has been shown to suppress the expression of the SA biosynthesis gene SA INDUCTION DEFICIENT 2 (SID2) (Berens et al., 2019). ABA also suppresses systemic acquired resistance by inhibiting upstream and downstream components of SA signalling in a manner that is independent of the JA/ET crosstalk (Yasuda et al., 2008) whereas Berens et al. (2019) have also shown a developmental age dependency of ABA–SA crosstalk in Arabidopsis, where different ages rosette leaves performed differently under exogenous ABA and SA application.

With respect to quinoa, initial elicitation of a specific stress signalling network such as quinoa's robust halophytic acclimation pathway could elevate general stress responsiveness of the plant through either pre-existing abiotic and/or biotic pathways, or alternatively, through unique combinatorial stress response pathways. This project hypothesises that quinoa's pre-existing halophytic adaptations will have molecular and morphological trade-offs or synergistic interactions with immunity, observable in both the basal and salt-inducible phenotype. For example, salt acclimation could 'prime' plant immune defences in quinoa via enhancing the availability (and thus functional readiness) of core stress signalling components

such as those shown in Fig.13 (MAPK, ROS, calcium signalling, antioxidant or antimicrobial secondary metabolites). This subsequently may have impacts on host-pathogen interactions. Equally, surveying quinoa's immune responses in the absence of salt could also reveal constitutive differences to glycophytic species such as Arabidopsis.

1.7. Rationale, Aims and Chapter Objectives

Chenopodium quinoa as a highly nutritious and naturally stress resilient crop with rich genetic diversity is a promising candidate crop for supporting food security in diverse climates and marginal lands. With high quality genomes and reference transcriptomes available for several genotypes and/or experimental designs along with the emergence of technologically advanced quinoa-specific breeding programmes, now is the time to contribute molecular level understandings of quinoa's stress response mechanisms. Given the prior focus of research groups on quinoa's abiotic stress tolerance, particularly on quinoa's exceptional salt tolerance traits, there is a need to turn our attention towards the understudied molecular basis of quinoa's biotic stress tolerance i.e., quinoa's immune system and its biotic stress/pathogen susceptibilities. This is important given quinoa's notable yield-limiting biotic stress vulnerability when grown outside of its native areas and a priority breeding trait for supporting continued expansion to new lands under unpredictable climate change.

We hypothesised that quinoa may show distinctive differences in its immune responses from glycophytic plants as a consequence of its halophytic adaptations. To investigate this, we aimed to develop a model system based on quinoa's interaction with the agronomically important pathogen *Pseudomonas syringae.* The choice of quinoa cultivar to use for this project was the commercial European-bred variety Atlas, one of the main varieties used by The British Quinoa Company on British fields between 2012 – 2020 (Stephen Jones, personal comms 2023).

Therefore, this thesis aimed to address the following aims:

Aim 1: Undertake a detailed characterisation of quinoa's immune system, focusing on PTI.

Aim 2: Interrogate how quinoa's halophytic adaptations influence its PTI, disease tolerance and host-microbe interactions with *P. syringae.*

The following four experimental chapters collectively addressed Aims 1 and 2:

Chapter 2: Tested and optimised several PTI assays in quinoa in order to characterise PTI responses at a molecular and biochemical level, which were then compared and contrasted to the glycophytic model species *Arabidopsis thaliana.* (C.2)

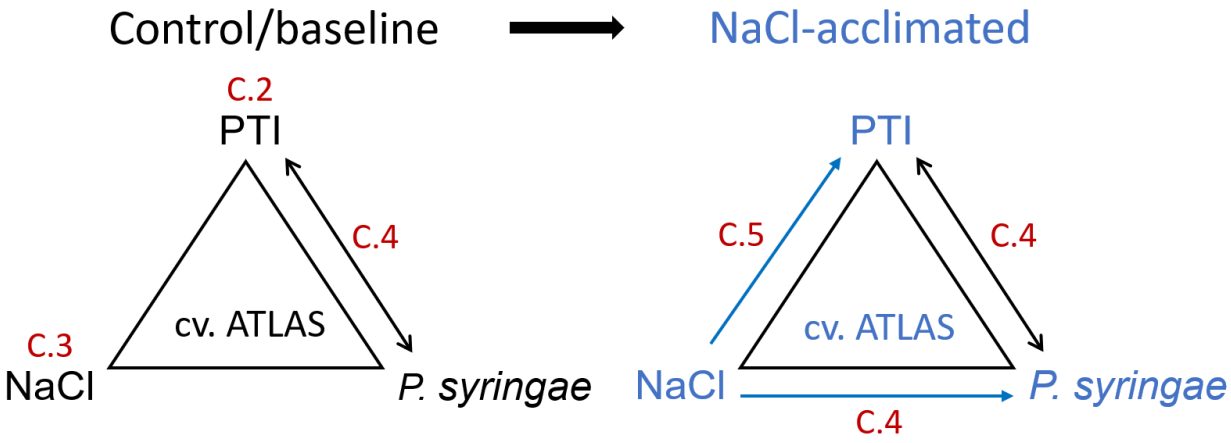
Chapter 3: Evaluated quinoa cv. Atlas's salt tolerance in order to establish a robust saline growth system for creating a significant salt acclimated foliar phenotype (which was needed for testing combinatorial stress responses when challenged with a secondary biotic stress in subsequent Chapters 4 and 5). (C.3)

Chapter 4: Established an informative and amenable pathosystem with the model pathogen *P. syringae* by screening a diverse panel of strains and evaluating how salt acclimation affected the plant's disease resistance and bacterial pathogenesis. (C.4)

Chapter 5: Brought together systems and insights from the previous chapters to specifically address how salt acclimation influenced quinoa's PTI mechanisms, and in doing so, evaluated the potential of quinoa as a model system for investigating abiotic x biotic combinatorial stress responses of plants. (C.5)

To conceptualise and guide the experimental approach, the high-level disease triangle framework introduced in Fig.1 is re-drawn with the specific components (combinatorial stress tools) used or evaluated in this thesis: NaCl is the abiotic stress, *P. syringae* is the biotic stress, and PTI is the specific aspect of quinoa's immune system focused on. Two disease triangle scenarios are shown: the baseline (left) and salt-induced/salt-acclimated (right) foliar phenotypes of quinoa. Red text (C.2-C.5) indicates which aspects are addressed by which

experimental chapter and the blue text highlights the influence of salt on the disease triangle: the direct effect of salt on quinoa's PTI (and thus on the subsequent disease interaction with *P. syringae*) and the direct effect of salt on the pathogen.



Lastly, a third non-experimental aim was to use quinoa's Andean heritage and position as a novel superfood crop, along with my own dual British-Bolivian nationality, to forge collaborations between the UK and Bolivia: connecting the University of Oxford with Bolivian quinoa scientists and the National Germplasm Bank INIAF and to develop relationships with local quinoa farmers in Bolivia, as well as with the British Quinoa Company. This aim aspired to create longer-term bilateral possibilities for exploring quinoa's wider scientific, agronomic and commercial potential as a novel food source.

Chapter 2: Exploring PAMP-Triggered Immunity in the halophytic crop *Chenopodium quinoa*; similarities and differences to the model species *Arabidopsis thaliana*

2.1. Introduction

Plants have evolved diverse immune strategies to combat microbial pathogen attack and colonisation. At the same time, selective pressure from the outcome of molecular plant-microbe interactions also drives pathogen evolution as an interdependent process known as a 'host-pathogen arms race'. Quinoa however, originated in the marginal lands of the Andean high plains where harsh environmental conditions limit the incidence of microbial-based biotic stresses as well as potentially influencing certain aspects of the plant immune system through interacting with abiotic stress adaptations. Only when temperatures and humidity become more temperate do opportunities arise, as has been found for quinoa adapted to lower, warmer regions of the country where the major (oomycete) pathogen *Peronospora variabilis* (Downy Mildew; DM) can take hold and cause severe crop losses. The quinoa-DM 'host-pathogen arms race' has led to the natural selection for resistance traits in certain ecotypes where plant pathology studies using panels of ecotypes with a range of genetic susceptibility will help elucidate the molecular basis for this specific tolerance (Colque-Little et al., 2021). In this opening experimental chapter, we first query what generic conserved immunity has evolved in quinoa and whether fundamental differences may exist to the canonical mechanisms described in other plant species. For example, the highly saline soils present in quinoa's regions of origin encouraged the evolution of halophytic adaptations, many of which are dependent on ABA signalling which could complement or antagonise ('crosstalk') with typical immune responses (Verma et al., 2016; Pizzio, 2022).

2.1.1. A PAMP-Triggered Immunity model for perception and signal transduction

Our current knowledge of the origin and evolution of key components of the plant immune system has mainly come from the model species *Arabidopsis thaliana, Nicotiana benthamiana* and an increasing number of economically important glycophytic crop species

such as rice, tomato and soybean (Jones and Dangl 2006; Goodin et al., 2008; Liu and Wang 2016; Takken and Rep 2010; Rao et al., 2023). As mentioned in Chapter 1, the plant immune system revolves around two interconnected and mutually potentiated systems, PAMP-Triggered Immunity (PTI) and Effector Triggered Immunity (ETI), which perceive and respond to pathogen infections in different spatiotemporal ways (Ngou et al., 2021).

Microbes, pathogens and insects carry conserved molecular patterns called MAMPs or PAMPs which are comparably ubiquitous and slow at evolving (as they are essential cellular or physiological components) compared to the pathogen specific effectors which specifically trigger ETI. This means that receptors for detecting P/MAMPs, pattern recognition receptors (PRRs), have been widely conserved among diverse plant families having evolved in very early lineages under purifying selection (Han 2018; Fischer et al., 2016). We hypothesised therefore that common PAMPs are likely to be perceived through PRRs as part of quinoa's PTI.

Considering also how PTI is typically the first immune system to be engaged following exposure to a biotic stress, the focus of this chapter will be the characterisation of quinoa's PTI. PRRs recognize P/MAMPs and heterodimerize, triggering downstream signalling initially orchestrated by phosphorylation and calcium-dependent signalling cascades which culminate in a range of conserved responses (Han 2018), details of which are summarised in Fig.1.

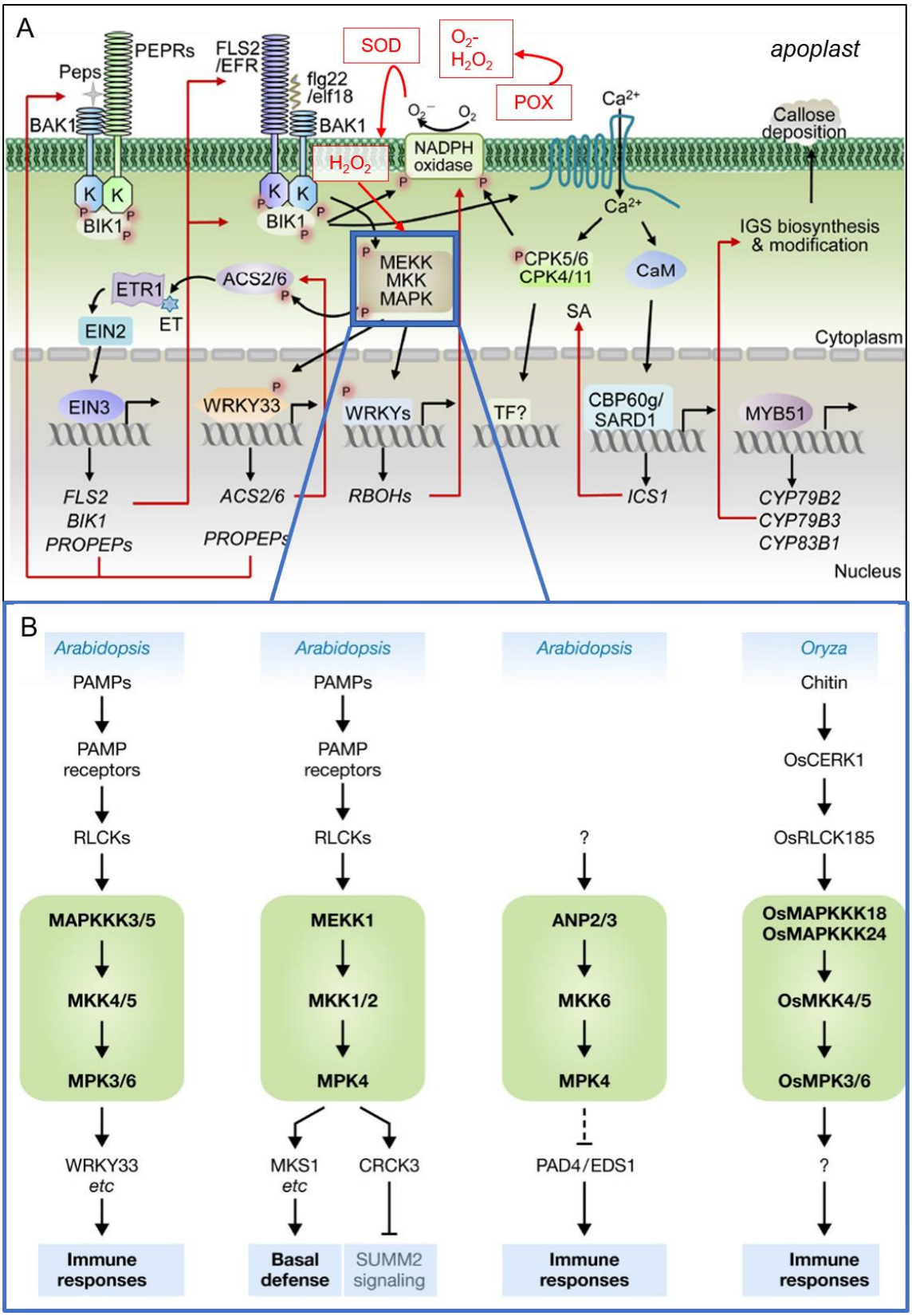


Fig.1. A depiction of core PTI components and signalling events elucidated from rice and model species. Figures compiled and adapted from Li et al. (2016) and Sun & Zhang (2022). **A)** Conserved plasma membrane (PM)-associated extracellular PRRs such as the well-characterised FLS2 or EFR

receptor detect highly conserved PAMPs such as flg22 or elf18 in the host apoplast to initiate PTI signalling. Co-receptors such as BAK1 instantaneously heterodimerize with the PRR which triggers the activation (phosphorylation) of a receptor like cytoplasmic kinase BIK1, which in turn directly phosphorylates the PM-located NADPH oxidase (RBOHD; RESPIRATORY BURST OXIDASE HOMOLOG D) as an early response. RBOHD produces a burst of pathotoxic apoplastic ROS such as O_2•, which can be rapidly converted to membrane permeable species H_2O_2 by apoplastic superoxide dismutases (SOD) which further amplifies downstream signalling. Cytoplasmic mitogen-activated protein kinase (MAPK) enzymes (MAPK kinase kinases, MAPK kinases and MAPKs) rapidly orchestrate an organised three-tiered signalling cascade to execute further activation of key immune actors, for example, phosphorylated immune-specific MAPK3, MAPK6 or MAPK4 enzymes directly activate immune transcription factors (TF) such as WRKY33. These MAPK enzymes are activated through the dual phosphorylation of threonine and tyrosine residues in the T-X-Y activation loop, assayable using immunoprecipitation on a western blot detected by antibodies such as the anti-ERK1p42/p44 (Pitzschke, 2018). (B) Apoplastic ROS is also generated by activated peroxidase enzymes (POX), whose expression is upregulated through downstream gene induction. Callose synthesis and deposition at the cell wall is another key later induced response which strengthens the first physical barrier to pathogen attack (along with ABA-mediated stomatal closure, not shown). The production of the phytohormone ethylene (ET) and antimicrobial components such as phytoalexins are also canonical inducible responses (not shown).

A diverse range of PAMPs have been characterised and purified for use as controlled immune elicitors via their specific cell membrane localised PRRs. Flg22 and elf18 are protein-derived PAMPs of bacterial origin, derived from flagella and the cytoplasmic protein EF-Tu (Elongation factor thermal unstable T) respectively, and are sensed by leucine-rich repeat receptor kinase (LRR-RK)-type PRRs FLS2 and EFR. Chitin and chitosan are polysaccharide-derived MAMPs found in the cell walls of fungi and oomycetes and in the cytoskeletons of insects which are detected by LysM-RKs LYK5 and VvLYK1-1 /VvLYK1-2. Other MAMPs include lipid-derived molecules such as lipopeptides or ergosterol (Schellenberger et al., 2019). Although not the focus of this study, damage-associated molecular patterns (DAMPs), can also trigger PTI as pathogen invasion disrupts plant cell walls and plasma membranes causing the release of cell wall or extracellular protein fragments, peptides, nucleotides, and amino acids, detected by LRR-RKs such as PEPR1/PEPR2 for the DAMP plant elicitor protein Pep1 or putative Wall-Associated Kinase (WAK) oligogalacturonides (Ogs) (Hou et al., 2019; Brutus et al., 2010).

Downstream of the FLS2/EFR receptors different MAPK cascades (Fig.1B) show partial functional redundancy by activating overlapping final gene targets: MPK3/MPK6 phosphorylate WRKY33, ERF6/ERF104 and BES1, while MPK4 appears to interact with a wider range of targets including heat shock proteins (HSPs). Mutant and overexpression genetic studies with MPK4 have revealed diverse roles in salt and osmotic stress adaptation, root growth, alterations of the JA/SA hormone balance and more recently MPK4 activation was shown to mediate the regulation of PAMP-induced alternative splicing (Bazin et al., 2020). Crucially, of particular interest, MPK4 appears to function in a species-specific manner, where phenotypic discrepancies have been found through gene silencing whereby ABA-mediated stomatal closure was impacted in one *Nicotiana* species but not in another (Hettenhausen et al., 2012).

2.1.2. Use of transcriptomics and proteomics for elucidating PTI response genes

Over the last 20 years a large number of microarray and RNA-sequencing studies have been performed to elucidate transcriptional level responses in plants (predominantly the model species Arabidopsis) to biotic stress. Diverse PAMPs, pathosystems and even damage stresses have been used to create differentially expressed gene lists which through functional enrichment analyses have helped reveal leads on core immunity 'hub genes' and processes for testing *in planta* (Gust et al., 2007; Wan et al., 2008; Zipfel et al., 2006; Li et al., 2016; Bjornson et al., 2021). Subsets of general non-self-response (GNSR) genes (Maier et al., 2021) and generic or biotic-stress specific co-expression networks (Amrine et al., 2015) have also been revealed which serve as reference points for uncovering novel responses in new species. Bjornson et al. (2021) used seven different PAMPs of different origin and biochemical nature to reveal how PTI-associated transcriptional responses are very similar at early time-points (<3h), suggesting converging signalling pathways, where specificity may lie at the level of individual gene induction dynamics and the amplitude of expression. GLUTAMATE RECEPTOR-LIKE (GLR) calcium-permeable channels and calmodulin proteins, cell-wall-associated proteins such as extensins and cell-wall-bound peroxidases, phytohormone synthesis genes, along with specific members of transcription factors WRKY, MYB, ERF and NAC are examples of key

upregulated genes, whilst photosynthesis-related processes are widely downregulated (Bjornson et al., 2021; Yuan et al., 2019; Maier et al., 2021; Li et al., 2016; Amrine et al., 2015).

Post-transcriptional regulation is a subsequent major orchestrator of rapid responses to biotic stress. A second high-throughput analysis at the level of the proteome which has recently been robustly established in plants is RNA-binding protein capture (ptRIC) (Bach-Pages et al., 2020), which helps to integrate responses between the biochemical and molecular gene levels. RNA-binding proteins (RBPs), which function through their differential association with RNA have recently been shown to contribute to plant immunity: 186 high confidence (and a total of 330 putative) flg22-responsive RBPs were found in Arabidopsis over early (2h) and/or late (12h) time-points (Bach-Pages et al., 2020). Differential RBP association with RNA can occur via changes in RNA-binding activity, RBP protein abundance or localisation, or by changes in the target RNAs themselves (Sysoev et al., 2016; Garcia-Moreno et al., 2019). After 2h of flg22 treatment, an enrichment of post-translational modification (PTM) sites was found among the flg22-responsive RBPs yet interestingly protein abundance was not significantly different to mock conditions. This suggests that early RBPs act as a layer of immunity receptive to PTMs from upstream signalling pathways. Complementary RNA-seq analyses were then performed and compared to the proteomic results to conclude that RBPome remodelling over longer timeframes also occurs via changes in RBP abundance. Different flg22-responsive RBPs include those involved in RNA metabolism (RNA helicases), heatshock proteins and glutathione S-transferases (GSTs) and it was found that mutant lines lacking individual flg22-responsive RBPs became differentially susceptible to *P. syringae* (Bach-Pages et al., 2020).

2.1.3. Translating our understanding of PTI from model species to crops

The core concepts of plant immunity and PTI mechanisms have been defined using non-salt tolerant plants such as the model plant species Arabidopsis and *Nicotiana benthamiana,* and more recently using the genetically modifiable crop species tomato and rice (Jones and Dangl, 2006; Goodin 2008; De Vleesschauwer et al., 2014). Important species-specific differences are being elucidated, for example, different roles of key defence hormones SA, JA and GA were found between rice and Arabidopsis in response to pathogens of different lifestyles and infection strategies, which could explain the plants' varying range of resistance (De

Vleesschauwer et al., 2014; Yang et al., 2013). Another study queried how PTI responses vary between *A. thaliana* accessions and between closely related *Brassicaceae* species, where species-specific patterns of gene cluster induction were found to be independent of phylogenic relatedness (Winkelmüller et al., 2021). This suggests that core PTI genes are under evolutionary selection and impacted by environmental conditions and so it will be fascinating to uncover how the unique and isolated conditions of the Andean Altiplano may have shaped the PTI of the halophytic crop quinoa.

2.1.4. Aims and rationale

To elucidate whether PTI responses are conserved in the novel halophyte quinoa, a range of synthetic PTI elicitors were used as probes for assaying the presence or absence of, or differences in key molecular signatures along the biotic stress perception to response axis. Given how MAPK signalling cascades and ROS are two of several key abiotic-stress transducers and quinoa is an exceptionally abiotic-stress tolerant species, we were intrigued to see if and how they are used for biotic stress perception. Does quinoa possess immune-specific MAPK and ROS-generating enzymes? Or how does the plant distinguish between individual stresses to induce specific responses? A combination of biochemical, transcriptional and bioinformatic experiments were performed to answer these questions.

Objectives:

- Test the perceptibility of different PAMPs in quinoa
- Optimise routine PTI assays in quinoa (appropriate PAMP concentrations, elicitation mode and timeframes)
- Qualitatively and quantitatively identify PTI differences between quinoa and Arabidopsis
- Generate transcriptional and proteome-level datasets for PTI responses in quinoa

2.2. Results

2.2.1. Establishing a series of biochemical PTI assays in quinoa using artificial PAMPs

To initiate the characterisation of quinoa's PTI, several distinct and well-characterised PTI elicitors (PAMPs) representing a variety of organisms were tested at standard concentrations for their perceptibility and elicitation effect in quinoa. Four established biochemical PTI assays were trialled and optimised for quinoa: MAPK activation, a reactive oxygen species (ROS) burst, upregulation of peroxidase activity (POX) and callose deposition using Arabidopsis as a positive control species. We hypothesised that quinoa may possess different immune-specific MAPK signatures (components or intensities of induction) to the less abiotic stress resilient species Arabidopsis and that ROS signalling may also be under tighter control in quinoa (abiotic stresses typically cause significant oxidative stress, invoking redox homeostasis mechanisms). Once a robust PTI-inducing set-up is established, transcriptional and proteomic experiments will be designed to add further integral layers to our understanding of conserved and differential immune responses in the halophytic crop species quinoa.

2.2.1.1. MAPK activation in response to PAMPs is conserved in quinoa but orchestrated by different MAPK enzymes to Arabidopsis

MAPK activation cascades are widely conserved abiotic or biotic signalling mechanisms in eukaryotes which play a pivotal role in the stress response of plants (Manaa et al., 2023). We therefore tested whether MAPK phosphorylation cascades also function in early biotic stress signalling pathways in quinoa where we compared the activation patterns to Arabidopsis as a positive control (Fig.2). Pilot comparative MAPK experiments which exposed quinoa, Arabidopsis and *N. benthamiana* to PAMPs via needless syringe infiltration (data not shown) revealed comparably strong phosphorylated MAPK signals under mock treatment for quinoa and *N. benthamiana* suggesting damage responses could be easily elicited. To eliminate the mechanical stress of leaf infiltration, a leaf-disc MAPK assay was developed (Methods) and a positive damage control was included for quinoa to help resolve clearer signals for immune elicitor MAPK responses in quinoa. An NaCl stress was also included for both species as a

putative abiotic-stress positive control to see if MAPK activation differed and thus whether immune-specific patterns could be visualised via western blotting.

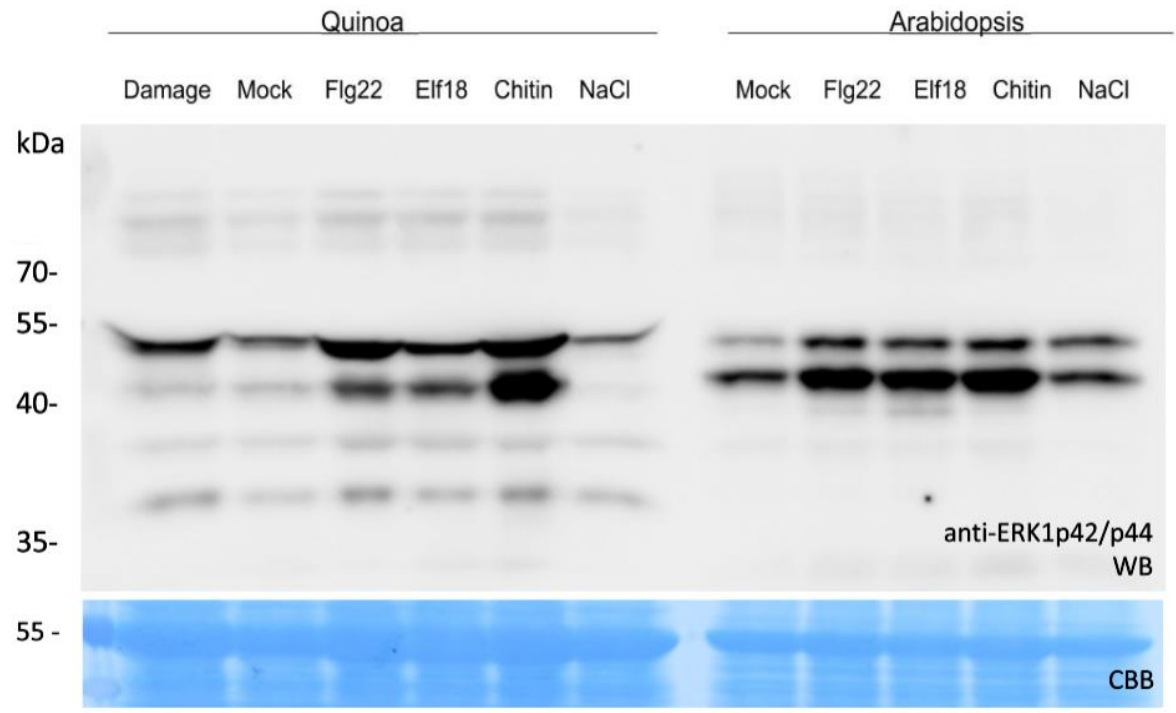


Fig.2. Detection of phosphorylated MAPK enzymes in quinoa and Arabidopsis in response to different PAMPs. Pre-equilibrated leaf discs were distributed across the wells of a 24 well plate containing 500 µL of elicitor solutions: 1 µM for flg22 and elf18 and 50 µg/mL of chitin, mock (Milli-Q water) or 500 mM NaCl and incubated for 30 minutes under continuous light. A positive damage control was achieved by applying exaggerated pressure to the edge of the leaf discs using the same tweezers and technique used for handling the leaf discs, making sure not to break the tissue. Each band represents 3 pooled samples per treatment, each sample represents 3 equivalent leaf discs harvested the day before from developmentally equivalent leaves of 4.5-week-old quinoa or Arabidopsis plants. Protein extracts were normalised by sample weight and the Rubisco enzyme used as the protein loading control. Phosphorylated MAPK enzymes were visualised via tagging with anti-ERK1p42/p44 and developed via chemiluminescence reaction captured on LAS4000 (GE Healthcare Life Sciences).

Species-specific MAPK activation signalling was observed. There was consistent but uneven protein loading between species due to quinoa leaf protein concentration being higher than Arabidopsis meaning qualitative comparisons should be drawn only. In future experiments sample normalisation was therefore done by protein concentration rather than tissue mass,

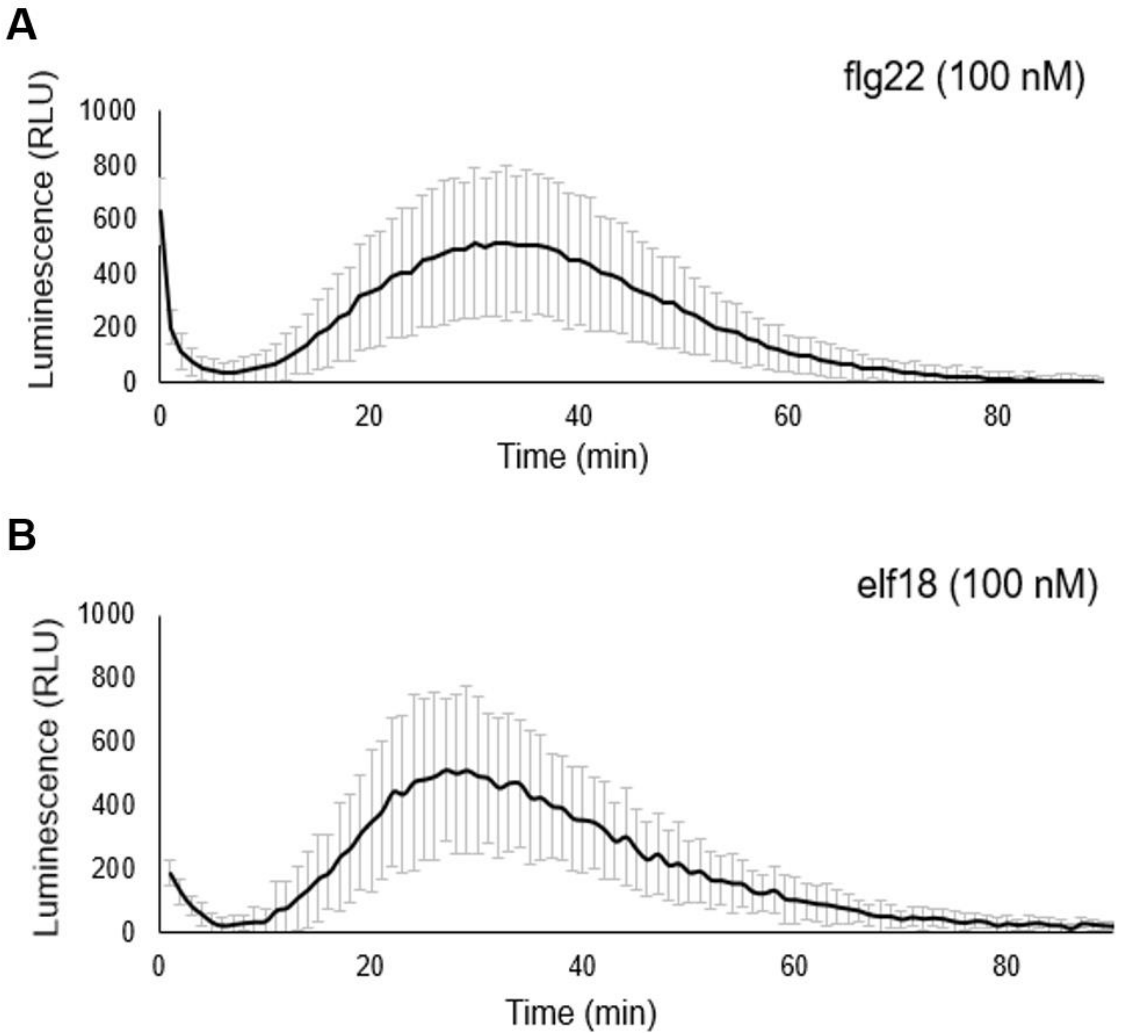
highlighting a key protocol adaptation to consider when working with non-model species. Surprisingly, all three PAMPs trigger phosphorylation of the conserved MAPK motif in quinoa, predominantly in a putative MPK4 orthologue at ~50kDa (Pitzschke 2018), which is much less significantly engaged in Arabidopsis (Fig.2) relative to canonical immune MAPKs atMAPK3 and atMAPK6 which are known to be 43kDa and 45kDa) respectively (TAIR website). The bands presumably representing MAPK3/6 in Arabidopsis are often seen as two distinct bands of equal activation which suggests they may be indistinguishable from each other but represented by the band around 43kDa. Exposure to the widely recognised fungal cell wall chitin PAMP elicited a distinct MAPK response in quinoa, strongly engaging smaller MAPK enzymes, putative MPK3/6 orthologs.

The positive damage control shows how the damage response in quinoa appears to engage one of the same putative 50 kDa MAPKs as those induced by the PAMPs, but to a lesser degree. Through observing how the mock and 500 mM NaCl also triggered a comparatively weak 50 kDa MAPK activation it suggests that either low levels of constitutive MAPK activation exist in quinoa, or that the experimental condition set-up (floating leaf disk) constitutes enough generic environmental stress (e.g., through osmotic stress) to trigger a 50 kDa MAPK activation. A higher NaCl stress occurred in Arabidopsis relative to the mock condition than in quinoa (despite protein concentration appearing half that in the quinoa blot). This result was expected given the comparably much lower salt tolerance (and osmotic stress buffering capacity) of Arabidopsis and further suggests the ~50 kDa MAPK in Arabidopsis is not specifically activated in response to PAMP detection. In conclusion, the presence of significantly higher activation of the ~50 kDa MAPKs under all three PAMP treatments along with the unique signature to chitin, damage and NaCl in quinoa suggests a capability for MAPK signalling to differentiate between biotic and abiotic stresses.

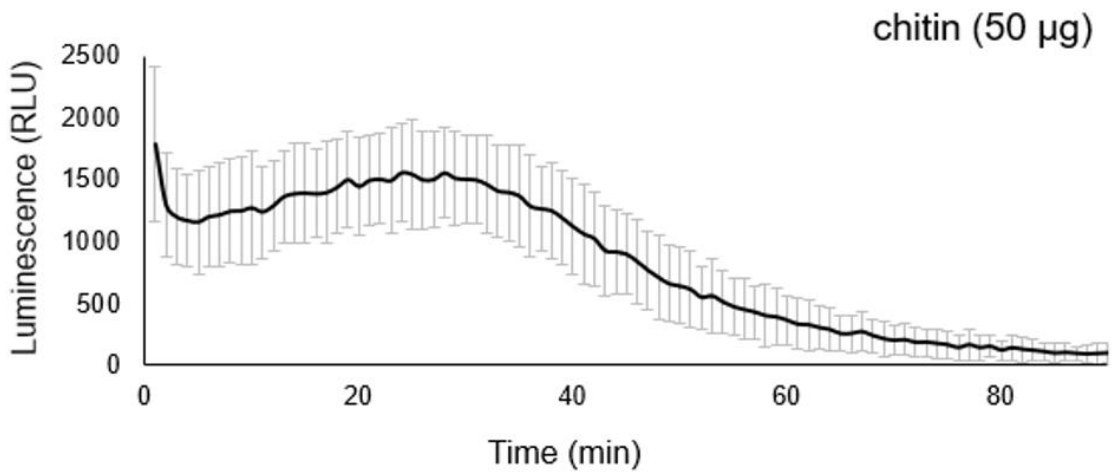
2.2.1.2. Quinoa produces ROS bursts in response to diverse PAMPs but at a delayed time and reduced intensity relative to Arabidopsis

An early downstream response from MAPK activation is the generation of extracellular ROS as toxic agents via plasma membrane anchored RBOH enzymes, and intercellular ROS at the chloroplast for additional signal propagation (Shapiguzov et al., 2012). Production of

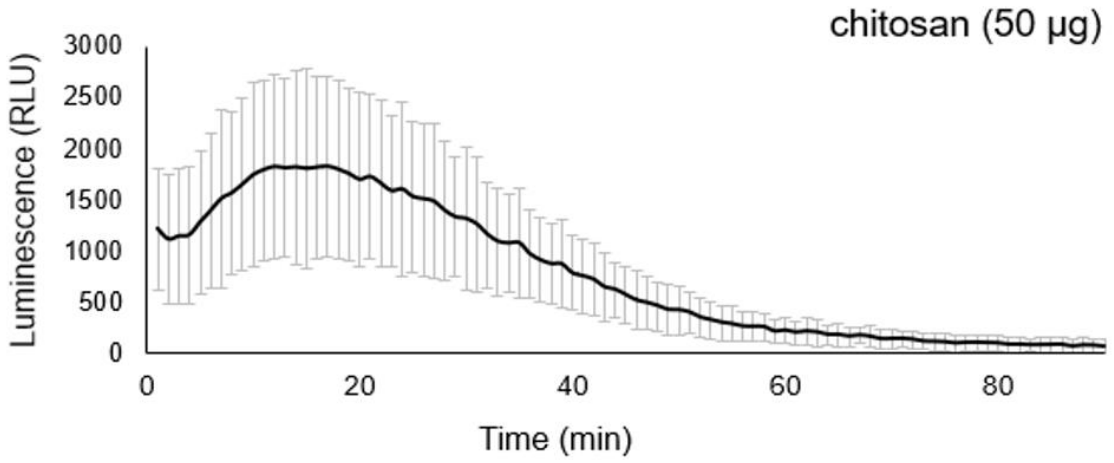
apoplastic ROS in quinoa was therefore tested using the routinely used *in vitro* 96-well leaf-disc assay (Melcher & Moerschbacher, 2016) to screen responses to different PAMPs. The flg22-Arabidopsis response was also tested as a positive control (Fig.3E).



C


chitin (50 µg)
Luminescence (RLU)
2500
2000
1500
1000
500
0
0
20
40
60
80
Time (min)

D


chitosan (50 µg)
Luminescence (RLU)
3000
2500
2000
1500
1000
500
0
0
20
40
60
80
Time (min)

E

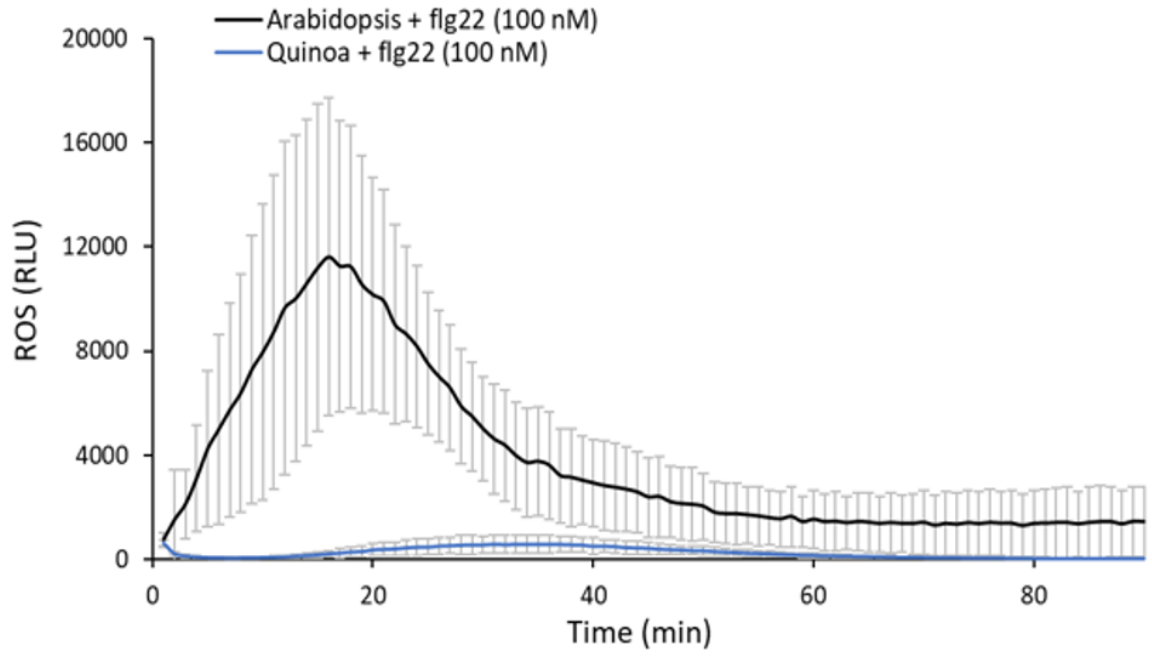
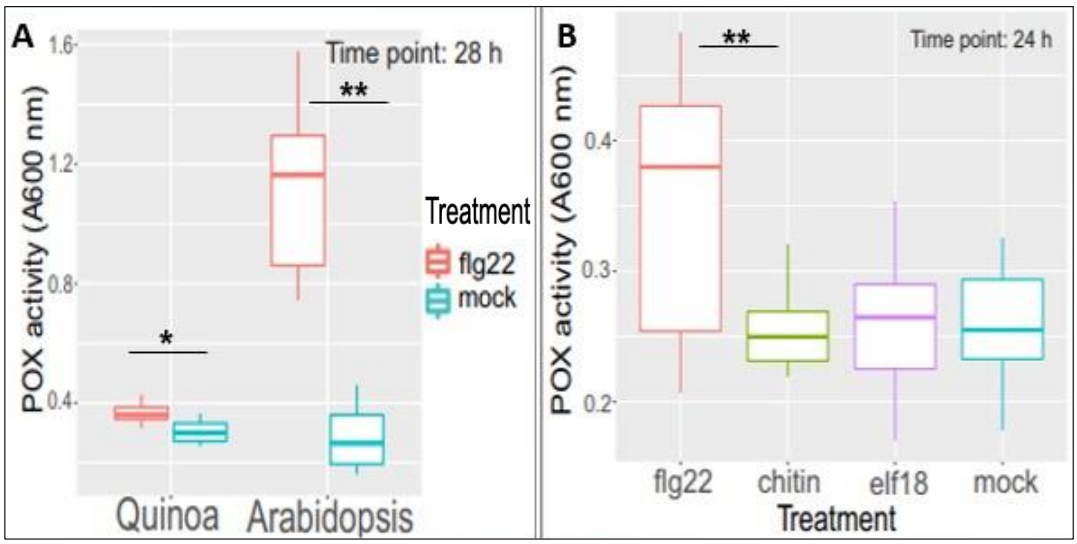

Arabidopsis + flg22 (100 nM)
Quinoa + flg22 (100 nM)
ROS (RLU)
20000
16000
12000
8000
4000
0
0
20
40
60
80
Time (min)

Fig.3. ROS production in quinoa leaf discs after treatment with different PAMPS and the ROS response to flg22 in Arabidopsis. The relative intensity of ROS production was measured using the L-012 -based assay (Melcher and Moerschbacher, 2016) after treatments with 150 µl of elicitor solutions flg22 (100 nM; A), elf18 (100 nM; B), chitin (50 µg/ml; C), chitosan (50 µg/ml; D) or mock (150 µl Milli-Q H_2O) (data not shown) and a comparison to Arabidopsis using 100 nM flg22 (E). Results are mean relative luminescence units (RLU) + SD from *n = 12* leaf discs pooled randomly from equivalent, fully expanded leaves from mature 4.5-week-old quinoa or Arabidopsis plants. Results are representative of two or more independently repeated experiments, and for D representative of 2 rows of 12 leaf discs each done on the same plate. Chemiluminescence readings were taken continuously over a 90-minute period using a TECAN plate reader.

Quinoa produces a ROS burst in response to the three previously tested PAMPs: flg22, elf18 and chitin and to the additional immune-inducer PAMP chitosan, a de-acetylated derivative of chitin (Hadrami et al., 2010) (Fig.3, panels A-D). No ROS burst was observed for mock conditions (data not shown). Quinoa's ROS response to flg22 (Fig.3A) and elf18 (Fig.3B) at equal concentrations of 100 nM was very similar: maximal ROS was produced at ~30 minutes. Chitin also induced maximal ROS at 30 minutes however the magnitude of the response was greater and the starting RLU was considerably elevated (1500 RLU). The ROS response curve for chitosan (Fig.3D) has similar magnitude and shape to chitin (Fig.3C) but the maximum was seen at half the time: 15 minutes. Further interrogation will be needed to confirm whether ROS production in response to different PAMPs in quinoa is binary, or if the differences in the ROS curve shape (ROS induction, amplitude and time till maximum) hold physiological relevance. Dose response curves would help elucidate this, where a range of PAMP concentrations from low to saturation in quinoa could be done (Melcher & Moerschbacher 2016; Mott et al., 2017). Lastly, it is important to note that the sensitive L-012 chromogenic substrate used in this assay is oxidised by various ROS (hydrogen peroxide, superoxide, or hydroxyl radical), making it difficult to conclude the enzymatic source of quinoa's apoplastic ROS response. Key enzymes of other species are the plasma membrane localized NADPH oxidases (RBOHs) and inducible cell wall peroxidases (Kámán-tóth et al., 2019). Given this test is for apoplastic ROS production only, we do not know whether ROS can also act as a biotic signalling component in quinoa as observed in other plant species, however we can study canonical downstream ROS-signalled responses to infer this such as callose deposition.

2.2.1.3. PAMP-induced peroxidase upregulation in quinoa is subtle and delayed relative to Arabidopsis

Peroxidase enzymes (POX) are released into the apoplast in response to stress (Minibayeva et al., 2015). Upon PAMP exposure, POX activation and induction of POX gene expression can be assayed as total apoplastic POX activity as an orthogonal read-out for an apoplastic ROS response (Daudi et al., 2012; Mott et al., 2017). To address the putative POX contribution to the apoplastic ROS burst observed in Fig.3, where we expected to find correlation with the data, we exploited a similar 96-well plate set-up devised by Mott et al., 2017.



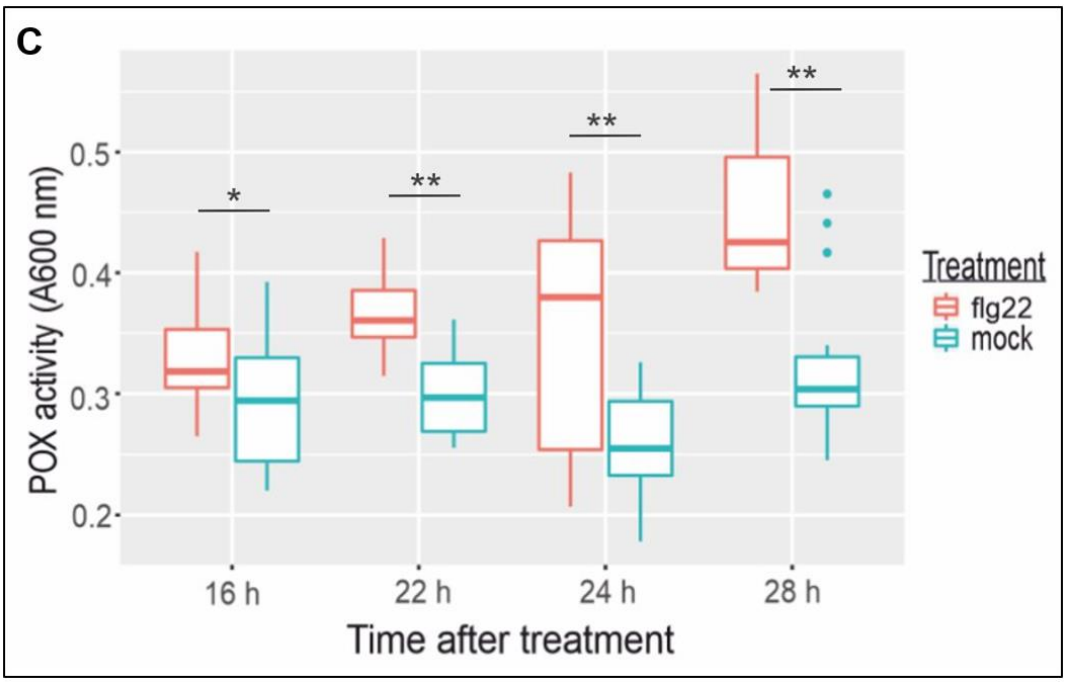


Fig.4: Differential POX activity of Arabidopsis and quinoa in response to flg22 elicitation at 28h. A) POX activity intensity differences of quinoa compared to Arabidopsis. **(B)** Differential POX activity in quinoa after treatment with the PAMPs panel at 24 hours **(C)** time-series of POX activity in quinoa in response to flg22 from 16 to 28 hours. Leaf discs from 4.5-week-old plants were incubated for the specified time-periods in incubator solutions (flg22: 100 nM, chitin: 50 µg/ml, elf18: 100 nM) or mock (Milli-Q water) then removed before quantifying POX activity via the chromogenic reaction between 5-aminosalycylic acid and hydrogen peroxide. The reaction was quenched at 2 minutes with 1 M NaOH for Arabidopsis to prevent oversaturation and at 4 minutes for quinoa. Total activity was quantified by measuring absorbance at 600 nm using a TECAN plate reader. Boxes show the first quartile, median and third quartile POX activity and whiskers extend to the highest and lowest POX activity measurements that are were identified as outliers (>1.5 times the interquartile range). Experiments are representative of 2+ experimental repeats. T-test was used for statistical significance where single and double asterisk indicate significance levels $P < 0.05$ and $P < 0.01$.

Upregulation of POX activity in response to flg22 was significantly lower in quinoa than in Arabidopsis ($P < 0.001$): flg22 at 100 nM concentration induced almost three times the enzymatic activity in Arabidopsis compared to quinoa (Fig.4A), whereas mock treatment (background POX activity) for both species were similar (statistical difference: $P = 0.22$). Although the magnitude of activity was much lower in quinoa, the induced POX response to flg22 was significant ($P < 0.05$). Four minutes reaction time was found to be the optimum timeframe for ensuring putative differentials between treatments were captured in quinoa (given the lower overall range of intensity of quinoa's inducible POX system). The assay was extended to evaluate the POX response to the PAMPs elf18 and chitin (Fig. 4B). Interestingly, no significant upregulation of POX activity was seen for these PAMPs compared to mock treatment, which were significantly different to flg22-induced POX ($P < 0.01$).

In a similar way to the flg22-induced ROS burst in quinoa, POX upregulation also appears to be a much less pronounced immune response than in Arabidopsis. However, the subtle increase in quinoa POX activity upon 100 nM flg22 treatment was found to become more significant over time. The experiment was repeated to generate a time series for quinoa POX activity in response to flg22 (Fig.4C). Whilst there was appreciable variation among biological replicates in the leaf-disc system, the mean POX activity showed a gradual increase and reached a maximum level again at 28 h.

Lastly, considering how 28 h is a much longer time to soak a leaf disc than the 16-20 h suggested in the original POX assay protocol, we hypothesised that the leaf disc edge would potentially be under greater osmotic (and/or submergence) stress or that the stability of the induced apoplastic POX enzyme activity was evaluated over time. Preliminary data from this experiment (data not shown) compared the POX activity observed at 23 h (when the leaf disc was removed) to a reading from an aliquot of the same leaf-bathing solution five hours later to simulate the effect of a longer incubation on existing POX activity. A significant 10% decrease (data not shown) was found suggesting the POX value measured at 28 h could be an underestimate of the true cumulative activity generated in response to flg22 over this time period. The use of bigger leaf discs could potentially reduce the proportion of tissue under osmotic stress when needing a prolonged incubation time.

2.2.1.4. Quinoa deposits callose papillae at the cell wall in response to flg22

A canonical inducible downstream PTI response from the ROS burst and upregulated POX activity of plants is the deposition of structural (b-1,3-glucan) polymer callose at the cell wall, typically at plasmodesmata or cell plates to reduce cell wall permeability (Wang et al., 2022).

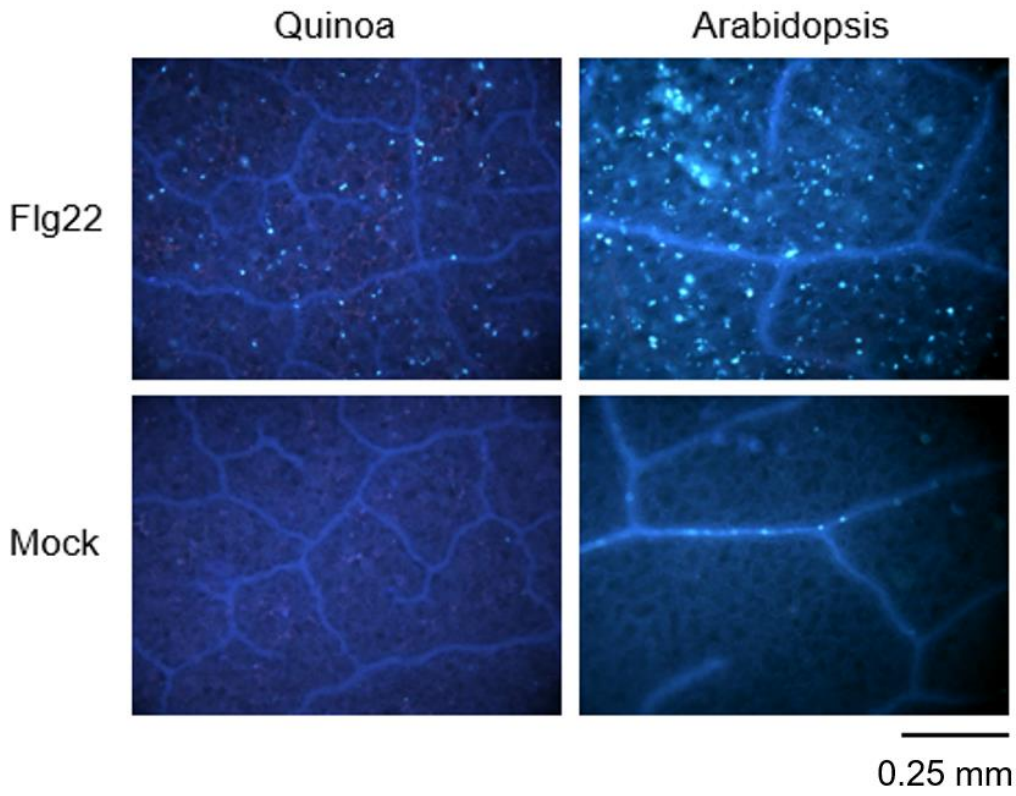


Fig.5. Quinoa, like Arabidopsis produces callose in response to flg22. 4.5-week-old quinoa and Arabidopsis leaves were infiltrated with 1 µM flg22 or Milli-Q (mock) and left for 24h. Whole quinoa and Arabidopsis leaves were harvested at the petiole, reduced to 4 cm^2 squares around the infiltrated area, fixed, cleared and stained with 0.01 % aniline blue stain overnight. Leaves were mounted in 40% glycerol and visualised immediately on the microscope Olympus B201 with a WU fluorescence cube (excitation filter BP330-385 nm, barrier BA420 nm) and photos captured by a QICAM Fast 1394 colour camera. Images are representative of five biological replicates and of two independent experiments. Images were taken 0.5 mm away from the infiltration zone to avoid any potential overlap with infiltration damage response and using a 20x lens.

Quinoa produces callose deposition by 24 hours in response to flg22, but qualitatively to a reduced intensity than Arabidopsis (Fig.5). Callose deposition was also induced around the point of syringe infiltration (data not shown) for both species as a damage response. Callose deposition is dependent on ROS signalling such as the H_2O_2 generated by NADPH oxidases or apoplastic peroxidases and so this reinforces the evidence for the conservation of key features of the PTI regulon in quinoa.

To validate these biochemical responses and to identify core PTI genes and putative key response pathways in quinoa an RNA-sequencing (RNA-seq) experiment was designed using the most robust PTI-inducing PAMP tested, flg22 (Fig.6). A dataset for the early PTI transcriptional response in quinoa will provide new molecular level resolution of a key part of quinoa's host immune defence system.

2.2.2. Profiling an early transcriptomic response of quinoa to flg22 treatment

Transcriptome profiling of quinoa leaves was performed using the widely used bacterial PAMP flg22 to identify early response candidate immunity genes in the quinoa genome via RNA-seq. Gene expression changes were captured at the 2h time-point in order to complement our molecular assays and to be comparable to studies done in other systems such as Arabidopsis. Two principal approaches were taken for identifying candidate PTI genes of interest in quinoa, firstly, a de-novo interrogation of quinoa's flg22 induced differentially expressed genes (DEGs), secondly, comparative analyses with a parallel Arabidopsis dataset to. query shared and distinct DEGs between the species. Both approaches started by obtaining global trends

in the form of genesets before focusing on individual DEGs of interest, the full data for which can be found in Supplementary Material.

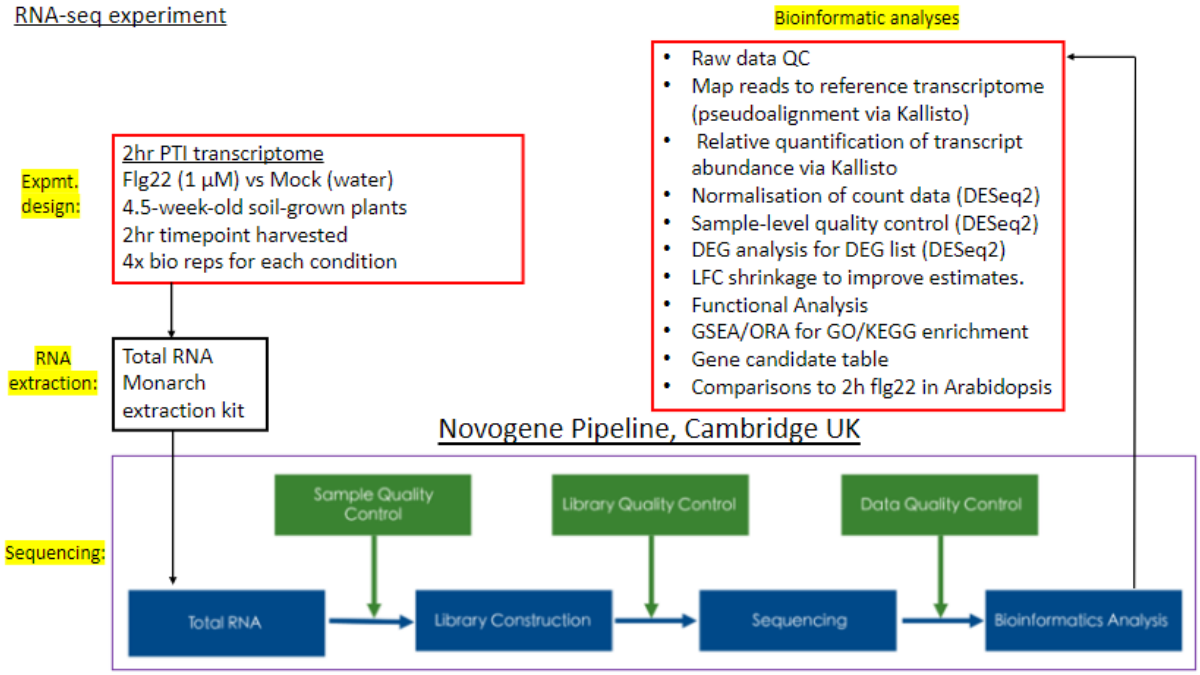
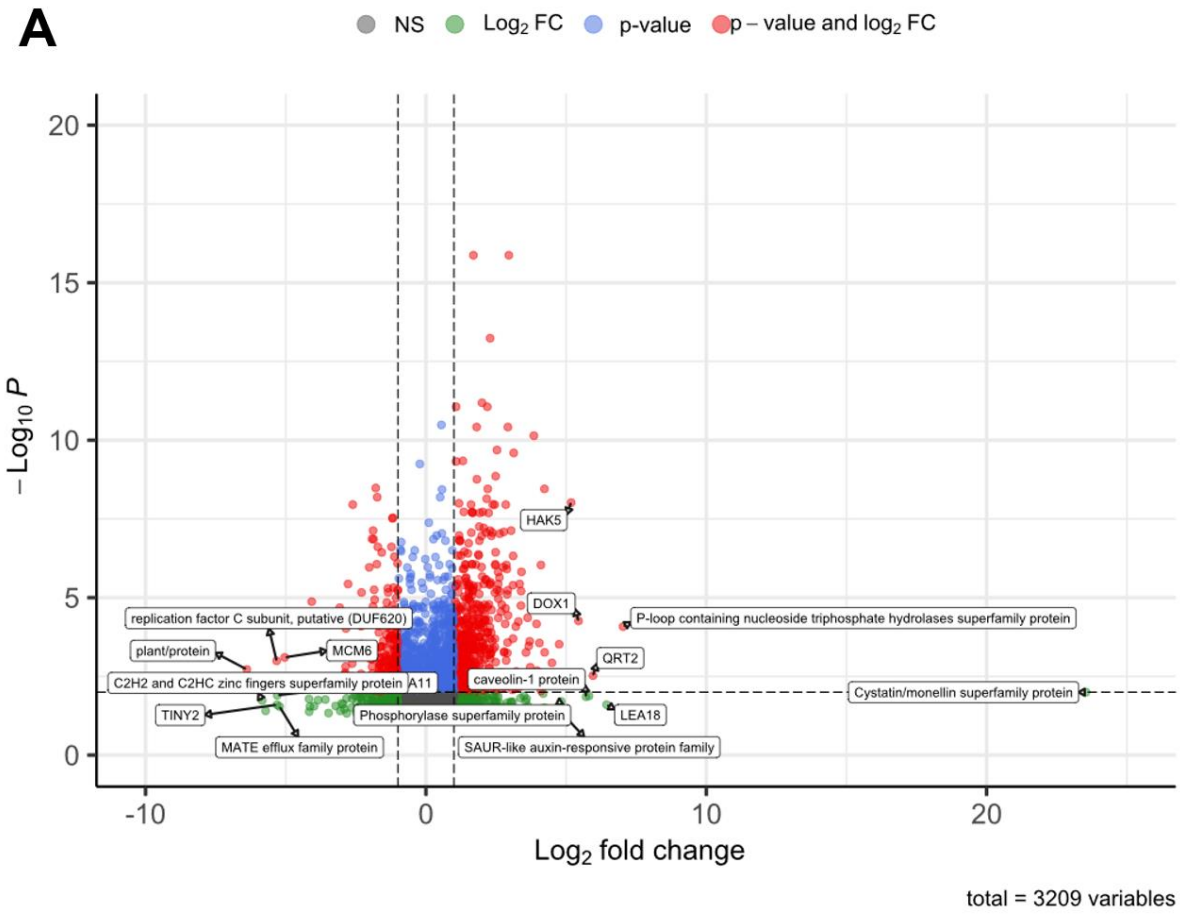


Fig.6 The RNA-seq pipeline for the flg22 experiment. The steps performed externally by Novogene are shown in the purple box.

The total number and distribution of DEGs in response to 2-hour treatment with 1 µM flg22 treatment (significant at $P < 0.05$) is visualized for quinoa and Arabidopsis by volcano plots (Fig.7). Immediately it is obvious by examining the shape of the plots, and particularly the range in magnitude of expression between the species, that the flg22-inducible transcriptomes of quinoa and Arabidopsis corroborate with the biochemical data whereby higher intensity responses were found for Arabidopsis. Several of the most highly expressed and suppressed statistically significant DEGs were annotated in case any were shared and indicative of canonical immune or stress-defence-related processes. To gain more biological significance within these plots, global functional analyses were next performed to investigate unifying biological themes among gene sets (rather than individual genes) and to assess affected pathways in response to flg22. At the individual gene level there is often very little overlap between datasets even in the same system, whereas similarities are confidently resolved at the gene set level (Subramanian, 2005). Furthermore, an increase of 20% expression in all genes of the same metabolic pathway or biological process may have a more

dramatic effect on the phenotype than a 20-fold increase in one single gene (Subramanian, 2005). In order to do this, we mapped the quinoa transcripts to the well-characterised high-quality Arabidopsis proteome and retrieved annotations to perform unbiased global functional enrichment analyses. This strategy enables us to draw clearer comparisons between independent quinoa transcriptome studies and crucially also to the PTI transcriptomes of other reference species. This approach is justified by how 80 % of all quinoa reference transcript queries were found to have a protein alignment covering at least 50%, where 32% of transcript queries had a 95% protein mapping coverage using Arabidopsis proteins via BLASTp (data not shown).



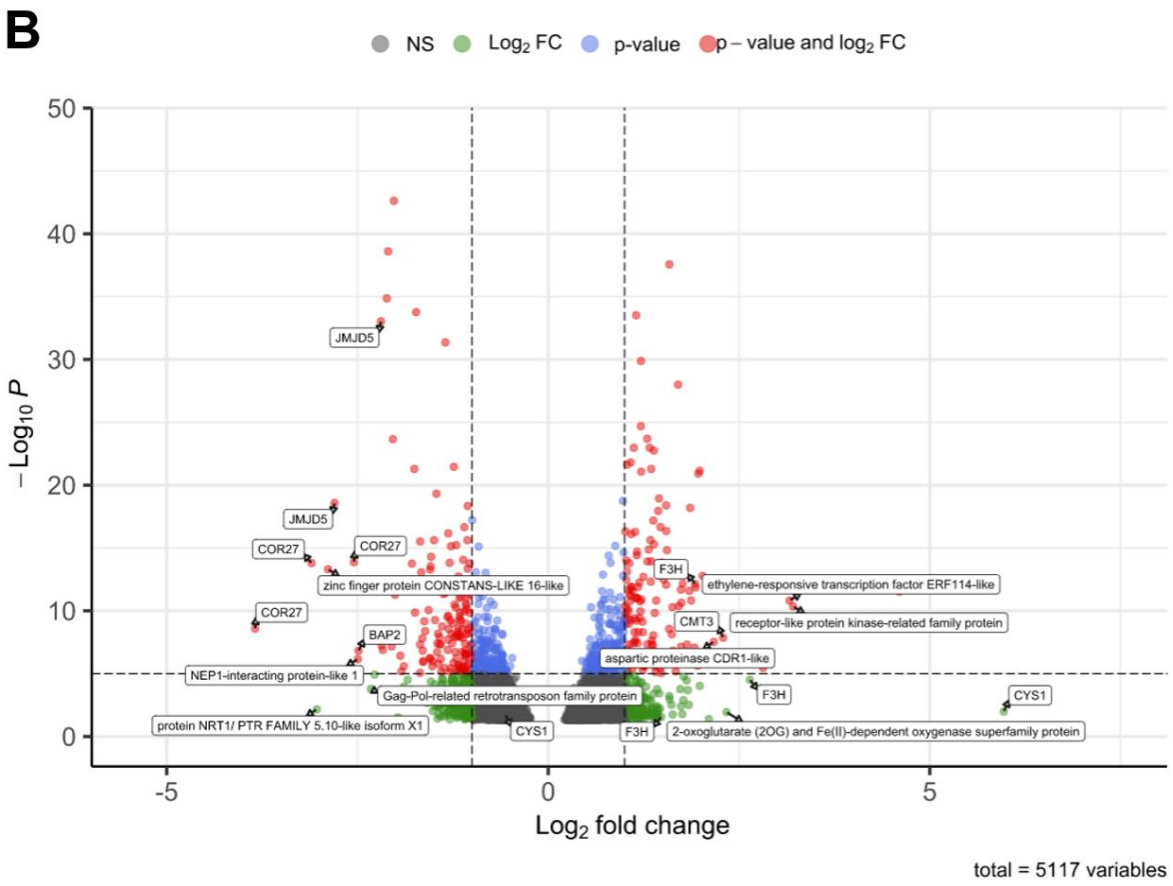


Fig.7. Volcano plots showing the distribution of DEGs in response to 2-hour treatment with 1 µM flg22 treatment (significant at *P < 0.05).* R was used with the Enhanced Volcano package to generate the graph (Blighe, Rana, and Lewis, 2018) and x-limits for the log2foldchange were set at 1 for both species, while the default adjusted p-value (padj; P) significance limits were used for quinoa (A) and Arabidopsis (B) datasets (-Log_{10}P of 5 and 2.5 respectively).

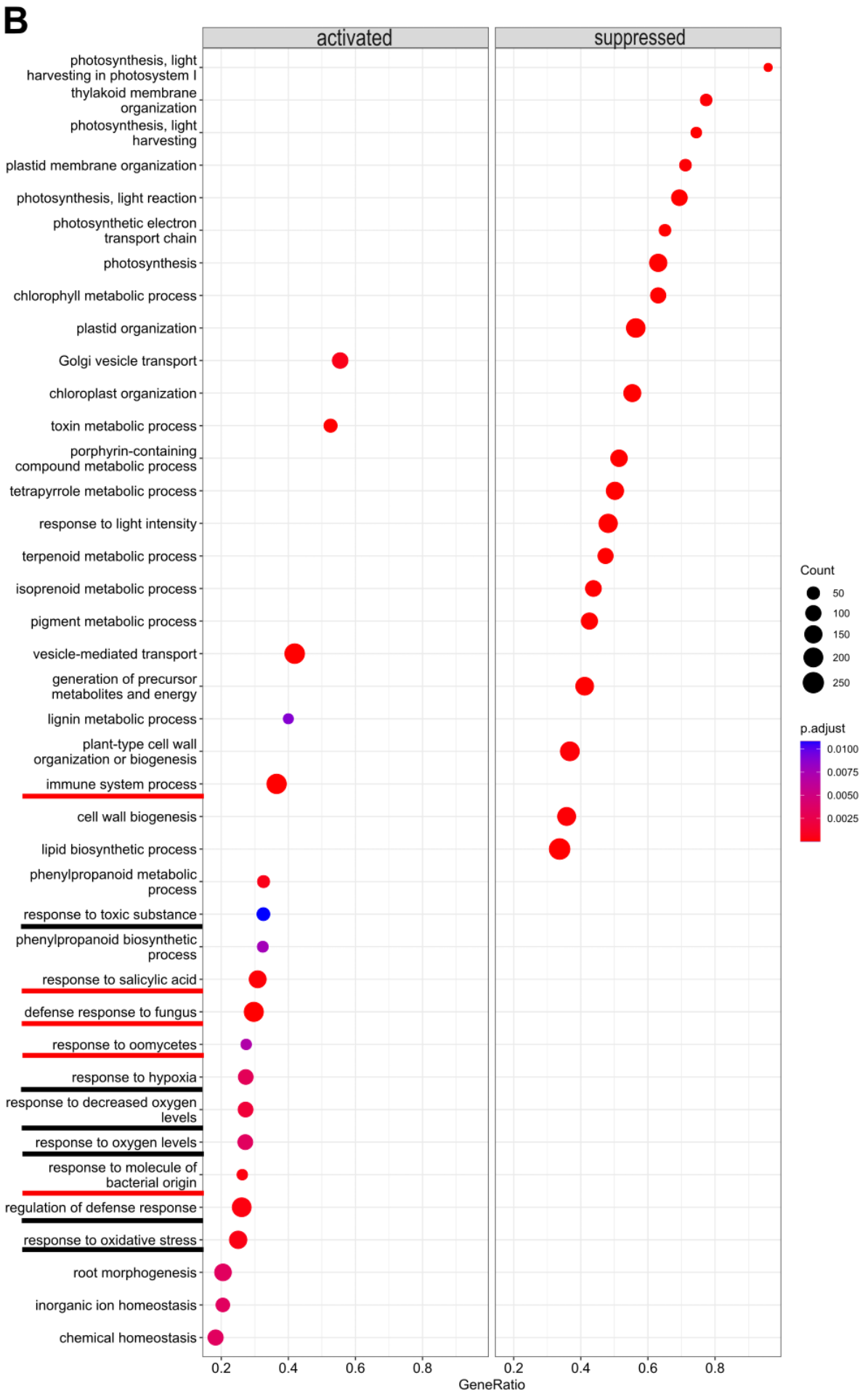
2.2.2.1. Global functional enrichment analyses reveal more differences than similarities between the two-hour flg22-induced transcriptomes of Arabidopsis and quinoa

The quinoa DEGs mapped to Arabidopsis gene IDs were next annotated with the biological function descriptors Gene Ontologies (GO) and Kyoto encyclopedia of genes and genomes (KEGG) terms and assessed for their enrichment using the Bioconductor clusterProfiler GSEA (Gene Set Enrichment Analysis) package. Enriched upregulated (activated) and downregulated (suppressed) terms were visualised by information-rich DotPlots (Fig.8) which reveal five key pieces of DEG information; the Y-axis shows the most significant highly enriched terms based on the normalized enrichment score and adjusted p value(padj) (Yu et al., 2014); the number of genes annotated with the enriched term (count) is represented by

dot size, the dots are coloured by padj for their multiple comparisons significance and spaced along the X-axis by 'gene ratio', which represents the proportion of genes in the quinoa flg22 DEG list annotated by the enriched term out of the total known number of genes annotated by this GO term i.e. the enriched gene count divided by the gene set size.

DotPlots were generated for each GO category but only the Biological Process (BP) and Molecular Function (MF) categories are shown as they highlighted a more diverse range of biological information with more specific terms from lower down the GO hierarchy, whereas the most significantly enriched Cellular Component (CC) terms described generic transcriptional or photosynthetic machinery.


A
activated
suppressed
starch catabolic process
photosystem I assembly
regulation of photosynthesis
cellular polysaccharide catabolic process
Golgi vesicle transport
photosynthesis, light harvesting
photosynthesis
plastid organization
photosynthesis, light reaction
abaxial cell fate specification
porphyrin-containing compound metabolic process
vesicle-mediated transport
negative regulation of carbohydrate metabolic process
organophosphate metabolic process
anion transport
organic substance transport
ion transmembrane transport
inorganic ion transmembrane transport
protein modification by small protein conjugation
cation transmembrane transport
nitrogen compound transport
carbohydrate derivative metabolic process
inorganic cation transmembrane transport
ion transport
carbohydrate derivative biosynthetic process
transmembrane transport
regulation of photosynthesis, dark reaction
regulation of reductive pentose-phosphate cycle
negative regulation of reductive pentose-phosphate cycle
cation transport
monocarboxylic acid metabolic process
metal ion transport
negative regulation of photosynthesis
response to bacterium
defense response to bacterium
0.5
0.7
0.9
1.1
1.3
GeneRatio
Count
100
200
300
400
p.adjust
0.04
0.03
0.02
0.01


B
activated
suppressed
photosynthesis, light harvesting in photosystem I
thylakoid membrane organization
photosynthesis, light harvesting
plastid membrane organization
photosynthesis, light reaction
photosynthetic electron transport chain
photosynthesis
chlorophyll metabolic process
plastid organization
Golgi vesicle transport
chloroplast organization
toxin metabolic process
porphyrin-containing compound metabolic process
tetrapyrrole metabolic process
response to light intensity
terpenoid metabolic process
isoprenoid metabolic process
pigment metabolic process
vesicle-mediated transport
generation of precursor metabolites and energy
lignin metabolic process
plant-type cell wall organization or biogenesis
immune system process
cell wall biogenesis
lipid biosynthetic process
phenylpropanoid metabolic process
response to toxic substance
phenylpropanoid biosynthetic process
response to salicylic acid
defense response to fungus
response to oomycetes
response to hypoxia
response to decreased oxygen levels
response to oxygen levels
response to molecule of bacterial origin
regulation of defense response
response to oxidative stress
root morphogenesis
inorganic ion homeostasis
chemical homeostasis
0.2
0.4
0.6
0.8
GeneRatio
Count
50
100
150
200
250
p.adjust
0.0100
0.0075
0.0050
0.0025

C

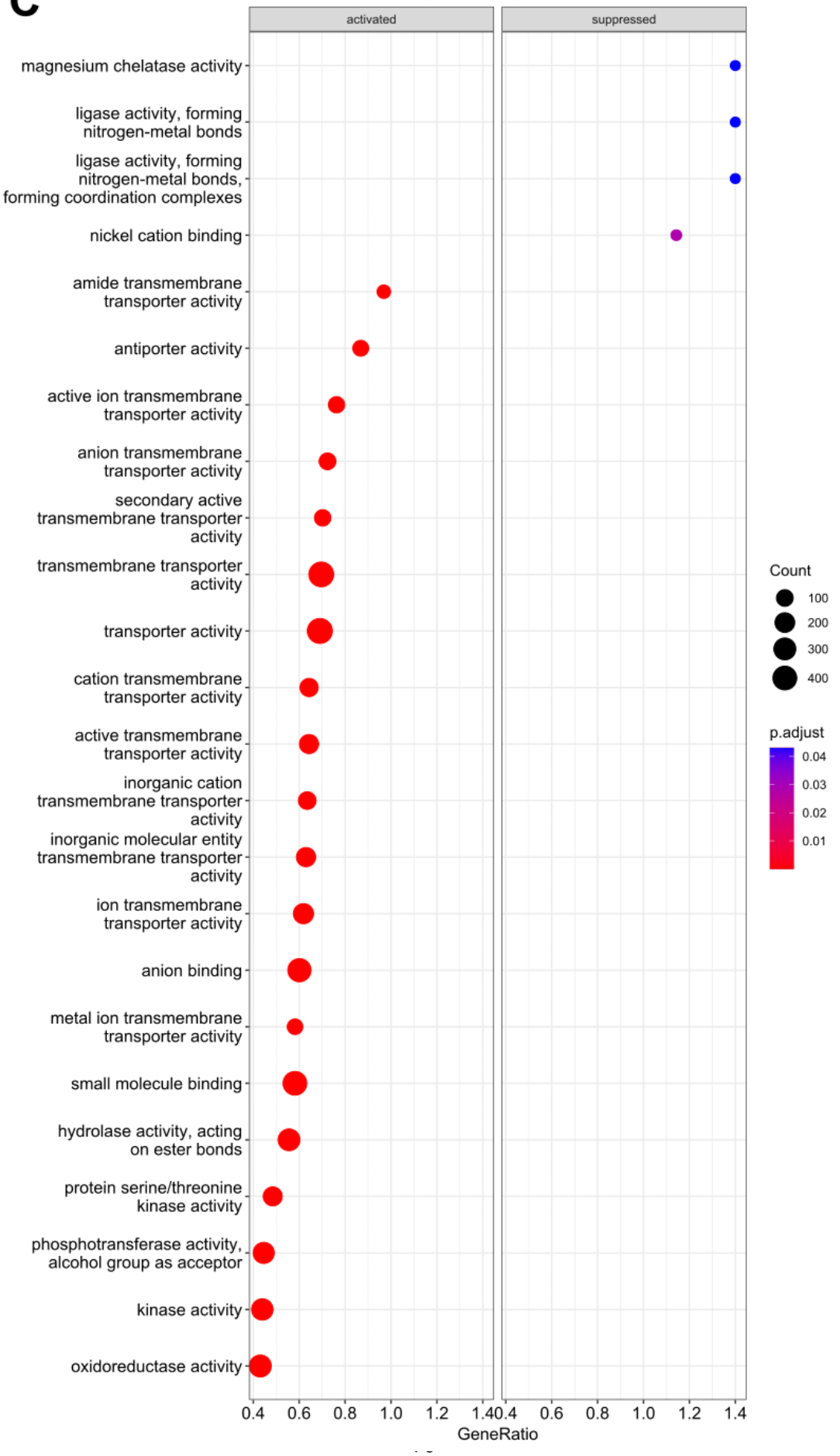

activated
suppressed
magnesium chelatase activity
ligase activity, forming nitrogen-metal bonds
ligase activity, forming nitrogen-metal bonds, forming coordination complexes
nickel cation binding
amide transmembrane transporter activity
antiporter activity
active ion transmembrane transporter activity
anion transmembrane transporter activity
secondary active transmembrane transporter activity
transmembrane transporter activity
transporter activity
cation transmembrane transporter activity
active transmembrane transporter activity
inorganic cation transmembrane transporter activity
inorganic molecular entity transmembrane transporter activity
ion transmembrane transporter activity
anion binding
metal ion transmembrane transporter activity
small molecule binding
hydrolase activity, acting on ester bonds
protein serine/threonine kinase activity
phosphotransferase activity, alcohol group as acceptor
kinase activity
oxidoreductase activity
0.4
0.6
0.8
1.0
1.2
1.4
GeneRatio
Count
100
200
300
400
p.adjust
0.04
0.03
0.02
0.01

Fig.8. Dotplots showing the top 20 enriched flg22-induced BP terms in Quinoa (A) Arabidopsis (B) and the top 20 enriched MF terms for quinoa (C). These plots were created by clusterProfiler and DOSE packages (Yu et al., 2014). The red and black lines in the dotplots A and B indicate canonical immune and generic stress related terms respectively. Terms were significantly enriched if their Benforroni-corrected p-value was less than 0.05 and the gene space used was the full list of DEGs, unfiltered by significance.

the top 20 activated (upregulated) and total 15 suppressed (downregulated) BP terms (ranked 71by enrichment score) are shown in Fig.8A. The majority of the 15 significantly enriched-suppressed BP terms were related to photosynthesis, which is a widely described immune response and reflective of results obtained for a 2h flg22 vs mock experiment in Arabidopsis (Fig.8B). A shift to a state of high metabolism and transport processes (vesicle-mediated, nitrogen, transmembrane and ion and metal ion transport) is observed for upregulated processes, however only two related canonical immune specific response terms were enriched-upregulated whereas for Arabidopsis five terms along with six generic stress response terms were found (underlined by red and black lines respectively; Fig.8B). The DotPlot showing the top 20 MF terms for quinoa (Fig.8C) reveals only four significantly suppressed terms involving metal chemistry and for Arabidopsis just three terms were suppressed: purine phosphoribosyltransferase activity, polygalacturonase activity and chlorophyll binding (data not shown). The top 20 significantly enriched-upregulated terms further reflect the active state of metabolite transport whilst also revealing key features of stress signaling modules such as kinase cascades, specifically of serine/threonine nature reaffirming the biochemical MAPK activation western blot results, where an increase in oxidoreductase activity validates our ROS and POX data. For Arabidopsis enriched MF terms, transmembrane, transporter and kinase activity did not populate the most enriched-upregulated terms (data not shown).

To validate the GSEA GO findings for quinoa and to visualise enriched pathways of interest, the GSEA was extended to test for enriched KEGG pathway terms, an orthogonal functional classification system which is less prone to redundancy of related GO terms (due to the hierarchical direct acyclic graph structure). As expected, the KEGG photosynthesis pathway was significantly suppressed, however this was the only term that was significantly

suppressed, suggesting indeed that the majority of suppressed BP and MF terms were likely to be interrelated and involved in photosynthesis (Fig.9). The most highly enriched term alpha-linolenic acid metabolism is part of the jasmonic acid biosynthesis module: linolenic acid is a precursor of the jasmonic acid (JA) phytohormone which mediates responses to both biotic and abiotic stresses and crosstalks with other stress-related hormones ethylene (ET), abscisic acid (ABA), salicylic acid (SA), brassinosteroids (BRs) (Wasternack and Strnad, 2018). Tryptophan metabolism is another pathway of interest given its involvement in defence responses against pathogens via serotonin production (Ishihara et al., 2008) or as a precursor of antimicrobial secondary metabolites such as phytoalexins and indole glucosinolates (IGS) (Costantini et al., 2020).

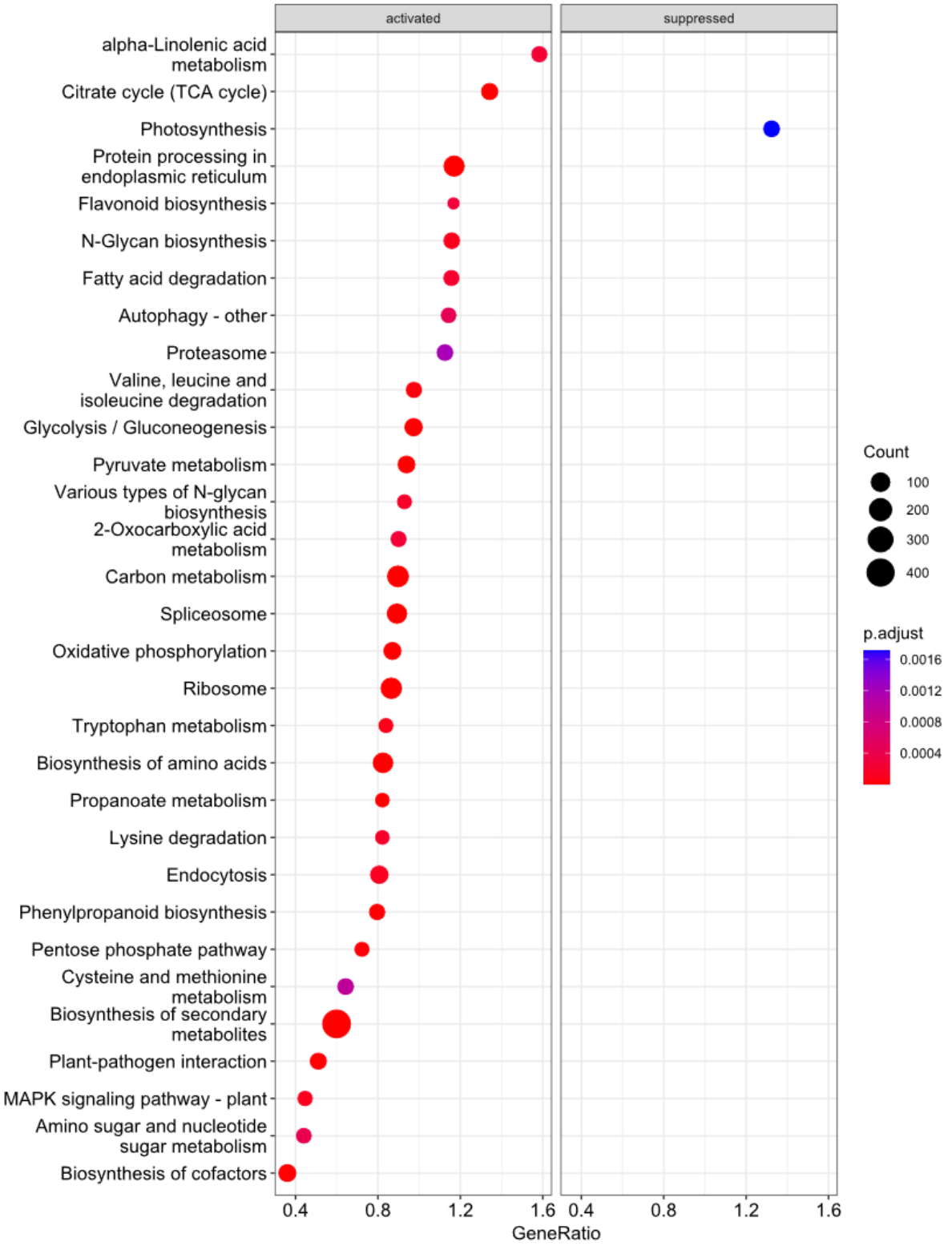


Fig.9. KEGG enrichment Dotplot showing the top 30 enriched flg22-induced KEGG terms in Quinoa clusterProfiler and DOSE packages were used Terms were significantly enriched if their Benforroni-corrected p-value was less than 0.05 and the gene space used was the full list of DEGs, unfiltered by significance.

The enriched KEGG term MAPK signalling pathway for both species was next examined in greater detail for its role in pathogen infection and ABA/salt/drought stress (Fig.10). Firstly, pathogen infection revealed several expected components in pathogen perception, the transmembrane receptor FLS2 and co-receptor SERK4 (BAK1) where for both species the genes were strongly upregulated (red colour) (Fig.10A). Further components with similarly directed gene expression changes between the two species were the MAPKK MKK1/2/MEK1, the downstream VIP1 gene, WRKY29/22 transcription factor and for the abiotic stress pathways the MAPKK MKK3. Contrasting expression patterns were found for pathogen infection end component SUMM2, and the PR1 gene, which were upregulated in quinoa and downregulated (green colour) in Arabidopsis, and the WRKY33 gene and MPK3/6 gene which were both upregulated in Arabidopsis and downregulated for quinoa. Interestingly, for the abiotic stress signalling pathway (Fig.10B) the first three components: PYR, PP2C and SNRK2 showed complete opposing patterns: downregulation in Arabidopsis and upregulation in quinoa. Several components also strongly differentially expressed in one species but not found to be either significantly induced or suppressed in the other (components with white or grey boxes).

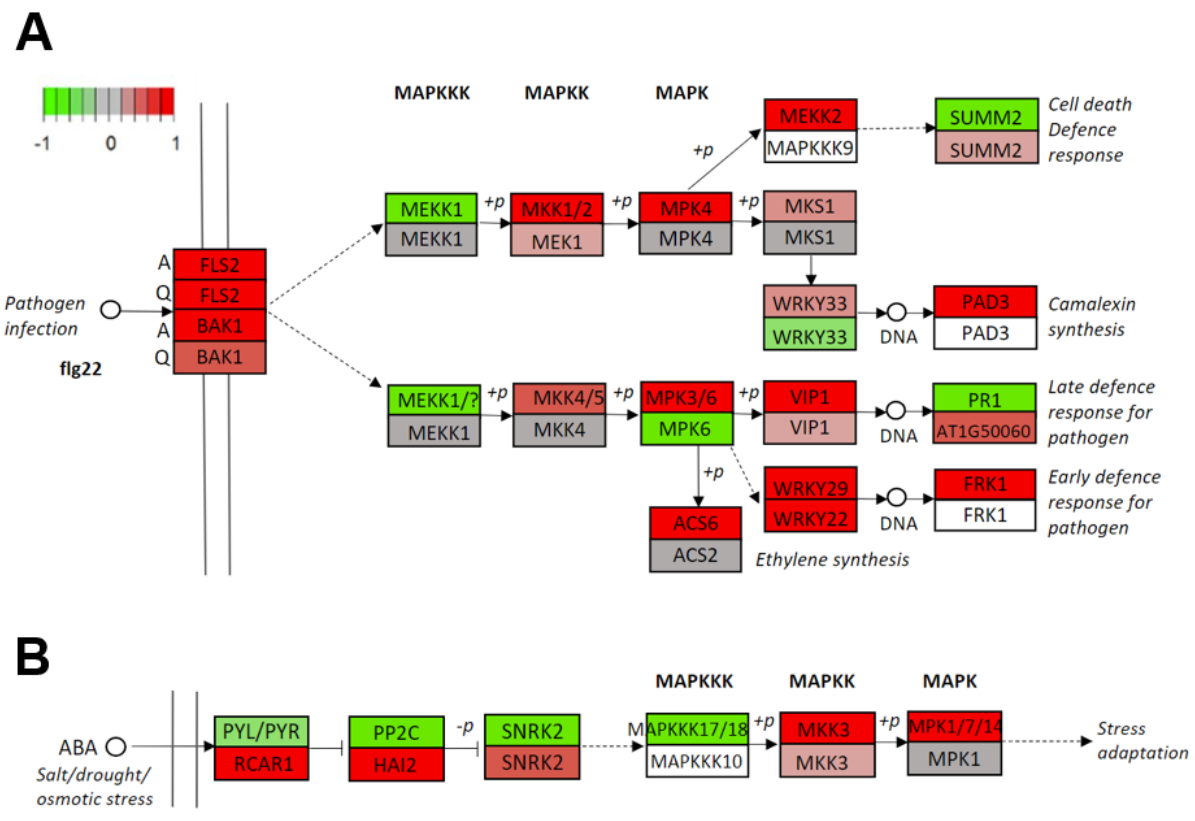


Fig.10. Composite KEGG Pathview comparisons for MAPK signalling components between Arabidopsis and quinoa. The graph is based off outputs for each species from the Pathview R/Bioconductor package (Luo and Brouwer 2013) and selectively shows just the pathogen infection (A) and abiotic stress related pathways (B), where Arabidopsis components are shown on the top line of each pathway (denoted in graph A by the letter 'A' and 'Q' for quinoa for the FLS2 and BAK1 genes). The relative change in expression is binary (-1, 0 or +1) and colour-coded where red is positive, green is negative, grey is no change and white suggests a lack of an orthologous gene was found for that component.

2.2.2.2. De-novo analysis of the DEGs annotated with enriched GO and KEGG terms reveal putative flg22-responsive candidate genes in quinoa

Having observed significantly enriched themes, the next step was to identify individual genes within these sets. Key terms of interest were selected from the GSEA output for MF, BP, CC and KEGG analyses on the basis of having a normalised enrichment score of > 2.0 and which were terms related to immunity, disease and abiotic stress. The chosen list contained 31 terms (Supplementary Table 1), for which the core enriched genes were extracted and thinned to remove duplication (i.e., where one gene was represented by multiple terms) which produced a list of 1233 significant DEG genes which represents ~25% of the full DEG list for quinoa (Supplementary Table 2) which were plotted on a volcano plot to highlight their distribution expression patterns (Fig.11).

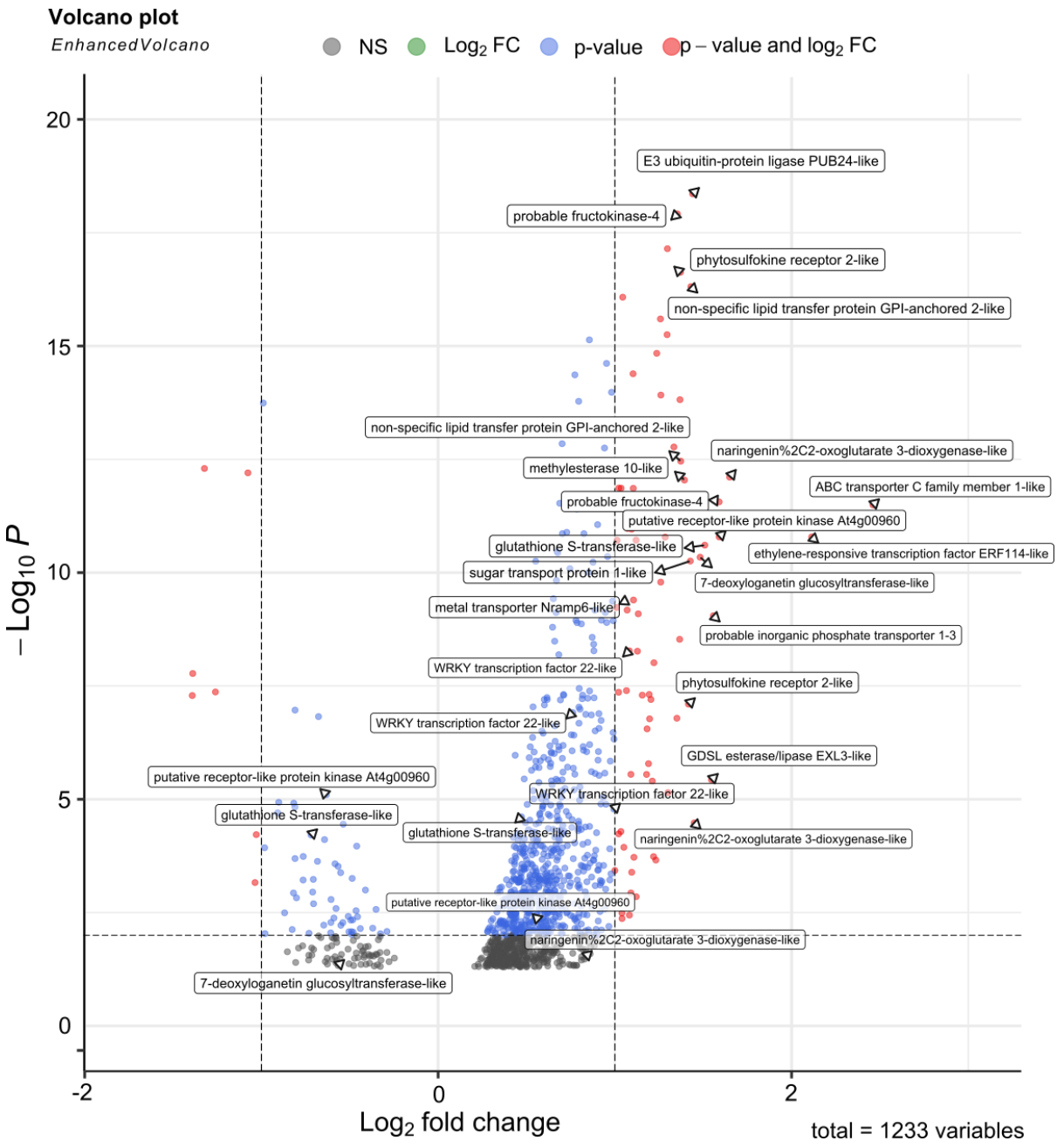


Fig.11. Volcano plot showing the distribution of core stress related DEGs induced in quinoa by flg22 treatment. 1233 significant DEG genes were plotted using Enhanced Volcano R package (Blighe, Rana, and Lewis, 2018) and the top 20 upregulated genes of this dataset were labelled by gene name or description when the gene name was not available. X-limits for the L2FC were set at 1 while the default adjusted p-value (padj; *P*) significance limits were -Log10P = 2.5.

An additional manual approach was used to zoom in on further genes of interest exploiting the finding that the output file of the GSEA ranks the genes in the core enrichment column by descending L2FC, allowing the most highly upregulated terms to be easily identified. The

longlist of 31 terms was reduced to a shortlist of 12 terms of specific interest (highlighted in bold in the grey cells of Supplementary Table 3) and the top genes with a L2FC >1.0 were extracted and mapped back to the full DEG list (unfiltered by padj) to discover their individual expression values and any gene copies.

One particularly interesting finding was the presence of several EFR annotated genes in the full list of unfiltered DEGs, which supported the elf18 induced MAPK and ROS burst responses observed in Fig.2 and Fig.3B, but which was previously thought to be restricted to the *Brassicaceae* plant family lineage (Boller and Felix, 2009). OrthoFinder (Emms and Kelly, 2019) was therefore used to generate a list of *C. quinoa* vs *A. thaliana* orthologs (primarily for helping to validate our BLASTp results for the quinoa vs Arabidopsis reference proteomes) but also to for querying the suggested existence of several homologs of the cognate elf18 EFR receptor gene (AT5G20480) in quinoa. This analysis revealed the presence of five AT5G20480 homologs in Arabidopsis which collectively mapped to 36 orthologs in quinoa. The BLASTp results were used to identify the protein with the highest percentage mapping identity, which revealed one protein with 45% amino acid identity to AT5G20480. From the BLASTp output file the reference protein could be mapped back to the gene loci identifier LOC110705634, suggesting that this is the EFR gene in quinoa. While this gene was indeed found in our transcriptome dataset, as expected, its expression was not found to be significantly induced by flg22 (L2FC of flg22 vs mock = 0.165; $P = 0.55$).

2.2.2.3. Quinoa and Arabidopsis share only a small set of flg22-induced DEGs with many genes opposingly regulated

Next, as done in the biochemical experiments, the 2h quinoa flg22 PTI transcriptome was compared directly to the 2h flg22-induced transcriptome in Arabidopsis (Aquino, Bach-Pages, Preston unpublished). The quinoa and Arabidopsis flg22-induced transcriptomes had 5117 and 3209 DEGs respectively (at $P < 0.05$). Quinoa's tetraploid genome (1.39 Gb) is significantly larger than the diploid genome of Arabidopsis (0.135 Gb) and many genes will have a copy due to quinoa's allotetraploid genome composition. This was demonstrated by filtering the quinoa significant DEG list to single copies of genes only, which reduced the dataset to 3663 genes. Interestingly when the same was done for Arabidopsis the dataset remained unchanged at 3209 (Supplementary Table 4). Quinoa's full significant DEG list was used for

subsequent comparative analyses, however. The datasets were first split into down and upregulated DEG subgroups, where in both quinoa and Arabidopsis there were slightly more upregulated (UR) genes than downregulated (DR) genes (52.4% and 55.8% respectively) (Fig.12). The DR and UR DEG lists were next compared between the two species finding 203 and 243 shared DEGs (Fig.12). To simply visualise any outstanding differences between the species' expression patterns within the shared UR and DR DEG lists, these lists were ordered by descending or ascending L2FC (based on the L2FC values of Arabidopsis) and plotted as line graphs (Fig.13).

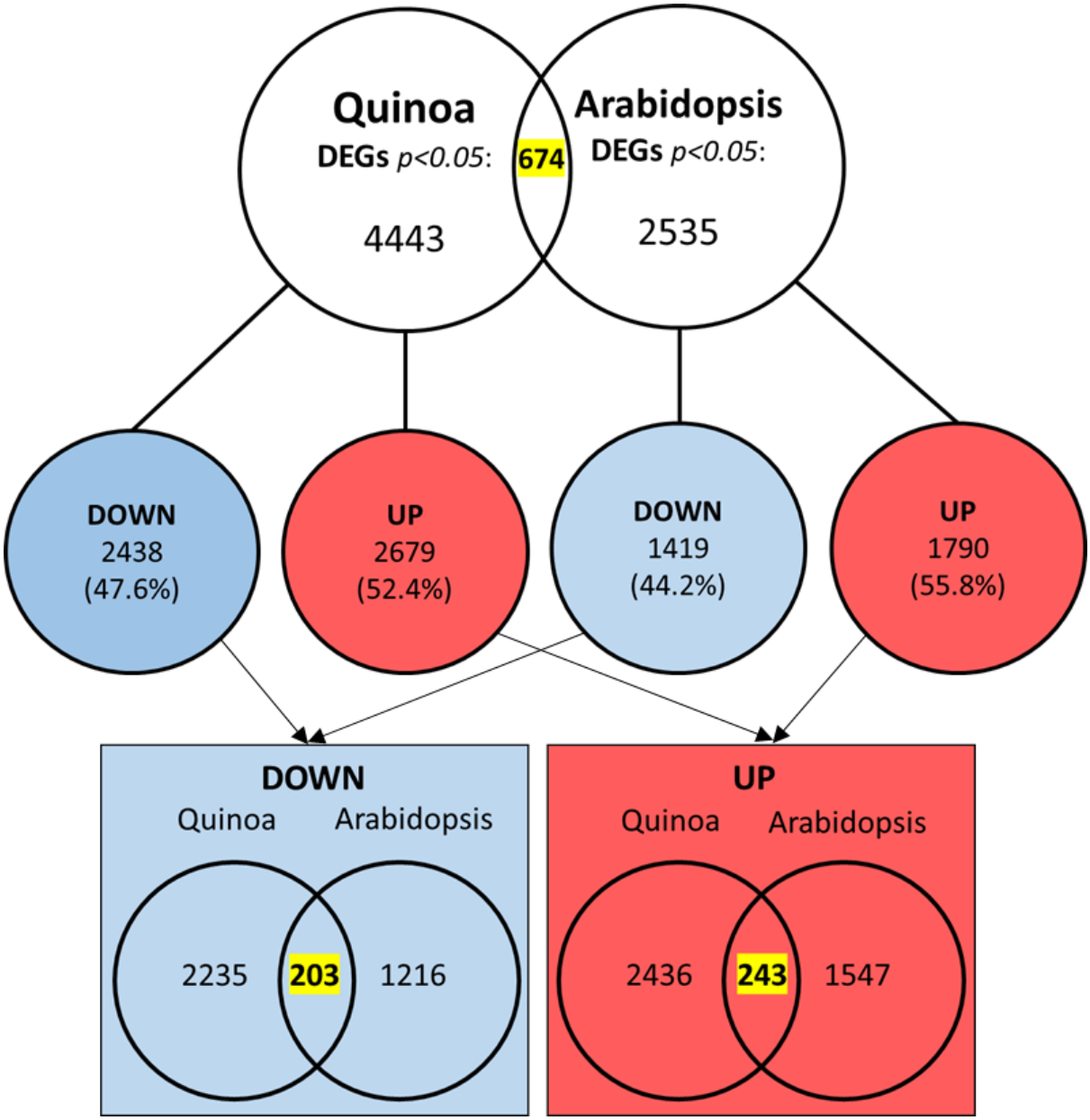


Fig.12. Venn diagrams showing unique and shared DEGs between quinoa and Arabidopsis plants in response to 2h 1 µM flg22 treatment. Intersecting number of genes are highlighted in yellow. Down and upregulated genesets are colour coded in blue and red respectively to highlight the comparisons made.

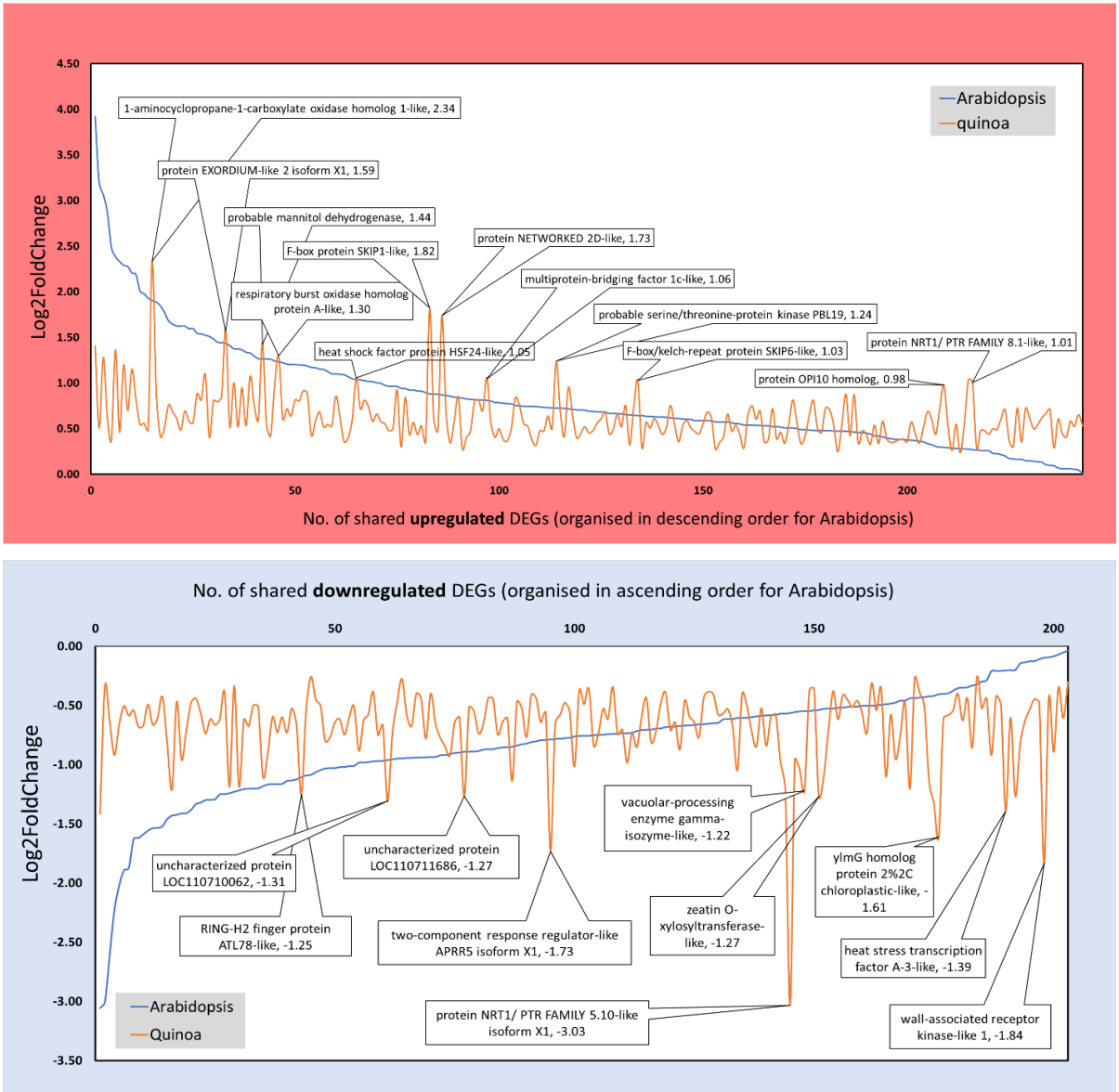


Fig.13. Line graphs of shared upregulated and downregulated DEGs highlight differences between the relative importance of genes in each species. The shared UR and DR DEG datasets were ranked and plotted in decreasing L2FC (top graph; shared UR DEGs; red background) and increasing L2FC (bottom graph; shared DR DEGs; blue background) based on the L2FC values of Arabidopsis. The blue smooth line in each graph therefore represents the changing L2FC values of Arabidopsis DEGs whereas

quinoa's corresponding trace is shown in orange. DEGs with pronounced contrasting L2FC values have been annotated with their gene description.

The line graphs reveal how the protein NRT1, one of the upregulated DEGs with the lowest L2FC in Arabidopsis is one of the more highly upregulated DEGs in quinoa, whereas the wall-associated receptor kinase-like 1 protein was one of the most highly suppressed DEGs in quinoa but only very mildly suppressed in Arabidopsis. These contrasts suggest a potential differential importance across the species. The 1-aminocyclopropane-1-carboxylate oxidase homolog 1-like gene however showed high expression for both species suggesting a conserved importance in PTI.

Fig.12 shows that the total shared number of DEGs between the two species was 674, which is 228 genes greater than the sum of the shared UR (243) and DR (203) genes meaning a significant subset (33%) of this list contains opposingly regulated genes. This can more clearly be visualised by a heatmap (Fig.14) which also highlights (via the darker colouration) the greater intensities in expression for Arabidopsis genes.

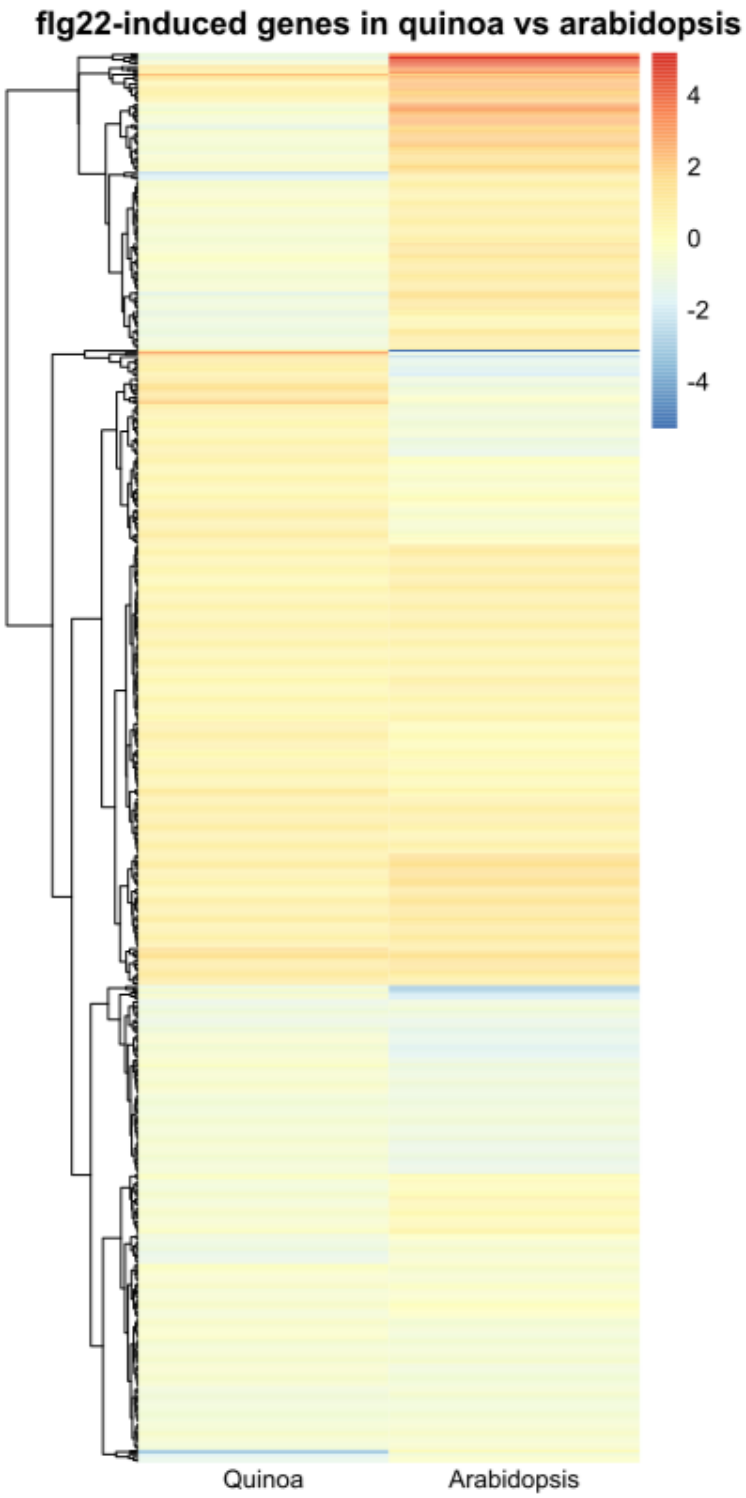


Fig.14. Heatmaps of the shared 674 flg22-induced genes between quinoa and Arabidopsis. Created by Pheatmap in R. Gene IDs were removed for clarity but can be found in Supplementary Table 5.

The 674 shared genes were next plotted using a four-quadrant scatter graph to allow a higher quantitative visual resolution of the genes, facilitate the identification of further genes of potential interest.

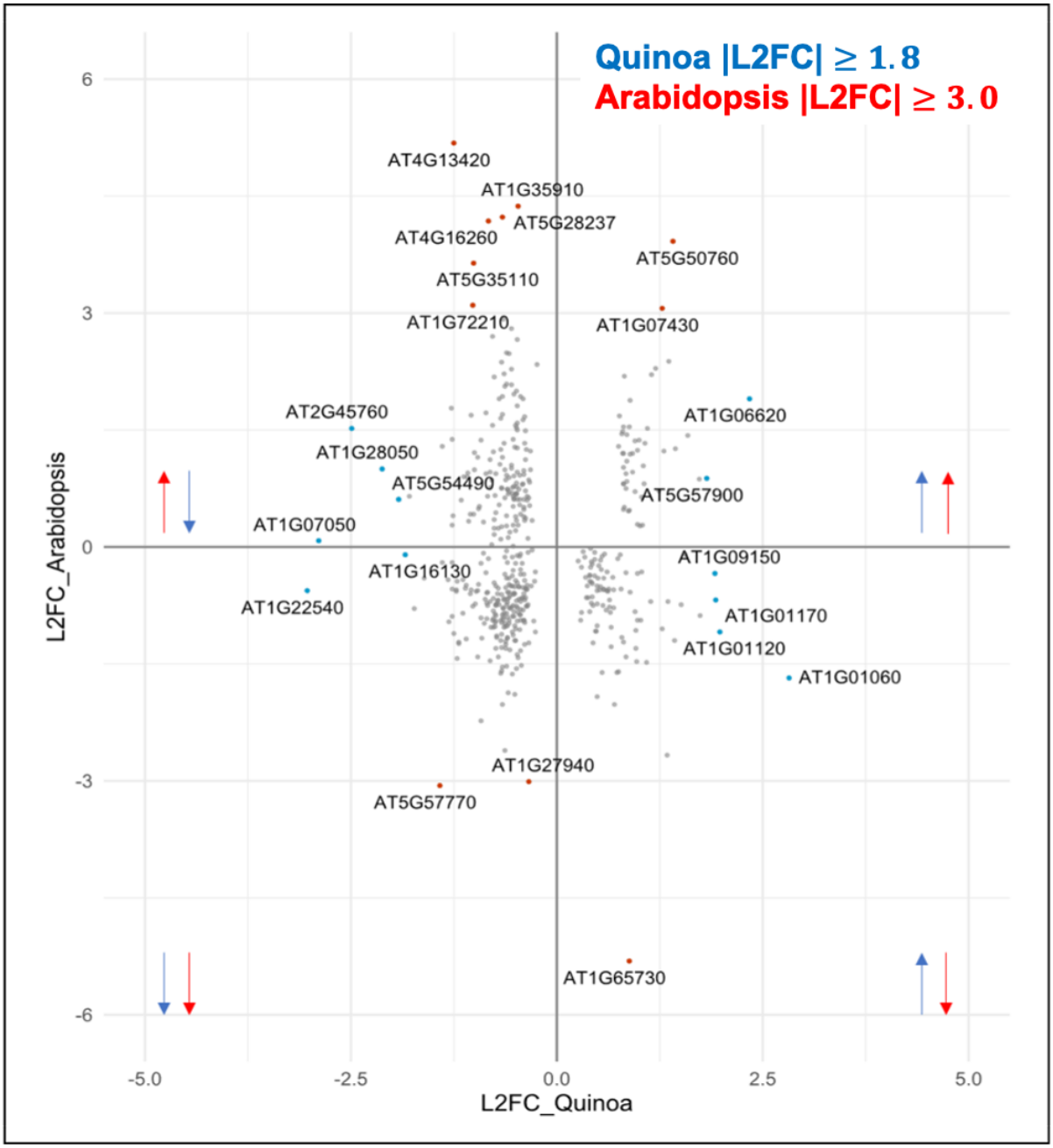


Fig.15. Scatterplot showing the distribution of the 674 shared genes between quinoa and Arabidopsis. A criterion of absolute L2FC (|L2FC|) values of ≥ 1.8 (blue dots; quinoa) and ≥ 3.0 (red dots; Arabidopsis) was set and used to identify a subset of 23 genes on the chart with most striking differences or similarities, for which the At gene identifiers are provided. These genes have been highlighted also in a separate sheet of Supplementary Table 5.

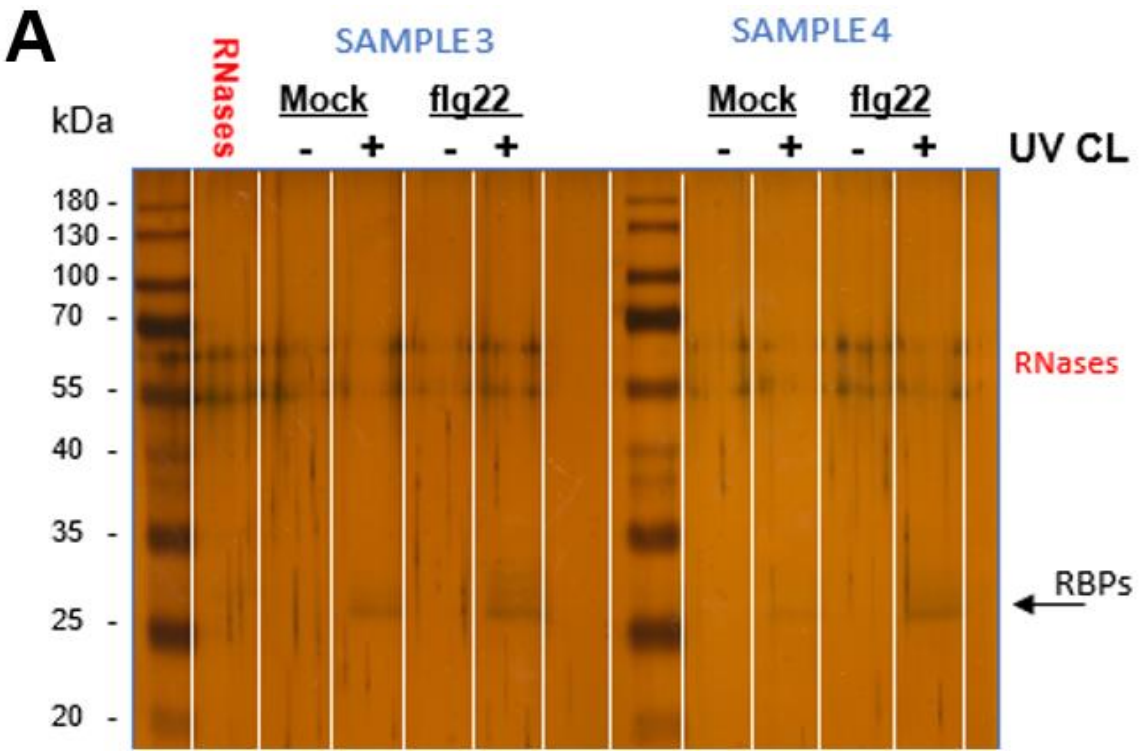
2.2.3. Profiling an early proteomic response of quinoa to flg22 treatment

2.2.3.1. The novel Plant RNA Interactome Capture method reveals preliminary background and flg22-induced quinoa RBPomes

The RNA-seq results confirm how several biochemically assayed PTI immune responses in quinoa depend on transcriptional reprogramming and can be confirmed as PTI related genes. Several of these genes are hypothesised to be core stress response genes in quinoa and will be confirmed by independent salt stress and combinatorial stress studies in subsequent chapters 3 and 5. To deepen our molecular understanding of PTI responses in quinoa we finally took a proteomics approach to identify RNA-binding proteins (RBPs). RBPs act as key regulators of gene expression by regulating RNA synthesis, as well as orchestrating diverse post-transcriptional functions: processing, (re-)localizing, translating or regulating the stability of RNAs (Bach-Pages et al., 2020). RBPs therefore offer plants fast ways to respond to stresses. M.Bach-Pages et al. (unpublished) have previously demonstrated the applicability of the improved plant RNA-interactome capture (ptRIC) protocol to a wide range of dicot and monocots to isolate the 'RBPome' of these plants, and recently, they determined how the RBPome responds to flg22 uncovering a new source of gene candidates important for plant immunity in Arabidopsis (Bach-Pages et al., 2020).

For quinoa, ptRIC was optimised by extending the incubation time from 1 hour to overnight for the first round of RBP capture to obtain higher yields from the plant tissue and two independent ptRIC experiments were conducted for all samples (using the same starting material) to ensure a high enough RBP yield for Mass Spectrometry (MS) analysis. While the total amount of eluates (RBP complexes) was approximately three times lower than Arabidopsis, and difficult to observe by silver staining (Fig.16A), the RBPs (and corresponding whole cell lysate proteins) were successfully purified by FASP (Filter Aided Sample Preparation) and sent to ACE (Analytics Core Facility Essen) for MS analysis. Unfortunately, one eluate sample (flg22 biological replicate 2) experienced an unexpected technical error of significant sample loss (either during transit to ACE or during the preparation for MS) and had to be discarded from the post-MS statistical analyses. Thorough quality control checks, statistical modelling and early post-MS analyses were all performed by Dr Wael Kamel in the

Castello group in Glasgow University. The 375 and 397 bonafide RBPs found for control (mock-treated) quinoa and flg22-treated leaves are shown by Fig.16B & 16C.



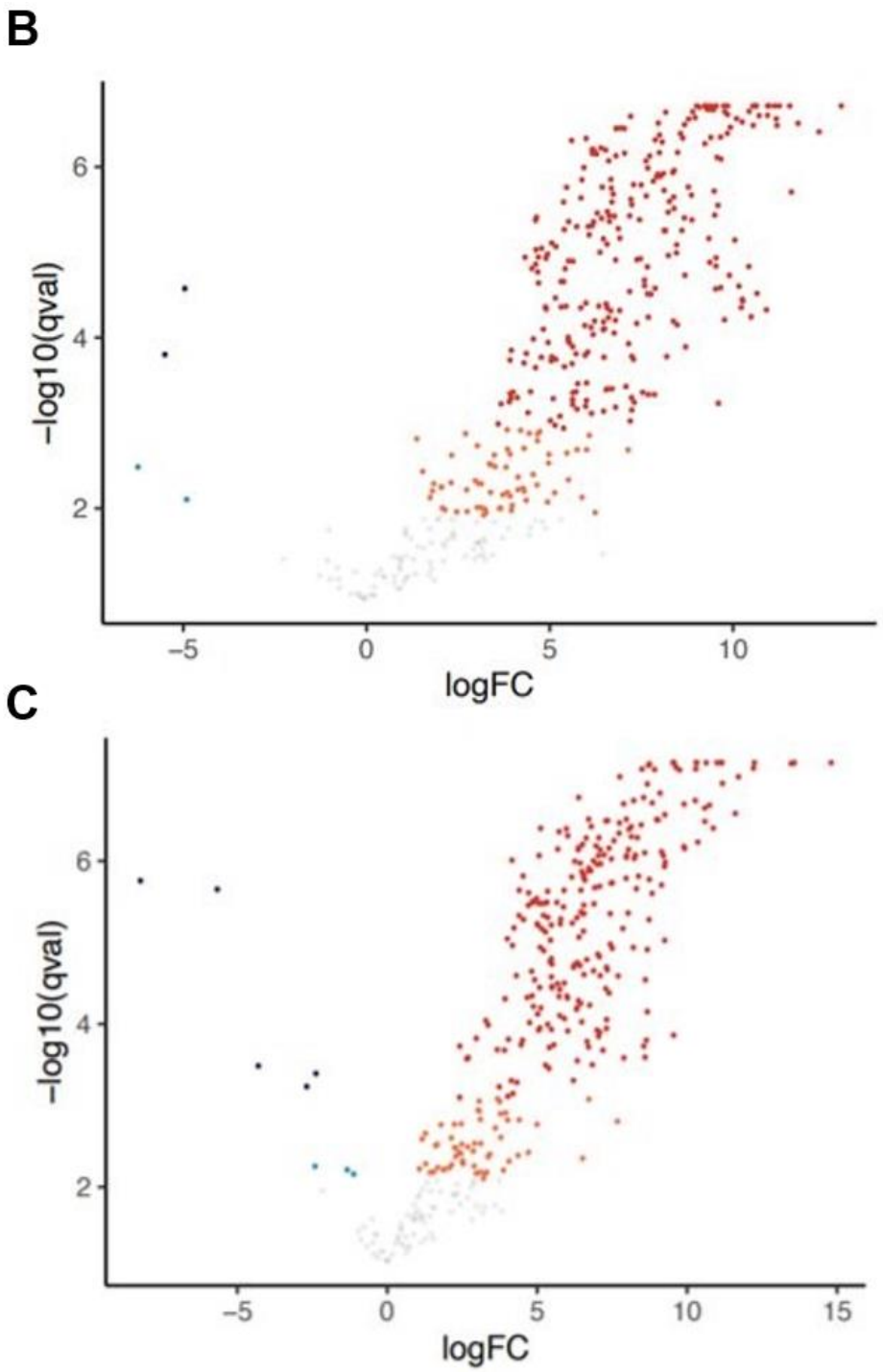


Fig.16. Identification of quinoa leaf RNA-binding proteins (RBPs) using plant RNA interactome capture (ptRIC). (A) Silver staining analyses of the eluates (RBPs) from ptRIC applied to quinoa leaves. "+" and "-" indicate 'with UV crosslinking; CL' or the negative control 'No UV crosslinking; NoCL' where UV crosslinking is needed to fix in place actively bound RBPs to RNA in order to be pulled-down ('captured'. Volcano plots for A and B depict the $\log_2$ fold change (L2FC[CL/NoCL]) and the significance value between UV crosslinking (CL) and no UV crosslinking (NoCL) treatments for each protein (dot) identified by MS. The data represent the mean of three biological replicates for both mock-treated (B;

top graph) and flg22-treated (C; bottom graph) quinoa leaves. The colour of the dots indicates the certainty (significance level) of the proteins representing true RBPs: red or dark blue = False Discovery Rate (FDR) ≤ 0.01 and orange or light blue = FDR ≤ 0.1. Non-significant or 'non-enriched proteins' are coloured in grey. As done by Bach-Pages et al. (2020) a combination of quantitative and semi-quantitative data analyses was used to identify high-confidence RBPs for each condition (Methods).

Next, these datasets representing the reference mock-treated ("CTRL") and the flg22-induced RBPomes were compared directly using a venn diagram to identify immune-specific RBPs (Fig.17). 332 RBPs were found to be shared which suggests these represent the (high confidence) core RBPs of quinoa. 74 unique flg22-induced RBPs were found, 16 of which were significant (FDR ≤ 0.05), whereas a lower number of unique flg22-suppressed RBPs were found, 35, of which 5 were significant (FDR ≤ 0.05).

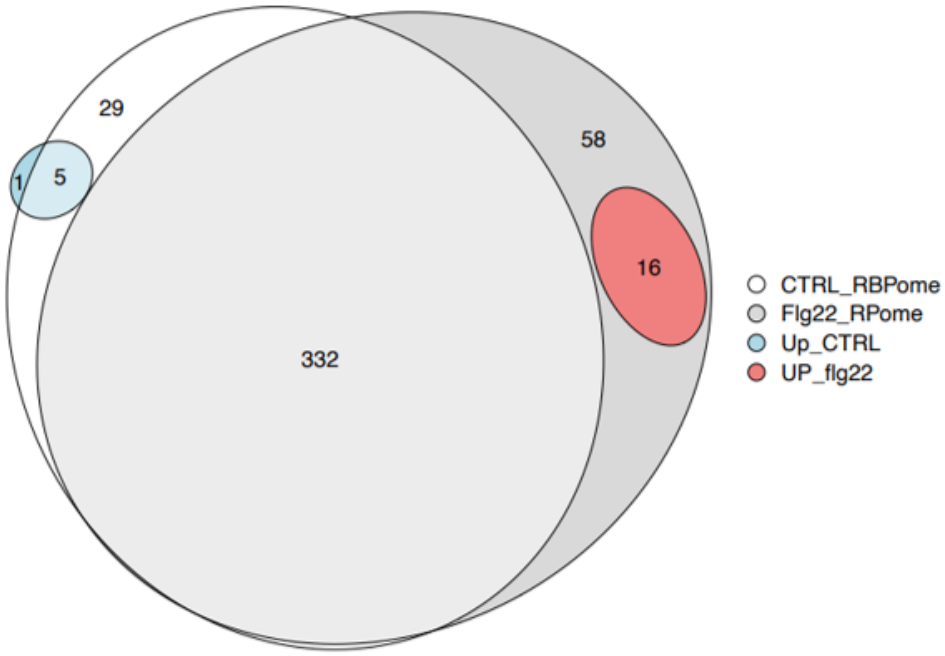


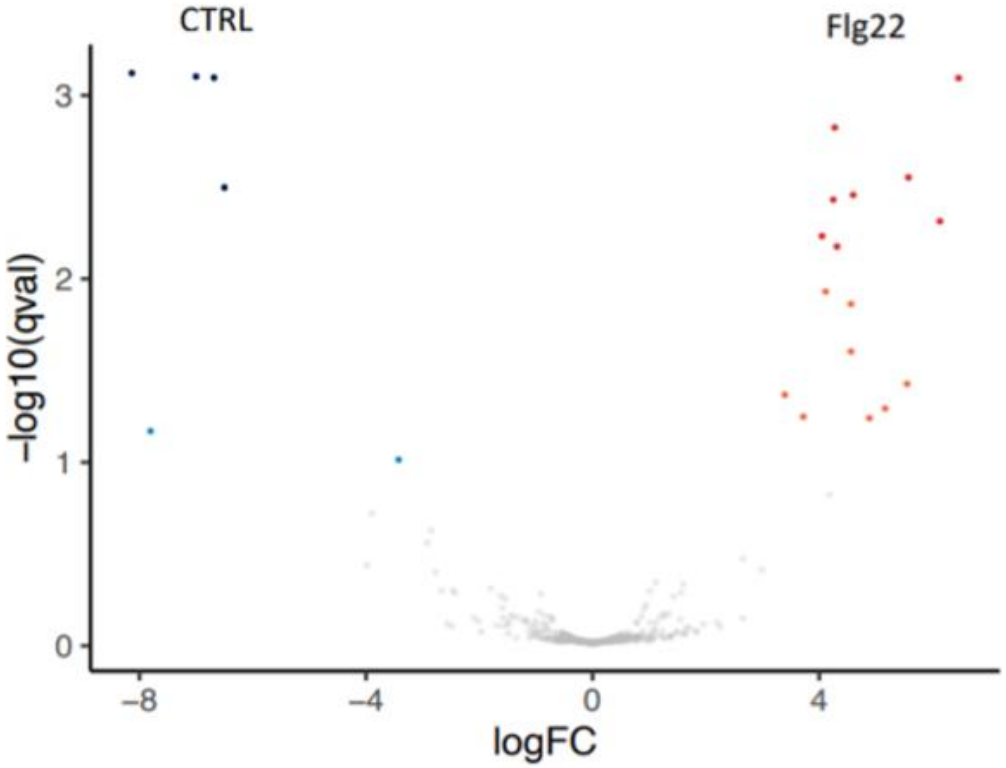
Fig.17. Venn diagram showing the overlap of RBPs found in both untreated and flg22-treated conditions. The subsets of RBPs that were significantly more active (red) in the flg22 or untreated condition (blue) at an FDR < 0.05 are also shown.

The next step was to evaluate the impact of flg22 on the quinoa RBPome at a quantitative level by comparing the intensity differences of shared RBPs between mock and flg22 samples (Fig.18A). This analysis revealed 24 differentially regulated RBPs at the more lenient stringency of FDR ≤ 0.1 after 2h flg22 treatment (Fig.18B). This is just 5.5% of the total number of RBPs identified for the flg22 vs mock samples (440). For Arabidopsis, 112 of the 1135 leaf

RBPs were identified by Bach-Pages et al. (2020) at the 2h time-point (also at FDR ≤ 0.1) which is 9.9% of the total. Given the reduced amount of RBPs captured by ptRIC applied to quinoa leaves, the discrepancy in the resolution of flg22-induced RBPs achieved between the datasets is understandable.

To gather functional insight on the flg22-responsive RBPs, the UniProt online database was used to call GO annotations via the UniProt identifiers for each RBP (Fig.18B). Out of the activated RBPs, three were annotated with the GO term 'RNA-binding', one was annotated with translation-structural GO terms (ribonucleoprotein complex; ribosome; structural constituent of ribosome; translation) and three were annotated by redox terms (oxidoreductase activity, acting on NAD(P)H, quinone or similar compound as acceptor, electron transfer activity and oxidoreductase activity, acting on a sulfur group of donors, disulfide as acceptor). One of the four strongly inhibited RBPs was annotated with phosphorylation (serine/threonine kinase) activity which could be involved in supporting specific phosphorylation signalling patterns, and which was also annotated with ATP-binding. Two of the activated RBPs were also annotated with ATP-binding, including and ATPase and heat shock protein (Fig.18.B).

A



B

qval	Quinoa_UniProt_ID	Quinoa Protein names	Gene Ontology (ALL terms)	logFC
0.00076	A0A803MH62	DUF4408 domain-containing protein		-8.1
0.00079	A0A803M2S3	Protein kinase domain-containing protein	ATP binding [GO:0005524]; protein serine/threonine kinase activity [GO:0004674]; protein phosphorylation	-7.0
0.0008	A0A803MKU5	Pentatricopeptide repeat-containing protein		-6.7
0.0008	A0A803LUY3	NAD(P)H-quinone oxidoreductase subunit N, chloroplastic	membrane [GO:0016020]; oxidoreductase activity, acting on NAD(P)H, quinone or	6.5
0.0015	A0A803LLQ2	PP28 domain-containing protein		4.3
0.0028	A0A803M4L5	Nucleolin-like	RNA binding [GO:0003723]	5.6
0.00318	A0A803N6L7	Mitochondrial uncoupling protein 1	integral component of membrane [GO:0016021]; mitochondrial membrane [GO:0031966]; mitochondrial transport [GO:0006839]	-6.5
0.00348	A0A803MTV1	60S ribosomal protein L23	ribonucleoprotein complex [GO:1990904]; ribosome [GO:0005840]; structural	4.6
0.0037	A0A803LX13	Pentatricopeptide repeat-containing protein		4.2
0.00485	A0A803MES7	YTH domain-containing protein	RNA binding [GO:0003723]	6.1
0.00584	A0A803MU40	14_3_3 domain-containing protein		4.0
0.00666	A0A803LVD9	Phytocyanin domain-containing protein	electron transfer activity [GO:0009055]	4.3
0.01173	A0A803MNF5	RRM domain-containing protein	RNA binding [GO:0003723]	4.1
0.01369	A0A803LIT2	Thioredoxin domain-containing protein	oxidoreductase activity, acting on a sulfur group of donors, disulfide as acceptor [GO:0016671]	4.6
0.02487	A0A803LU25	Mitochondrial carnitine/acylcarnitine carrier-like protein	integral component of membrane [GO:0016021]	4.6
0.03735	A0A803MPN5	Plasma membrane ATPase (EC 7.1.2.1)	[GO:0016021]; plasma membrane [GO:0005886]; ATP binding [GO:0005524]; ATP hydrolysis activity [GO:0016887]; P-type proton-exporting transporter activity	5.6
0.04282	A0A803LEM3	Heat shock 70 kDa protein 14	ATP binding [GO:0005524]; ATP-dependent protein folding chaperone [GO:0140662]	3.4

Fig.18. Response of the quinoa RBPome to flg22 perception. (A) The Volcano plot depicts the direct comparison of 2h flg22-treated vs mock-treated cross-linked samples. Proteins (dots) are distributed

by L2FC and significance and representative of three biological replicates. Red and orange proteins represent the RBPs stimulated upon flg22 perception, whereas dark blue and light blue represent RBPs inhibited upon flg22 perception. The colours of the dots also indicate the significance of the protein's differential response to flg22: red indicates an FDR ≤ 0.05 and L2FC [flg22/mock] > 0, orange when FDR ≤ 0.1 and L2FC [flg22/mock] > 0, then dark blue indicates an FDR ≤ 0.05 and L2FC [flg22/mock] < 0 and light blue an FDR ≤ 0.1 and L2FC [flg22/mock] < 0. Non-significant proteins are coloured in grey. (B) Summary table of the 13 flg22-stimulated (red cells; FDR < 0.05) and four flg22-inhibited (blue cells; FDR < 0.05) RBPs in quinoa, ordered by decreasing significance (qval), with protein name and GO ontologies (where possible) obtained through the UniProt database.

2.2.3.2. Comparison of the quinoa flg22-RBPome to the Arabidopsis flg22-RBPome reveals little overlap (and could not be used to retrieve additional putative flg22-responsive RBPs)

It was hypothesised that the low number of statistically significant RBPs found for quinoa could be due to relatively higher levels of noise due to the smaller sample size owing to technical (or biologically related) limitations in the quinoa ptRIC RBPome capture, or due to the comparably smaller differences in L2FC changes between the flg22 and mock in quinoa, a feature seen throughout the PTI assays performed in this chapter. To search for additional putative flg22-responsive RBPs in quinoa a cross-species comparison was next made with the higher resolution flg22-RBPome dataset from Arabidopsis. It was hypothesised by RIC expert collaborators Dr Alfredo Castello & Dr Wael Kamel (University of Glasgow) that if non-significant flg22-induced quinoa RBPs showed the same direction of activity as high confidence flg22-induced Arabidopsis RBPs then they may represent additional candidate flg22-stimulated RBPs in quinoa (whose significance was missed originally due to the aforementioned 'noise' in the dataset) (Fig.20).

To do this, all candidate flg22-responsive RBPs from Bach Pages et al. (2020) (including those identified at 2h and 12h flg22 timepoints and at the two confidence levels FDR < 0.20 and FDR < 0.05) were compared to the complete list of unfiltered differentially activated RBPs for quinoa (i.e., the shared but differentially regulated RBPs between quinoa flg22 and mock datasets) (Fig.19). Importantly, these RBPs were not filtered by qval in order to maximise the space for capturing additional RBPs in quinoa. This approach can be justified when considering the FDR for these RBPs represents the statistical difference in the *detected* RBP

peptide intensity (interpreted as RBP activity; Bach-Pages et al., 2020) between flg22 and mock only.

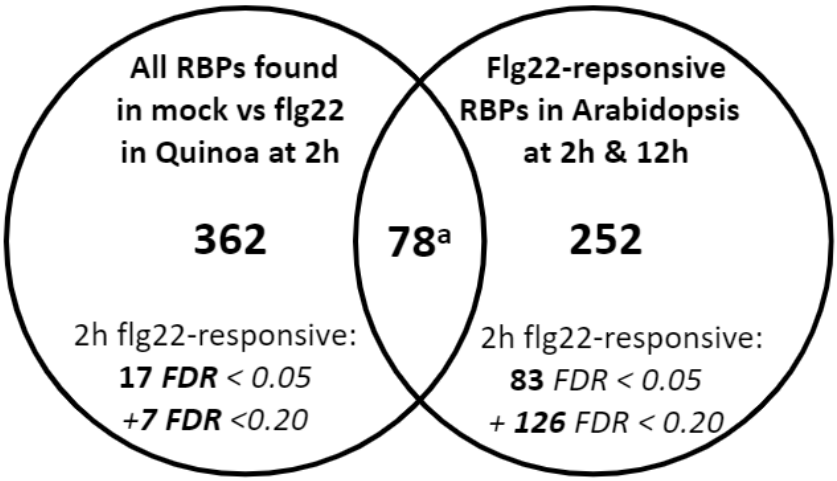


Fig.19. Comparisons of quinoa RBPs against the flg22-responsive RBPome of Arabidopsis. The shared RBPs between quinoa and the flg22-responsive RBPs in Arabidopsis are shown by the intersect, where the [a] signifies how of the 78 shared RBPs, none were found to be jointly significant at FDR < 0.05 under 2h flg22 treatment in both species. Number of RBPs at two significance thresholds are shown for 2h flg22 treatment for each species.

Just 78 shared RBPs were found between the datasets and only three of the 24 statistically significant flg22-responsive RBPs in quinoa were also found in the Arabidopsis flg22-RBPome (Table 1) all of which were significant at the later time-point 12h rather than 2h. 18 shared RBPs which had an FDR < 0.05 and an additional 23 shared RBPs at the FDR < 0.2 threshold were found at the 2h timepoint in Arabidopsis.

Table 1: Identities of the three shared flg22-responsive RBPs in quinoa and Arabidopsis

Protein ID(s)	L2FC Quinoa 2h	FDR Quinoa 2h	Percent Identity match	L2FC Arabidopsis 2h	FDR Arabidopsis 2h	L2FC Arabidopsis 12h	FDR Arabidopsis 12h
Q9LFF1	**4.25**	**0.004**	**69.1**	**-0.26**	**0.383**	**-0.80**	**0.012**
P19456 F4JPJ7	**5.55**	**0.037**	**87.1**	**0.54**	**0.346**	**2.09**	**0.002**
P54609Q9L ZF6Q9SCN8	3.72	0.056	90.1	0.35	0.664	1.32	0.088

Out of a list of 20 RBPs which were both upregulated in both species, six were statistically significant for Arabidopsis 2h FDR < 0.05 and one RBP (AT4G30190) was found at FDR < 0.05 for quinoa, with an additional candidate RBP (AT5G03340) at FDR = 0.056. The RBP AT3G53700 was found to have a large positive L2FC of +4.25 in quinoa (FDR = 0.0037) but a modest negative L2FC of –0.26 for Arabidopsis (FDR = 0.38 at 2h and FDR = 0.012 at 12h) (Table 1).

The distribution of the direction of activity of the 78 shared flg22-induced RBPs between quinoa and Arabidopsis is visualised in Fig.20, where mutually upregulated and downregulated candidates are highlighted. The RBPs which were both reduced in intensity/downregulated in response to flg22 in both species (blue dots in bottom left quadrant) had minor L2FC values and none were significant in quinoa (the lowest FDR = 0.89), so it none of these shared mutually downregulated RBPs should be considered flg22-responsive candidates. Looking at the top left quadrant, no downregulated RBPs in quinoa were significant either and because they were opposingly regulated (activated) in Arabidopsis it further shows that these RBPs can be ignored. There were two RBPs which were non-significantly downregulated in quinoa and significantly upregulated in Arabidopsis: AT5G50920 (FDR = 0.046) and AT5G02500 (FDR = 0.010) but their L2FC changes were modest, 0.56 and 0.87 respectively so were discarded for further analysis also.

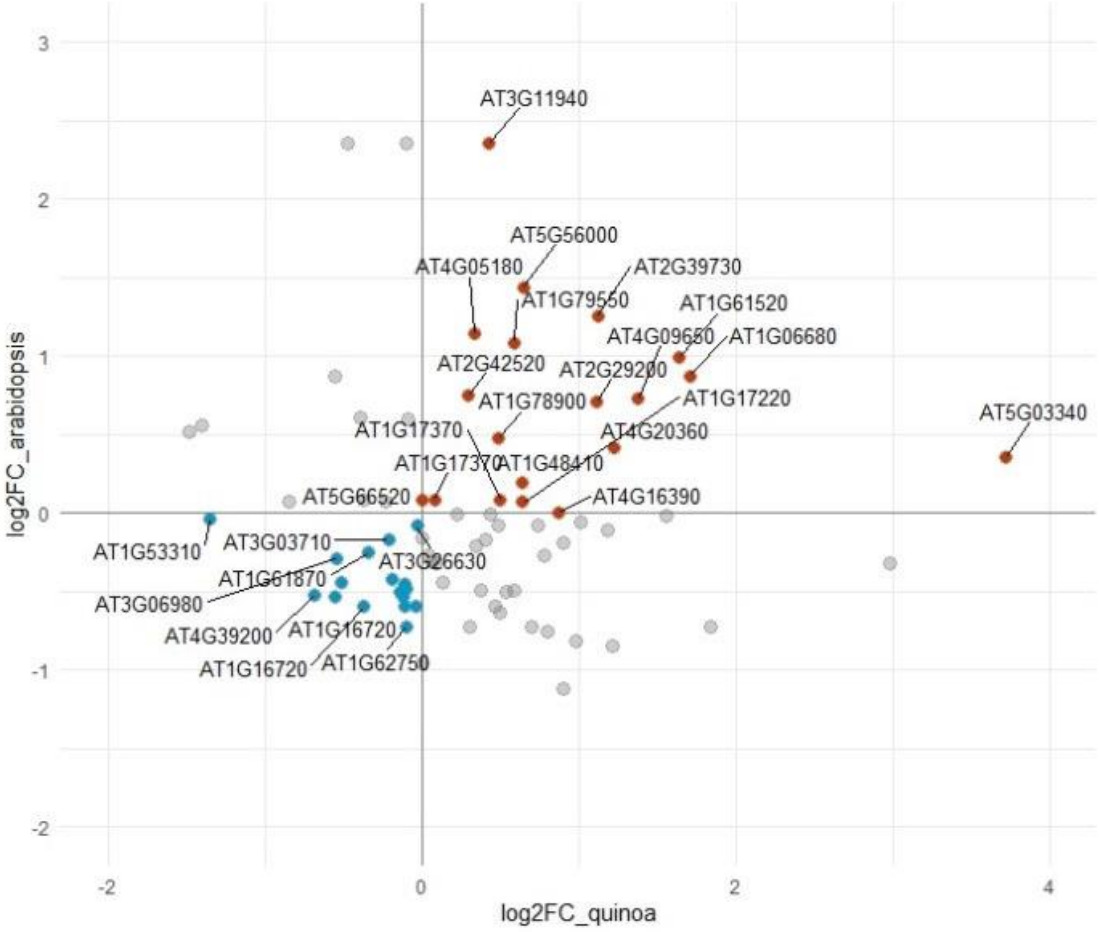


Fig.20. The distribution of the direction of activity of the 78 shared flg22-induced RBPs between quinoa and Arabidopsis. Red dots highlight the shared positively activated RBPs, and the blue dots highlight the shared downregulated RBPs, with their AtGene IDs shown. The plot was created in R.

2.3. Discussion

The objectives of this chapter were to apply routine biochemical, transcriptional and novel proteomic PTI assays to quinoa to evaluate the responses of this halophyte to different PAMPs and how they compare with the model species Arabidopsis. Two novel transcriptome and proteome-level datasets for PTI responses in quinoa were generated and initial bioinformatic analyses conducted. For the first time to our knowledge, quinoa's molecular PTI immune responses were studied and across several regulatory levels. Canonical features of plant PTI such as the oxidative burst, MAPK activation, callose deposition and upregulation of peroxidase activity were observed in quinoa, with the first two responses found for all PAMPs

tested (bacterial elicitors flg22 and elf18 and the fungal cell-wall/insect cytoskeleton components chitin and chitosan), but with differing measurable levels of intensity relative to Arabidopsis. Most striking differences between the species were found in the 2h transcriptional and RBPome responses to flg22 which are contextualised in the following sections.

2.3.1. Quinoa's PTI responses show a mix of expected, unexpected and novel results relative to Arabidopsis

As mentioned in the introduction, the ubiquitous and slowly evolving nature of PAMPs and their cognate plant receptors meant that it was expected that quinoa would also show signs of downstream signalling events from cell surface PRRs. The suite of biochemical assays used were useful here, where at least one positive downstream response was found for each PAMP suggesting that quinoa has evolved functional FLS2, EFR, LYK5/CERK1 PRR orthologs for flg22, elf18, chitin and chitosan perception. Arabidopsis was run in parallel as a positive immune response control and so that results could be validly compared for evaluating species similarities and differences.

Considering MAPK signaling cascades and ROS are two of several key abiotic-stress transducers (Raja et al., 2017) it was interesting to observe their evident role in quinoa's biotic stress signaling and response. Compared to Arabidopsis, quinoa appeared to use alternative MAPK homologs showing a prioritized engagement of MAPKs of higher molecular weight than Arabidopsis. Previous studies in quinoa had profiled various MAPK orthologs during seed germination under control and highly saline conditions and found that quinoa displayed a dynamic and highly complex MAPK activation signatures (Pitzschke, 2018). MAPK activation can also be triggered by mechanical stress such as that from rain or insects and Matsumura et al. (2022) demonstrated how Arabidopsis trichomes act as mechanosensory cells that transduce stress through MAPK signalling. Given how quinoa leaves are covered with enormous halophyte-specialised trichomes, EBCs, it will be necessary to consider the potential mechano-activation of MAPKs and continue to include zero damage controls in future experiments. Further work using structurally more specific monoclonal (rather than polyclonal) antibodies paired with additional abiotic stresses and higher concentrations of salt could be used to delineate more precisely potential signaling differentiation between PAMPs

and abiotic stresses by specific MAPK homologs or protein isoforms. Quinoa's ROS burst was evaluated using the 96-well plate ROS assay using the sensitive L-012 probe which allowed the non-specific measurement of apoplastic ROS. The specific type and spatiotemporal dynamics of ROS generated could therefore be further elucidated using ROS-species specific differential staining and POX selective chemical inhibitors such as potassium cyanide or sodium azide to isolate RBOH dependent superoxide generation (O'Brien et al.,2012).

The biochemical assays could be further supplemented with bioinformatic analyses using available reference genomes and quinoa transcriptomes beyond the analyses performed in this chapter. For example, Orthofinder (Emms and Kelly 2019) could be used to query the presence of orthologs for key components of PTI which may have been missed due to the single 2h time points used here, or as a way to orthogonally validate results, as was exemplified for the elf18 EFR receptor.

Receptor gene copy number and qRT-PCR gene expression profiles could be evaluated using various concentrations of PAMPs to provide higher resolution of quinoa's sensitivity and amplitude of response to different PAMPs which could then add molecular evidence to quinoa's major evolutionary biotic pressures.

We noticed repeatedly that oxidative responses such as the ROS burst and POX upregulation were notably subtler, delayed and less reliably induced in quinoa compared to Arabidopsis. This suggests that quinoa may have a greater heterogeneity within its leaf tissue or that a higher biological variability exists between individual plant replicates or that quinoa leaf tissue has a higher threshold for triggering a response due to genetic or inducible differences in RBOH/peroxidase enzyme production or activity. Comparing our POX results to other crop species such as tomato and bell pepper studied by other groups it was also found that significant POX upregulation was observed at later timepoints relative to Arabidopsis (20 h rather than 16 h) (Mott, Desveaux and Guttman, 2017). Quinoa also showed differential responses to different PAMPs which could be an inherent feature of the plant's immune system which could be further elucidated by conducting dose-response experiments and repeating downstream response assays such as callose deposition for the extended PAMP panel. The positive callose deposition response was perhaps the most expected PTI response

given its key role against haustorium-forming pathogens such as the oomycete *Perenospora variabilis* for halting further cell wall penetration (Ellinger et al., 2013).

The most unexpected and novel results were revealed at the transcriptome and proteome level. Specific genes might not be the same, but it was expected that more commonalities may be found at the global functional level (Subramania et al., 2005). However, only two enriched GO terms for quinoa were directly related to biotic stress responses, whereas five were found in Arabidopsis and further disparity was found at the gene level where a third of all shared genes were opposingly regulated, suggesting how quinoa has evolved unique immune features. To understand how many of these are due to quinoa's halophytic adaptations, either as constitutively expressed or inducible features, a comparison to quinoa's salt-acclimated and combined stress transcriptomes is needed. Expected PTI signatures such as the downregulation of photosynthesis were however found at the transcriptional level suggesting a shift of resources towards pathogen defence is maintained in quinoa (Amrine et al., 2015).

The RBPome of quinoa was hard to capture probably due to tissue differences, for example, thicker cell walls and a higher content of UV-protecting phenolics as well as light-diffracting EBCs (Hinojosa et al., 2018; Shabala et al., 2012; Imamura et al., 2020) and there was insufficient time to optimise the ptRIC protocol for higher yields. 375 RBPs represent the background (mock-treated) RBPome for quinoa, which is a comparable number to the RBPome of rice (370 RBPs) and bean (420 RBPs) (Bach-Pages et al., unpublished) and further highlights the need for species-specific ptRIC optimisations. This more limited number of RBPs was further complicated by the unexplainable loss of material for one of four biological replicates for flg22 between the internal protein purification step and externally sourced Mass Spectrometry analysis step. The proportion of flg22-induced RBPs as a proportion of the total number of constitutively expressed 'basal' quinoa RBPs was however similar. When comparing the unfiltered flg22-induced RBPs between quinoa (2h) and Arabidopsis (2h plus 12h) only three candidates were shared, none of which were significant for Arabidopsis at the 2h time point suggesting further temporal PTI differences exist between the two species. Curiously, the shared flg22-induced candidate RBP with the highest significance (FDR < 0.05) showed opposing regulation between the two species: a chloroplastic RBP, with description pentatricopeptide repeat (PPR)-containing protein and MATERNAL EFFECT EMBRYO ARREST

40 (gene ID and Uniprot identifier: AT3G53700 and Q9LFF1), showed a +4.25 L2FC in quinoa (FDR = 0.004) and –0.80 L2FC in Arabidopsis (FDR = 0.012). Bach-Pages et al., 2020 had previously identified a larger proportion of RBPs localising to the chloroplasts than anticipated, and PPR domains were also one of the more prominent non-classical RNA-binding domains found. Lastly, future work could compare the intensity of flg22-induced RBPs in quinoa ("eluates") with their existence and intensity in their corresponding whole cell proteome samples ("inputs") as was done by Bach-Pages et al. (2020). These analyses could also provide further evidence for "moonlighting" RBPs, enzymes with alternate roles such as peptidyl-prolyl cis-trans isomerases, heat shock proteins, or mono- or di nucleotide-binding proteins [ATP/ADP, NADP/NADH] but which also act as RBPs when activated by flg22. The two latter functional descriptions were also found enriched in the small sample of significantly activated RBPs in quinoa. Specific analysis of the inputs vs eluates samples is work still in progress with our collaborator lab at the University of Glasgow.

2.3.2. Oxidoreductase activity plays an important role in quinoa's biotic stress response

Out of the small number of flg22-responsive RBPs found, a majority were annotated by redox terms such as oxidoreductase activity, acting on NAD(P)H, quinone or similar compound as acceptor, electron transfer activity and oxidoreductase activity, acting on a sulfur group of donors, disulfide as acceptor. This was also reflected at the transcriptional level, where the oxidoreductase term was also significantly enriched with a large number of genes annotated including cytochrome P450s, flavanone 3-hydroxylase, cinnamyl alcohol dehydrogenase 4 and glutathione S-transferase-like and naringenin-oxoglutarate 3-dioxygenase-like. The latter two genes were also represented in the overall top 20 flg22-upregulated genes in quinoa.

Interestingly glutathione S-transferase-like, putative receptor-like protein kinase At4g00960 and 7-deoxyloganetin glucosyltransferase-like also had gene copies which were significantly downregulated, suggesting quinoa's allotetraploid genome may contain homeologs (owing to the hybridisation of its ancestral species) with functional divergence.

The ROS-generating NADPH Oxidase RBOH, previously assayed biochemically through the ROS burst assays, is also shown to be upregulated, confirmed through evaluating positive L2FCs of quinoa RBOH genes, for which three out of eight putative homologs were

significantly induced. Only two however had orthologs in Arabidopsis: LOC110722611 (AT1G64060; RBOHF) and LOC110719599 (AT4G11230; RBOHI), expressed at +1.25 ($P < 0.001$), and +0.54 ($P < 0.05$) respectively. Interestingly, the RBOHF NADPH oxidase isoform (one of a total of 10 RBOH genes in Arabidopsis) has been shown to play a critical role in the soil-salinity tolerance of Arabidopsis: its root localised expression and ROS generation helps limit Na^+ uptake to maintain favourable shoot Na^+/K^+ homeostasis and is part of the plant's ethylene mediated salt tolerance (Jiang et al., 2012 & 2013). Canonical features of the MAPK signalling pathway were also further highlighted through KEGG Pathview analyses which organised DEGs into sequences of known stress response components as visual pathways where the many opposing differences in expression observed further suggests that conventional biotic and abiotic stress MAPK-signalling pathways are differentially engaged between quinoa and Arabidopsis. For example, a quinoa homolog of the immune central MPK6 kinase and TF WRKY33 were downregulated and the one key WRKY33 target shown PAD3, which is responsible for synthesising the antimicrobial camalexin, was found to be absent in the quinoa DEG list (Zhou et al., 1999).

2.4. Conclusion

In conclusion, quinoa's immunity includes canonical features of PTI, with differential responses to the PAMPs tested and to Arabidopsis which could be reflective of historic differences in quinoa's exposure to native microbial stresses. Whilst several layers of PTI regulation and responses were evaluated in this chapter, many more features exist and should next be explored and at additional time-points. Of particular interest would be calcium signalling and stomatal responses given their involvement in ABA/abiotic stress responses. Future work could also evaluate the response of quinoa to exogenous hormone treatment such as SA and JA to see what immune defence responses are specifically induced and how they compare to vast work done in Arabidopsis (Berens et al. 2019; Mur et al., 2006). The canonical PTI features found present in quinoa through this chapter are summarised by Fig.21., which is an updated version of Fig.1.

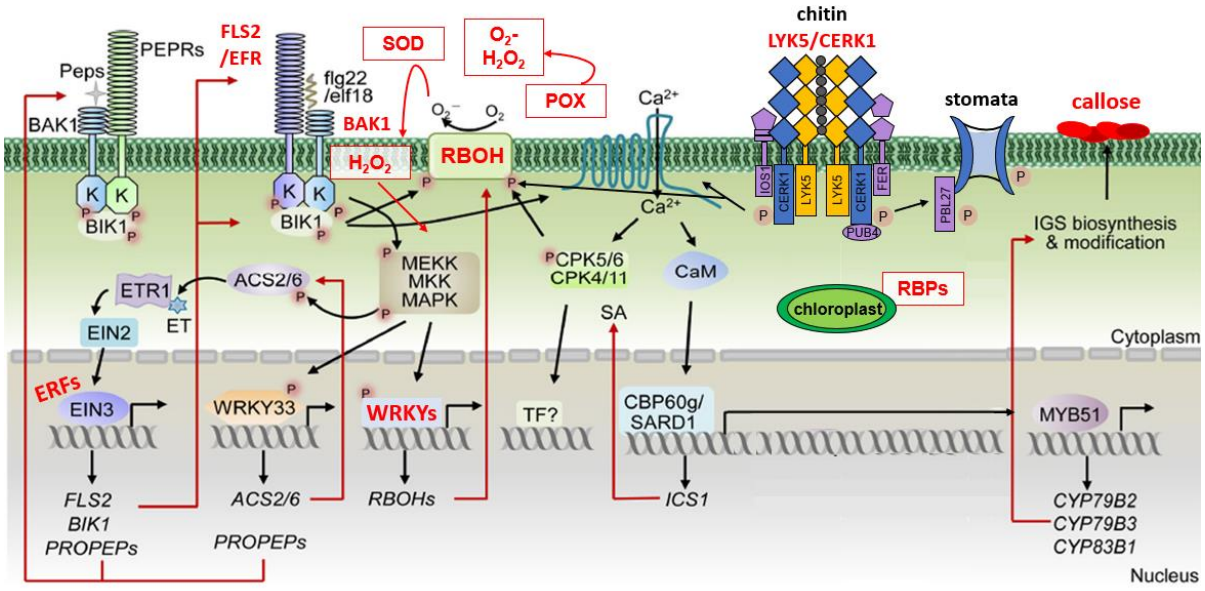


Fig.21. Updated figure adaptation showing core PTI components and signalling events of plants. This figure originally shown in Fig.1 now includes additional components relevant to quinoa's PTI response, highlighted in red text since their observation in quinoa. These include a positive chitin response via MAPK and ROS signalling, where the PRR LYK5 and co-receptor CERK1 have since been cross-validated through OrthoFinder/BLASTp results and through observing a subtle but significant flg22-induced upregulation of CERK1 in soil-grown flg22 treated quinoa. The FLS2 and EFR PRRs were also found to be functional. Outstanding features to investigate are shown including the role of calcium signalling and stomatal responses. The identity of proteins in black text originating from the original figure by Li et al. (2016) have not been changed. A role for WRKY TFs and ERFs was also found through the transcriptomics experiment and are shown in red, whereas ptRIC revealed the role of chloroplastic RBPs (shown in association with a chloroplast for clarity) as per their functional description.

But of these responses queried, what would be the most indispensable PTI factors for quinoa? It is logical to think that such core PTI genes could represent core general stress genes for quinoa that remain intact even in the presence of salt, or other environmental stresses. Distinguishing core PTI genes and core general stress genes would be highly advantageous for developing combinatorial stress tolerant cultivars; if quinoa's abiotic hardiness could be extended to improve its comparably weak biotic stress resilience, then a major aspect for boosting the crop's yield security would be provided.

2.5. Methods

Plant material and growth conditions

Quinoa seeds of the Atlas variety were used for all experiments, and provided by
The British Quinoa Farm, Shropshire, England in 2018 (harvest date 2016) from which plants were cultivated to seed in the Oxford Greenhouses and harvested in the summer of 2018.
Plants used for PTI experiments were grown in the greenhouse for 4-5 weeks under 16h day/8h night in a ratio of 4:1 M2 soil: medium size vermiculite. 3 seeds per $8cm^2$ pots were sown and thinned at 1 week to 1 plant per pot, with 8 pots per tray which were watered 3 days per week as 1-inch into the trays.

Chemicals

Flg22 (Anaspec), Chitin (Sigma), Chitosan (Sigma), Elf18 (a collaborator), horseradish peroxidase (HRP) enzyme (Thermo scientific), 5-aminosalycylic acid (Sigma), hydrogen peroxide (Sigma), L-012 (Sigma), NaOH (Sigma), Aniline blue (Sigma), K_2HPO_4 (Sigma), Ethanol (Sigma), Acetic acid (Sigma).

MAPK

The assay performed was based on Flury et al. (2013), with the following amendments:
4 x 4.5-week-old plants with 2 equivalent fully expanded leaves were chosen and 4 x 1cm Ø leaf discs were harvested (2 from each leaf half avoiding veins). Leaf discs were soaked in water overnight under continuous light to remove the wounding response. Pre-equilibrated leaf discs were carefully transferred into individual wells (3 per well) of a 24 well plate containing 500 µL of elicitor solutions and left for 30 minutes, elicitor concentrations were: 1 µM for flg22 and Elf18 and 50 µg/ml of chitin, or mock (Milli-Q water) or 500 mM NaCl. A damage control sample was also included whereby exaggerated pressure was applied to the edge of the mock-floated leaf discs using the same tweezers and technique used for handling the leaf discs, making sure not to break the tissue. After 30 minutes samples were quickly but carefully removed from the well and placed in safe lock 2 mL eppendorfs containing 2 metal beads and frozen on liquid nitrogen. Proteins were extracted and normalised by sample weight before loading on a 12% SDS gel and the western blot followed standard procedures (Bass et al. 2017) using the anti-ERK1p42/p44 antibody. The blot was imaged via chemiluminescence captured on LAS4000 (GE Healthcare Life Sciences).

ROS

The relative intensity of ROS production was measured using the L-012 -based assay (Melcher and Moerschbacher, 2016) and chemiluminescence readings were taken continuously over 90-minutes using a TECAN plate reader (following script used in Buscaill et al., 2019). 150 µl of elicitor solutions used were: flg22 (100 nM), elf18 (100 nM), chitin (50 µg/ml), chitosan (50 µg/ml) or mock (150 µl Milli-Q H2O). 0.4 cm Ø leaf discs were harvested from fully expanded leaves and soaked in water overnight under continuous light to reduce the wounding response before their careful transfer into an opaque 96 well-plate using a P200 pipette end as a lever to minimise damage. The plate was set-up in rows of treatments and a multichannel pipette used for simultaneous delivery across treatments.

POX

This assay was performed according to the protocol by Mott et al. (2017). Amendments include: 0.4cm Ø leaf discs from 4.5-week-old quinoa and Arabidopsis were incubated in elicitor solutions: flg22 (100 nM), chitin (50 µg/ml), elf18 (100 nM) or mock (Milli-Q H2O) then removed before quantifying POX activity via the chromogenic reaction between 5-aminosalicylic acid and hydrogen peroxide. The reaction was quenched at 2 minutes with 1M NaOH in for Arabidopsis and at 4 minutes for quinoa. Total activity was quantified by absorbance at 600 nm using a TECAN plate reader.

Callose

Protocol was adapted from Schenk S et al., 2015. 4.5-week-old short-day grown quinoa and Arabidopsis plant leaf halves were syringe-infiltrated with 1 µM flg22 or Milli-Q (mock) using a needleless syringe. After 24 hours whole quinoa and Arabidopsis leaves were harvested at the petiole and treatment samples (5 per treatment) were pooled into labelled 50 mL falcon tubes, for quinoa, leaf size was reduced to 4 cm^2 squares around the infiltrated area for ease of handling. Samples were fixed and cleared of chlorophyll in 1:3 solution of acetic acid at 50*C for 1h (Arabidopsis) and 2h (quinoa, including a solution refresh). The solution was replaced again, and the samples left at room temperature until leaves were white-translucent. Half the solution was poured out and Milli-Q water added and left for 10 mins, this was repeated once more until samples were being rinsed in 100% Milli-Q, ensuring a gradual reduction of brittleness of the leaves and to fully remove the acid. The Milli-Q was

replaced with 150 mM K_2HPO_4 and left for 1 hour, before it was replaced with the 0.01% aniline blue stain (dissolved in 150 mM K_2HPO_4 solution). The falcon tubes were wrapped in foil and placed in a dark box and left overnight. Leaves were mounted in 40% glycerol and visualised immediately. The microscope Olympus B201 with a WU fluorescence cube (excitation filter BP330-385 nm, barrier BA420 nm) at 20x magnification was used with a QICAM Fast 1394 colour camera to acquire digital photos.

RNA-sequencing experimental design, sample preparation and sequencing (via Novogene)

A randomised block design was used to split 4.5-week-old soil-grown quinoa plants into 4 blocks for staggered infiltration with 1 µM flg22 via a needleless syringe. Each set of leaves was then harvested at the petiole with a scalpel exactly 1.95 hours later, placed on ice for 5 minutes and snap frozen in 50 mL falcons in liquid nitrogen at exactly 2h for storage at -80°C. Four biological replicates for each treatment were sequenced. *RNA extraction*: first, frozen leaves were ground to a fine light green powder using a sterile mortar and pestle under liquid nitrogen. Total RNA was isolated from ground tissue using the Monarch® Total RNA Miniprep Kit following the manufacturer's instructions, where columns were loaded twice to maximise yield of RNA from each sample with minimal trade-off with sample end purity. *RNA QC:* total RNA amount and purity was measured using the NanoPhotometer® spectrophotometer giving values >100 ng/µL and A260/A280 > 2.0 and A260/A230 >1.6 respectively. RNA integrity (RIN) was evaluated using an Agilent 2100 BioAnalyzer with Nano6000 kit and RIN values were sufficiently high >7.5 (ranging from 7.6-8.1). Subsequent steps were performed by Novogene, Cambridge: *Preparation of sequencing libraries:* using the NEBNext® Ultra TM RNA Library Prep Kit for Illumina® (NEB, USA) mRNA was purified via positive selection from total RNA using poly-T oligo-attached beads, cDNA synthesis was performed using NEBNext reagents and library fragments were purified with AMPure XP system (Beckman Coulter, Beverly, USA). *Library quality* was assessed on the Agilent Bioanalyzer 2100 system. *Sequencing:* Paired-end sequencing of read length 150-bp at a depth of 20 million reads per sample was performed using Illumina NovaSeq6000 to produce 6GB of data. *Data quality check and filtering*: Raw reads of FASTQ format were processed through fastp to remove reads containing adapters, poly-N sequences (N>10%) and reads with low quality nucleotides (where base quality < 5 for > 50% read), so that all samples had > 97% Q20 > 92% Q30.

RNA-seq data bioinformatic analysis

Mapping reads and quantifying transcripts: a virtual Conda environment was used to perform QC on the cleaned raw reads via fastqc and then kallisto was used to pseudo-align them to the *C. quinoa* reference transcriptome for cultivar QQ74 (Jarvis et al.,2017) and transcripts were quantified. The reference transcriptome assembly and gtf annotation file were obtained from the NCBI site.

The following steps were all performed locally in R. The R Bioconductor package DESeq2 (Love MI, Anders S, Kim V, Huber W 2014) was used to normalise the count data, perform sample-level quality control and DEG analysis as well as shrinkage of the L2FC values via the apeglm method (Love, Zhu & Ibrahim, 2018). Genes with an adjusted P value < 0.05 and |fold change|>1 i.e., a |L2FC| > 0.2 found by DESeq2. *Enrichment analysis:* the quinoa transcripts were mapped to the TAIR Arabidopsis reference transcriptome using BLAST with an expected value cut of e ≤ 0.001. Then biological gene ontologies GO terms (biological processes, molecular functions, and cellular component) and pathway enrichment information Kyoto Encyclopaedia of Genes and Genomes KEGG terms were called for the genes (now identified using Arabidopsis geneIDs) using the R BiocManager package clusterProfiler and gene set enrichment analyses GSEA was performed (adjusted *P value < 0.05*) to identify significantly enriched functions. DOSE package was used for visualisation of results. DEG and GSEA analysis were performed at $P < 0.05$. *Gene level analyses:* genes in the core enrichment column from the GSEA outputs were extracted and further gene description information was called from the full DEG lists in R. DEG list comparisons to Arabidopsis were done in R and data generated were visualised and explored further using R or Excel.

Plant Interactome Capture (ptRIC)

The same block of plants used for RNA-seq were utilised here, where during the 5 minutes on ice the cross-linked samples were exposed to UV light at 254 nm to promote crosslinking between RNA and proteins that are in intimate contact. The remaining ptRIC procedure was done exactly as reported in Bach-Pages et al. (2020) (UV Crosslinking, Cell Lysis, Oligo(dT) Capture, Downstream Applications of Isolated RNA–Protein Complexes including Silver Staining and Filter-Assisted Sample Preparation for Mass Spectrometry). One key amendment to the protocol was made, whereby the first round of interactome capture on Oligo(dT) beads

lasting usually 1 hour was extended to a long (16 h) incubation period as this was found to substantially increase RBP yield for quinoa. Parameters for statistically analysing the peptides found from MS are shown by the figure below, analysed by Dr Wael Kamel, University of Glasgow according to the analysis pipeline used in Bach-Pages et al., 2020.

Search and analysis parameters:

- Nobiorep2
- MatchBetweenRun: ON
- Normalization: default VSN
- Imputation: Global mindet for ON/OFF proteins
- Pvalue:Limma testing with Block setting
- FDR: fdrtools with qval

Samples Names

CTRL CL
"Intensity.02"
"Intensity.10"
"Intensity.14"
Flg22 CL
"Intensity.04"
"Intensity.12"
"Intensity.16"

Chapter 3: Establishing saline phenotypes in the European Quinoa variety Atlas

3.1. Introduction

3.1.1. Land salinization and food security solutions with halophytic crops

Land salinization is a serious threat to agriculture. In 2015 the damage was calculated to affect 20% worldwide and is only predicted to intensify with climate change, the continuation of unsustainable irrigation practises and a need to expand food production into more marginal lands to keep up with population growth (Mickelbart et al., 2015; Zeng et al., 2018). Halophytes are naturally salt-tolerant plants which have evolved unique strategies for thriving under high salinity (200 mM NaCl upwards) and thus offer promising solutions for food security if edible. Halophytic crops include the nutritious pseudocereals quinoa and amaranth and vegetables wild beet, capers and wild tomato species *S. pennellii* which maintain high yields where other crops fail to grow (Egea et al., 2023; Petropoulos et al., 2018).

Furthermore, halophytic species are often richer in antioxidants (e.g., vitamin C and phenolic compounds) and contain higher proportions of key minerals and trace minerals due to their enhanced selective capacity to uptake and sequester inorganic ions, heralding them as new functional foods (Srivarathan et al., 2023; Lombardi et al., 2022; Agudelo et al., 2021; Petropoulos et al., 2018). Some halophytes also produce high amounts of antimicrobial chemicals such as saponins, which has encouraged their use in traditional medicine (Petropoulos et al., 2018).

3.1.2. Salt stress adaptations

Salinity stress has a large and complex effect on many aspects of plant physiology due to the ionic and osmotically active properties of salt ions which ultimately limit plant growth (Kumari et al., 2015; Munns & Tester, 2008; Ruiz et al., 2017). The salt tolerance of glycophytes (salt-sensitive species) and halophytes largely depends on widely conserved responses: the maintenance of ion and redox homeostasis via a tight control over ion transport and an effective antioxidant system, and the resourceful utilisation and biosynthesis of osmolytes for osmotic adjustment (Munns & Tester, 2008; Volkov, 2015; Grigore and Vicente, 2023). However, the relative efficiency of these responses and the specific dependence on certain tolerance mechanisms over others varies widely across different species, and even between genotypes within the same species (Shabala & Mackay, 2011; Ruiz et al., 2017). For example, halophytes have evolved the resourceful capacity for using salt ions as 'free osmotica' to immediately counteract osmotic stress, whilst organic compatible solutes are also produced to higher amounts and include proline, polyols, glycine betaine and betalains which help maintain optimum cell turgor (Shabala, 2013; Ruiz et al., 2017; Petropoulous et al., 2018). Halophytes have also evolved adaptive traits for salt sequestration and compartmentalization into internal vacuoles and/or via external salt glands or bladder cells to prevent their disruption to the core metabolism of cells. Transcriptomic and metabolomic studies have suggested that halophytes constitutively express certain stress tolerance genes typically induced in glycophytes reaching a state of "stress-anticipatory preparedness" (Kazachkova et al., 2018; Ruiz et al., 2019; Taji et al., 2004; Gong et al., 2005).

With an increasing demand for salt-tolerant crops and the development of new improved research techniques many halophytic adaptations have been revealed at the molecular level.

This is thanks to the availability of genome sequences and transcriptional datasets for halophyte models such as *C. quinoa, Atriplex hortensis* and *Mesembryanthemum crystallinum* (Jarvis et al., 2017; Hunt et al., 2020; Shen et al., 2022) and the applicability of techniques such as advanced transmission electron tomography, orthologous transport protein expression systems, electrophysiology techniques, and/or fluorescent tracer ion flux studies which have directly resolved solute flow at the cellular level (Bazihizina et al., 2022; Kiani-Pouya et al., 2017; Bohm et al., 2018).

3.1.3. Salt tolerance mechanisms in quinoa

Salt tolerance genes which underpin the sub-traits of ion homeostasis, osmotic balance and ROS regulation are categorised by function: controlling the rate of salt uptake, translocation, and compartmentalisation; adjusting ionic and osmotic balance; and regulating developmental processes especially at the leaf-organ-level for example by a 'slow growth phenotype' (Munns, 2005). Important ion genes in quinoa revealed over the years have largely been related to ion homeostasis, and include: two allelic variants for the canonical sodium transporter gene SOS1 which exist as distinct homeologs (cqSOS1A and cqSOS1B from the A and B sub-genomes of quinoa) were both found to contribute to salt tolerance via Na^+ elimination in roots (Maughan et al., 2009; Orsini et al., 2011); the Na^+ antiporter gene CqNHX1 (Na^+/H^+ exchanger 1) was shown to support ion homeostasis in leaves under high salt stress (Ruiz et al., 2016); and Böhm et al. (2018) identified two co-orthologs of AtHKT1 in quinoa, where CqHKT1.1 is predominately expressed in roots and CqHKT1.2 predominantly in leaves and induced significantly in response to salt, along with a Cl^- ion transporter gene CqClC-c.

As seen in Fig.7 of Chapter 1, quinoa leaves (and stems and petioles) are covered in enormous balloon-like osmolyte-sequestering specialised epidermal bladder cells (EBCs). The direct role of EBCs in quinoa's salt tolerance has been argued for and against by several groups over the last several years, where discrepancies could be due to the age of leaves tested and the differences between quinoa cultivars and techniques used (Ruiz et al., 2016; Kiyani-Pouya et al., 2017; Böhm et al. 2018; Kiyani-Pouya 2019; Otterbach et al., 2021; Kiyani-Pouya et al., 2022; Moog et al., 2022). The initial hypothesis was that, like *M. crystallinum,* quinoa EBCs act

as salt-sequestering ‘salt dumps’, alleviating the levels of salt in the leaf cell cytosol. However, recent studies by Moog et al. (2022) were not able to reproduce the high levels of Na^+ in EBCs found by Kiani-Pouya et al. (2017) and Bohm et al. (2018), nor were the significant increases in expression of key NHX1 transport protein found in EBCs and most significantly of all, an EBC-free mutant was found to be as salt tolerant as the WT. Moog et al. (2022) suggested that much higher salt is instead sequestered into leaf intracellular vacuoles. It is in wide agreement however, that K^+ plays an important role in EBCs (Hariadi et al., 2011; Turcios et al., 2021; Böhm et al. 2018; Moog et al., 2022) where recently Moog et al. (2022) showed a sharp increase from an already high 0.5 M in control conditions to 1.7 M K^+ under high salinity and that Cl^- also increased substantially, but from much lower starting levels, 10 mM which, following treatment with 400 mM NaCl increased to 800 mM NaCl. Old leaves of quinoa were also shown to accumulate higher proportions of Na^+ than intermediate and young leaves.

The role of osmolytes in quinoa were explored in the salt tolerant Chilean variety PRJ where high amounts of proline were found in response to 300 mM NaCl (Ruiz et al., 2016), and quinoa leaves have since been described as ‘proline factories’ able to increase levels 16-fold upon salt exposure (Kiani-Pouya et al., 2017). Quinoa’s extensive germplasm and agricultural niches have inspired explorations of genotype-dependent salt tolerance: Ruiz et al. (2016) compared coastal-lowlands with salares landraces to reveal similar polyamine (PA) and PA biosynthetic gene expression profiles, and strong induction of ABA biosynthetic enzyme NCED, however, the rate of induction of transcriptional changes was significantly faster for salt-tolerant salares varieties. These data suggest constitutive and inducible salt-induced defences vary among quinoa cultivars; it is interesting to speculate the stability of such defences in the context of new environments and in combination with other (biotic) stresses.

When revaluating the relationship between growth maintenance and salt tolerance traits for screening purposes, Agirresarobe et al. (2022) compared the previously identified tolerance mechanisms of succulence, osmotic adjustment, ion homeostasis and antioxidant metabolism between nine quinoa varieties from different origins and found variety-specific differences in the relative importance of each, except for antioxidant enzyme activity which underwent similar degrees of upregulation in response to salt stress across all varieties.

A recent study by Rasouli et al. (2023) looked at the role of guard cells (GCs) in the salt response of quinoa relative to related glycophytic species spinach. Genes related to ABA signalling, ABA biosynthesis, transporters of amino acids, proline, sugars, sucrose and potassium, the cell wall plasticity gene Pectin methylesterase3 and genes involved in the inhibition of stomatal development and differentiation were all found to be strongly induced in quinoa but not in spinach. The action of these genes collectively helped to improve quinoa's water use efficiency and support the observation of salinity-induced reduction in stomatal density previously documented by Shabala et al. (2012) and Kiani-Pouya et al. (2019). Kiani-Pouya et al. (2017) also found EBC density increased under saline conditions in the majority of 114 quinoa accessions screened irrespective of their variable salt tolerances.

3.1.4. Salt stress administration

Salt stress is known to affect different plant tissues and developmental stages to different extents and therefore careful experimental design using a range of concentrations, timings and modes of salt treatment/administration/exposure is critical. In-vitro seed germination and seedling root growth assays are space, resource and time-efficient systems routinely used for producing clear phenotypes (Jiang. et al., 2013; Raney et al., 2014), whilst full life cycle viability and yield studies are particularly useful for evaluating agronomic traits and often performed in soil-filled pots or in the field (Roman et al., 2020; Grigore and Vicente 2023). Hydroponic systems are best for bridging the gap between early growth and late growth stages, where vegetative developmental stages and sensitivity to different nutrients or ambient conditions can be controlled extremely tightly (Hoagland and Arnon 1950; Nguyen et al., 2016). All these strategies have been trialled in quinoa previously but given the differences in available growing resources, quinoa genotypes and underlying research questions, a mix of growing systems and salt application modes will be tested in this chapter. Another important consideration is the desired intensity of the salt stress imposed on the species. Salt stress can be achieved by gradual increments allowing acclimation, typical of natural scenarios, whereas a salt shock can be imposed by applying high concentrations directly, which results in distinct differences at the transcriptome and morphological levels, seen whereas salt shock induces toxicity and cell death (Skorupa et al., 2019). Salt stress is more valid therefore for elucidating salt adaptation mechanisms of plants. Likewise, one

simple and agronomically relevant method for ascertaining salt tolerance thresholds of a plant species is to compare the extent of growth inhibition (e.g. plant height or biomass) and visual signs of toxicity (e.g. leaf discolouration) across a range of salinities, and to decide on a level that causes for example 50% growth inhibition (reported as LD_{50} or EC_{50} values), or a significant reduction of other key phenotypic components such as chlorophyll concentration (Yeo and Flowers 1983). Other measures used in toxicology research use the first sign of a statistically significant change relative to control i.e., the highest non-observed effect concentration (NOEC) (Soudek et al., 2010).

3.1.5. Aims and rationale

The purpose of this chapter is to understand the halophytic phenotype and salt tolerance threshold of the quinoa variety Atlas for establishing a robust saline growth system for future infection and immunity assays. Therefore, the long-exposure salt–induced transcriptomic dataset generated in this chapter will be evaluated for global significant differences only, before being interrogated to greater depth in the context of plant immunity and combinatorial stress responses in Chapter 5 to start unravelling specifically how salt tolerance and immunity intersect in quinoa.

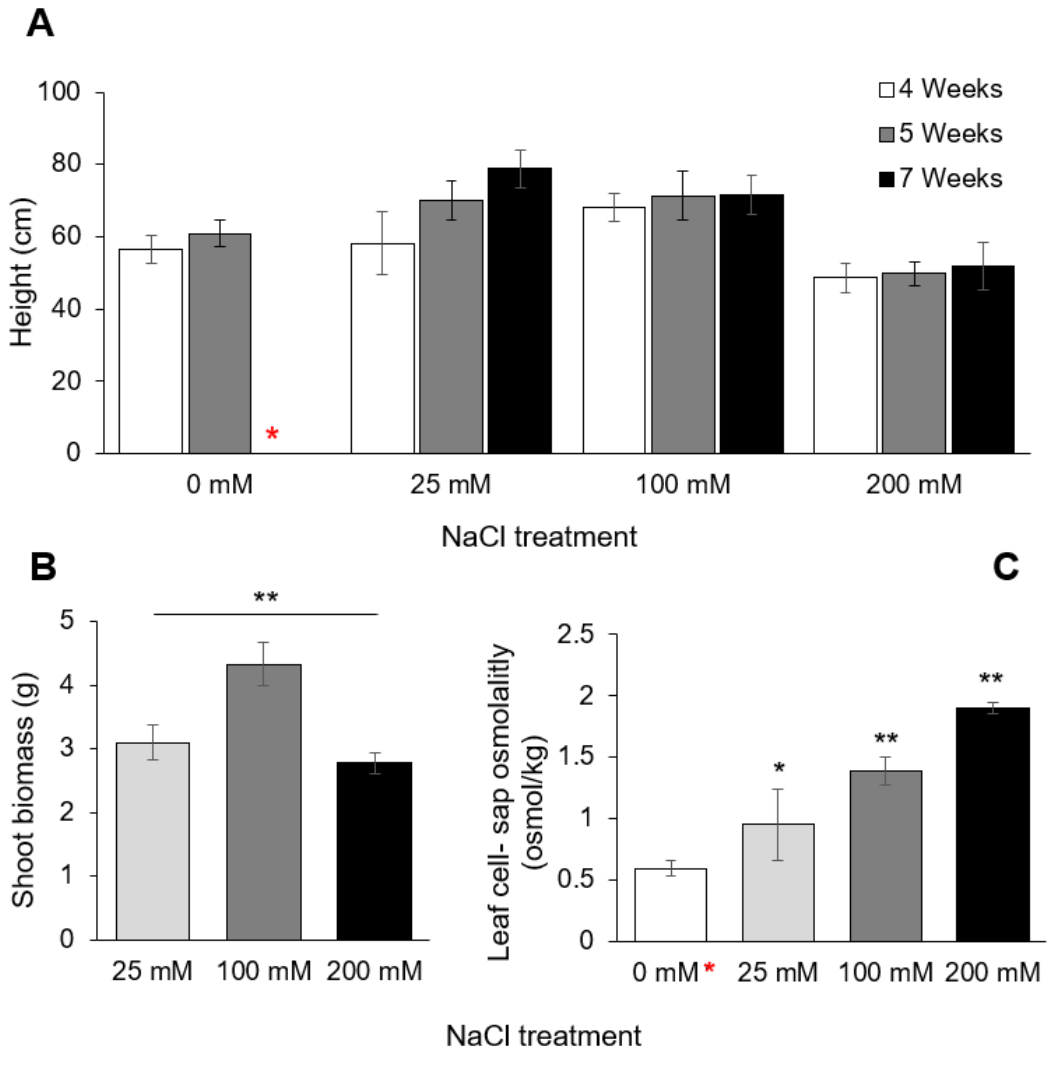
Objectives:

- Evaluate the salt tolerance of the European-bred quinoa variety Atlas
- Establish a growing system for administering controlled and reliable levels of salt
- Characterise the halophytic phenotype of Atlas

3.2. Results

3.2.1. Evaluating the salt tolerance of the European-bred quinoa cultivar Atlas

A series of preliminary salt-stress experiments were performed to evaluate the salt tolerance of Atlas throughout its lifecycle, from seed germination through seedling growth and leafy phenological stages and up to final seed production (as a measurement of yield) using a range of salt concentrations and experimental growth systems guided by the literature. A similar range of salt concentrations to native quinoa varieties 0 – 400 mM NaCl was able to be used for creating a gradient of significantly different halophytic phenotypes in Atlas. The mode of salt supplementation was successfully administered *in vitro* via salt-supplemented 1/2MS media, a soil-based system via salt-water irrigation and lastly through a saline hydroponics deep flood system.



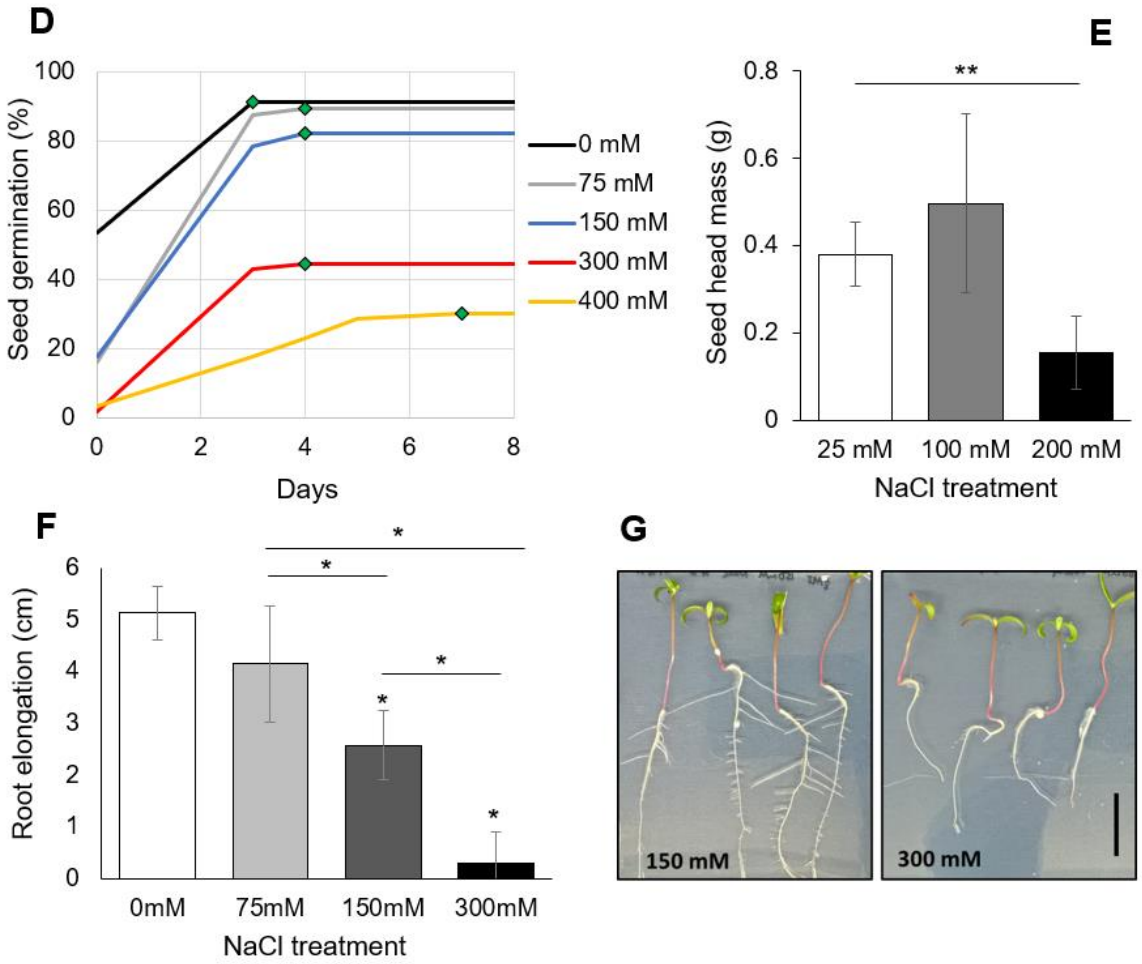


Fig.1. The effect of salt on growth parameters of Atlas plants at different developmental stages

A) Heights of 9-week-old quinoa plants grown in the greenhouse after 7 weeks of different concentrations of salt irrigation. Plants were watered to soil saturation once per week with solutions of salt at different concentrations (further details in Methods). Height measurements were made in ImageJ using the segmented tool to measure stem elongation (length) from the root/shoot divide and up to the top of the flower head. Red asterisk signifies loss of control (0 mM) plants by 7 weeks after 5 weeks due to an unforeseen heatwave, which meant graphs B and E do not have yield parameter data for the low salt control for comparing to **B) Final dry biomass of the shoots of each salt treatment.** Samples were harvested and oven-dried for 24h at 50°C. Values represent mean ± SD of *n = 4* plants. **C) Leaf cell-sap osmolality of fully expanded quinoa leaves from each salt treatment.** 50 µL samples of leaf cell-sap was obtained through centrifugation of freeze-shocked leaf samples and measured using an OSMOMAT 030 cryoscopic osmometer. Red asterisk signifies results taken from equivalent leaves of a separate batch of 11-week-old control (0mM NaCl) plants grown under the same conditions during the same period. **D) In-vitro germination proficiency of quinoa seeds on different salt concentrations over time.** The seed germination time course for quinoa seeds plated

1/2 MS media supplemented with different NaCl concentrations was followed for 8 days and scored to provide a percentage germination value at each time point. Green marker highlight time point where maximal germination % is reached. Seeds were stratified for 3 days prior to growth in TCR1 at 16h photoperiod, and germination was scored at the first sign of hypocotyl emergence. Sample size *n = 56* (2 plates of 28 seeds). **E) Final dry biomass of just the seed heads from each treatment F) The sensitivity of quinoa seedling root growth to varying salt concentrations**. Stratified seeds were grown vertically for 4 days on 1⁄2 MS media and transferred to salt-supplemented plates for a further 4 days and the primary root growth over this period was measured. ImageJ was used for analysis of photos taken at day 4 and 8 with a Microsoft Lumia Phone camera and primary root elongation calculated. Values are means ± SD (*n = 12* individual seedlings. **G) Complete root growth phenotypes of seedlings grown on different salt concentrations.** Representative images of *n = 12* seedlings for 150 mM and 300 mM 8-day-old seedlings showing pronounced lateral root growth differences observed. Seedlings grown on 0 mM and 75 mM NaCl had similar levels of lateral root growth as for 150 mM (data not shown). Scale bar = 2 cm. A, B, C, E are the mean data from the same set of plants ± SD from *n = 4* biological replicates and representative of a single experiment. Single and double black asterisk above samples' error bars indicate statistical difference relative to control plants (0 mM NaCl) (where applicable) to $P < 0.05$ and $P < 0.001$ respectively. Statistical differences between specific samples are indicated by brackets and asterisk, assessed by one-way ANOVA with posthoc Tukey's test. B & E do not have 0 mM NaCl plants and only a one-way ANOVA was performed.

3.2.2. In-vitro salt-supplemented growth systems are amenable for evaluating the early growth responses of Atlas

Quinoa seeds (from the British Quinoa Company's 2016 harvest) showed 90% germination proficiency on normal (0 mM NaCl) 1⁄2 MS media after three days, representing basal levels of germination (Fig.1D). This proficiency was almost identically mirrored for seeds plated on 75 mM NaCl, while 81% germination was maintained at 150 mM NaCl. Both 75 and 150 mM NaCl plated seeds took four days to reach maximal germination. 400 mM NaCl significantly inhibited germination rate reaching maximal germination capacity at the delayed time of seven days and to only 33% proficiency relative to control. A greater and more lineal sensitivity to increasing salt concentrations was found at the seedling growth stage, where significantly different extents of root elongation inhibition were found between each salt increment ($P < 0.001$), approximately 25% inhibition with doubling concentration (Fig.1F). 300 mM NaCl inhibited root growth almost entirely longitudinally and secondary root hair growth was completely inhibited (Fig.1G). Interestingly, there were no obvious differences in degree

of root hair growth between 0 – 150 mM NaCl conditions implying Atlas may prioritise lateral root hair growth over total root length. Lastly, the 300 mM NaCl treated seedings showed no other signs of toxicity beyond stress-induced growth inhibition as cotyledon and shoot pigmentation were consistent with lower salt treatments showing that adaptive mechanisms were effective for maintaining tissue viability in Atlas even at 300 mM NaCl.

3.2.3. Longer term salt exposure from two-week-old plants reveals a halophilic phenotype in Atlas grown under 100 mM NaCl

A 7-week salt irrigation experiment was devised to assess the impact of salt on later phenological stages up to full maturity, where final shoot height and dry shoot and seed biomass were measured as yield parameters. Having seen how early salt supplementation caused significant effects on germination and seedling growth rates, this experiment was designed to start salt exposure in pre-established 2-week-old plants. 100 mM NaCl irrigation caused a growth increase (assessed by height) in Atlas during the first four weeks relative to control and 25 mM NaCl treatments, whereas the higher salt stress of 200 mM (Fig.1A) was inhibitory. Between four, five and seven weeks however, the growth rate (assessed by mean plant height increments) reduced for 100 mM and especially the 200 mM salt treatment relative to 25 mM NaCl. Data for 0 mM NaCl plants beyond five weeks was lost due to failing greenhouse temperature control during an unexpected heatwave. A series of end-point experiments were performed after seven weeks irrigation (9-weeks-old biological age) where, contrary to the height measurements at seven weeks, a significantly heavier shoot biomass was found for 100 mM treated plants (Fig.1B) relative to 25 mM and 200 mM NaCl treatments.

3.2.4. Quinoa plants accumulate high concentrations of salt in their leaves in response to salt irrigation

To complement the whole-plant biophysical data, leaf organ-specific chemical composition of the leaves was assessed via leaf-cell sap osmolality measurements, as a standard parameter for quantifying salt accumulation in halophytes (López-portillo et al., 2014; Puniran et al., 2014). This revealed a pronounced salt-induced leaf phenotype and a positive statistically significant ($P < 0.05$) relationship between salt concentration and leaf cell-sap osmolality in quinoa for the range 0 – 200 mM NaCl (Fig.1C). Basal levels of osmolyte levels (0.6 osmol/kg)

for control plants increased three-fold up to a maximum of 1.9 osmol/kg for 200 mM NaCl treated plants (Fig.1C). The leaves harvested from 200 mM NaCl-watered plants for these experiments were notably more dehydrated and thinner than equivalent leaves at lower salt concentrations (data not shown) and so the relative water content of the leaf sap may have been less, concentrating the osmolytes. Considering there was notable yellowing (nutrient deficiency) of all leaves harvested for this experiment by 9-weeks, it was decided younger plants grown in a higher soil/nutrient volume should be used for future infection and immunity experiments to minimise confounding stress factors.

3.2.5. Establishing a hydroponics system in quinoa for improved control of salt exposure and saline phenotype development

A limitation to salt-irrigation experiments is the difficulty in quantifying actual salt exposure to the plant at any time as salt accumulates in the soil by binding to soil particles (affecting ion-availability). While a soil-based system is more agriculturally relevant, it would be invalid for evaluating precise interactions between salt and immunity (or pathogen infection) in future experiments and could reduce the reproducibility of phenotypes in a dual stress system. Hydroponics growth systems offer a reliable means to control salt-related phenotypes and so a series of hydroponics growth trials were performed to find an optimal regime with comparable fitness to soil-grown phenotypes for Atlas. Considerations included non-biotic (equipment), biotic (plant-based) and abiotic (mode and intensity of the salt exposure) factors which were addressed over iterative trials.

The most appropriate hydroponics vessel was the larger-volume (1.5 L) relatively shallower Araponics© tubs, which were optimised using robust and reusable hand-made plugs to support the stems and to facilitate flexibility in changing the plants-per-tub density from six up to 18 equally spaced plants as required. By changing the growing density, quinoa was found to be highly adaptive to the surrounding space available, meaning the growth rate and end-leaf size could be tailored to end analysis use e.g. a six-plant-per-tub density produces bigger leaves, more suitable for extracting higher yields of apoplastic fluid, whereas a 12-plant density produces smaller but more homogenous plants suitable for higher replicate infection assays or when multiple same-aged plants are needed for several end-uses.

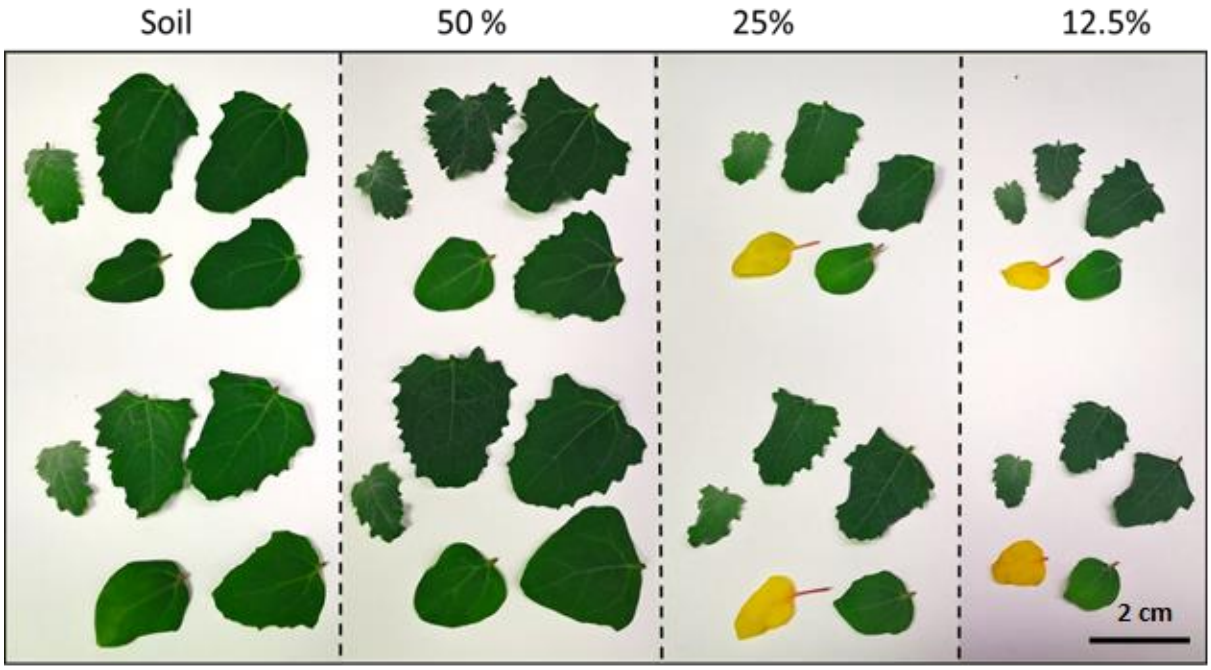


Fig.2. Nutrient strength dependency of quinoa on Hoagland's hydroponic solution. Same aged plants 4.5 weeks old grown on soil or under 2-fold dilutions of Hoagland's solution. Two replicates of *n = 6* plants are shown to highlight the high reproducibility of each growth system.

Use of a supportive matrix such as vermiculite, plastic or clay beads for quinoa root anchoring was tested but concluded not to be necessary, simplifying the set-up. Quinoa is known to grow on marginal soils so the standard Hoagland's solution (Hoagland and Arnon, 1950) at full strength (100%) was diluted by half and set as the upper percentage to be tested alongside soil, 25% and 12.5% strengths to compare plant fitness and growth at the standard 4.5-week fully expanded leaves time-point (Fig.2). Hydroponically grown quinoa in 50% Hoagland's solution at a six-plant density showed near identical growth and pigmentation to individual soil-grown plants in 8cm^2 pots while using considerably less water.

The final trials aimed to define the mode of salt exposure to the plants on hydroponics to establish a halophytic pathosystem with clear phenotypic saline gradients. Results from previous salt-stress studies at different developmental ages guided the selection of time-points for the growth procedure on hydroponics (Fig.3). Seedling establishment was quickest and most homogenous when done in soil (in the absence of salt), where after ~10 days (season-dependent) same sized seedlings where first true leaves have started to appear are transferred to hydroponic tubs (Phases 0-1).

After a minimum of three days initial growth on the hydroponics solution (Phase 1), salt (NaCl) is introduced to the system via 50 mM increments every two days until the final concentration is reached (Phase 2). Plants are grown for a further 10-14 days (size-dependent, influenced by plant density) (Phase 3) and then harvested for various end-point analyses when plants are 4-5 weeks old (Phase 4). Replacement of old with new Hoagland's solution is signalled by the red arrows (in Fig.3) between phases 1 and 2 and once within Phase 3 and ensures nutrient and water availability are not limiting while also minimising potential composition changes (Hoagland and Arnon, 1950).

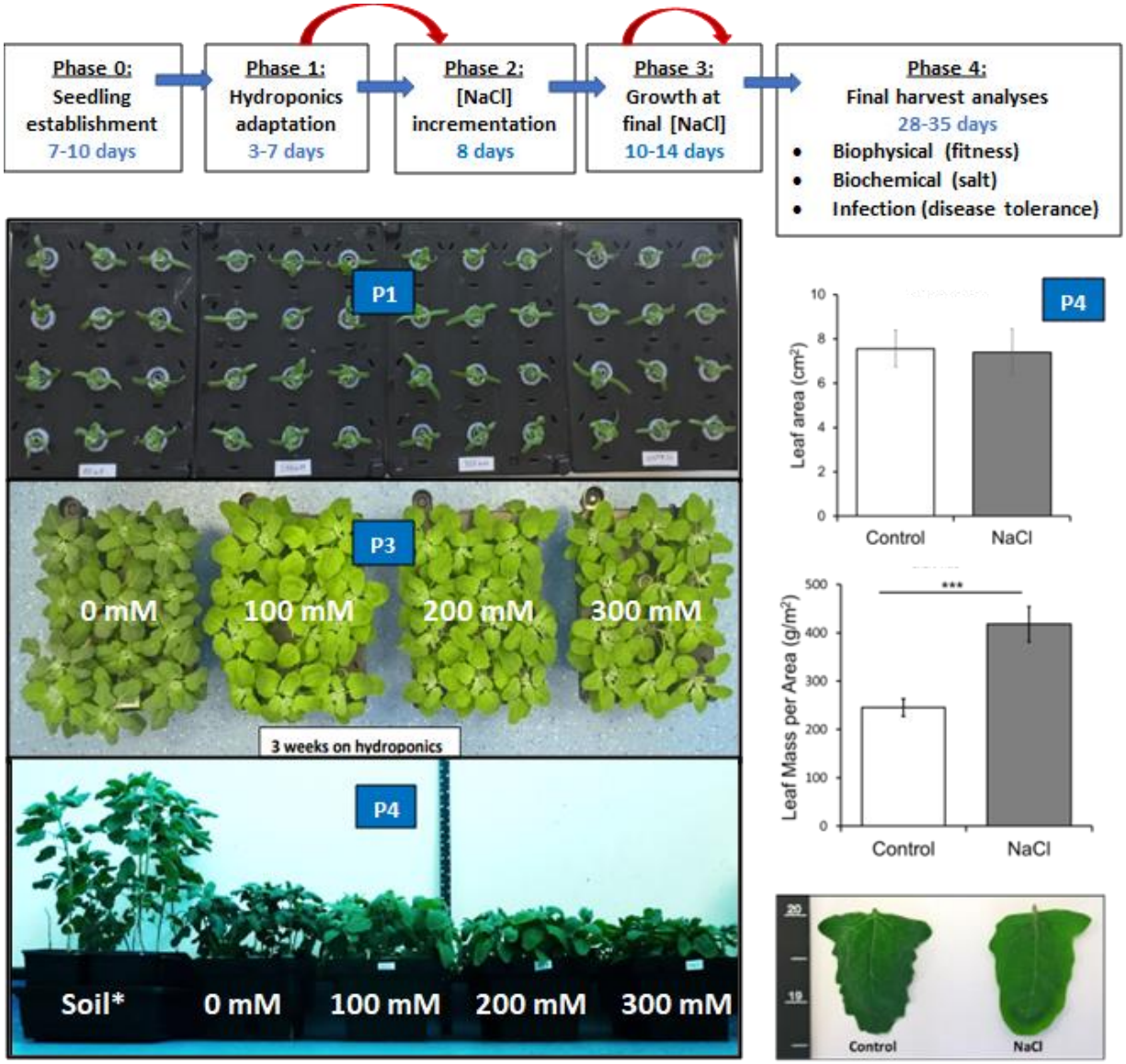


Fig.3. The establishment of a saline hydroponics growth system for quinoa. Key growth phases are shown at the top and corresponding phenotypes at key stages P1, P3 and P4 are shown. Red curved arrows indicate where old nutrient solution was removed and replaced with fresh solution at the same

salt and nutrient concentration. Leaf mass per area between treatments was statistically different (T-test; $P < 0.001$) while no significant difference was found for leaf area. Data represent mean +/- SD from four representative leaves each taken from four independent control or 100 mM NaCl plants. Leaf mass per area was calculated as per De La Riva et al. (2016) but using fresh weight. Representative plants of control and a range of salt-grown plants (0 - 300 mM NaCl) are shown to highlight the distinct colour differences and plant heights between them and also relative to soil-grown plants in the lower panel. Ruler scale bar is in inches (2.5 cm). Asterisk next to the word "soil" signifies how plants were grown in F8 pots with comparably more space (approximately double the space) for growth than in the hydroponics plants arranged at a 12-plant-per-tub density which could have influenced the final height. Therefore, height comparisons should be limited to between the four hydroponically grown plants.

3.2.6. Ultrastructural analyses reveal unique constitutive and salt-induced phenotypes in quinoa

Salt and control-grown quinoa at six-plant density show comparable end biometric sizes but distinct phenotypic differences exist at the leaf-organ level for: colour, shape, density and turgidity (Fig.3), which were investigated further through ultrastructural analyses (Fig.4). Leaves from (hydroponically) salt-grown plants show comparable distribution of EBCs but differential EBC morphologies: salt increases the turgidity of individual EBCs and increases the topological uniformity of the leaf surface (Fig.4E). Moreover, autofluorescence signals were captured externally (whole leaf) (Fig.4D) and at the ultrastructural level revealing a higher leaf lamina penetration in control leaves (shown by the visualisation of stalk cells) and thicker, more robust cell walls in high salt plants (Fig.4E) which indicate certain auto-fluorescing biochemicals or structural properties of the plants vary under salinity.

To evaluate potential differences in cell shape or density of cells between low and high salt leaves cross sections were prepared and stained. Similar to the confocal microscopy analyses, high salt grown leaf tissue showed higher integrity and relative thickness compared to low salt grown leaves, with a more cuboid shape at the leaf edge (Fig.5).

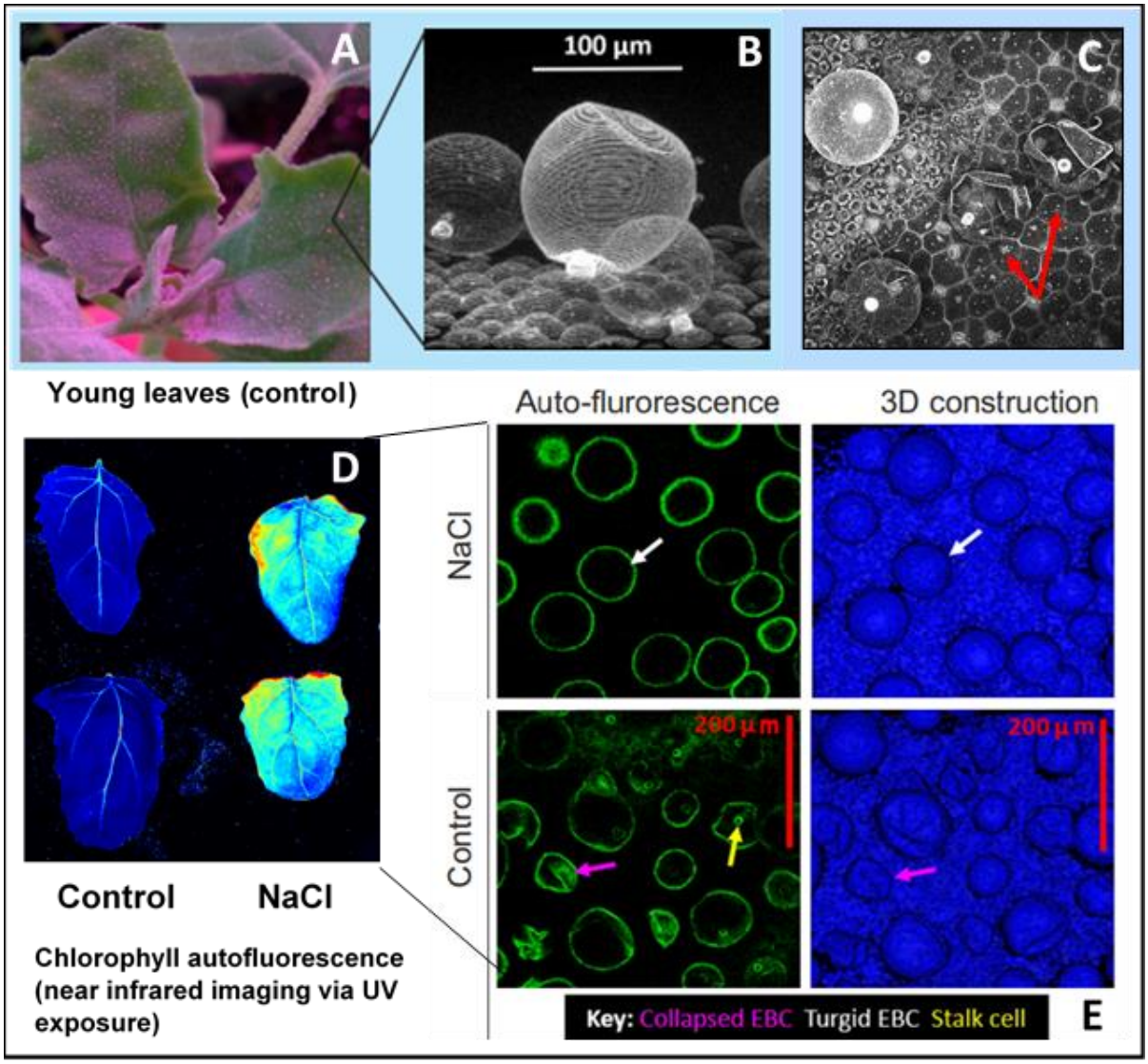


Fig.4. Atlas constitutively produces EBCs on the adaxial and abaxial sides of leaves and salt treatment creates a unique leaf surface topology by increasing EBC turgidity and altering leaf auto fluorescence. Microsoft Lumia phone camera captures the shiny light diffracting properties of EBCs on the adaxial side of young leaves grown under control conditions (A). Balloon-like EBCs are significantly larger than epidermal pavement cells and are firmly propped up on highly auto fluorescing stalk cells (B). EBCs can burst open to release their contents across the leaf (C) signalled by the red arrows. Differential autofluorescence of quinoa leaves grown +/- NaCl (D). EBCs on the abaxial side of quinoa leaves grown +/- NaCl can be observed in 2D via autofluorescence when excited with 480 nm (emission at 680 nm) or reconstructed from brightfield confocal slices in ImageJ plug-in '3D Viewer' setting 'surface' (E). Images B, C and E were taken on the Zeiss confocal microscope, B at x40 magnification and C & E at x25, both are representative of 2+ frames. The raw images were then reconstructed in ImageJ 3D viewer using a z-stack of confocal slices across the abaxial leaf surface.

Before analysis leaf samples were fixed and chlorophyll cleared gradually in ethanol by reducing strength concentration.

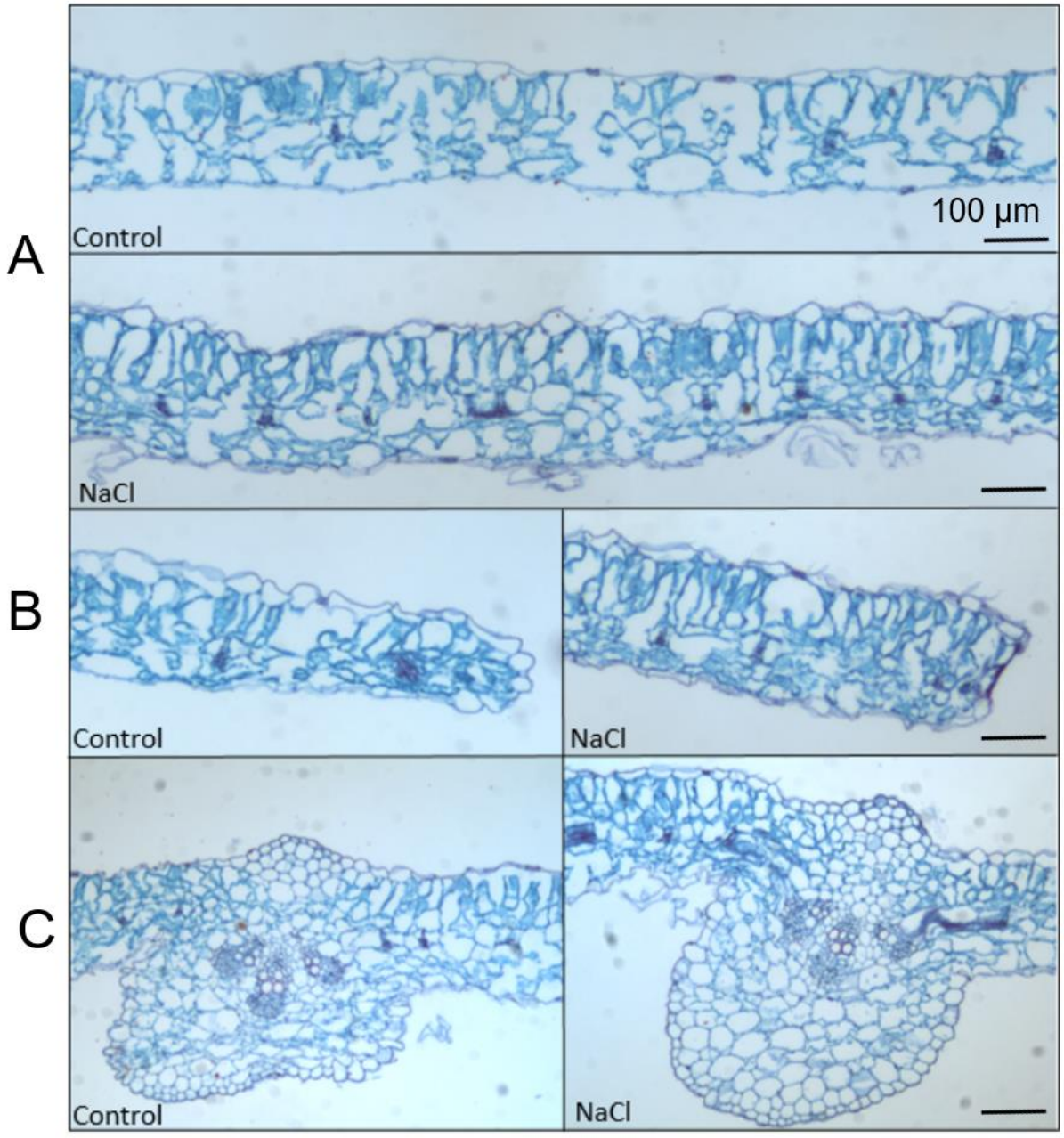


Fig.5. Cross-sections of low and high salt hydroponically grown quinoa leaves. Leaves were sampled from the mid-point of fully expanded leaves, fixed, sectioned, stained with Safranin O (for lignified structures) and the counter stain Fast Green (non-lignified cell walls) and imaged by a Leica DMRB microscope with a DFC7000T camera (Hughes, Sedelnikova & Langdale 2018). Images are representative of *n = 6*. A) leaf centre, no vein, B) leaf edge no vein and C) midrib vein. Images are x20 magnification and scale bar is 100 µm.

3.2.7. Transcriptional analysis of the 200 mM NaCl foliar phenotype in Atlas reveals a typical halophytic expression profile

A preliminary salt-induced RNA-seq experiment was performed to understand the molecular basis of (and salt-activated background for) the 200 mM NaCl foliar phenotype in Atlas. This would also facilitate the comparison of common themes and the identification of any unique signatures found against the several pre-existing salt-induced transcriptomes of other quinoa varieties, performed under different salt concentrations and lengths of salt treatment.

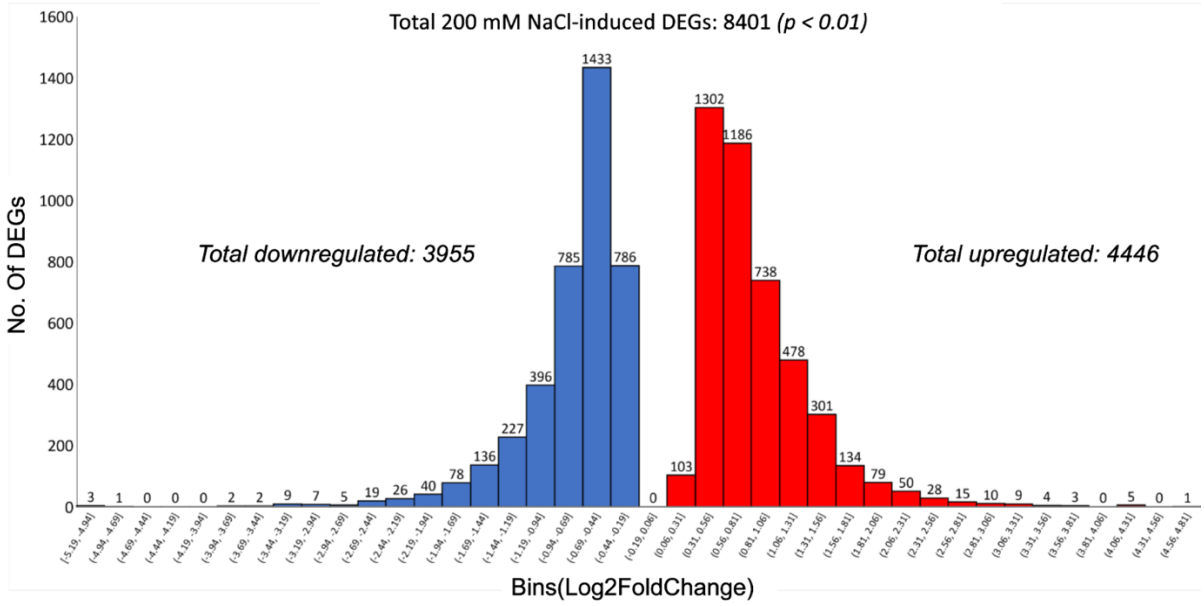


Fig. 6. Histogram showing the distribution of the total number of salt-induced differentially expressed genes (DEGs) found in the leaves of hydroponically grown Atlas plants under 200 mM vs 0 mM NaCl. The histogram was divided into 40 bins with a bin width of 0.25 Log_2 Fold Change (L2FC) where blue and red bars represent downregulated and upregulated DEGs respectively. *n = 4*, where 6-8 fully expanded leaves harvested from two plants were pooled to represent each biological replicate. DEGs are significant to *P < 0.01*. See Material and Methods for sample preparation.

A large number (8401) of significant DEGs were found (*P < 0.01*) with very similar total numbers of up (4446) and down (3955) regulated genes (Fig.6). The majority of DEGs experienced subtle L2FCs as shown by the shape of the histograms clustering around ± 0.5 L2FC (Fig.6) whereas just 0.7% (29 genes) and 1% (47 genes) were contained within the 10 and 9 bins beyond the mid-point of the total down and upregulated bins respectively. Before querying candidate DEGs with especially high L2FCs, functional enrichment analysis was

performed to gather a global impression of the salt-induced foliar phenotype. To do this, the normalised transcript reads were mapped to the reference quinoa transcriptome (Jarvis et al., 2017) and then BLASTed against the Arabidopsis proteome (TAIR) to call a higher resolution of protein descriptions using Gene Ontology (GO) annotations. This was the same method (bioinformatics pipeline) used in Chapter 2 to facilitate direct and valid future comparisons to the quinoa PTI transcriptome generated.

The majority of the 86 most significantly enriched GO terms found belonged to the Cellular Components (CC) category (43; 50%) followed by Biological Processes (BP) (31; 36%) and lastly Molecular Function (MF) (12; 14%). CC terms related to photosynthesis, translation (ribosome), cell wall, apoplast and extracellular region were most enriched (Fig.7).

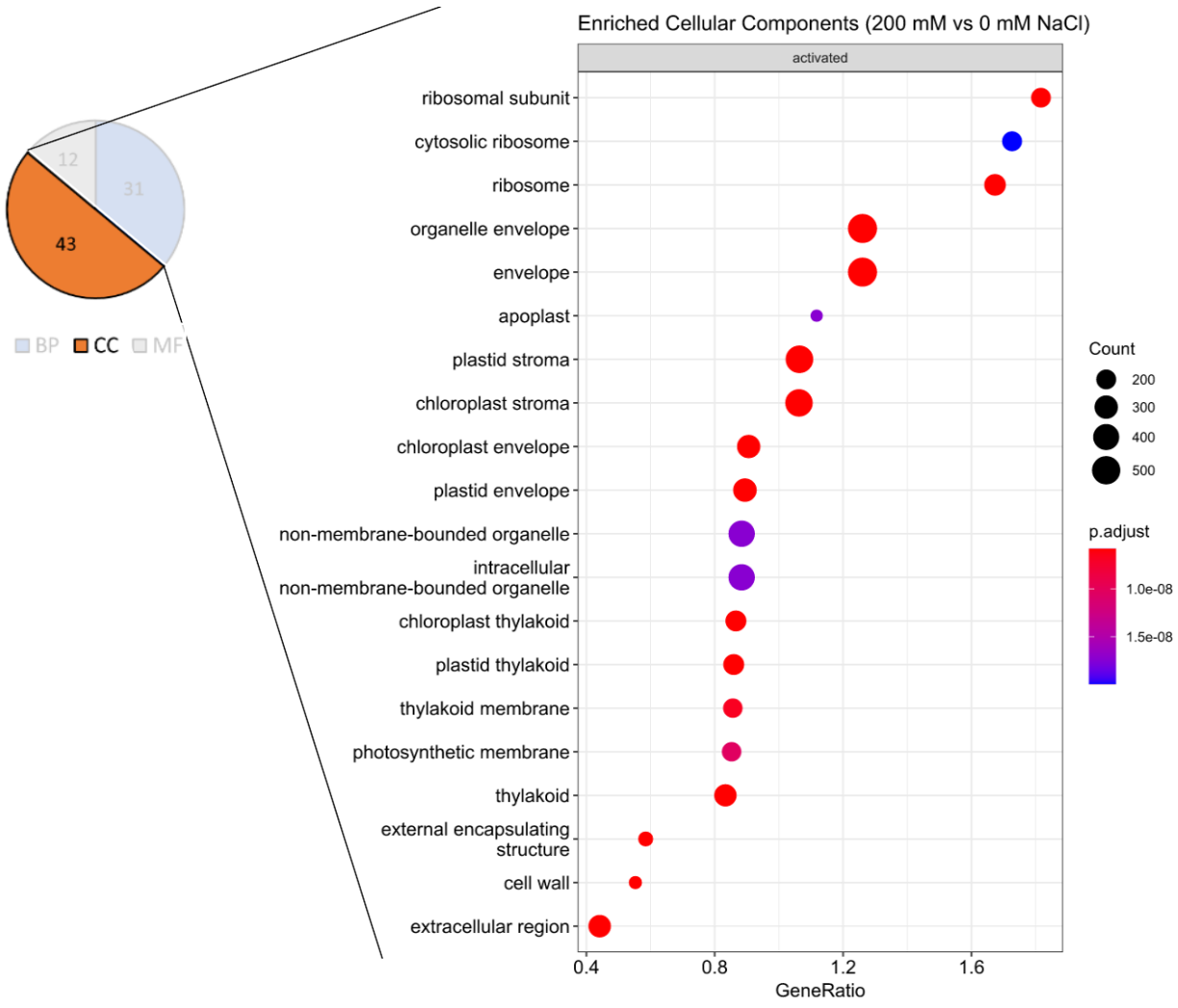


Fig.7. Pie chart showing the proportions of most highly enriched salt-induced GO terms within the DEG list, by subcategory. B) Dot Plot showing the top 20 enriched upregulated CC terms in response to salt (200 mM NaCl leaves vs 0 mM NaCl). The enrichment analysis was performed by the GSEA function in the clusterProfiler and DOSE packages using the DEG gene list (*P < 0.01*) as the gene space. CC = Cellular Component, BP = Biological Process and MF = Molecular Function.

In our functional enrichment analyses using GO annotations, a clear increase in protein synthesis, metabolism and ultrastructural reorganization at the level of the cell wall, apoplast and organelles, particularly related to photosynthesis occurs, with relative inhibition of DNA-replication processes and related cellular components along with MAPK signalling, and specific ion transport. Additional specific insights from enriched upregulated MF and BP include the upregulation of copper ion binding, fatty acid metabolism, oxidoreductase activity and organonitrogen, peptide, amide and secondary metabolite biosynthesis.

The most highly upregulated gene in response to salt was found to be 1-Aminocyclopropane-1-Carboxylic Acid Oxidase (ACO) with a L2FC of +4.1, found in three copies with the other two expressed to a lower degree, < +0.7 L2FC. ACO was also the most highly expressed gene annotated by the enriched term 'oxidoreductase activity'. Ethylene response factor (ERF) transcription factors (TFs) were also found to be strongly enriched, along with WRKY TFs, NAC domain-containing proteins and abscisic stress-ripening proteins and abscisic acid 8-hydroxylases.

Another highly expressed and widely represented salt responsive gene in Atlas was S-adenosylmethionine synthase 3/4 (AT3G17390: SAM synthase 3 or 4/METK4 or METHIONINE ADENOSYLTRANSFERASE 4) which was annotated with 16/86 of the significantly enriched GO terms. The SAM synthase gene was found in duplicate where both gene copies had high L2FCs of +3.4 and +3.2. Example annotations of the SAM synthase function are diverse reflecting the prominent role of its product SAM (catabolised from methionine and ATP) in cell wall processes, lignin biosynthesis, mRNA-binding and response to abiotic stimulus, for which this SAM synthase 4 was the second most expressed gene annotated with this term. The most highly expressed gene annotated with the enriched GO term 'response to abiotic stress' was inorganic pyrophosphatase 1-like (AT1G73010) with a L2FC of +4.8 and +4.1 and considerably lower expression for its inorganic pyrophosphatase 2-like isoform.

3.3. Discussion

The main objectives of this Chapter were, sequentially, to evaluate the salt tolerance of the Atlas cultivar, to establish a robust saline growth system, to produce and characterise the halophytic foliar phenotype of Atlas for use in future combinatorial stress assays. The objectives were successfully met through an informative and complementary range of *in vitro*, hydroponic and soil-based growth systems, from which transcriptional, micro and macroscopic halophytic phenotypes were defined. Salinity impacts many different traits, and we chose to focus on growth rates and yield parameters of different developmental stages to determine the 0 – 300 mM NaCl salt range used in the hydroponics system, before dedicating our focus to exploring the 0 mM vs 200 mM NaCl foliar phenotype. Several interesting opportunities for follow-on work have arisen. Firstly, a new prolonged exposure salt-induced foliar transcriptomic dataset was generated for a genotyped European quinoa variety Atlas. This experiment was performed twice under the same growth conditions but with 1.5-years between experiments, where the repeat dataset formed part of the combinatorial stress system (Chapter 5). This offers researchers the chance to robustly compare quinoa's longer-term medium-level salt-stress adaptations to the previously generated transcriptomic datasets for quinoa's shorter-term 'salt-shock' responses (Ruiz et al., 2017 & 2019). Secondly, the process of establishing varied growth systems and salt stress assay screens in Atlas has provided a pipeline with technical considerations for handling novel plants (or new ecotypes). This pipeline has already shown promise for guiding the establishment of other Chenopods and novel plant species under controlled conditions in Oxford and Warwick (Scrafton & Preston unpublished).

3.3.1. Salt treatment of *C. quinoa* cv. Atlas produces halophilic and halophytic phenotypes at the macroscopic to ultrastructural and biochemical Levels

Salt tolerance in quinoa is known to be genotype dependent (Ruiz et al., 2015; Cai and Gao 2020; Mizuno et al., 2020; Qureshi & Daba 2020) and so in the establishment of a saline growth system it was imperative to evaluate the salt threshold of Atlas. A high salt tolerance and even halophilic properties under 100 mM salt exposure (which produced a greater shoot and seed biomass) were found, which corresponds with biomass data of another European bred quinoa variety used in previous studies as well as native highland and lowland South

American varieties (Hariadi et al., 2011; Ruiz-Carrasco et al., 2011; Ruiz et al., 2016). The denser shorter plant height found for 100 mM NaCl-irrigated plants along with its higher seed yield is an agronomically attractive inversion of energy, especially valuable for climates susceptible to extreme wind stress, which is a major yield-limiting stress on the high plains of Bolivia (Barrientos-Perez et al., 2023, Bonifacio and Torrico Gonzales, personal comms 2018). Hariadi et al. (2011) also found that shoot biomass was conserved better in the Danish variety cv. 5206 than shoot length under high salinity stress: 500 mM NaCl irrigated plants showed a 20% and 50% reduction in shoot biomass and shoot length respectively.

The salt stress tolerance of Atlas plants exceeds 300 mM NaCl. This was demonstrated clearly using hydroponics whereby visibly healthy plants were produced, with no signs of chlorosis or necrosis at the foliar level and where leaf size and plant height only suffered minor reductions in proportion to hydroponic salt concentration. This is typical of the salt adjustment strategies described for quinoa in other studies (Hariadi et al., 2011; Zeng et al., 2018; Manaa et al., 2019). Our results have since been validated by Roman et al. (2020) who found that European sweet varieties (including Atlas) are extremely salt tolerant and could produce seed under salinities beyond 400 mM NaCl. We found that the later phenological stages of Atlas such as the 2-3-week-old leafy were more salt tolerant than germinating seeds and seedlings. This could partly be explained however by the more gradual mode of salt stress application used (increments of 50 mM NaCl every two days until 300 mM NaCl was reached), which gave the plants sufficient time to adapt, as opposed to a ‘salt-shock’ scenario (Shavrukov et al., 2013). Schmöckel et al. (2017) also used 50 mM NaCl increments administered to similarly aged 2–3-week plants but in the shorter timeframe of 12h increments to reach a final concentration of 300 mM NaCl, then held for 7-days. This saline growth strategy allowed the researchers to delineate varying salt tolerances among different quinoa varieties. These studies reinforce the potential for creating controlled halophilic, halophytic, salt-stressed and salt-shocked (although not desired in this project) phenotypes in quinoa to evaluate the interaction between abiotic and biotic stress mechanisms.

Pronounced changes occurred at the biochemical level where leaf cell sap osmolality experienced a progressive increase under salt treatment, which reflects previous studies done in quinoa cv. 5206. The highly significant differences in osmolality readings between each salt

treatment in the salt irrigation experiment demonstrated the mechanistic physiological sensitivity of Atlas and the technical ease for establishing foliar saline gradients for the subsequent creation of a 'halophytic pathosystem' with *P. syringae*. The osmolytes known to contribute the most were shown to be the inorganic ions Na^+, Cl^- and K^+ (Hariadi et al., 2011) and thus under our conditions, the 200 mM vs 0 mM growth system created an effective NaCl concentration difference of 485 mM vs 205 mM. The relationship between external salt concentration and leaf osmolality found in Atlas was not directly linear but was easy to reproduce, whereby multiple repeat experiments showed a narrow range of variance in osmolality readings of just 2% for 200 mM NaCl plants and 15% for control (0 mM NaCl) plants. Hariadi et al. (2011) showed a tight correlation between a genotype's leaf osmolality and xylem Na^+ load, which negatively correlated with overall salt tolerance (as defined by biometric parameters). Interestingly, the difference in effective salt concentration in the leaves of Atlas plants grown at 200 mM vs 0 mM NaCl under our growth regime (incrementation of 8 days, plus 14 days held at 200 mM) was a lot lower than for the aforementioned regime by Schmöckel et al. (2017), which produced a 5 to 8 times difference in shoot NaCl concentration of 250-400 mM vs 5-20 mM NaCl (depending on the accession). This demonstrates the phenomenal halophytic plasticity and rapid adaptability to saline conditions using inorganic ions as cheap osmotica.

Osmotic adjustment through actively sequestering (and synthesising) osmolytes in the cytosol maintains cell turgor and supports a more efficient uptake of water from the external medium (Flowers et al., 2015). Reduction in transpiration (via stomatal closure or reduction in density) also occurs to boost leaf cellular water retention needed to dilute the ionic stress component of high concentrations of Na^+ and Cl^- ions. We spotted macroscopic, microscopic and physiological evidence of these adaptations in Atlas whereby water requirements (and thus, water use efficiency) were significantly reduced as salt treatment increased, along with tissues becoming more succulent, denser, thicker and cells more cuboid in shape. The molecular basis for structural tissue changes has been further explored in quinoa and other less tolerant species such as *Lycium barbarum L*. (goji berry) previously by Manaa et al. (2019) and Yao et al. (2023). The hydroponic system revealed a linear increase in water use efficiency from 0, 100, 200 and 300 mM NaCl (data not shown) whilst the loss of control 0 mM irrigated soil plants, but not 25 mM, 100 mM or 200 mM plants during an unexpected period of heat

stress suggests that even small amounts of salinity can 'prime' Atlas for broader abiotic stress resilience.

Lastly, it appears that salt-adapted tissue is much more resistant (recalcitrant) to fixing and clearing solutions based on ethanol and/or acetone, whereby significantly longer incubation periods plus heat were needed to penetrate the tissues and dissolve chlorophyll. These observations support the understanding of thicker cell walls and fewer natural openings such as stomata under saline conditions. The thinner weaker tissue of control plant leaves is further supported by the comparable loss of leaf lamina ultrastructure (integrity) found for the histological analyses of control leaf cross-sections. The EBCs reconstructed using confocal microscopy imaging suggested how saline leaves possessed inflated, more turgid and robust EBCs than control leaves, however, experiments performed since have suggested that this could also reflect higher levels of tissue damage for control leaves. Scanning electron microscopy studies were initiated with Dr Niloufer Irani where tissue preparation conditions were optimised for live tissue imaging of quinoa grown under low and high salinity using home-made 'nano-shield-suits' (Chapter 1 Fig.7; Irani and Scrafton unpublished) and the EBCs were found to be fully inflated and turgid for growth conditions.

In future work it will be interesting to query whether the salt-induced increase in osmolytes and changes in water status and leaf lamina spatial boundaries of the quinoa plant directly impact the microenvironment experienced by invading bacterial pathogens.

3.3.2. Global functional analysis of the salt induced DEGs provides a snapshot of the halophytic mechanisms underpinning the saline foliar phenotype of Atlas

A pronounced shift in foliar gene expression (extensive transcriptional reprogramming) reflects the pronounced phenotypic changes observed in response to prolonged gradual salt exposure. This is shown by the large number of differentially expressed genes (DEGs) found where 90% of PCA variation between samples (four biological replicates under each condition) was explained by salt treatment, minimising the impact caused by the variation between biological replicates to just 4% (data not shown).

Ruiz et al. (2019) found the total number of salt induced DEGs increased from 945 for 1h to 1471 for 120h (five days) exposure to 300 mM NaCl in the highly salt tolerant Chilean salares

ecotype R49. Unlike our system, this type of salt treatment represents a salt shock in quinoa considering how the leaves of R49 wilted showing toxicity. This shift in DEG numbers was accompanied by a concomitant increase in the number of TFs expressed and the overrepresentation of the biological processes oxidation-reduction, response to stress, response to abscisic acid (ABA), and cell wall organization (Ruiz et al., 2019).

The most highly upregulated gene in response to salt consistently found in our salt stress dataset (in this chapter and in an equivalent dataset produced as part of Chapter 5's combinatorial stress experiment) was the 1-Aminocyclopropane-1-Carboxylic Acid Oxidase (ACO) enzyme, which makes the developmental and stress responsive hormone ethylene (ET), which is a key hormone in salt stress responses (Jiang et al., 2012 & 2013). The ACO gene as well as AC synthase 1 and 2 genes, growth related expansin genes, lipoxygenase genes and oxidoreductase GO term were also all found to be strongly induced in the transcriptome of R49 following short (1 h and 120 h) high intensity (300 mM NaCl) salt shock treatment (Ruiz et al., 2019). Other key factors previously described as salt responsive in quinoa and other halophytes such as *Suaeda maritima* and glycophytes Arabidopsis, wheat and tomato were also found to be upregulated in our dataset: ERF, WRKY, NAC TFs and abscisic stress-ripening proteins and abscisic acid 8'-hydroxylases (Gharat et al., 2016; Vaseva et al., 2021; Gharbi et al., 2017; Ma et al., 2021; Yue et al., 2019; Rong et al., 2014). SAM is a precursor for many salt-adaptive compounds such as ethylene, the organic osmolytes polyamines (PAs) and glycine betaine, and cell wall structural component lignin, which have all been shown to be involved in salt-adaptations in quinoa and other halophytes, and was unsurprising therefore to be highly upregulated in Atlas (Bueno and Cordovilla et al., 2019; Ruiz et al., 2017; Orsini et al., 2011; Jiang et al., 2012 & 2013). Inorganic pyrophosphate phosphatases (PPiases) were also upregulated, and catalyse the specific cleavage of pyrophosphate (PPi) from phosphorylated substrates as an immediate metabolic adaptation where PPi is known to be an alternative source of energy especially under stress (May et al., 2011, Gutiérrez-Luna et al., 2018) and which can support phosphate-limiting growth conditions.

A key potential limitation of our approach compared to other abiotic stress induced transcriptomic studies performed in quinoa was the use of Arabidopsis proteome annotations, having previously mapped raw reads onto the reference quinoa transcriptome. Whilst this approach yields higher functional resolution especially for comparing to our PTI

dataset, fundamental differences in the genomes between the species exist: quinoa is an allotetraploid halophyte, with an expansion of salt-adaptive features (Schmöckel et al., 2017) whereas Arabidopsis is diploid glycophyte, the genetic and thus transcriptomic coverage is less, and it is likely that some of Atlas's salt-responsive genes were missed entirely. This could explain any unusual absences of previously identified candidates, as well as being a skewed Arabidopsis-centred or glycophyte-centred representation of Atlas's salt response. Our At gene annotated quinoa DEG dataset however does have the potential advantage of identifying features which could be more easily applied to plants with genomes and orthologs similar to Arabidopsis. Furthermore, for the purpose of this project, to establish an experimental system for robustly administering combinatorial stress to compare points of abiotic and biotic crosstalk in quinoa, our approach to use a smaller but higher resolution comparative dataset is valid. Further work using our raw data could be done to pin-point Atlas-specific salt responsive DEGs in the future.

Lastly, it is interesting that photosynthesis related terms were significantly enhanced in salt-grown plants because these functions are typically suppressed in plant immune responses, where Chapter 2 confirmed this to also be true in quinoa. It will be fascinating therefore to query how these relations change under the combination of salt and immune stress.

3.4. Conclusion

This chapter confirmed that Atlas can be grown hydroponically under differential salinity to produce significant salt acclimated phenotypes with high (and tightly controlled) concentrations of osmolytes in the leaves, whilst maintaining high overall plant viability. We conclude that 100 mM, 200 mM and 300 mM NaCl concentrations could be used as complementary salt treatments to induce differential phenotypic gradients relative to low salt conditions (0 mM or 25 mM NaCl). In the establishment of a dual stress system with salt and biotic stress this wide range of salinities would enhance the scope for observing macroscopic and subcellular phenotypes indicative of putative salt-priming effects or crosstalk. However, to initiate these combinatorial stress studies, just two concentrations of salt which produce significantly different phenotypes will be used. The two chosen final salt concentrations are: low salt ("control": 0 mM NaCl) and high salt ("NaCl": 200 mM NaCl), which is a high enough concentration to cause a significant effect on the salt adaptive traits

e.g., pronounced differential transcription, tissue structural changes and leaf osmolalities, without causing significant growth rate trade-offs. 0 mM NaCl was chosen because quinoa is a facultative halophyte and Atlas grows equally well in the absence of salt (Fig.2 of this thesis) and similarly to Han et al. (2023) we also found that 100 mM was growth-enhancing (at the foliar and shoot biomass level) especially during early growth stages (4-5 weeks; Fig.2A) before the effective salt concentration in the soil likely became higher upon subsequent irrigations due to salt accumulation. Importantly, a gradual mode of salt administration has been established for the purpose of inducing salt acclimation in quinoa rather than a salt shock response (Skorupa et al., 2019; Ruiz et al., 2019). This not only more closely mirrors natural salt exposure in field settings, but also allows a more valid interaction between how the plant's halophytic adaptations crosstalk with immunity.

The adaptive biochemical, physiological, structural and transcriptional changes observed and characterised in this chapter could have significant impact on plant immunity and pathogen susceptibility. To uncover these, a pathosystem will next be established with model pathogen *P. syringae* and infection assays carried out under low and high salinity before repeating the set of PTI assays in saline quinoa leaf tissue in the final experimental chapter. It will be important to consider structural and ultrastructural facultative changes and constitutive features of quinoa as well as the biochemical differences.

3.5. Methods

Salt stress assays

All height/length measurements of full-grown plants or *in vitro* grown roots were analysed by photographing and using ImageJ calibrated with a featured ruler. Weight measurements were performed on suitably sensitive scales for material (error ± 0.0005g or 0.005g). Dry biomass was calculated using samples harvested and oven-dried for 24h at 50°C.

Soil-based salt-irrigation growth experiments

Individual quinoa plants were grown in 8 cm^2 pots and watered 3 days per week with tap water for 2 weeks before starting 7 weeks of a salt watering regime: On Mondays 100 mL of salt solution (prepared in batches of 0 mM, 25 mM, 100 mM, 200 mM NaCl) was carefully poured onto the soil surface of each pot until saturated i.e., liquid just starts dripping from

bottom. On Wednesdays and Fridays, the bottom of each tray was filled with 500 mL tap water.

Osmolality measurements

Leaf cell sap (cytosolic, vacuolar and apoplastic fluid combined) was obtained by centrifuging freeze-shocked leaf samples at 4000 rpm for 10 minutes, ambient temperature. An OSMOMAT 030 cryoscopic osmometer was calibrated with milli-Q water and 300 mM NaCl standard (readings of: 0 osmol/kg and 0.30 osmol/kg) and then 40 µL leaf cell-sap samples were measured in 4-5 technical replicates until or until two readings were consistent to within 0.001 osmol/Kg.

Histology

Fixing, sectioning, staining and imaging were performed identically to the histology protocol in Hughes, Sedelnikova & Langdale 2018.

Confocal microscopy

Tissue preparation, fluorescence microscopy confocal analysis was done as per Dettmer et al. (2006) with specific as follows: Zeiss 880-Airyscan1 confocal laser-scanning microscope, with a 40X or 25X 1.2 water objective was used. Autofluorescence of quinoa structures such as stalk cell and EBCs were observed following excitation with 480 nm for emission at 680 nm. 3D or surface images were reconstructed from brightfield confocal slices in ImageJ plug-in '3D Viewer' setting 'surface'.

RNA-sequencing experimental design, sample preparation and sequencing (via Novogene)

This protocol was performed identically to Chapter 2, except for the experimental design: A randomised block design was used to choose four blocks of six plants from total 24 4.5-week-old hydroponically grown quinoa plants, growing in two separate Araponics hydroponics tubs at the 12-plant density and all mature fully expanded leaves were harvested at the petiole to represent one biological replicate, out of total four per hydroponic condition. Two conditions were prepared: 0 mM NaCl and 200 mM NaCl, with the salt exposure administered as previously described. Each set of leaves were snap frozen in 50 mL falcons in liquid nitrogen for storage at -80°C.

Chapter 4: Establishing a pathosystem in quinoa with *Pseudomonas syringae*

4.1. Introduction

In Chapter 2 it was found that quinoa's early inducible PAMP-Triggered Immunity (PTI) comprised several canonical features including intracellular MAPK signalling, an apoplastic ROS burst, callose deposition at the cell wall, and unique transcriptional and RNA-binding responses to Arabidopsis. To investigate quinoa's later, longer-lasting and pathogen-specific immune responses, and specifically how salt may influence disease resistance in a halophytic crop, an amenable pathosystem needed to be established. The primary candidate for doing this was the model pathogen *Pseudomonas syringae (P. syringae)* due to its rich genetic diversity, ease of culturing and genetically modifying, and to the wealth of gene-level information available on its pathogenesis mechanisms.

4.1.1. *P. syringae* pathosystems

P. syringae is responsible for major crop losses of economically important crops such as kiwi, tomato, bean and sugar beet which stimulated early efforts to sequence the species' genomes so pathogenesis processes could be interrogated at a molecular level (McCann et al., 2017; Buell et al., 2003; Arnold et al., 2011; Ranković et al. 2023). Bioinformatic analyses and creation of virulence mutants can greatly support the determination of the genes underpinning host specificity (and thus host immune processes) (Preston, 2000; Mansfield, 2012). *P. syringae* can also be transformed via plasmid-based or chromosomally incorporated genes to produce traceable signals (e.g., YFP or luminescence) for improving the throughput of infection assays, to track colonization dynamics or as a read-out for changing virulence gene expression under different (micro)environment conditions (Soldan et al., 2020; Laflamme 2020).

4.1.2. *P. syringae* biology, diversity and its crop host and environmental niches

P. syringae are gram negative 1.5 µm long rod-shaped, plant-associated bacteria with an optimal growing temperature of 22–30 °C, however some non-pathogenic isolates can be found in water sources whilst others can endure near-zero temperatures and even trigger

crop frost damage through the production of ice-nucleating proteins (Arnold and Preston, 2019). As an endophyte and plant pathogen, *P. syringae* can colonise all tissues from leaves to seeds, fruits and tree bark endophytically (by entering through natural openings like stomata or through wounds) and can also live epiphytically (Arnold and Preston, 2019).

P. syringae is a genetically diverse species and 60 pathovars have been discovered already, organised into a '*P. syringae* complex' currently divided into 13 phylogenetic groups (phylogroups). These comprises even 'primary' monophyletic groups and six 'secondary' phylogroups within which some strains previously identified as *P. syringae* have recently been identified as new species (Baltrus et al., 2017). Members of the same phylogroups contain more similar types and numbers of virulence factors (effector proteins and phytotoxins). These factors contribute to the bacteria's host specificity, that is, the ability to tolerate and grow in specific host apoplast microenvironments (Chapter 1, Fig.11).

4.1.3. Virulence factors

The unifying infection mechanism of all *P. syringae* pathovars is their ability to mount a Type III secretion system (T3SS) to translocate type III effector proteins (T3E) into plant host cells. T3Es promote infection by suppressing or altering key host physiology and immune responses in a specific way (Lindeberg et al., 2012), an interaction fundamental to the 'host-arms race' that drives evolution of host specificity. From the plant side, perception of effector sets or their activity occurs (typically) via intracellularly located NLR receptor proteins which initiates Effector Triggered Immunity (ETI). Most strains contain between 10-40 T3Es and some significantly fewer such as CC1557, which contains just five but has evolved other means to be highly virulent on diverse plant hosts (*N. benthamiana* and sugar beet) despite being originally isolated from snow (Hockett, 2014).

Other virulence determinants include non-ribosomal peptides (NRPs), phytotoxic secondary metabolites, plant hormones and plant hormone mimics, which can be equally critical to the successful colonization of tissues (Zheng et al., 2012; Hockett 2014; McClerklin et al., 2018). Phytotoxins can induce chlorosis (coronatine, phaseolotoxin, and tabtoxin), necrosis (syringomycin and syringopeptin) or interfere with core metabolic processes (Bender, 1999) to create a more suitable microenvironment in the apoplast. Therefore, it will be important to correlate the propagation potential and disease symptom development of strains from

different *P. syringae* phylogroups in quinoa with their genetic composition to understand what virulence factors and processes are key for causing disease in quinoa.

4.1.4. The influence of external environment and leaf microenvironment on pathogenesis

High environmental humidity has correlated with the majority of *P. syringae* disease outbreaks in crop fields where nearby biotic or abiotic reservoirs of bacteria can suddenly become a threat; high humidity increases bacterial aggregates on leaf surfaces and aids motility whilst also keeping a higher proportion of stomata open to facilitate entry into the host apoplast (Xin et al., 2018). Once there, T3Es such as AvrE and HopM1 in the tomato pathovar DC3000 (from here on pv. DC3000) create an aqueous apoplast visible as "water soaking" which increases nutrient supply (Xin et al., 2018). Laboratory-based pathosystems can be used to study epiphytic survival, adaptation and more natural colonisation processes of pathogens via spray inoculation, aided by maintain high humidity conditions. Alternatively, pathogens can be inoculated directly into the apoplast, a method which favours the study of *in planta* virulence factors, such as those governing the suppression of host immunity or the establishment of a conducive apoplast microenvironment for propagation.

Shifting the focus to the plant host side, any environmental stress that reduces the fitness of the plant is likely to enhance the susceptibility to pathogen infection. For example, for salt-sensitive crops cucumber and tomato (Li et al., 2018; Gao et al., 2019) sequential application of salt and pathogen stress (infection with *P. syringae*) intensified disease symptoms due to unfavourable shifts at the phytohormone and prooxidant/antioxidant levels (Chojak-Koźniewska et al., 2017 & 2018; Li et al., 2018; Gao et al., 2019). Quinoa, being a salt-tolerant facultative halophyte therefore presents a unique opportunity for evaluating how disease susceptibility changes under a wider range of salt stress. Depending on how saline the microenvironment of the quinoa apoplast becomes, an analysis of how salt and apoplastic adaptations to salt (such as an increased production of antioxidants and osmolytes or alterations to ion homeostasis) directly impacts the bacteria will also be needed. Previous studies (Rahme et al., 1992; Freeman et al., 2013) and preliminary work by McCraw and Preston 2013 have shown that the expression of the virulence gene hrp (hypersensitive and pathogenicity) is affected by pH, osmolarity and salt.

4.1.5. Aims and rationale

To start interrogating disease susceptibility in quinoa, an infection system with the agriculturally important model bacterial pathogen *P. syringae* was established using pathovars of a range of virulence to help determine key susceptibility mechanisms in the host. Although not a highly damaging pathogen in quinoa, a laboratory study demonstrated the pathogenicity of a pathovar isolated from the closely related species sugar beet (pv. *aptata*) in quinoa (Maraite, 1997) and more recently a natural infection in Colombia was found (Fonseca-Guerra et al., 2021). Considering the ubiquitous distribution and broad genetic diversity within the *P. syringae* species complex worldwide (Dillon et al., 2019; Morris, 2019) it was hypothesised that certain pathovars might be able to infect and cause disease, or elicit PTI, ETI or non-host-resistance (NHR) in quinoa. It was also hypothesised that pathogenesis and disease resistance in quinoa may differ significantly under saline foliar microenvironments.

Objectives:

- Determine the parameters for an amenable and robust model pathosystem in (the halophytic crop) quinoa with *P. syringae* (with and without the presence of salt)
- Determine which *P. syringae* pathovars are most virulent on quinoa i.e., model pathogens
- Sequence and compare the genomes of model pathogen strains and initiate comparative functional genomic analyses to generate leads on candidate virulence factors in quinoa
- Evaluate how salt influences bacterial growth and virulence gene expression *in vitro*

4.2. Results

4.2.1. Infection assays

4.2.1.1. *P. syringae* pathovars from distinct phylogroups can infect quinoa and cause differential symptoms in a type III secretion system dependent manner

Following the successful establishment of an inoculation procedure in quinoa (see Discussion and Methods) a series of infection assays using representative pathovars from five diverse *P. syringae* phylogroups (PGs) along with one T3SS-defective virulence mutant and a low effector carrying strain were performed in quinoa. Certain PGs and pathovars within each PG were found to produce a wide range of disease interactions, summarised by growth and symptoms severity in Table 1, where key interactions are covered in detail in the following subsections.

Table 1: *P. syringae* - *quinoa* infection assay metadata, colour-coded by phylogroup.

Strain & phylogroup		Plant host species	Country	Symptom description, severity and growth	
pv. *spinaciae*[a] *NCPPB3788*	1	*Spinacia oleracea* (spinach)	Italy	severe leaf coiling, chlorosis, necrosis at higher CFU	++
pv. *spinaciae*[b] *NCPPB3550*	1	*Spinacia oleracea* (spinach)	Italy	severe leaf coiling, chlorosis, necrosis at higher CFU	++
pv. *maculicola*[b] *NCPPB2038*	1	Cabbage/Brassicas	UK	very light chlorosis	+
pv. tomato DC3000[a]	1	Radish, tomato, (*N. benthamiana* if hopQ effector is removed)	Jersey	light chlorosis	+++
pv. tomato DC3000 hrpA-[a]	1	NA – defective virulence mutant	NA	no symptoms	-
pv. *syringae* B728a[a]	2	various, bean *N. benthamiana*	USA	light chlorosis	+++
pv. *aptata*[a] *NCPPB 3539*	2	*Beta vulgaris* (sugar beet)	UK	severe leaf coiling, chlorosis, necrosis at higher CFU	+++
pv. *aptata*[b] *NCPPB2664*	2	*Beta vulgaris* (sugar beet)	Italy	severe leaf coiling, chlorosis, necrosis at higher CFU	+++
pv. *aptata*[b] *NCPPB603*	2	*Beta vulgaris* (sugar beet)	not specified	severe leaf coiling, chlorosis, necrosis at higher CFU	+++
pv. *aptata*[b] *NCPPB871*	2	*Beta vulgaris* (sugar beet)	USA	severe leaf coiling, chlorosis, necrosis at higher CFU	+++
pv. *glycinea* KN44[c]	3	*Glycine max* (soy bean)	not specified	no symptoms	-
pv. *phaseolicola* 1448A[c]	3	*Phaseolus vulgaris* (bean)	Ethiopia	very light chlorosis	-
pv. *oryzae I_6*[a]	4	*Oryza sativa* (rice)	not specified	extreme chlorosis	++
CC1557[c]	10	Isolated from snow, alpine meadow, infects *N. benthamiana*	France	severe leaf coiling, chlorosis, necrosis at higher CFU	++++

Key: number of repeats of experiments performed is coded by a subscript next to the strain names, where a= 3+, b=2, c=1. Ability to grow in quinoa, 'growth', was assessed by taking colony counts of plated leaf homogenate samples and ranges from no growth i.e., static or declining titres by comparing 2 dpi to 0 dpi (-) through to the highest increase in titres observed by 2 dpi e.g., by 100-fold (++++) representing Log10CFU ≥ 10^6. Symptoms and severity are shown by descriptions and a colour code in

the adjacent column where from white (denoting asymptomatic leaves) to black (most severe disease symptoms). Starting inoculum density for all experiments were 5 x 10^5 CFU/ml except for CC1557 at 10^6 CFU/ml, which was studied alongside three other strains inoculated at this density shown in Fig.2.

The choice of pathovars (in Table 1) included isolates from related species to quinoa, sugar beet (pv. *aptata*, various isolates, see Table 1; PG2) and spinach (pv. s*pinaciae,* various isolates, Table 1; PG1) which were hypothesised to be more virulent, whilst several well-studied pathogens (with available genome sequences) from key crops of economic importance were also tested. These included isolates from bean (pv. B728a; PG2 and pv. *phaseolicola* 1448A; PG3), tomato (pv. DC3000; PG1), soybean (pv. *glycinea* KN44*;* PG3), brassicas (pv. *maculicola* NCPPB2038; PG1) and rice (pv. *oryzae* 1_6; PG4). Two additional strains were also tested to determine early on whether successful establishment of the pathogen in the novel host quinoa was dependent on the T3SS, and then later, how strains carrying a much smaller effector repertoire behaved in quinoa. These two strains were the hrp virulence mutant *hrpA*- of the tomato pathogen DC3000, which lacks a functional copy of the gene encoding the T3SS pilus, and the PG10 snow-isolated low effector carrying strain CC1557, respectively.

DC3000 *hrpA*- was found to be virulence-defective in quinoa, quantified by comparably reduced bacterial growth and an absence of virulence symptoms (Fig.1B). This indicates that T3SS effector proteins (T3Es) are needed to successfully colonise the quinoa leaf apoplast (Xin et al., 2018; Arnold and Preston, 2019), and that quinoa's PTI defences are sufficient to significantly inhibit growth over both the 0-2 and 2-3-day period (data not shown).

4.2.1.2. Sugar beet *P. syringae* pathogen pv. *aptata* NCPPB3539 is especially virulent on quinoa

From the first round of infection experiments performed in Atlas, it was found that *P. syringae* pv. *aptata* NCPPB3539 (an isolate of sugar beet grown in the UK) caused the most aggressive symptoms in quinoa: leaf curling at 2-days-post-inoculation (2 dpi) compared to mild chlorosis in pv. B728a and pv. DC3000 (Fig.1A). Severe necrosis and full leaf collapse occurred for pv. *aptata* NCPPB3539 by 3 dpi which could also be produced at the earlier timepoint 2 dpi when inoculated at a higher starting density, 10^6 CFU /ml (data not shown).

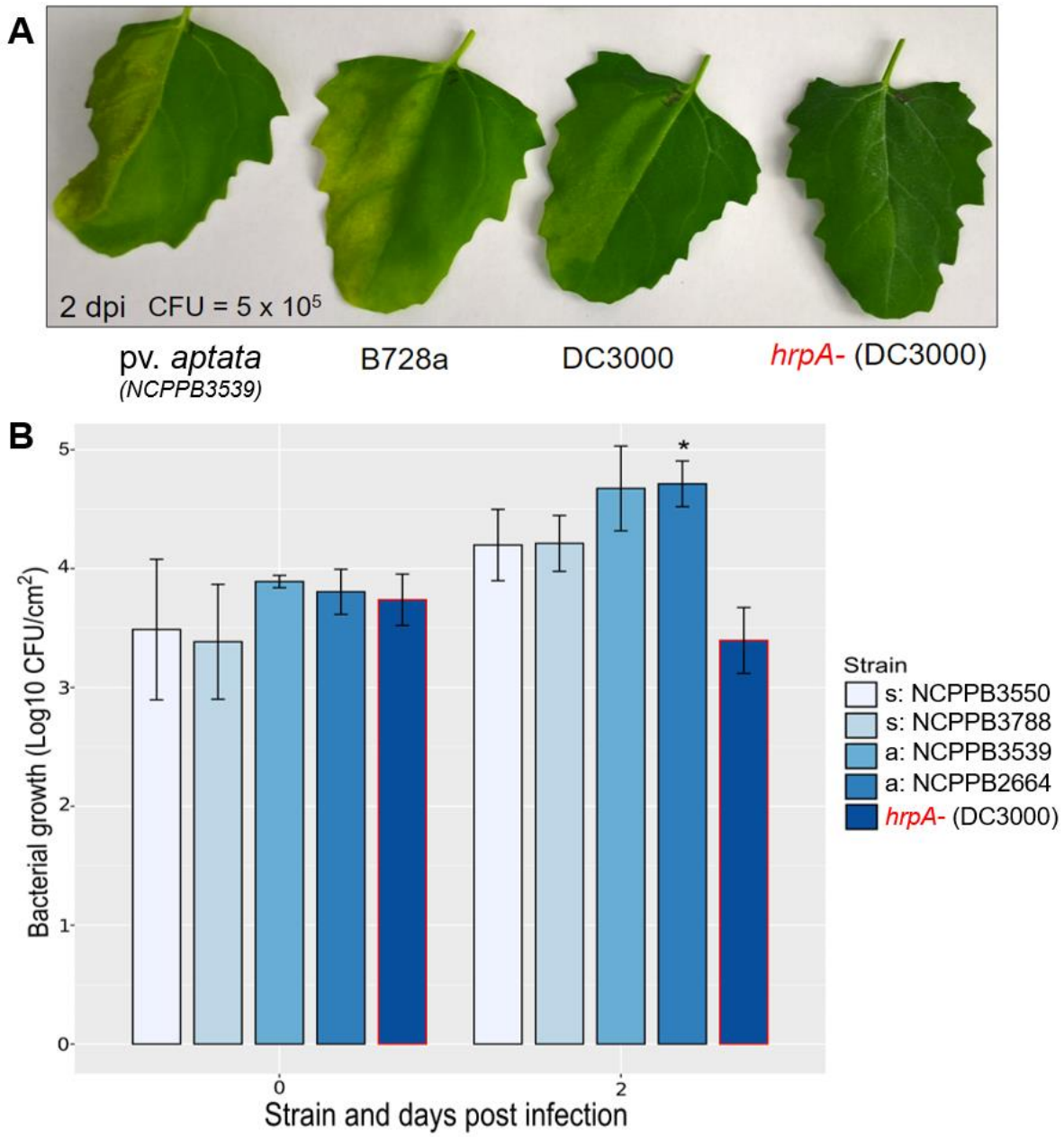


Fig.1. Pathovars of related Amaranthaceae species sugar beet and spinach cause most severe disease symptoms in quinoa. A) Overnight cultures of strains pv. a*ptata* NCPPB3539*,* pv. B728a (PG2), pv. DC3000 (PG1) and DC3000-*hrpA*- were suspended at CFU = 5 x 10^5 CFU/ml in 10 mM $MgCl_2$ along and inoculated into quinoa leaves of 4.5-week-old soil-grown plants and symptoms were imaged under visual light at 2 dpi. A mock treatment of just 10 mM $MgCl_2$ was also prepared (data not shown). **B)** A separate experiment was conducted using a panel of different pv. *aptata* and pv*. spinaciae* isolates designated by the letter 'a' and 's' followed by their NCPPB number respectively, alongside the virulence-defective mutant DC3000-*hrpA*-. Strains were inoculated at CFU = 5 x 10^5 CFU/ml in 10 mM $MgCl_2$ and colony counts taken as previously described. Bar graph means are representative of three-four biological replicates and colony counts were performed as triplicate technical replicates.

Single asterisks show significance between 2 dpi and 0 dpi titres of the same treatments to *P < 0.05* assessed by an un-paired T-test.

4.2.1.3. The PG1 pathovar isolated from spinach causes more severe disease symptoms than other PG1 pathovars isolated from tomato and brassicas

Since spinach is phylogenetically (evolutionarily) closer to quinoa than sugar beet (Chapter 2; Fig.2*),* we next obtained and tested the virulence of two independent isolates of the spinach pathogen *P. syringae* pv. *spinaciae* (NCPPB3550 and NCPPB3788). Positive, but differential disease symptoms and a slightly reduced growth was found in comparison to two different pv. *aptata* isolates (NCPPB3539 and NCPPB2664) (Fig.10C). All four pv. *spinaciae* and pv. *aptata* strains grew from 0 dpi to 2dpi, with pv. *aptata* NCPPB3539 showing the most pronounced proliferation (*P = 0.0173*) while the growth of negative disease control strain DC3000-*hrpA*- decreased 0 dpi – 2 dpi, reaching final titres that were significantly lower than all WT strains *(P < 0.05).*

Next, with the assistance of Morgan Wade we prepared lower and higher inoculum for phenotyping disease symptoms at a higher resolution, uncovering differential aggressiveness of infections in a time-sensitive manner (data not shown). Only the *P. syringae* pv. *aptata* NCPPB3539 and pv. *spinaciae* NCPPB3550 model strains caused notable phenotypes at the lowest inoculum 1 x 10^5 CFU: discrete yellow specks were seen for pv. *aptata* NCPPB3539 and chlorosis observed for pv. *spinaciae* NCPPB3550 (data not shown). We also tested additional strains including a third PG1 strain, the brassica pathogen *P. syringae* pv. *maculicola* NCPPB2038, which unlike PG1 strains pv. DC3000 and both pv. *spinaciae* isolates could not grow in quinoa by 2 dpi but which also caused chlorosis, but to a much milder extent than the other two PG1 strains (data not shown), suggesting this effect is due to conserved genetic factors within PG1.

In summary, we deemed strains to be pathogenic in quinoa if their growth increased from 0 dpi to 2 dpi and where severe necrosis or chlorosis symptoms developed, even at lower starting inoculation titres (as necrosis arising from high inoculation titres can be indicative of effector triggered immunity (ETI) or toxin-induced necrosis rather than virulence).

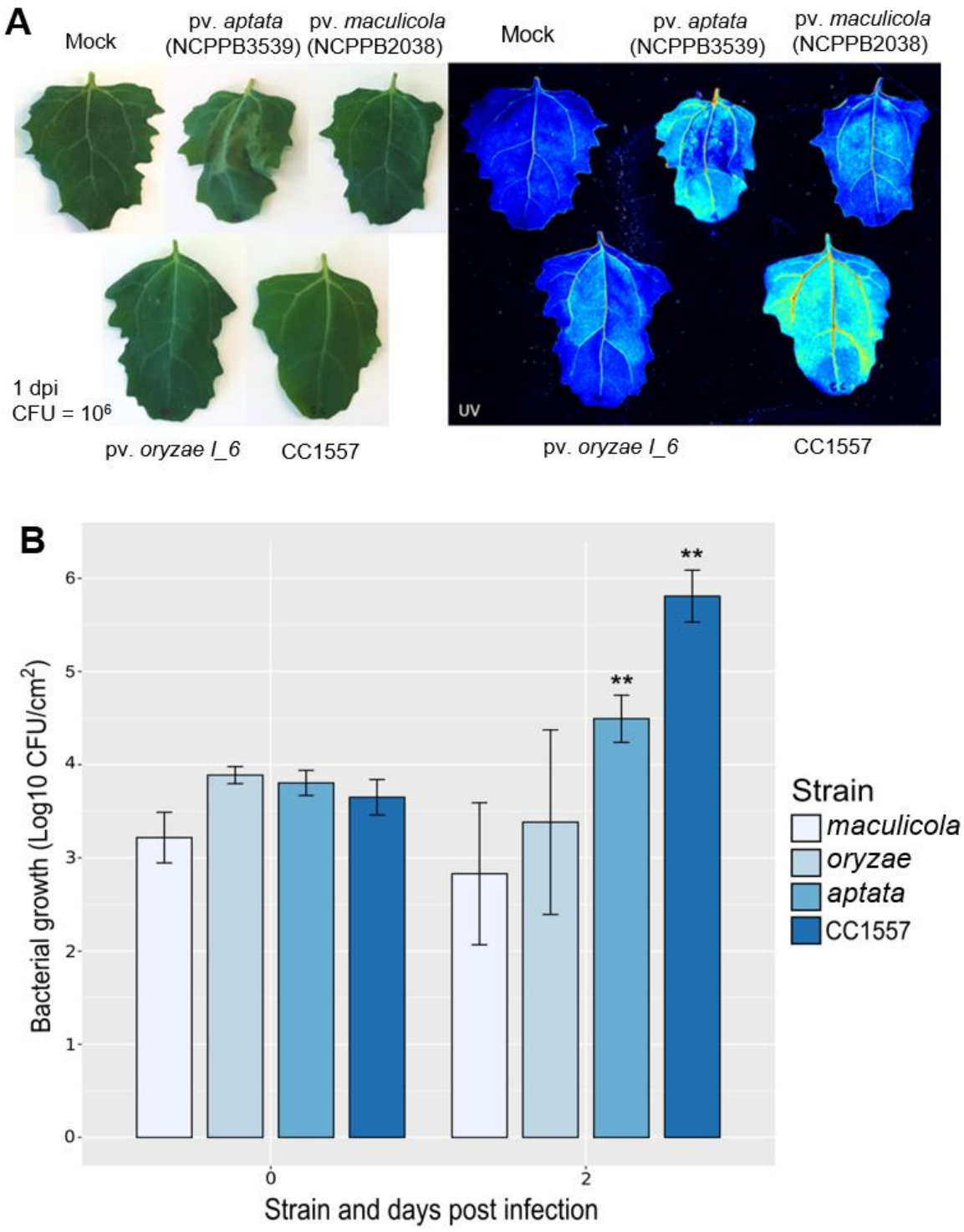


Fig.2. Different pathovars of *P. syringae* cause differential disease symptoms and grow to differential population densities. Overnight cultures of strains pv. *oryzae* 1_6 *(*PG4), pv. *aptata* NCPPB3539 (PG2), pv. *maculicola* NCPPB2038 (PG1) and CC1557 (PG10) were suspended at CFU = 10^6 CFU/ml in 10 mM $MgCl_2$ and inoculated into quinoa leaves of 4.5-week-old soil-grown plants. **A) UV transilluminator leaf images of infected leaves at 1 dpi can reveal earlier symptom differences than visual light.** UV excitation at wavelength 302 nm and fluorescent images were captured by a CCD

camera (ChemiDoc™ MP Imaging System) with standard emission filter and show accumulated defence compounds in the leaves. **B) Colony count data for the strains.** Two leaf discs were harvested per leaf and pooled for each biological replicate. Sample pictures and bar graph means are representative of five-six biological replicates and colony counts were performed as triplicate technical replicates. Double asterisks show significance between 2 dpi and 0 dpi titres of the same treatments to $P < 0.001$, assessed by an un-paired T-test.

4.2.1.4. PG3 strains cannot grow in quinoa whilst PG4 rice pathogen pv. *oryzae 1_6* causes pronounced chlorosis

As part of the infection assay series performed with Morgan Wade, PG4 and PG3 strains were tested for the first time, these were: the rice pathogen *P. syringae* pv. *oryzae* 1_6 (PG4), soybean pathogen *P. syringae* pv. *glycinea* KN44 (PG3) and a second bean pathogen, *P. syringae* pv. *phaseolicola* 1448A (PG3) along with PG1 and PG2 strains previously tested. PG3 strains pv. *phaseolicola* and pv. *glycinea* KN44 could not grow in quinoa as bacterial titres reduced from 0 dpi to 2 dpi and inoculated leaves were asymptomatic (data summarised in Table 1). PG4 strain pv. *oryzae* 1_6 was able to induce the most pronounced chlorosis/yellowing observed and leaf collapse at higher inoculum (data summarised in Table 1), but while mean bacterial titres increase from 0 to 2 dpi, replicate leaves infected with pv. *oryzae* 1_6 were consistently found to be highly variable (Fig.2B).

4.2.1.5. The alpine snow-isolated, low effector carrying *P. syringae* strain CC1557 is highly virulent on quinoa

A late addition to the pathosystem toolbox was the PG10 strain CC1557 which was able to grow extremely well in quinoa leaves, reaching a population size that was 1.5x more than the model pathogen strain pv. *aptata* NCPPB3539 and which caused similar degrees of necrosis. Apoplastic water soaking was induced across the leaf infiltration zone by 1 dpi which was the first time this had been observed for a strain. UV fluorescence imaging was used to reveal early signs of pathogenesis, or induced plant responses such as the production of fluorescing compounds such as phenolics, which were otherwise missed under white light (Fig.2A). Interestingly the two most virulent strains pv. *aptata* NCPPB3539 and CC1557 caused the most pronounced full-leaf fluorescence, whereas pv. *oryzae* 1_6 and pv. *maculicola* NCPPB2038 showed fluorescence more localised to the infiltration zone.

4.2.2. Sequencing the complete genomes of model pathogen strain isolates of *P. syringae* pv. *aptata* and pv. *spinaciae*

Considering how strains across different clades could successfully propagate in quinoa and cause different severities of macroscopic symptoms, a comparative bioinformatic analysis of existing effectors and other potential virulence factors could reveal the molecular basis for these differences. To be able to do this, the model pathogen strain isolates of *P. syringae* pv. *aptata* and pv. *spinaciae* genomes needed sequencing to compare against the published genomes of the other strains. We obtained several isolates of each of these model disease-inducing strains and sequenced their genomes with MicrobesNG. Global sequencing data is summarised below in Table 2.

Table 2: Sequencing summary for model pathogen strains (data from MicrobesNG)

Strain	Sequencing	Bases (Kb)	GC content (%)	CDS (protein coding sequence)	tRNA	tmRNA
pv. *aptata* NCPPB3539	EGS_strain	6083.080	NA	5232	63	1
pv. *aptata* NCPPB2664	WGS_DNA	6001.303	58.97	5125	65	1
pv. *aptata* NCPPB871	WGS_DNA	6022.780	58.76	5146	67	1
pv. *aptata* NCPPB603	WGS_DNA	6019.329	58.94	5182	65	1
pv. *spinaciae* NCPPB3788	WGS_DNA	6503.531	58.42	6002	60	1
pv. *spinaciae* NCPPB3550	WGS_DNA	6492.826	58.42	5987	60	1

With the genome sequences now available for the model strains, comparative genomic analyses relative to other *P. syringae* pathovars was possible and undertaken in collaboration with Chloe Harper, Jasmine Dodd and Nattapong Sanguankiattichai. First, a phylogenetic tree was constructed to reveal the genetic relationships between all strains tested in quinoa (Fig.3) which was consistent with PG designations. Next, virulence factors such as T3SS effector repertoires (Fig.4) and phytotoxin secondary metabolites thought to be important for

successful colonization (Fig.5) were mapped using OrthoFinder and AntiSMASH software respectively.

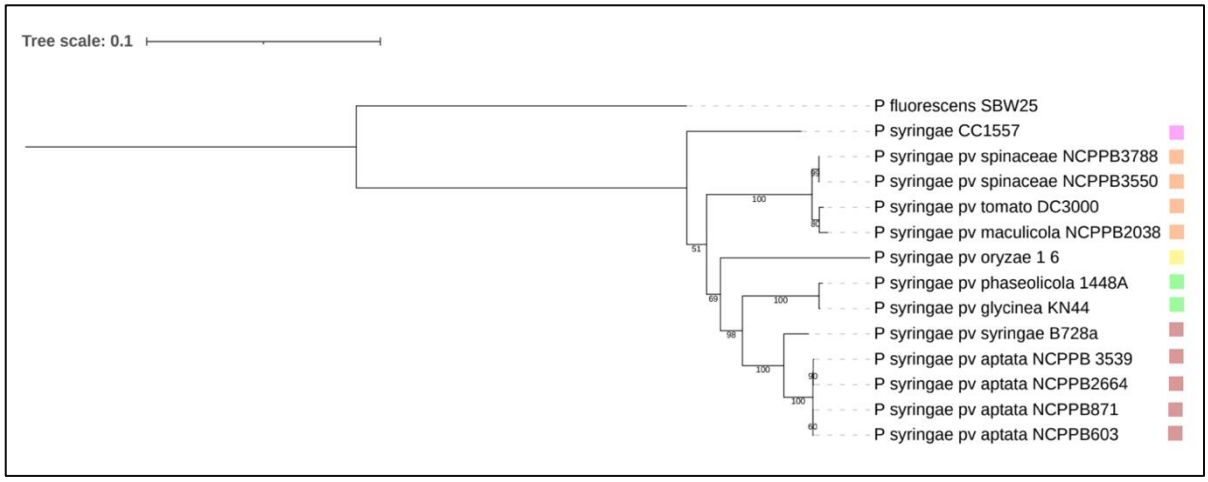


Fig.3. A reconstructed phylogenetic tree showing the relationship between all *P. syringae* strains tested in quinoa. The maximum likelihood tree was reconstructed using alignments of four concatenated housekeeping genes (rpoD, gyrB, gltA and gapA). *P. fluorescens* SBW25 was used as an outgroup. Strain phylogroups (PG) are indicated by their respective colours: PG1 = orange, PG2 = red, PG3 = green, PG4 = yellow and PG10 = pink. Further details are found in the Methods.

4.2.3. Comparative genomic analyses of *P. syringae* pathovars reveals key differences and similarities in effector and phytotoxin repertoires

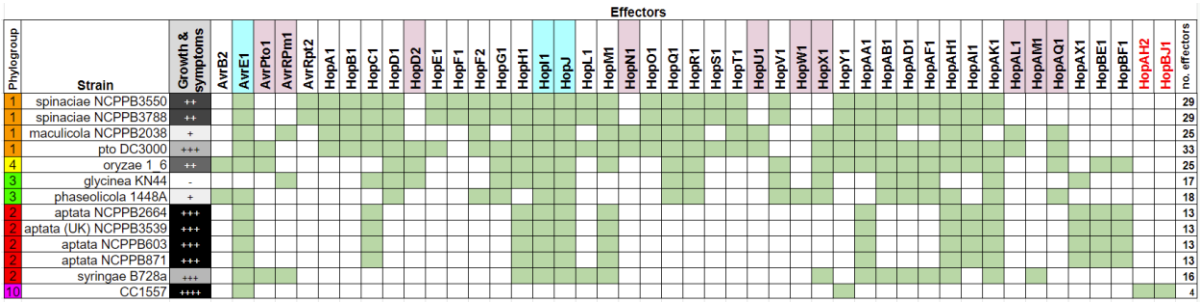


Fig.4. The T3E protein repertoire within *P. syringae* strains is diverse and varies according to pathovar. A matrix of representative T3E proteins present (green box) or absent (white box) across *P. syringae* strains as assessed by OrthoFinder. Strains are ordered in accordance with their core-genome phylogenetic tree topology (Fig.3). Blue highlighted cells indicate common effectors that are shared by all but one of the strains, while rose-coloured cells show effectors not found in any of the pathogenic strains pv. *aptata*, pv. *spinaciae* and CC1557. Total number of effectors is given in the final column. Columns colour-coding each strain's phylogroup, growth capacity and symptoms in quinoa, which was previously used in Table 1 are also included here. The darker the colour of 'Growth &

symptoms' column the more severe the virulence symptoms and the increasing number of pluses indicates higher bacterial growth titres (same as in Table 1).

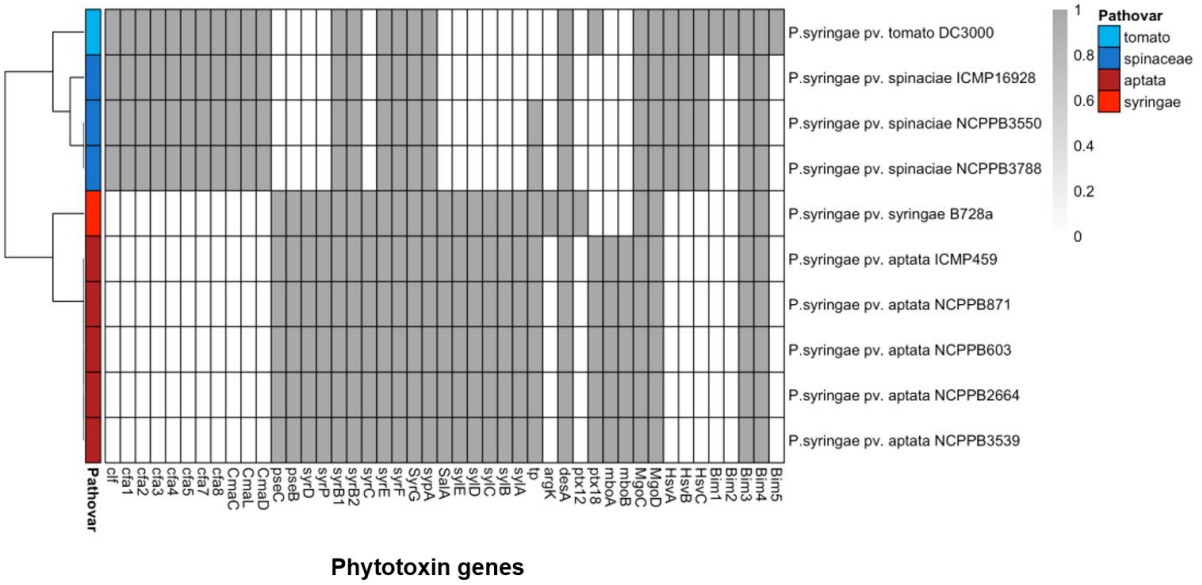


Fig. 5. Phytotoxin compositions of different isolates of the same pathovar were found to be largely conserved and higher similarities were found between pathovars from the same phylogroup. Heatmap of phytotoxins present (grey boxes) and absent (white boxes) in pathogenic *P. syringae* strains and non-pathogenic control strains (from the same phylogroup) according to OrthoFinder. Strains are clustered by their phytotoxin composition through hierarchical clustering calculated by euclidean distance in Pheatmap (R package).

OrthoFinder (Emms and Kelly, 2019) was used to identify orthologs of known T3E proteins in the genomes of *P. syringae* pv. *spinaciae* and pv. *aptata* isolates (Fig.4) and their presence and absence were compared to the T3E repertoires of the other *P. syringae* strains tested in quinoa. The total number of T3Es in the PG2 pathogenic strain *pv. aptata* (all isolates) was 13, which was the lowest observed number of T3Es from a crop source (after CC1557 which has just 4) and which was less than half the number of T3Es of pathogenic strain pv. *spinaciae* (29), but more similar to the other PG2 strain B728a (16). pv. DC3000 had the highest number of T3Es at 33. All strains except the null growth pv. *glycinea* KN44 strain possess a copy of AvrE1, whilst 10 T3Es (rose-coloured cells) were absent in all pathogenic strains. No T3Es were exclusively found in all the pathogenic strains, and considering how a smaller T3E repertoire

is often compensated for by the production of phytotoxins, a comparative analysis of phytotoxins was next performed to identify putative complementary virulence factors for successful growth in quinoa.

Phytotoxins are secondary metabolites that (unlike T3Es) play non-host-specific roles in pathogenesis. All *P. syringae* pv. *spinaciae* and pv. *aptata* isolates were found to possess syringomycin, syringopetin, phaseolotoxin and mangotoxin orthologs as well as genes from the *bim* cluster responsible for glucosidase-inhibitor production (Sanguankiattichai, unpublished). Unique features found were coronatine and Phevamine A orthologs in the isolates of pv. *spinaciae,* and several additional syringolin orthologs present in the isolates of pv. *aptata*.

4.2.4. Salt-adapted quinoa plants are significantly more resistant to infection by *P. syringae* pv. *aptata* NCPPB3539

In Chapter 3, we demonstrated how salt treatment of Atlas, whether supplied via salt-irrigation to soil-potted plants or added to the nutrient solution of hydroponic plants, results in significantly higher concentrations of salt accumulated in the leaves along with notable macroscopic and ultrastructural leaf changes without affecting plant viability.

Two infection assays in saline quinoa leaves were therefore performed to test how quinoa's halophytic adaptations influence the interaction with a model pathogen. Firstly, the hydroponic growth system established in Chapter 3 was used to grow batches of 0 mM (control) and 200 mM NaCl (NaCl) plants before inoculating individual leaves (as done previously) with the model strain *P. syringae* pv. *aptata* NCPPB3539. Equivalent leaves were harvested for leaf-cell sap osmolality measurements to quantify differences of salt/osmolyte accumulation in the pathosystem. Significantly lower (>5-fold) bacterial growth was found in the leaves of 200 mM NaCl grown plants by 2 dpi relative to control plants in two independent experiments (Fig. 6B).

The osmolality values were significantly different between the leaves of plants grown under 200 mM and 0 mM NaCl for both independent repeats ($P < 0.0001$): 0.93-0.95 osmol/kg and 0.41-0.47 osmol/kg respectively (Fig. 6A). These values approximate 480-490 mM NaCl and

190-220 mM NaCl respectively, calculated by use of a standard curve prepared with the osmometer and using a range of 0 mM – 1 M NaCl standards (data not shown).

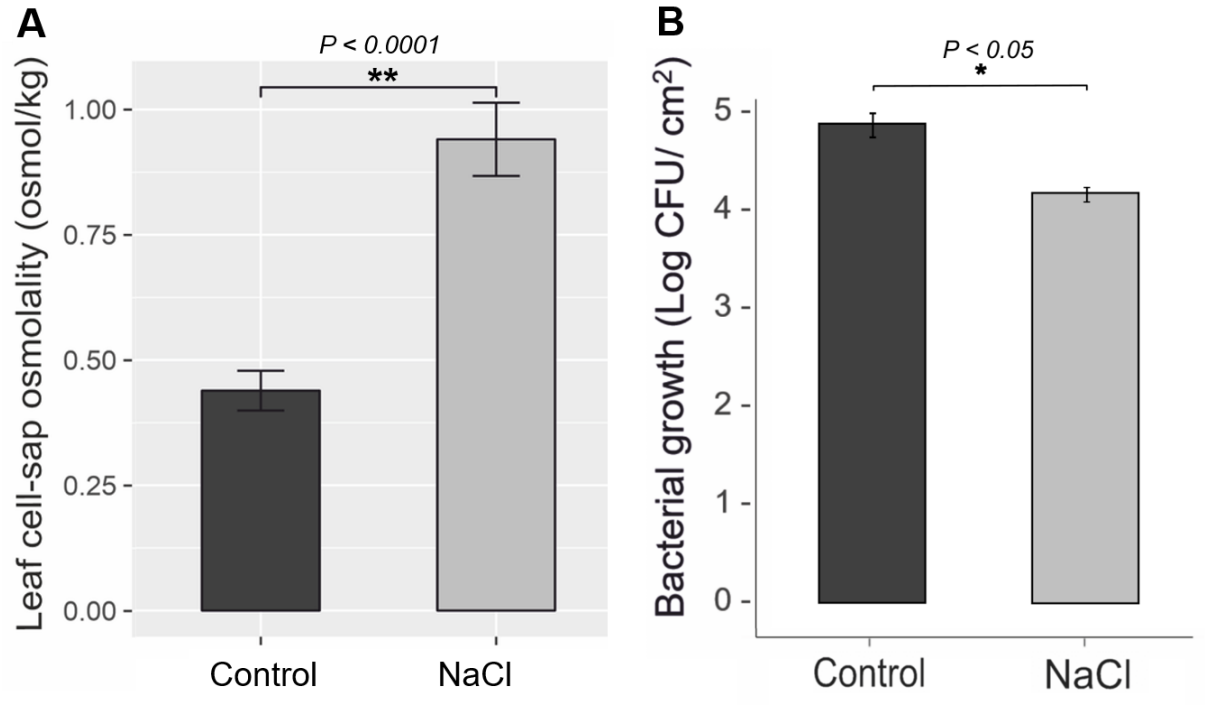


Fig.6. The effect of salt on quinoa leaf cell sap osmolality and disease resistance. 12 x 4.5-week-old plants were grown across two hydroponics tubs at a 6-plant density in 50% strength Hoagland's solution supplemented with 0 mM or 200 mM NaCl **A)** Fully expanded leaves of four of these randomly chosen plants were used for osmolality measurements, performed as described previously. **B)** Fully expanded leaves of six randomly chosen plants were infiltrated with *P. syringae* pv. *aptata* NCPPB3539 (5 x 10^5 CFU/ml) or mock (data not shown) as described previously. Each biological replicate represented two pooled leaf discs taken from one leaf from one plant. Each plant had four equivalent leaves of which two were inoculated with pv. *aptata* NCPPB3539 (or mock) for 0 and 2 dpi samples but growth by the 2 dpi comparison stage is only shown here. Data are representative of two independent experiments for osmolality measurements, whereas a similar trend of inhibition under salt was found for a repeat of the infection experiment, but a 50-fold instead of 5-fold was found and so the colony count (and respective osmolality) data were not combined in one graph. Single and double asterisks show significance between treatments of $P < 0.05$ and $P < 0.001$ respectively, assessed by an un-paired T-test.

Secondly, considering how the 100 mM irrigation regime was found to be growth enhancing for Atlas in Chapter 3, it was hypothesised that overall plant fitness and immunity may be

enhanced. The salt-water irrigation experiment was thus repeated using 100 mM or control (0 mM NaCl) until the 5-week growth stage and the leaves of each plant were infected with *P. syringae* strains of interest: pv. *aptata* NCPPB3539, pv. *oryzae* 1_6 or mock. As was found for hydroponically grown saline plants, soil-grown salt irrigated plants became more resistant to both *P. syringae* pathovars (Fig 7.B). Significant growth of both strains pv. *aptata* NCPPB3539 and pv. *oryzae* 1_6 was found in control (0 mM NaCl) plants, *P = 0.0048* and *P = 0.0077* respectively, whereas neither strain grew to a statistically higher population density in NaCl (+) plants, *P = 0.0890* and *P = 0.4960* respectively. The starting 0 dpi titres for pv. *aptata* NCPPB3539 in both control and NaCl plants were identical, which enabled a valid comparison to be made between their final 2 dpi titres where a 5.4-fold growth inhibition was found in NaCl leaves (*P = 0.0092).* By comparing the mean 0 and 2 dpi titres for pv. *oryzae* 1_6 in control and NaCl plants, the same trend is also observed, however due to the high variability among biological replicates at 2 dpi for NaCl plants infected with pv. *oryzae* 1_6 the statistical power was very low *(P = 0.5221).*

Under UV light, as was found for hydroponically grown saline plants in Chapter 3, a stronger background fluorescence signal was found in the leaves of mock-inoculated salt-irrigated plants compared to the mock-inoculated control. Leaves from salt-irrigated plants when infected by pv. *oryzae* 1_6 and pv. *aptata* NCPPB3539 strains then also produced much stronger autofluorescence signals in the infiltration zone than the leaves of their respective control plants (Fig.7A).

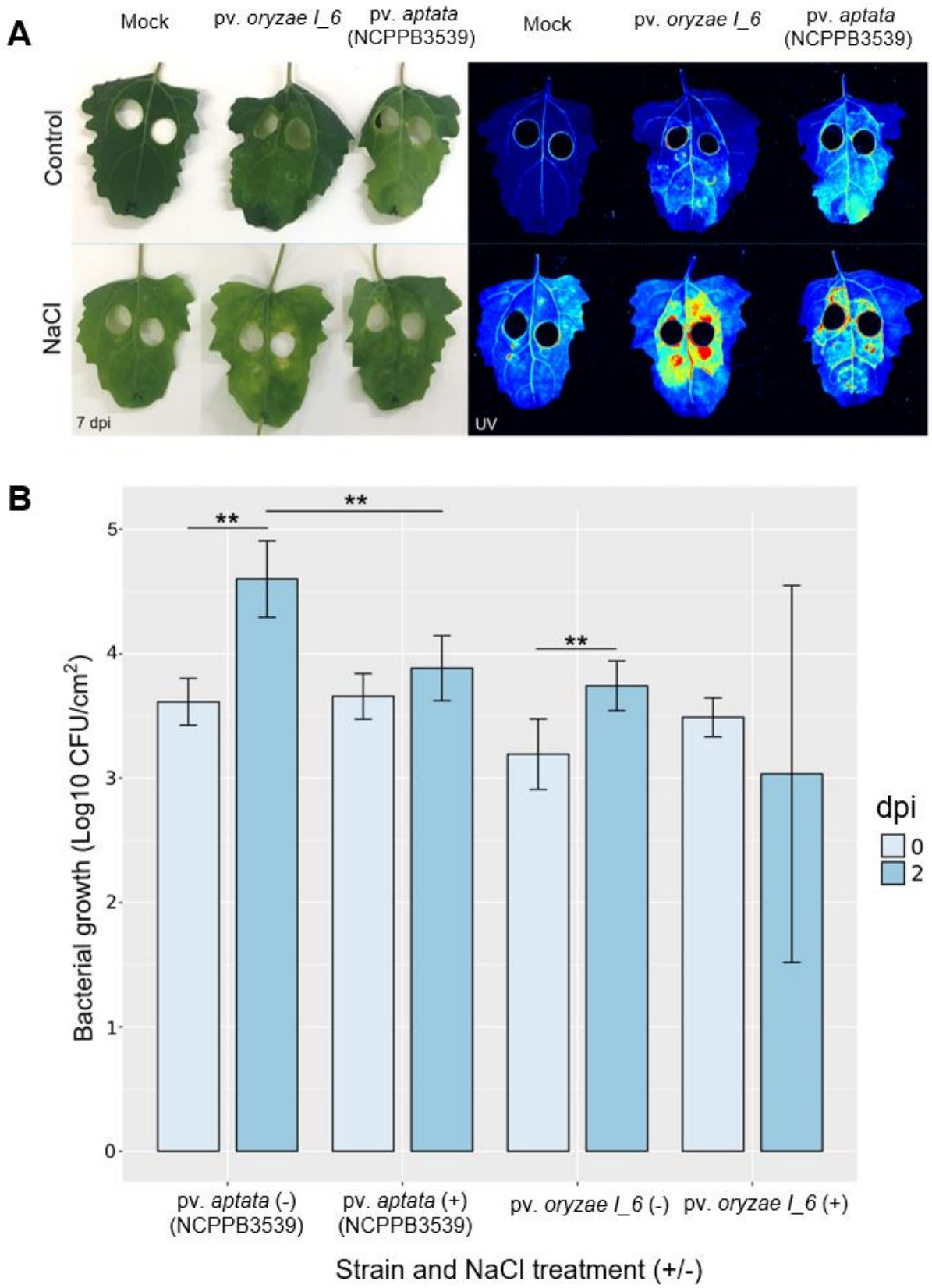

A
Mock
pv. oryzae I_6
pv. aptata (NCPPB3539)
Mock
pv. oryzae I_6
pv. aptata (NCPPB3539)
Control
NaCl
7 dpi
UV
B
**
**
**
Bacterial growth (Log10 CFU/cm2)
0
1
2
3
4
5
dpi
0
2
pv. aptata (-) (NCPPB3539)
pv. aptata (+) (NCPPB3539)
pv. oryzae I_6 (-)
pv. oryzae I_6 (+)
Strain and NaCl treatment (+/-)

Fig. 7. Soil-grown 100 mM salt-irrigated plants are more resistant *to P. syringae* pv. *aptata* NCPPB3539 and pv. *oryzae* 1_6 and accumulate higher levels of fluorescing compounds. Fully expanded leaves of 4.5-week-old potted plants were infiltrated with *P. syringae* pv. *aptata* NCPPB3539 or pv. *oryzae* 1_6 at 10^6 CFU/ml or with mock ($MgCl_2$) as described previously, and bacterial growth quantified (B). Each biological replicate represented two pooled leaf discs taken from one leaf from one plant, where each plant had three leaves inoculated, one for each treatment for one time-point and $n = 6$ per treatment per day. A) UV fluorescence of infected, leaves at 7 dpi alongside corresponding images under visual light, as described previously. The holes in the leaves are due to previously harvested tissue for the infection assays shown in Fig.7B. Double asterisks show significance level of $P < 0.001$ between the treatments grouped by the ends of the bracket, assessed by an un-paired T-test.

4.2.5. Saline quinoa leaves have a higher apoplastic fluid osmolality and extracts inhibit the *in vitro* growth of *P. syringae*

The inhibitory effects observed in the halophytic pathosystem of quinoa - *P. syringae* in the previous sections could be due to active mechanisms in the plant where salt acclimation primes the plant's immune responsiveness to pathogens, and/or due to the direct toxicity of the apoplastic microenvironment via ionic and/or osmotic effects. Given the high osmolality differences of whole leaf cell sap extracts representative of the total apoplast plus cytosolic and vacuolar fluid, it was hypothesised that the apoplastic fraction may also have significantly different osmolalities. To investigate the impact of salt acclimation on quinoa's apoplast composition and approximate how this may affect bacterial growth *in planta,* apoplastic washing fluid (AWF) was extracted from control and NaCl plant leaves (O'Leary et al., 2014). The osmolality value for AWF-NaCl was found to be significantly higher, 0.45 osmol/kg vs 0.1 osmol/kg for AWF-control ($P < 0.0001$) (Fig. 8A). Important to note is these values represent the NaCl concentration of the plants' AWF and not that of their true apoplastic fluid. The AWF values represent a diluted sample of the apoplast due to the method by which it was collected (using water infiltration and extraction; O'Leary et al., 2014), and so differences between control and NaCl plants can only be approximated here. The dilution factor of the AWF extraction technique could however be calculated for quinoa by following additional methods provided in O'Leary et al. (2014).

The growth potential of *P. syringae* pv. *aptata* NCPPB3539 was tested in the AWF of each plant type alongside a nutrient rich (LB) and a minimal nutrient media (M9) (Fig. 8B). The growth curve dynamics were notably different between different growth medium: bacteria reached a maximum optical density (absorbance at 600 nm; OD) of 1.0 in LB by 13 hours, an OD of 0.33 by 25 hours (end of the experiment) in M9, an OD of 0.56 by eight hours in AWF-NaCl and an OD of 0.69 by 13-hours in AWF-control. Although initial growth rates were similar, *P. syringae* reached a higher maximum population density in AWF-control compared to AWF-NaCl, which could suggest limitations in nutrient availability in AWF-NaCl. However, it should be noted that the process of apoplast fluid extraction results in the dilution of apoplastic solutes, and the loss of unstable or volatile compounds such as ROS or cyanide which could be important for inhibiting growth *in planta* (O'Leary et al, 2014). Thus, results obtained using apoplastic washing fluid are not wholly representative of the bacterial growth observed *in planta.*

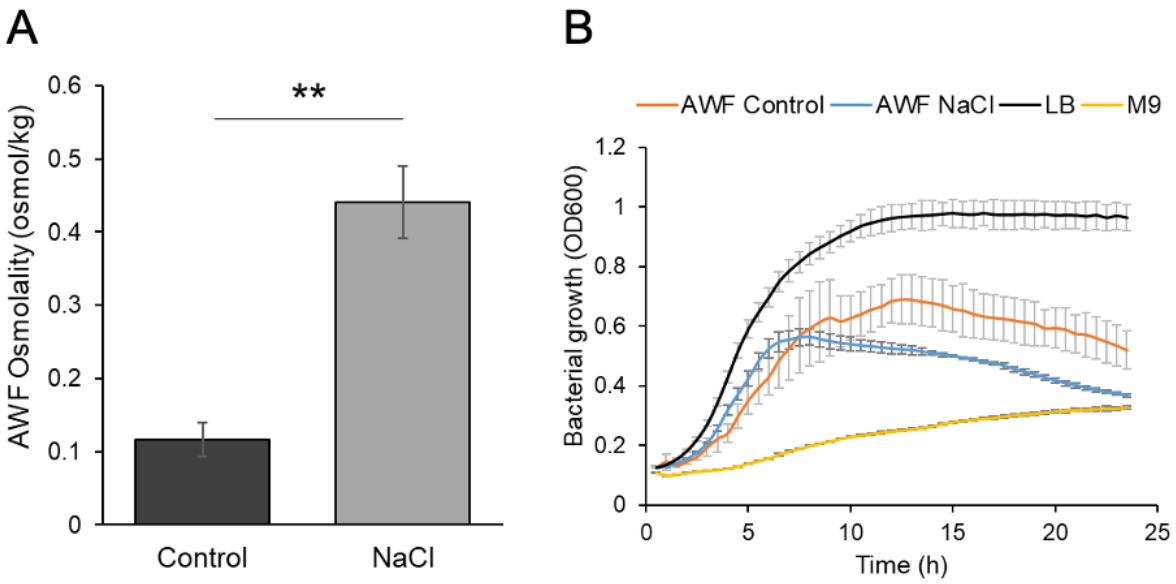


Fig. 8. The osmolality of apoplastic washing fluid (AWF) extracted from hydroponically grown 200 mM NaCl plants is four times higher than the AWF of control plants. A) AWF was extracted from six equivalent leaves of each plant type and the osmolality of AWF extracts was measured for three technical replicates of 40 µL aliquots using the OSMOMAT 30 osmometer. ***P. syringae* pv. *aptata* NCPPB3539 reaches a higher population density in AWF from control plants than 200 mM plants.** B)

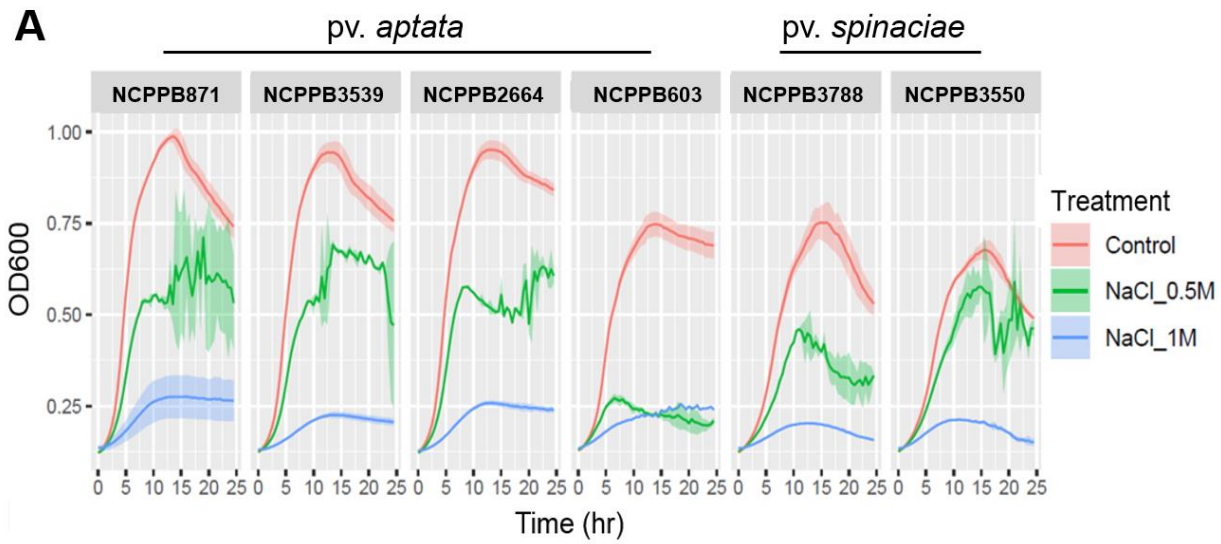
AWF samples were pooled by treatment and filter-sterilised before performing growth curves for *P. syringae* pv. *aptata* NCPPB3539. LB and minimal nutrient media M9 were used as maximum and minimum growth controls, performed as three technical replicates. Only two technical replicates were done for AWF samples due to the limited total volume available. Error bars represent standard deviation and double asterisk represents a significance of $P < 0.01$ between the treatments, assessed by an un-paired T-test.

4.2.6. Salt x pathogen *in vitro* stress studies reveal differential salt tolerance of model strains

To better isolate the specific effect of salt stress on bacterial growth, assays were next performed by maintaining the composition of the growth medium constant but varying the concentration of salt. LB media was chosen as the background medium to ensure nutrient availability was not a limiting or variable factor. The growth of selected *P. syringae* strains was tested in a range of NaCl concentrations around the approximated *in planta* NaCl levels found in low and high salt grown plants using high-throughput in-solution and solid-state set-ups (Fig. 9). NaCl disassociates into Na^+ and Cl^- ions depending on the availability of H_2O, therefore we thought the use of liquid and solid LB media might produce differential ionic and osmotic stress on the bacteria (due to differential solvation of NaCl). Solid media also affects interactions by limiting ion diffusion. The 24h in-solution growth curves revealed different growth rates and dynamics between strains: maximum population density for the pv. *aptata* strains occurs between 12-14 hours (isolate-dependent) and between 15-16 hours for the pv. *spinaciae* strains and reach different maximal ODs 1.00 and 0.75 respectively.

Pv. *aptata* strain NCPPB603 was notably slower growing in LB compared to the three other isolates and was also found to be the most sensitive to salt showing isolate-specific differences in the pathovar (Fig.9A). All strains' growth were significantly inhibited under 1 M NaCl. The growth of all pv. *aptata* isolates (except for pv. *aptata* NCPPB603) in 1 M NaCl plateaus once the maximum OD600 is reached, suggesting a bacteriostatic effect of salt. This maximum OD is ~0.25, which is ~25% relative to the maximum under control (0 mM) conditions. For the pv. *spinaciae* strains, the maximal OD600 reached was 0.2, again approximating to ~25% of the maximum reached under control conditions, however, the growth curve shape was found to be similar under all salt concentrations.

Growth proficiency on the presence of salt supplemented solid media was tested for an extended panel of *P. syringae* strains to complement the in-solution growth curves (Fig.9B). Solid-LB growth reflected the trends found by the in-solution growth curves, however salinity stress administered by a solid growth matrix (which could hypothetically represent salt on the leaf surface following EBC damage or salt gland excretion) could be more inhibitory seen by how no colony forming units were found at 0.5 M NaCl for either of the pv. *spinaciae* strains and 1 M NaCl completely inhibited the growth of all strains, even when plated at the high inoculum starting density of CFU 10^7/ml. Both pv. *spinaciae* isolates (NCPPB3550 and NCPPB3788) followed by pv. DC3000 and pv. *aptata* NCPPB603 are salt-sensitive, showing reduced (or slowed) growth even at control conditions (171 mM NaCl) and full or near-full inhibition at 500 mM NaCl compared to the most salt-tolerant strains which grew at 500 mM NaCl when plated at the minimum inoculum CFU 10^5/ml and were the PG2 pathovars pv. *aptata* (with the exception of NCPPB603) and B728a and *P. fluorescens* strain SWB25.



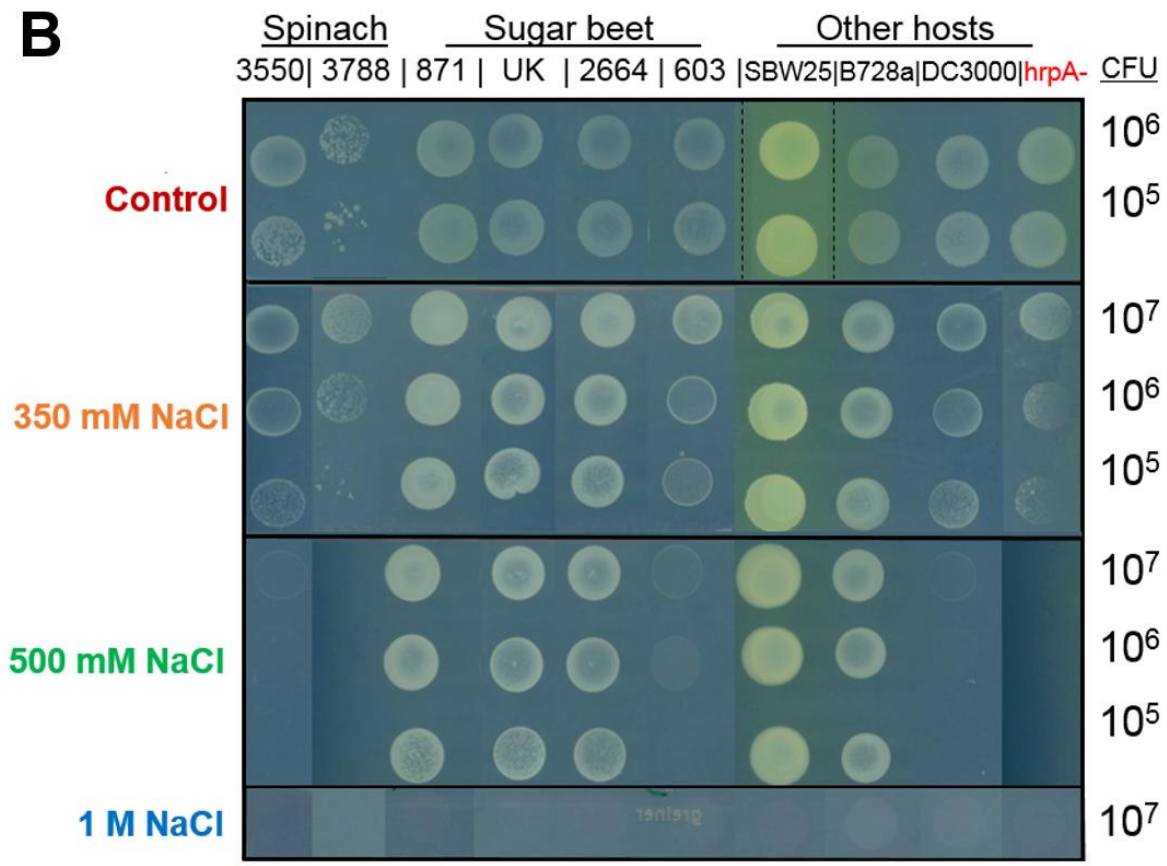


Fig. 9. Comparisons of *in vitro* bacterial growth under varying concentrations of salt. A) *P. syringae* pv. *aptata* strains (NCPPB3539, NCPPB807, NCPPB2664, NCPPB603) and pv. s*pinaciae* strains (NCPPB3550, NCPPB3788) were grown to log phase in LB then inoculated into 150 µL of NaCl-supplemented LB to a starting OD of 0.1 and growth was tracked over 24 h at 28 °C. Error bars show standard deviation between three technical replicates. Results are representative of two independent experiments. **B)** The solid-state salt-tolerance of model pathogen strains was compared to a wider panel of strains previously used along with the non-pathogenic epiphyte *Pseudomonas fluorescens* SBW25. 'Control' represents the standard LB NaCl concentration (171 mM), then two, three and six times this concentration was used i.e., 342 mM, 513 mM and 1026 mM NaCl. Bacteria were adjusted to three different CFUs 10^5-10^7 /ml and 20 µL of each were plated onto 10 cm^2 plates of varying NaCl. Images show representative growth from two technical replicates after 48 h incubation at 28 °C. Raw plate scanner images were cut only to align strain and treatments together in a more suitable order than was originally chosen when plated.

4.2.7. Pv. *aptata* strains contain an expanded number of genes encoding proteins containing Na^+ Transporter domains relative to PG1 pathovar pv. *spinaciae* and pv. DC3000 and PG2 pathovar pv. B728a

Next, the genomes of model strains were queried for genes containing putative salt associated Pfam domains (such as ion transport proteins) to see if gene copy numbers correlated with *in vitro* salt tolerance results, where HMMER was used to search for homologs across the reference protein database, Pfam (Fig.10). Both *P. syringae* pv. *spinaciae* isolates contained very similar numbers of protein domains associated with salt tolerance to the reference PG1 strain *P. syringae* pv. *tomato* DC3000. The four *P. syringae* pv. *aptata* isolates contained similar numbers of protein domains to the reference PG2 strain B728a, except for in their number of sodium exporter Na^+H^+ exchanger domains: just five were found in B728a compared to eight in pv. *aptata* NCPPB2664 and pv. *aptata* NCPPB3539 and six and seven in pv. *aptata* NCPPB603 and pv. *aptata* NCPPB871 respectively. PG1 strains pv. DC3000 and both pv. *spinaciae* isolates contained just six and five Na^+H^+ exchanger domains.

Phylogroup	Isolate	SNF	SDF	SSF	Na_sulph_symp	Na_H_exchanger	Na_Ala_symp	Na_Ca_ex	SBF	Ion_trans	TrkH	NQR2_RnfD_RnfE	MnhB	MadM	Ion_trans_2	Na_H_antiport_1	NHaB	NQRA	Cation_ATPase_C	Cation_ATPase_N	MNHE	Na_Pi_cotrans	PhaG_MnhG_YufB	Na_H_antiporter	MrpF_PhaF
1	P. syringae pv. spinaciae NCPPB3550	1	3	3	0	5	1	2	2	1	1	0	1	1	3	2	0	0	0	0	1	1	1	0	1
1	P. syringae pv. spinaciae NCPPB3788	1	3	3	0	5	1	2	2	1	1	0	1	1	3	2	0	0	0	0	1	1	1	0	1
1	P. syringae pv. tomato DC3000	1	3	3	0	6	1	2	4	1	1	0	1	1	3	2	0	0	0	0	1	1	1	0	1
2	P. syringae pv. aptata NCPPB2664	1	3	3	0	8	1	2	2	1	1	0	1	1	1	2	0	0	0	0	1	1	1	0	1
2	P. syringae pv. aptata NCPPB3539	1	3	3	0	8	1	2	2	1	1	0	1	1	1	2	0	0	0	0	1	1	1	0	1
2	P. syringae pv. aptata NCPPB603	1	3	3	0	6	1	2	2	1	1	0	1	1	1	2	0	0	0	0	1	1	1	0	1
2	P. syringae pv. aptata NCPPB871	1	3	3	0	7	1	2	2	1	1	0	1	1	1	2	0	0	0	0	1	1	1	0	1
2	P. syringae pv. syringae B728a	1	2	3	0	5	1	2	2	1	1	0	1	1	1	2	0	0	0	0	1	1	1	0	1

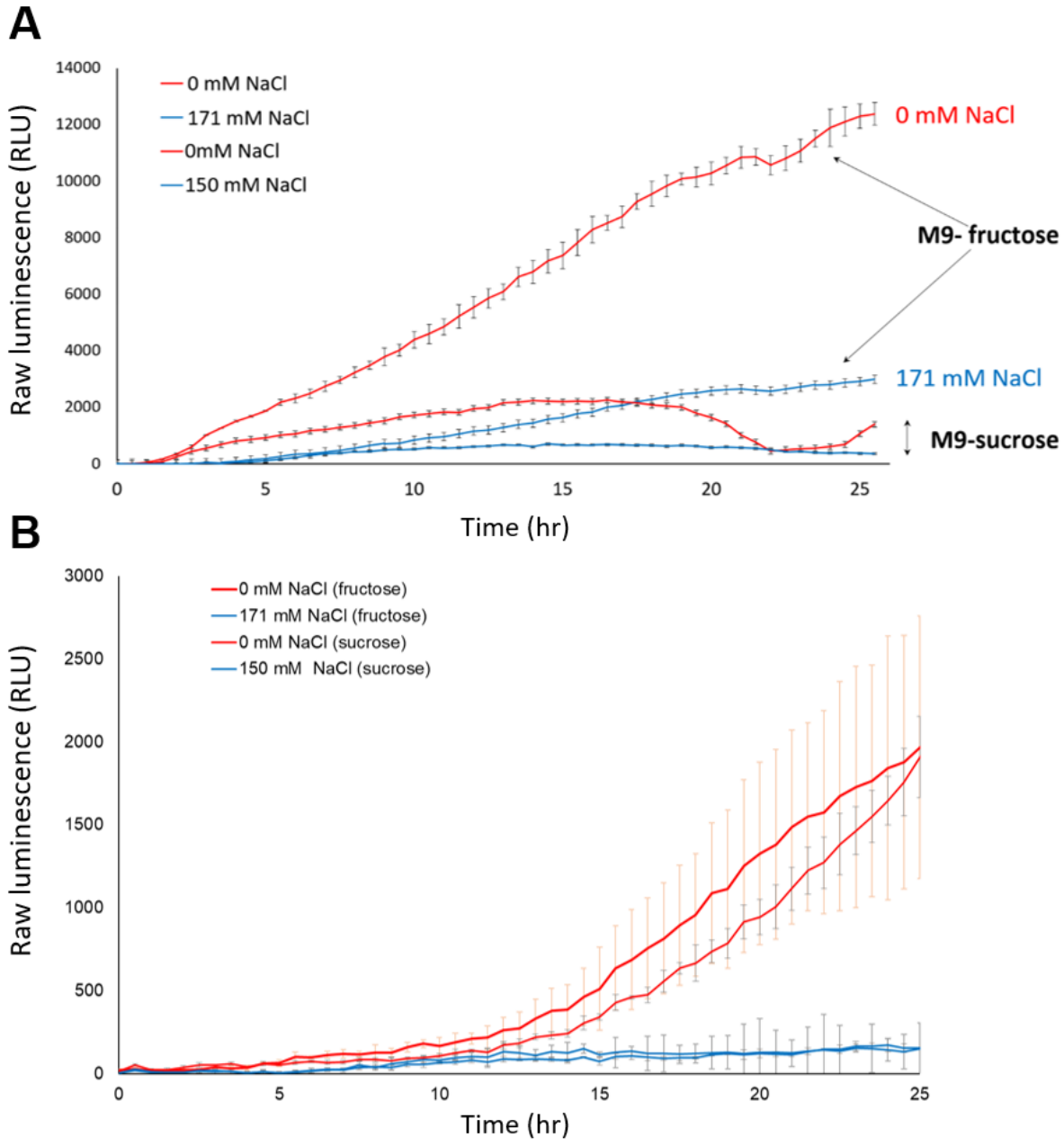
Fig.10. Salt transport associated Pfam protein domain numbers vary between pathovars and within pathovars but are more consistent within phylogroups. A matrix which shows the variation in salt tolerance Pfam protein domains between *P. syringae* strains. Cell numbers correspond to the number of domains identified in each strain where domains showing the most variation between strains are highlighted in yellow.

4.2.8. Salt inhibits virulence gene expression

Previous experiments shown earlier in this Chapter (Fig.1) proved the critical dependency of the T3SS for successful virulence in quinoa, which was expected based on other *P. syringae* pathosystems (Cunnac et al., 2011; Dillon et al., 2019). And so lastly, we evaluated the direct effect of salt on *P. syringae* T3SS expression by using its positive regulator gene hrpL as a virulence reporter system. NaCl was supplemented to minimal M9 media to approximate a nutrient composition more typical of the plant apoplast and to ensure virulence gene expression (Rahme et al*.,* 1992). PG1 strains pv. *spinaciae* and pv. DC3000 were transformed with the pBS63 LUX plasmid (phrpL::luxCDABE) so that light intensity could represent virulence gene expression. To establish conditions, two different carbon sources sucrose and fructose (which is known to be T3SS-inducing) for supplementing M9 salts were trialled, guided by concentrations used in previous studies (McCraw & Preston, unpublished). The growth of both strains showed a strong preference for sucrose over fructose for both control (0% NaCl) and NaCl (~1% NaCl) conditions however the mild salt stress inhibited growth by similar amounts relative to controls (12% and 15% for sucrose and fructose respectively, data not shown). Pv. *spinaciae* growth in both minimal media was very minimal however M9-sucrose was most amenable for the experiment showing a 14% growth increase over 25 h but just 4% for M9-fructose under control conditions. Under 1% salt, growth was negligible: 3% in M9-sucrose and 0.8% in M9-fructose and again, this growth inhibition relative to control for both media was very similar: 21% in sucrose and 20% in fructose. The higher inhibition of *in vitro* growth under saline conditions for pv. *spinaciae* vs pv. DC3000 corroborates with the solid-phase salt assays (Fig.9).

In M9-fructose, pv. DC3000 hrpL expression under control and saline conditions steadily increased over the 25 h period where 1% (171 mM) NaCl caused a significant 6-fold inhibition (Fig.11A) by 25 h. HrpL expression in M9-sucrose was comparably suppressed under both control and saline conditions where after 15 h levels for both conditions decreased (Fig.11A). In contrast, the dynamics of hrpL expression for pv. *spinaciae* grown under different carbon sources were very similar (Fig.11B) and salt was also shown to inhibit expression 12-fold in both media. The impact of salt on growth and hrpL expression is summarised by the derived graphs showing the total integrated LUX over integrated OD600 across the 25h time-course

for each strain (Fig.11C). The maximal hrpL expression levels reached in pv. *spinaciae* were over 6-fold lower than in pv. DC3000 (Fig.11D), which, alongside the comparably lower growth consistently found in all *in vitro* systems tested suggests a more specific niche environment might be created by this strain *in planta.*



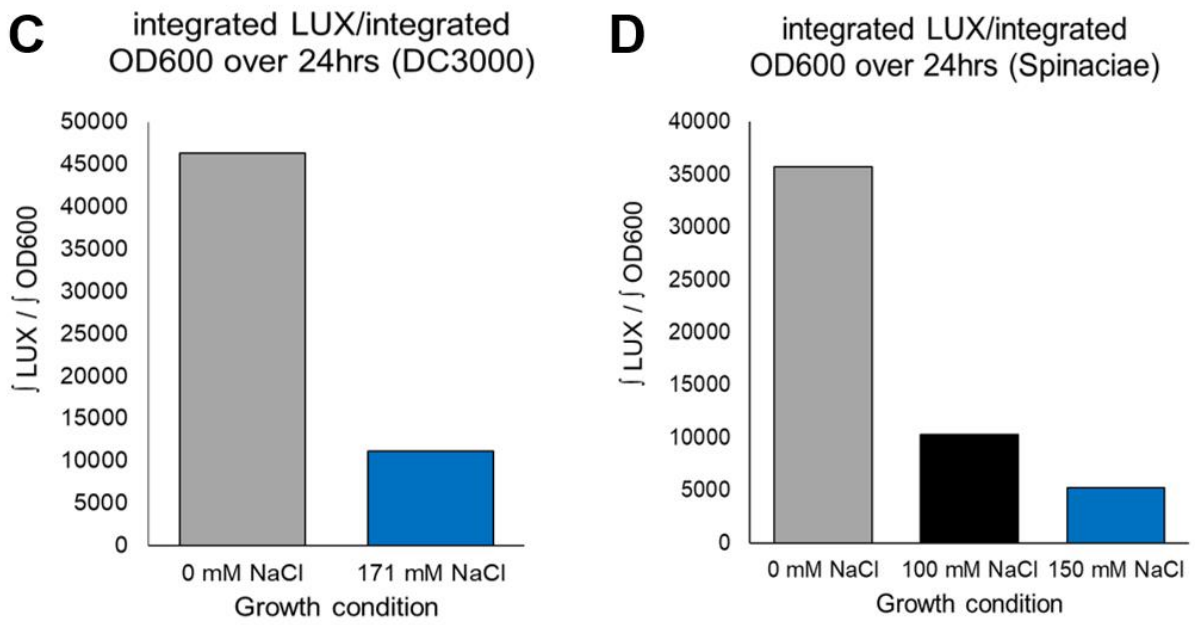


Fig.11. The effect of salt on hrpL gene expression for pv. DC3000 and pv. *spinaciae* NCPPB3550 under salt. 5 mM M9-sucrose and 10 mM M9-fructose supplemented by 0 mM NaCl, 100 mM and 150 mM or 0 mM NaCl 171 mM NaCl respectively for pv. *spinaciae* (A) and pv. DC3000 (B) respectively and used to induce varying effects on bacterial growth and hrpL expression. A) Luminescence traces over 25 h performed in triplicate technical replicates, error bars show standard deviation B) Integrated hrpL expression over integrated bacterial growth between 0 and 25 h for pv. DC3000 (C) and pv. *spinaciae* (D). Each technical replicate was performed as 150 µL solution in a 96-well plate with opaque sides but transparent well bases and run on the TECAN plate reader as described in methods.

4.3. Discussion

This chapter aimed to establish an amenable model pathosystem in quinoa with *P. syringae* where pathogenic and non-pathogenic strains could be classified and the impact of salt on disease resistance could be assessed. These results were then interpreted using additional insights from bioinformatic analyses (comparative genomics) of the strains at the level of effectors, secondary metabolite and salt-associated factors. The second part of the chapter addressed the hypothesis that infections in saline quinoa caused direct (plant-independent) and indirect (plant immunity-dependent) inhibitory effects of salt on pathogen growth. All initial experimental objectives were met but to differing levels of resolution after our focus shifted towards exploring the major finding that disease resistance to *P. syringae* increased significantly in salt-acclimated quinoa plants.

The relationship between the ubiquitous bacterial pathogen *Pseudomonas syringae* and quinoa had only been documented in one study (Maraite et al., 1997) prior to this project starting where quinoa was found to be highly susceptible to all pv. *aptata* isolates tested (causing leaf wilting) with varying susceptibility to pv. *atrofaciens* isolated from other hosts wheat and barley, whereas no symptoms were induced by a citrus isolate (pv. *syringae*). Since then, one natural field infection and another controlled infection study with a native *P. syringae* strain were described in Colombia and Egypt (Fonseca-Guerra et al., 2021; Badran et al., 2023). However, the interaction between British-grown quinoa cv. Atlas and the British sugar beet isolate pv. *aptata* NCPPB3539 was not known, nor was infection data available for pathovars from other phylogroups, or for pathovars of other important Amaranthaceae crops such as the spinach pathogen pv. s*pinaciae.* With genome data available for many strains across the core *P. syringae* phylogeny, genetic factors were matched with phenotypic data to understand pathogenicity of *P. syringae* to quinoa.

4.3.1. The bacterial species *Pseudomonas syringae* is an amenable model pathogen for investigating disease and resistance processes in *Chenopodium quinoa*

Molecular-level pathology research in quinoa trails far behind research investigating quinoa's abiotic stress tolerance mechanisms. *P. syringae* was seen as a strategic candidate for elucidating disease processes in Atlas given its ubiquitous prevalence and agricultural relevance as a pathogen (of varying specificity) to many economically important crops, paired with the technical advantages of being genetically modifiable, genetically diverse and with accessible research expertise and tools available for functional studies. Furthermore, highly informative model *P. syringae* pathosystems had previously been established between *P. syringae* and non-native hosts such as Arabidopsis and *N. benthamiana,* demonstrating the practicality of establishing novel pathosystems for yielding plant immunity and bacterial pathogenicity insights (Dong et al., 1991; Goodin 2008).

The major milestone of this Chapter therefore was the successful establishment of a *P. syringae* pathosystem in quinoa with high technical convenience: up to four different strains can be tested per plant facilitating comparative growth experiments; quinoa leaves are comparably easy to inoculate via needleless syringe infiltration; and a short time-course of

just two days was sufficient to observe differences in pathogenicity/virulence between pathovars. The dynamics are different to those observed in other plant – *P. syringae* pathosystems however, where unlike our system (where for virulent strains infection progresses rapidly to necrosis with no further growth by 3 dpi) the infection in other hosts continues progressing to three, five, seven and even 14 dpi (Katagiri et al., 2002; Zumaquero et al., 2010; Nunes de Silva, 2020). A semi-quantitative approach for tracking early to late symptom development in quinoa leaves was also developed using a UV-transilluminator and visible light imaging which captured striking leaf pigment changes and fluorescence-emission induced by saline plant growth conditions or specifically by certain pathovars such as the PG4 rice isolate pv. *oryzae* 1_6. The fluorescing compounds may be stress-inducible antioxidants such as phenylpropanoids (Sharma et al., 2019) and/or antimicrobial phytoalexins (Großkinsky et al., 2014) or potentially might represent changes in photosynthetic pigment levels. A more sensitive fluorescent compound-specific and less invasive method could interrogate the spatiotemporal dynamics of fluorescence production and shed light on the complexity of salt-host, salt-pathogen and host-pathogen interactions in the halophytic pathosystem. For example, Hupp et al. (2019) developed a method for monitoring infection in intact leaves by combining Pulse-Amplitude Modulation (PAM) fluorescence and conventional binocular microscopy with suitable wavelengths and filters to simultaneously track *P. syringae* (constitutively expressed) GFP, plant chlorophyll (Chl-F) changes and phenolic compound accumulation. The viability of the bacteria would need to be checked post-exposure to UV light however or compensated for by preparing sufficient levels of replication. Preliminary work with Morgan Wade demonstrated an ease of creating virulence gradients in quinoa leaves by changing the starting inoculum density of strains in 5-fold increments which allows a higher resolution of comparative symptom development, colonization and proliferation dynamics to be studied.

Lastly, the ease of accessibility to high genetic diversity on both the plant and pathogen side provides scope for identifying resistance processes i.e., specific resistance or susceptibility genes, which could be applicable to other pathogens and incorporated into quinoa breeding programmes. This study trialed five of the 13 known phylogroups of the *P. syringae* species complex using nine different pathovars, yet over 500 *P. syringae* pathovars from over 100 plant hosts from 28 different countries exist (Dillon et al., 2019) and are accessible from public

banks such as NCPPB or through strain exchange with other groups' collections. Therefore, it would be easy to extend our pathosystem to include further *P. syringae* diversity. Unfortunately, it proved impossible to obtain the only published quinoa-specific *P. syringae* isolate from field-grown quinoa in Colombia (Fonseca-Guerra et al., 2021). Future work therefore should aim to isolate further natural isolates of quinoa to understand how native growth dynamics compare to those observed in this study where it is assumed they would be better at establishing a niche in quinoa's microenvironment and suppressing host defences. Two attempts at doing this from diseased quinoa leaves of quinoa plants grown in British (2019) and Bolivian (2022) fields were unsuccessful and only non-pathogenic bacterial endophytes were found (Supplementary Figure 1). Quinoa as a species, also has immense genetic diversity thanks to the work of small-holder Andean farmers who for thousands of years grew and maintained multiple landraces (for subsistence farming) at a time, and more recently to the conservation efforts of National and regional germplasm banks such as at INIAF and UTO of Bolivia and at INIA in Peru. During this project we obtained a panel of 30 accessions from INIAF which represented varying abiotic and biotic stress tolerance in situ and future objectives would be to screen these using our 'halophytic pathosystem' established in Atlas.

4.3.2. Limitations of the *C. quinoa* – *P. syringae* pathosystem

Several technical and biological limitations of the pathosystem were identified throughout this project. The space available for growing enough plants, along with the time needed to inoculate and process a sufficient number of samples for robust results limited the number of strains testable at one time. The syringe infiltration technique used in this study, while a direct way to study endophytic growth potential, is relatively time-sensitive given how bacteria viability in the nutrient-deficient inoculation solution ($MgCl_2$) reduces with time (Preston Lab, unpublished). Likewise, preparing tissue for colony counting is laborious and also requires additional technical replication at the plating stage. Three solutions for improving throughput are proposed: firstly, the development of a dip or spray inoculation technique (Jacob et al., 2017; Buscaill et al., 2019) would speed up the inoculation step whilst also providing a chance to study a more natural infection process through quantifying epiphytic as well as endophytic colonization; secondly, the LUX reporting system for

quantifying *in planta* growth could be further optimised for use in our pathosystem (Soldan et al., 2021); and lastly, to save space and maintain high replication levels, both these techniques could be trialed on smaller/younger plants, as done for Arabidopsis (Martel et al., 2020) guided by preliminary *in vitro* early-stage growth studies developed in Chapter 3. If the trends found for mature plant infection assays could be recapitulated in quinoa seedlings, then a high-throughput, space-efficient system such as a 12 or 24-well plate could be implemented. A recent study successfully used a quinoa seedling infection set-up to investigate the protective effect of pre-inoculation with beneficial *Bacillus* endophytes to reduce *P. syringae* pathogenicity (Badran et al., 2023).

A biological limitation of the pathosystem was the finding that even the most pathogenic strains were not able to grow beyond 3 dpi, nor did they appear to colonise tissue much beyond the infiltration zone, which could be expected for true specific pathogens of quinoa based on the dynamics other pathosystems (Katagiri et al., 2002; Zumaquero et al., 2010; Nunes de Silva, 2020). The overall outcome of *P. syringae* is a balance between defence triggering and defence-suppressing factors (Katagiri et al., 2002; Laflamme et al, 2020) and so we could be observing the unfavorable effect (for the pathogen) of excessive necrosis induced by pathogen-secreted phytotoxins which cause full tissue collapse and limits further growth, or alternatively, perhaps by 3 dpi the plant has recognized certain effectors and triggers an ETI hypersensitive response (HR) to prevent further spread of the bacteria. Given how none of the strains were natural isolates of quinoa and therefore have not had time to evolve around this, it could be hypothesised that the former reason (as a result of non-host resistance; NHR) is more likely. Testing the phenotypic effect of specific known cell-death inducing T3SS effectors such as syringolin could be achieved using the PsyTEC system (Laflamme et al., 2020) whereas the TUNEL assay (Tripathi et al., 2017) or Trypan Blue stain (Bach-Pages and Preston, 2018) could be used to look for microscopic and macroscopic signs of defence-induced HR.

The limit of bacterial colonisation beyond the infiltration zone could also be due to ultrastructural, physiological or biochemical restrictions of the quinoa apoplast microenvironment, which could disfavor apoplastic colonisation of bacterial pathogens and become even more recalcitrant to infection in salt-acclimated tissue.

Another curious observation of the pathosystem was the absence of macroscopic signs of effector triggered immunity (ETI) for pathogens that showed no or declining growth in quinoa. Thus, canonical avirulent interactions could not be concluded for any of these strains and adds more evidence to such outcomes being a sign of NHR. Additionally, to the aforementioned PsyTEC, TUNEL and Trypan Blue assays for ETI, other strategies for increasing the chances of observing canonical ETI in quinoa include testing pathovar representatives from the remaining untested *P. syringae* phylogroups as well as other T3SS virulence-dependent bacterial species such as *Xanthomonas* spp. (Wichmann et al., 2013).

The identification of pathogen effectors that elicit ETI, termed avirulence 'Avr' proteins, in other pathosystems has led to the identification of the specific disease resistant proteins in the host plant and some have shown translational value for improving the resistance mechanisms of other species. For example, Pto kinase and the LRR protein Prf together form a resistance protein complex that specifically recognises the effectors AvrPto and AvrPtoB of the *P. syringae* tomato pathovar DC3000. Pto/Pfr when heterologously co-expressed in *N. benthamiana* secured full resistance to the pathogen pv. *tabaci,* (which also carries AvrPto and AvrPtoB orthologs) (Balmuth and Rathgen, 2007). Therefore, it would be important to next investigate quinoa's ETI as well as deepening our understanding of the plant's basal and salt inducible PTI mechanisms.

Lastly, to date, only one report of *P. syringae* bacterial spot disease has been reported in the wild and therefore does not currently represent the most economically important and pressing pathogen to study for quinoa farmers. Through a BSPP-Junior Fellowship I undertook in 2022 I was unable to isolate *P. syringae* from seven ecotypes of Bolivian quinoa grown in fields at one central (Caracollo) and one southern (Salinas de Garci Mendoza) altiplano location. Only *Bacillus* spp. bacterial strains were isolated from diseased leaves harvested in the field, with identities similar to those isolates by Badran et al. (2023), and they were found to be asymptomatic on cv. Atlas suggesting their role as non-pathogenic endophytes (Supplementary Figure 1). Interestingly, Badran et al. (2023) suggests *Bacillus* spp. endophytes might be beneficial against *P. syringae* pathogens.

4.3.3. Abiotic stress tolerance and host-relatedness to quinoa influences the virulence potential of *P. syringae* isolates on quinoa

Without native quinoa *P. syringae* isolates it is difficult to accurately investigate and define host-related specificity factors, however, the key finding that isolates from host related crops sugar beet and spinach were also aggressive on quinoa is interesting. Not only does it suggest host-genetic relatedness may be a better predictor of virulence in quinoa than pathogen genetic relatedness, but it raises agricultural concerns where fields of these staple vegetable crops may rotate with or lie close to quinoa crops. A recent comparative genomics study of 102 different *P. syringae* pathovars by Rankovic et al. (2023) with a focused analysis between differentially virulent pv. *aptata* isolates (six from sugar beet and one from rice) revealed a large range of different effectors (T3Es) globally. They proposed that 3% of total T3Es across all strains were 'core' whereas 97% were classified as 'accessory genes'. Between the six sugar beet pv. *aptata* strains 32 different T3Es were found, and three (AvrRpm1, HopAW1, and HopAU1) were uniquely present in one of the highly virulent and broad host-range strains, pv. *aptata* P21, which together demonstrates the high propensity for horizontal gene transfer within the pv. *aptata* pathovar. It will be interesting to obtain and test several of these differentially virulent pv. *aptata* isolates on quinoa.

Host compatibility depends on the presence of specific effectors, secondary metabolites and stress-tolerance factors acquired to withstand the apoplast microenvironment of their host species and to suppress host immunity (Preston, 2017). Plants of the Amaranthaceae family are renowned for their abiotic stress tolerance, where constitutive and facultative adaptations to their local environment such as salt or osmolyte accumulation and other physiological changes related to heat or drought stress tolerance could create a unique leaf apoplast microenvironment. Interestingly, a recent Amaranthaceae crops comparative growth and nutrient profiling study we performed last winter demonstrated sugar beet leaves grown in research grade peat irrigated with non-saline tap water in long-day greenhouse conditions accumulated four times more sodium than quinoa plants (Scrafton and Preston, unpublished). Sugar beet is also a salt-tolerant vegetable crop (Skorupa et al., 2019) and so the biological value for accumulating sodium is understandable and could explain also why its native pathogen pv. *aptata* was found to have high salt tolerance *in vitro*. The strain copy

number of genes with Na^+H^+ exchanger domains seemed to correlate with their *in vitro* plate and solution-based salt tolerance results where all pv. *aptata* isolates (excluding the least salt tolerant isolate pv. *apata* NCPPB603) contained an expanded number relative to less salt tolerant PG1 strains pv. DC3000 and both pv. *spinaciae* isolates.

The snow-isolated strain CC1557 was also found to propagate very well in quinoa which could be related to its high environmental stress hardiness. Further genomic and *in vitro* stress studies will need to be extended to this strain in future work (this strain was acquired at the end of this project). Given this strain has a small T3E repertoire, the phenotypic effect of T3E deletion or addition could be evaluated more readily to identify key T3Es for virulence, as well as putative avirulence, in quinoa, or whether alternate virulence factors are important.

Lastly, bioinformatic analyses revealed an expanded number of genes for the syringolin phytotoxin in all isolates of pv. *aptata* and pv. B728a relative to pv. DC3000 and pv. *spinaciae*. Syringolin A has been shown to function as an irreversible proteasome inhibitor which promotes bacterial colonization in the apoplast by inhibiting stomatal closure (Schellenberg et al., 2010) which could antagonise the innate immune response of ABA-induced stomatal closure in quinoa. It will be important therefore to investigate basal ABA levels in quinoa cv. Atlas and how they change under PTI-induction or following infection by certain *P. syringae* strains (Goel et al., 2007). Interestingly, mangotoxin genes were only found in pv. *aptata* which, like the well-studied phytotoxin phaseolotoxin, disrupts amino-acid biosynthesis pathways, specifically ornithine/arginine biosynthesis (Arrebola et al., 2007) which could highlight the importance of these amino acids for disease resistance in quinoa. Mangotoxin production is critical for the full virulence of *Pseudomonas syringae* pv. *syringae* on mango, manifested as apical necrosis (Arrebola et al., 2007) and so it will be interesting to test the dependence of amino-acid biosynthesis inhibiting toxins across the pathogenic vs. non-pathogenic strains. AvrE1 also appears crucial for infecting quinoa given how all strains except the null growth pv. *glycinea* KN44 strain possess a copy, whilst 10 T3Es (Fig.4; rose-coloured cells) were absent in all pathogenic strains which could indicate some may contribute to non-compatible interactions in quinoa. HopM1 and HopAH1 could be important T3Es for establishing initial growth in quinoa considering how the two null-growth strains pv *glycinea* KN44 and pv. *phaseolicola* 1448A are the only strains lacking a copy, except for the low-

effector virulent strain CC1557, but where the CC1557-specific T3Es HopAH2 or HopBJ1 might counterbalance this loss.

4.3.4. Salt accumulation in quinoa leaves creates an inhibitory microenvironment which could be exploited as a defence strategy against apoplast-colonising pathogens

The fascinating finding that quinoa cv. Atlas grown under saline conditions becomes much more resistant to the model pathogen pv. *aptata* NCPPB3539 could be due to a direct and indirect inhibitory bacterial growth effects of salt. For example, salt was shown to directly inhibit growth and the gene expression of the master regulator of T3SS-virulence hrpL *in vitro*, however it is possible that the pronounced salt-induced phenotypic and transcriptional changes observed in quinoa (characterised in Chapter 3) could indirectly restrict bacterial growth. A less favourable microenvironment ultrastructure along with inhibitory biophysical, physiological and biochemical changes within the halophytic apoplast could limit growth or effect the colonization dynamics of bacteria. Interestingly, it was found on several instances during preliminary work that saline quinoa tissue becomes more recalcitrant to intercellular water flow or uptake via the petiole, which along with the significantly higher osmolality of both leaf cell sap and AWF could affect relative water status (data not shown).

The composition of high salt AWF extract was found to be more inhibitory to pv. *aptata* NCPPB3539 in the 96-well plate *in vitro* growth study. Curiously, a significant colour change from light grey to mustard yellow was observed in these wells at the end of the experiment but not in the wells of the high salt AWF negative control (no bacteria) nor in the respective low salt AWF (+/- bacteria) wells. This suggests differential use of nutrients by the bacteria growing in the AWF of high salt plants, and when we performed preliminary ICP-MS analysis of low and high salt AWF samples, striking differences in metal composition were found, most notably: a 147-fold increase in Na ($P < 0.001$), a 7.3-fold increase in Zn ($P < 0.0001$), +3.6-fold in Mg ($P < 0.0001$), +1.7-fold in K ($P < 0.0042$), +1.5-fold in Fe ($P < 0.0004$) and reduced levels of Ca and Mn, -3.2-fold ($P < 0.0001$) and –1.9-fold ($P < 0.0002$) respectively. Kiani-Pouya et al. (2017) found a large and significant decrease in the metabolite oxalate in high salt leaf extracts and calcium oxalate precipitates were also only observed in the leaf cell sap extracts from low salt plants (Scrafton and Preston, unpublished).

The enhanced fluorescence of saline leaves pre and post infection relative to low salt leaves suggests a higher content of fluorescing polyphenols and lignified tissue, where phenols not only confer higher antioxidant capacity but also have antimicrobial effects, shown to increase the permeabilisation and destabilisation of the bacterial plasma membrane or to inhibit extracellular enzymes produced by bacterial strains (Tako et al., 2018; Miklasińska-Majdanik et al., 2018; Aldulaimi et al., 2017).

Lastly, an elevated level of ABA signaling found in saline quinoa (Ruiz et al., 2019; this thesis, Chapter 3) could keep stomata closed antagonising the effects of pv. *aptata* NCPPB3539 syringolin A and reducing the transpiration rate, which could also affect the osmotic and biochemical balance in the apoplast. To shed light on whether salt influences the immune system of quinoa triggering enhanced immunity mechanisms a combinatorial experiment was designed and tested in the next Chapter.

4.4. Conclusion

The model pathogen *P. syringae* has demonstrated high potential (and amenability) for investigating disease and resistance processes in quinoa. Likewise, the halophytic phenotype of quinoa, which can be controlled precisely, provides a fascinating novel microenvironment for studying combinatorial abiotic and biotic stress effects on bacterial growth *in planta*.

The core finding underpinning the direction of experiments in this chapter, the subsequent chapter and future follow-on work was the significant 5-fold inhibition of bacterial growth in saline plants, grown both hydroponically and in soil when irrigated by salt water. A direct inhibitory effect of salt on both bacterial growth and virulence gene expression in-vivo was found, where different pathovars were affected to different extents, which could be explained by the relative salt-tolerance of the host plant species, or to the bacteria's propensity for environmental stress hardiness (CC1557) as an epiphyte (B728a). The higher number of Na^+H^+ exchangers, the presence of syringolin biosynthetic genes and potentially the unique presence of mangotoxin found in all pv. *aptata* isolates tested could explain the greater virulence of the strain in quinoa relative to others tested.

Next it will be interesting to obtain pathogenic *P. syringae* strains isolated from quinoa in the field and test how they behave in the series of *in planta* and *in vitro* differentially saline protocols developed in this Chapter.

4.5. Methods

Infection assays

Overnight (ON) cultures of single colonies of each strain were prepared in liquid LB from LBA plates (of single colonies originally streaked from glycerol stocks which had been kept at 80°C). The ON cultures were washed twice and resuspended in 10 mM $MgCl_2$ and adjusted by serial dilutions to the required inoculum density - all results shown in this thesis were in the range of 0.0002 - 0.1 OD600 (~$1x10^5$ – $1x10^7$ CFU/ml) OD600. Individual strains were (needless) syringe infiltrated into the abaxial side of equivocal fully expanded quinoa leaves from 4-5-week-old soil-grown plants. If leaves were particularly tough (due to different growth conditions) a needle prick was used to aid gentle infiltration into the apoplast to reduce syringe-impact damage to the leaf (visible in some images), and all samples were infiltrated this way. All infiltrations were completed within <90 minutes and most within <60 minutes to minimise the stress to the bacteria which could have caused potential differentials in early *in planta* fitness. However, readings at 0 dpi readings were always taken (bar the first infection experiment –data not shown) so that 2 dpi titres and thus growth in quinoa could be evaluated validly. All leaf infiltrations were performed between 09:30-12:00 and the 0 dpi measurements were taken 3hrs after the mid-point of the infiltration window, 2 dpi was taken 48 hours after the 0 dpi measurement. The colony count experiment was performed as per (Buscaill et al., 2019). Strains were plated typically on solid LBA, but fast-growing strains (pv. *aptata* NCPPB3539) were often inoculated on LBA + nitrofurantoin antibiotic (1 µg/ml) to slow growth and force tighter colonies to form for easier counting. Plates were incubated at 28 °C for 16h-32h depending on the strain's growth rate and removed and stored at 4°C until the time of colony counting (usually done immediately).

In-vitro bacterial growth assays in rich and minimal media and apoplastic fluid

For in-solution growth curves: liquid cultures of single colonies were grown to log phase in LB and inoculated into a 150 µL fresh LB (or fresh minimal media, or apoplastic washing fluid details below) in the wells of a 96-well transparent plate to a final OD of 0.1.
The LB used was prepared in batches of three different salt concentrations: control LB with no extra NaCl added (final concentration: 171 mM NaCl), then LB adjusted to 500 mM and 1 M NaCl (autoclaved and cooled to RT before use). Minimal M9 media (for the virulence gene expression experiments) was prepared by diluting pre-made 10x M9 salts into sterile distilled water supplemented by 5 mM sucrose or 10 mM fructose (diluted from 10x stocks), $CaCl_2$ and $MgSO_4$ (final concentrations of 0.1mM) and sterile NaCl was added to reach 50mM, 100mM and 150 mM. For the apoplastic washing fluid (AWF) growth curves, 500 µL was obtained using the protocol by O Leary et al. 2014 and stored at –20 °C until it was thawed and used neat for inoculations.

The OD600 of each well was measured over 24 h using an Infinite M200 plate reader (Tecan Group Ltd, Switzerland) with the temperature controlled at 25 °C and measurements taken every 30 min. The plate was prepared as three technical replicates per strain and treatment and results were plotted and analysed by R.

For solid-phase growth on differentially saline media

Square agar plates were supplemented with four different salt concentrations: LBA control (174 mM NaCl), one with twice as much salt (348 mM NaCl), three times salt (522 mM NaCl) and six times salt (1.04 M NaCl). Bacterial cultures were resuspended in fresh LB from overnight cultures and adjusted to one of three OD600s (0.02, 0.002, 0.0002) and pipetted as 20 µL spots and left to dry before incubation at 28 °C. Plates were imaged using a scanner at 1-4 days post-plating to track growth.

DNA extraction and genome sequencing

For 5 of the 6 strains DNA was extracted using the DNA NucleoSpin Microbial DNA from Macherey-Nigel and eluted in EB buffer (10 mM Tris-HCl pH 8.5) with no EDTA, concentrations were measured by the NanoDrop and ranged between 250 - 600 ng/µL which were

normalised and sent as 40 µL aliquot to MicrobesNG for sequencing. The DNA integrity of the samples was checked by running samples on a 0.75% agarose gel and strain purity was confirmed by visual assessment of the LBA feed plates used. The pv. *aptata* NCPPB3539 strain was sent as a suspended pellet in 0.5 mL of 1x DNA/RNA Shield buffer obtained from a liquid culture at exponential growth phase. Genomic DNA extraction and sequencing was performed by MicrobesNG.

Soil-based salt-irrigation growth experiments - *as described in Chapter 3, but salt irrigation was performed using 100 mM NaCl and for 3 weeks only.*

Osmolality measurements – *as described in Chapter 3*

Hydroponics – *as described in Chapter 3*

***P. syringae* bioinformatic analyses** (Chloe Harper, Jasmine Dodd and Dr Nattapong Sanguankiattichai)

Phylogenetic Tree: The phylogenetic tree was constructed using concatenated DNA coding sequences of 4 conserved housekeeping genes (rpoD encoding sigma factor 70, gyrB encoding DNA gyrase B, gltA encoding citrate synthase and gapA encoding glyceraldehyde-3-phosphate dehydrogenase) similarly to the genes used by Hwang et al. (2005). Genome sequences were obtained from NCBI or sequenced by MicrobesNG (www.microbesng.com). Housekeeping gene sequences were identified by a local BLAST+ search (Camacho et al., 2009) using *P. syringae* pv. DC3000 as a query against genome sequences of all other strains. Sequences of each housekeeping gene were aligned using L-INS-I algorithm of MAFFT software (Katoh and Standley, 2013) and multiple sequence alignments of all genes were concatenated. IQ-TREE 2 software (Minh et al., 2020) was used for maximum likelihood phylogenetic tree reconstruction with the General Time-Reversible (GTR) DNA substitution model with empirical base frequency (+F), gamma distributed evolutionary rate heterogeneity among sites with 4 discrete categories (+G4), allowance for invariant sites (+I) and partitioning by gene. Branch support values were calculated from ultrafast bootstrap method with 1000 replications. *P. fluorescens* SBW25 was used as the outgroup and the tree was visualized using iTOL (Letunic and Bork,2019). *P*. Phylogroups were assigned according to previous literature (Baltrus et al., 2017).

Effector, phytotoxin and Pfam analyses:

43 core T3Es of interest were identified using Laflamme et al. (2020) Supplementary Dataset Table 2. Bacteria.ensemble.org and the NCBI database were used to ascertain the effectors' Reference Sequence Selected Product WP codes: effector cluster names were inputted to bacterial.ensemble.org to obtain their assembly accession numbers used to then identify effector WP codes in NCBI's Reference Sequence (RefSeq). The NCBI Assembly database was used to acquire amino acid sequences of protein coding genes for each strain (FASTA .faa files). The proteome .faa files were inputted into the OrthoFinder algorithm by Emms and Kelly (2019) to infer Orthology between the *P. syringae* strains of interest. OrthoFinder was run with default settings, utilising DIAMOND (Buchfink et al., 2015) to estimate sequence similarity scores. Ergo, de novo orthogroup inference was achieved for the selected strains. OrthoFinder produced considerable comparative genomic statistical outputs, from which the "Orthogroups.tsv" database was used to identify effector orthologs through identification of the effectors' WP codes. Effector orthologs were visualised in a presence/absence matrix in Excel which displayed common or pathovar-exclusive effectors within strains of interest.

This process was repeated for the identification of the strains' phytotoxins: assembly accession numbers were identified using Hulin et al's. (2018) Supplementary Dataset Table S4., inputted into NCBI RefSeq to obtain WP codes and searched for in the "Orthogroups.tsv" database. A toxin presence/absence matrix were created to expose potential patterns within the strains of interest using the Pheatmap R package.

Pfam (the protein family database) was used to identify protein domain architecture of P. syringae strains of interest (Mistry et al., 2007). FASTA faa. files were inputted to the HMMER hmmscan search to examine their sequences using the UniProt Knowledgebase (UniProtKB). Salt tolerance proteins were identified from the literature (Choudhury et al., 2001) and searched for in the Pfam output. A presence/absence protein matrix was created in R to display the quantity of protein families in each strain.

Chapter 5: The influence of quinoa's halophytic adaptations on PAMP Triggered Immunity

5.1. Introduction

This chapter builds on the previous chapters using the established saline hydroponics growth system and optimised PTI assays in quinoa to interrogate how salinity affects immune responses. The experimental set-up more generally hopes to yield insights on how abiotic stress adaptations interact (crosstalk) with biotic stress responses in plants, and specifically for quinoa, to what extent this can explain the increased disease resistance found in salt acclimated plants (also referred to as 'the saline phenotype' or 'high salt grown plants'). Therefore, the conceptual framework used to guide experiments for this chapter focuses on the interactions between the 'salt stress vertex' (NaCl) and the 'immune system vertex' (PTI) in the Halophytic Disease Triangle (Fig.2) to test the hypothesis that quinoa's biotic stress responses may be enhanced either directly through 'priming' of pre-existing immune mechanisms, or indirectly through inducing pre-existing halophytic traits when the plants are grown under saline conditions.

5.1.1. Plant responses to combinatorial or sequential stresses

Crops continuously face simultaneous or sequential abiotic and biotic stresses in the field which must be counteracted in efficient, prioritised ways to avoid significant growth penalties due to the overuse of energy reserves "the growth-versus-defence" trade-off (Huot et al., 2014). For example, from the rhizosphere to the phylosphere, plants may be subjected to longer term continuous stresses such as nutrient deficiency or high salinity of the soil first sensed at the roots. Later, the plants may experience a sudden onset of drought, high temperatures and/or UV stress sensed systemically (at the shoots and roots) or be challenged by biotic stresses such as the infection or infestation of specific tissues. The extent to which these stresses affect the plant from discrete tissues (such as individual leaves dying) to whole-plant lethality depends on the adaptive capacity and stress-responsiveness of the plant.

An increasing number of studies have therefore been designing experiments to mirror these field scenarios using multifactorial combinations of individual biotic and abiotic stresses over

varying durations to uncover core regulatory networks and metabolic pathways (Rasmussen et al., 2013; Kissoudis et al., 2015; Coolen et al., 2016; Olivas et al., 2016; Gupta et al., 2017; Saijo and Loo 2019; Zandalinas et al., 2021; Zandalinas and Mittler 2022). The combinatorial stress transcriptional (and proteomic) responses were consistently found to be unique from the single stress responses (Li et al., 2011; Rasmussen et al., 2013; Zandalinas et al., 2021 and reviewed by Suzuki et al., 2014) suggesting significant stress signalling crosstalk (molecular communication) occurs. This has significant implications for the applicability of findings from controlled single stress research systems to field based settings, where identifying crosstalk candidates such as 'hub genes' and core stress regulatory networks may offer promising strategies for conferring broader spectrum stress resilience in crops (Da Ros et al., 2023).

A unique combinatorial stress response is unsurprising considering how different single stress response pathways can depend on different hormones that antagonise each other in certain plants species, for example, the jasmonic acid (JA) vs salicylic acid (SA) antagonism that exists in Arabidopsis for dealing with biotrophic and necrotrophic pathogens respectively (Spoel et al., 2007). However, different species use hormone signalling pathways differently depending on the mode of defence evolved, for example, Ullah et al., 2022 found that in the woody tree species Black Poplar (*Populus nigr*a) SA and JA interact positively with each other to counteract the rust pathogen *Melampsora larici populina.* Resistance was found to correlate with an accumulation of antimicrobial flavonoid phytoalexins, and the expression of pathogenesis-related (PR) proteins was induced proportionally to the extent of overall pathogen infection rather than simply to SA content as typically found in Arabidopsis (Nawrath and Métraux, 1999). Abscisic acid (ABA) has predominant roles in abiotic stress tolerance to cold, drought and salinity but has also been shown to antagonise biotic stress hormones SA and JA and to suppress plant immunity in glycophytic crops (Acosta-Motos *et al.*, 2017; Kundu and Gantait, 2017; Berens et al., 2019; Rezzonico et al., 1998).

5.1.2. Combinatorial stress experimental systems: theories and practicalities

A summary of potential interactions between different combinations of environmental stresses was provided by Anwar et al. (2021) who visually summarised the interactive results from 42 single stress and combinatorial stress studies performed in several important glycophytic species (wheat, maize, tobacco, Arabidopsis, sugarcane, rice, strawberry,

sunflower, soybean, tomato, lettuce) tree species (beech and birch) and one halophyte *Suaeda salsa* by the following graphic (Fig.1):

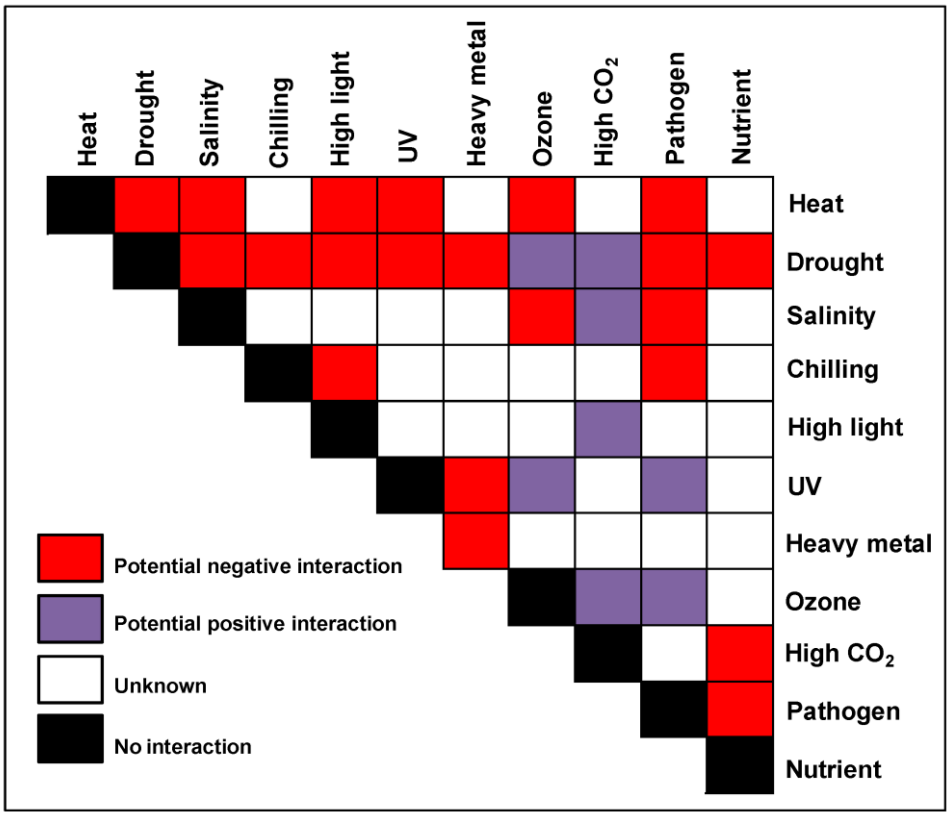


Fig.1. Summary figure 'The stress matrix' from Anwar et al. (2021): "Different combinations of potential environmental stresses that can affect crops in the field are shown in the form of a matrix. The colour of the matrix indicates stress combinations that were studied with a range of crops and their overall effect on plant growth and yield." See Table 2 of this paper for the full list of studies used.

Combinatorial stress studies for salt and pathogen interactions are in a minority compared to other stress combinations. For example, one study by Xiong and Yang (2003) showed a potential negative interaction between salt and disease resistance signalling pathways in rice where it was found that silencing the ABA inducible OsMAPK5 gene significantly improved fungal and bacterial pathogen resistance but decreased abiotic (salt, drought and cold) tolerance. Further examples in the literature have focused on glycophytic species tomato, cucumber, Arabidopsis and maize, finding negative and positive stress interactions on plant fitness (Kissoudis et al., 2015-2018; Chojak-Koźniewska et al., 2012 & 2017; Rasmussen et al., 2013; Zandalinas et al., 2021; Soliman and Kostandi, 1998).

Two comprehensive series of experiments by Kissoudis and Bai et al. (2015-2018) and Chojak-Koźniewska et al. (2012, 2017 & 2018) performed in tomato and cucumber respectively, revealed interesting findings at the level of R gene dynamics and changes in photochemistry, antioxidant capacity, and SA and ABA contents/dynamics. Kissoudis and Bai et al. (2015-2018) evaluated the effect of genotype and different degrees of salt stress on powdery mildew (*Oidium neolycopercisi; PM)* resistance in different tomato introgression and near-isogenic lines of varying monogenic PM resistance. They found the interaction outcome depended upon the specific PM resistance genes introgressed and their associated mechanisms: full resistance conferred by *ol-2* (an *mlo* mutant associated with papilla formation), and *Ol-4* (an *R* gene associated with a fast hypersensitive response; HR) was unaffected by salt, whereas susceptible and partially resistant lines became significantly more susceptible to PM at low salinity (50 mM) and more tolerant at high salinity (150 mM). This led the authors to propose that the higher foliar Na^+ and Cl^- content in the leaves helped to suppress PM growth through direct pathotoxicity (Kissoudis et al., 2015 & 2016).

Frameworks for interpreting different outcomes have been proposed by Rasmussen et al. (2013) who proposed that a response of a given transcript to two single stresses may be neutral, agonistic, antagonistic, or unrelated, whereas the response to combined stresses may be a combination of such responses. This led the researchers to defining five combinatorial stress transcript response behaviours, termed 'modes', which were: 'combinatorial', 'similar', 'cancelled,' 'prioritized' and 'independent', where just two of these modes (independent and similar) represent scenarios where the combined stress outcome (transcript response) could be predicted from results obtained using the single stress.

Zandalinas et al. (2021) challenged Arabidopsis seedlings with multifactorial combinations of six different abiotic or biotic stresses applied at low enough levels that single-stress effects were negligible and found that all fitness parameters (seedling survival, root growth and chlorophyll content) declined with increasing stress combinations. Whole-plant levels of key stress response signal ROS increased linearly with increasing numbers of stresses, and genes relating to iron and ROS homeostasis and all major stress-related hormones (ABA, SA, JA, ET) were upregulated in all conditions, but showed very dynamic and unpredictable patterns.

In Arabidopsis, high temperature reduces expression of the immune receptor FLS2, which suppresses immunity to the tomato pathogen *P. syringae* pv. DC3000 (Janda et al.,2019). Cheng et al. (2013) demonstrated how plant immune responses to pathogens differ with changing temperatures, suggesting PTI signatures become more important than ETI at higher temperatures. Light intensity is another important abiotic factor known to have a profound effect on plant immunity and disease susceptibility in a range of species (Jua, 2013).

As mentioned in the introduction section of Chapter 4, salt exposure typically reduces fitness and pathogen resistance of glycophytic crops, whereas our pathosystem with the halophyte species quinoa and *P. syringae* showed the opposite effect. This chapter aims therefore to contribute molecular and transcriptional evidence for this by investigating quinoa's PTI responses now in the presence of NaCl.

5.1.3. Aims and rationale

Previous studies have shown that identifying overlapping gene sets regulated by two distinct individual stresses is an invalid approach for identifying crosstalk candidates and therefore responses to combinatorial stress must be evaluated directly, and on a species-by-species basis. The major hypothesis for this thesis was that quinoa's salt adaptations may influence immunity, and so the experimental set-up for this final chapter is a prolonged salt exposure followed by a discrete PAMP exposure to emulate what may happen in a field setting. The salt exposure and PTI experiments were performed in identical ways to the previous procedures established in Chapters 2 and 3. Having found in Chapter 4 that the saline phenotype was significantly more disease resistant to *P. syringae* pv. *aptata* than non-saline plants, and that salinity had a direct inhibitory effect on *P. syringae* growth and virulence gene expression, here we queried whether salt acclimation of the halophyte quinoa confers cross-tolerance by priming PTI mechanisms of its plant immune system (Fig.2).

Objectives:

- Optimise PTI assays for use in saline quinoa leaf tissue
- Evaluate biochemical PTI differences between low and high salt-grown quinoa
- Design and perform a combinatorial RNA-seq experiment with salt (NaCl) and biotic stress elicitor (flg22) in quinoa

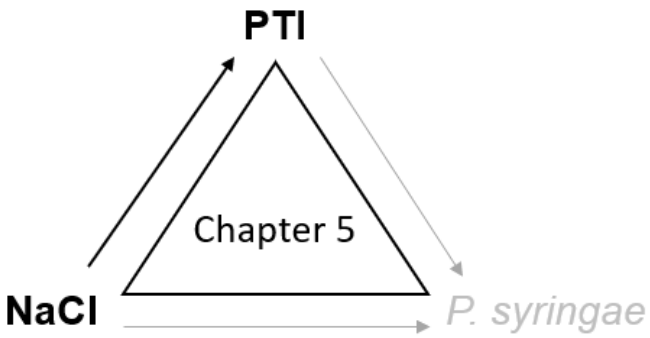


Fig.2. The Halophytic Disease Triangle experimental framework used for this chapter. Highlighted in bold are the components of the quinoa research system focused on: the NaCl and (flg22 induced) PTI single stress responses and the direct influence (black arrow) of NaCl acclimation on PTI. As established in Chapters 2 and 3, the biotic stress is administered by using the PAMP flg22 as a transient treatment when the plants are 4.5 weeks old, and the salt stress refers to the background growth conditions: an incremented and then consistently held 200 mM NaCl exposure to Atlas (which produces a significant saline phenotype but without toxicity relative to the control/ 0 mM NaCl/ low salt plants). As defined at the end of Chapter 3, 200 mM NaCl salt is not a severe salt stress for quinoa cv. Atlas but for simplicity of language in this chapter (especially for the transcriptomics experiment) it will be referred to as the 'single salt stress' whereas 'combined stress' refers to the saline phenotype challenged by flg22 treatment.

5.2. Results

5.2.1. Upstream and downstream PTI responses MAPK activation and callose deposition are conserved in high salt-acclimated quinoa

In Chapter 2, early MAPK activation was found to be triggered by a range of PAMPs in non-saline (soil-grown) grown quinoa leaves, and so the MAPK responsiveness was next queried in plants grown in the hydroponics system to see if responses are conserved in saline (hydroponically grown) leaves. This test was also used as a quality control step to validate leaf tissue responsiveness to flg22 treatment preceding the preparation of samples for a combinatorial stress (salt x flg22) transcriptomics experiment. The full leaf infiltration method (i.e., not the *in vitro* optimised leaf-disc assay of Chapter 2) was used for flg22 elicitation in the MAPK assay to mirror the set-up used for infection assays.

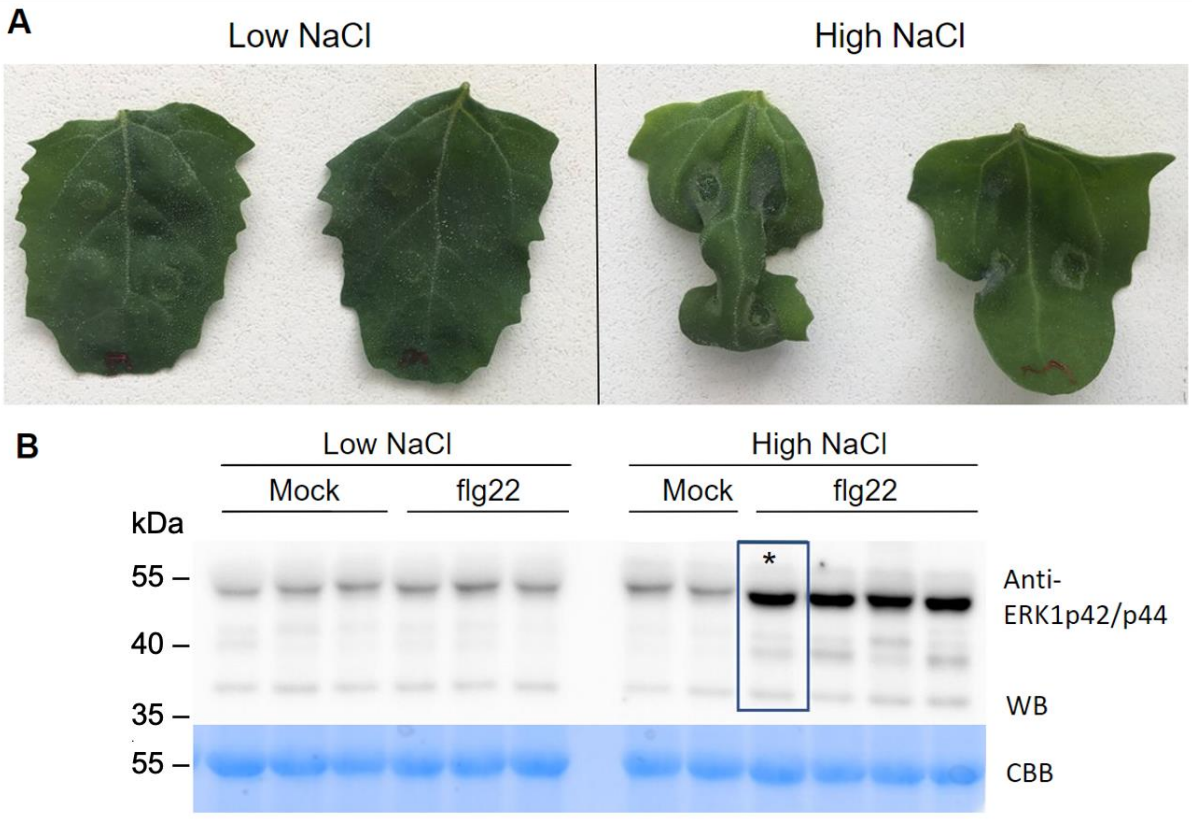


Fig. 3. MAPK enzymes are more strongly activated by flg22 in high salt plants compared to low salt plants. A) Phenotypes of representative mock-treated leaves of low and high salt plants directly before harvesting (i.e., 2h post-infiltration). B) Western blot showing activated MAPKs (phosphorylated ERK1p42/p44) as dark bands for each of three biological replicates. The starred and bordered sample

shows a clear human error made at the point of infiltrating biological replicates. The abaxial side of equivalent fully expanded leaves from three individual 4.5-week-old quinoa plants were infiltrated with 1 µM flg22 or water (mock) and harvested 2h later. Protein extraction and western blotting were done as per Chapter 2 except for sample normalisation was done by protein concentration (via the BioRad DC assay kit) instead of sample weight to account for the higher tissue mass of high-salt-grown plants found in Chapter 3.

Flg22-induced MAPK activation was found to be conserved and heightened in the leaves of high salt plants compared with low salt plants, which failed to show a clear differential MAPK activation signal between flg22 and mock treated leaves (Fig.3B). An unavoidable (but expected) effect of the leaf infiltration method was tissue damage, more notably seen for high salt leaves (Fig.3A) which could also influence biotic stress specific MAPK and transcriptional responses. Therefore, when this experiment was repeated as part of the QC for the combinatorial RNA-seq experiment, four biological replicates per treatment and additional zero-damage (untreated) controls were included for both sample types (low and high salt). In this repeat experiment (data not shown) clearest differences in MAPK activation were found between the infiltrated samples (with either mock or flg22) and untreated samples and to a lesser degree between flg22 and mock treated samples.

Next, the later 24h PTI response of callose deposition was examined in hydroponically grown quinoa leaves infiltrated with flg22 (as had been done in soil-grown plants in Chapter 2) and clear callose deposits were found in both low and high salt plants, suggesting this canonical signalling pathway is still activated in the saline phenotype (Fig.4).

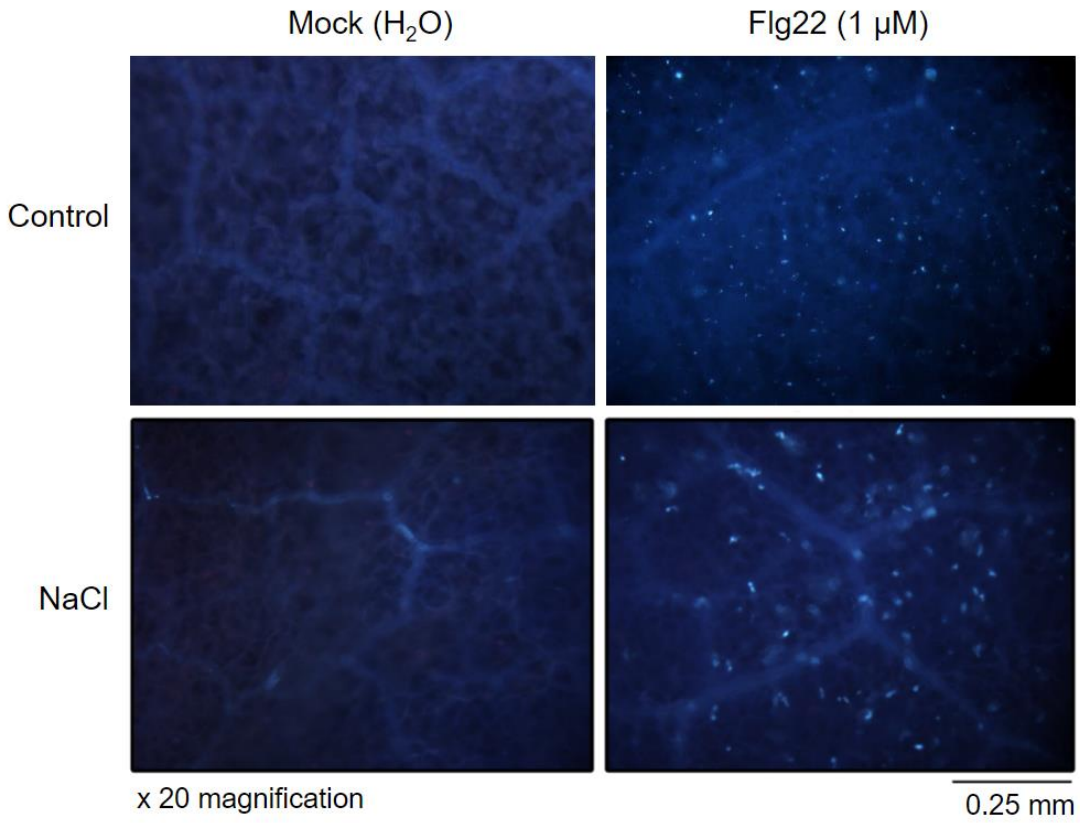


Fig.4. A callose deposition response to flg22 can be observed in high salt quinoa plants. Light specks represent fluorescing callose deposits observed in both low (control) and high (NaCl) salt leaves treated with flg22 (1 µM) stained by alanine blue and captured by the QICAM Fast 1394 colour camera connected to the Olympus B201 with a WU fluorescence cube. The protocol was performed identically to the method described in Chapter 2, except that the high salt plant leaf samples required a longer chlorophyll-clearing incubation time (2-3h at 50°C instead of 1 h at RT) in the 1:3 solution of acetic acid: ethanol solution. Images are representative from several camera shots of fully expanded leaves taken from *n = 3* individual plants per growth condition and treatment.

5.2.2. High concentrations of flg22 cannot elicit an observable ROS signal in the leaves of high salt quinoa

The earliest PTI response evaluated in soil-grown plants in Chapter 2 was the canonical ROS burst assayed from <1-minute post PAMP exposure using the 96-well plate ROS assay (Melcher Moerschbacher, 2016; Buscaill et al., 2019). It was also found that quinoa produced a delayed and less intense ROS burst than the model species Arabidopsis. This experiment was repeated for hydroponically grown quinoa plants and whilst low salt plants showed a positive ROS burst response (Fig.5), this was repeatedly found to be absent in high salt plants,

and even in plants grown under the lower salt concentration of 100 mM NaCl when treated at much higher doses of flg22 (Fig.5B).

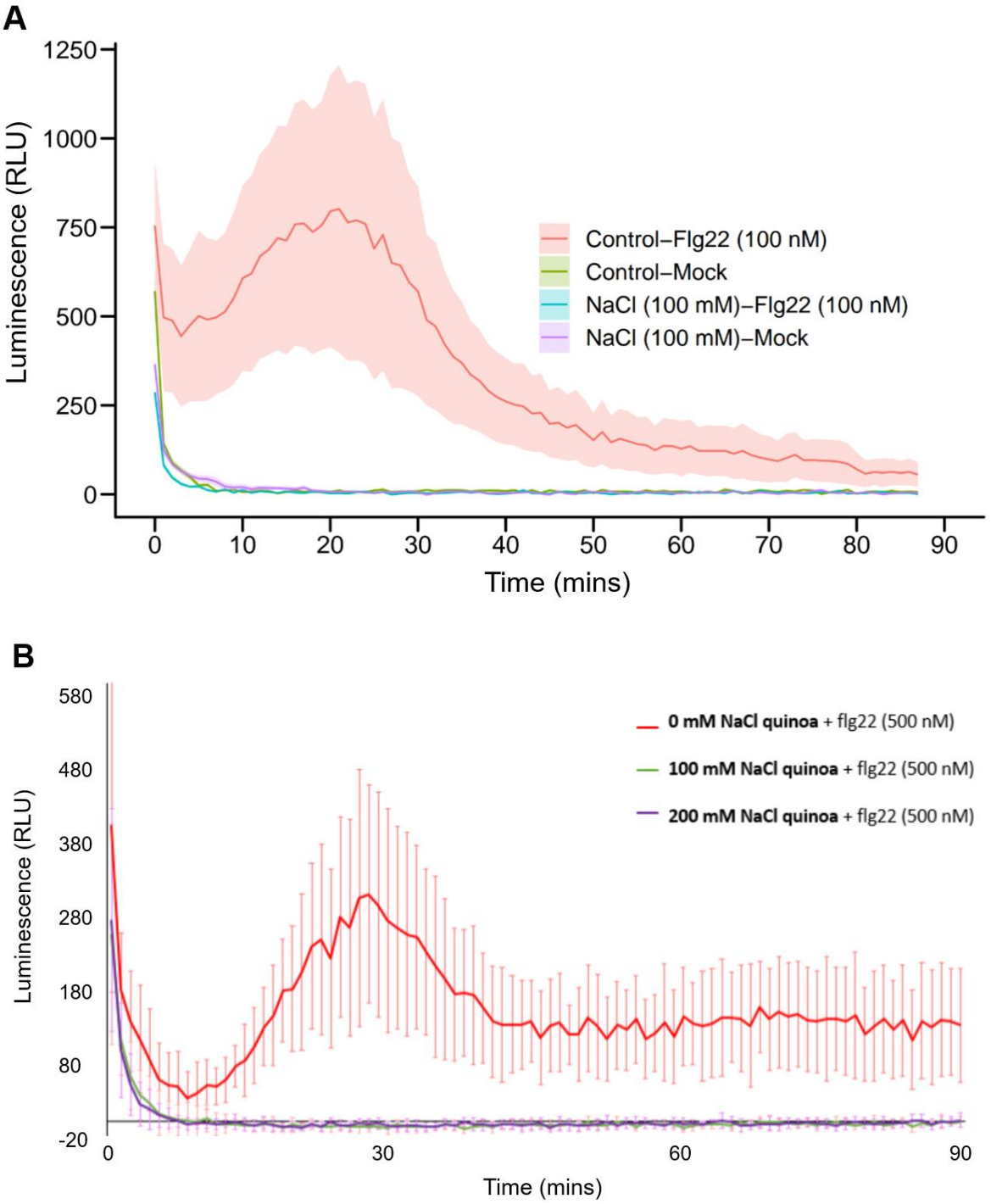


Fig 5. The ROS burst is absent in the leaves of high salt plants (A) and even under higher flg22 concentrations (B). Results are mean relative luminescence units (RLU) + standard deviation from *n = 12* leaf discs pooled randomly from four equivalent 4.5-week-old quinoa plants and are representative

of two or more independently repeated experiments. The protocol was followed identically to the method described in Chapter 2 where chemiluminescence readings were taken continuously over a 90-minute period using a TECAN plate reader. Flg22 concentration used was 100 nM or 500 mM.

The experimental set-up of the ROS assay was next dissected using a series of experiments to elucidate the cause of the null ROS response observed in high salt quinoa (Fig.6A). Fig.6B depicts the identified possible causes for the loss of luminescence categorised into plant-dependent factors and technical factors and numerated to represent different hypotheses. For example, no ROS is produced in the first place due to the RBOH enzyme being inactive in the saline phenotype or due to an inducible ROS-burst being inhibited by an alternate overriding stress imposed by the leaf disc set-up (hypothesis 0; H0). For the latter point, the leaf-disc assay set-up could compound the ability of saline leaf discs to respond to flg22 using a ROS burst if the tissues' cells prioritise responding to the hypoosmotic stress potentially imposed on saline leaf discs when incubated in hypoosmotic bathing solutions. Alternatively, it was hypothesised that a ROS burst is inducible by flg22 in saline leaf tissue (H1), but a technical limitation occurs where excess salt ions leak into the reaction wells and interact with and inhibit the function of core components of the assay, the L-012 probe or hydrogen peroxidase (HRP) enzyme (H2). High-salt leaf tissue is known to be significantly more saline (Chapter 3 & 4) and given how the leaf disc edges represent a large surface area of damaged (cut) cells, Na^+ and Cl^- ions could leak into the reagent wells, and more if further cell-death occurs due to hypoosmotic stress. Lastly, it was hypothesised that saline tissue may have higher amounts of endogenous antioxidants which diffuse or leak into the wells and quench any ROS produced before it oxidises the probe and luminescence is produced (H3) (Fig.6.B).

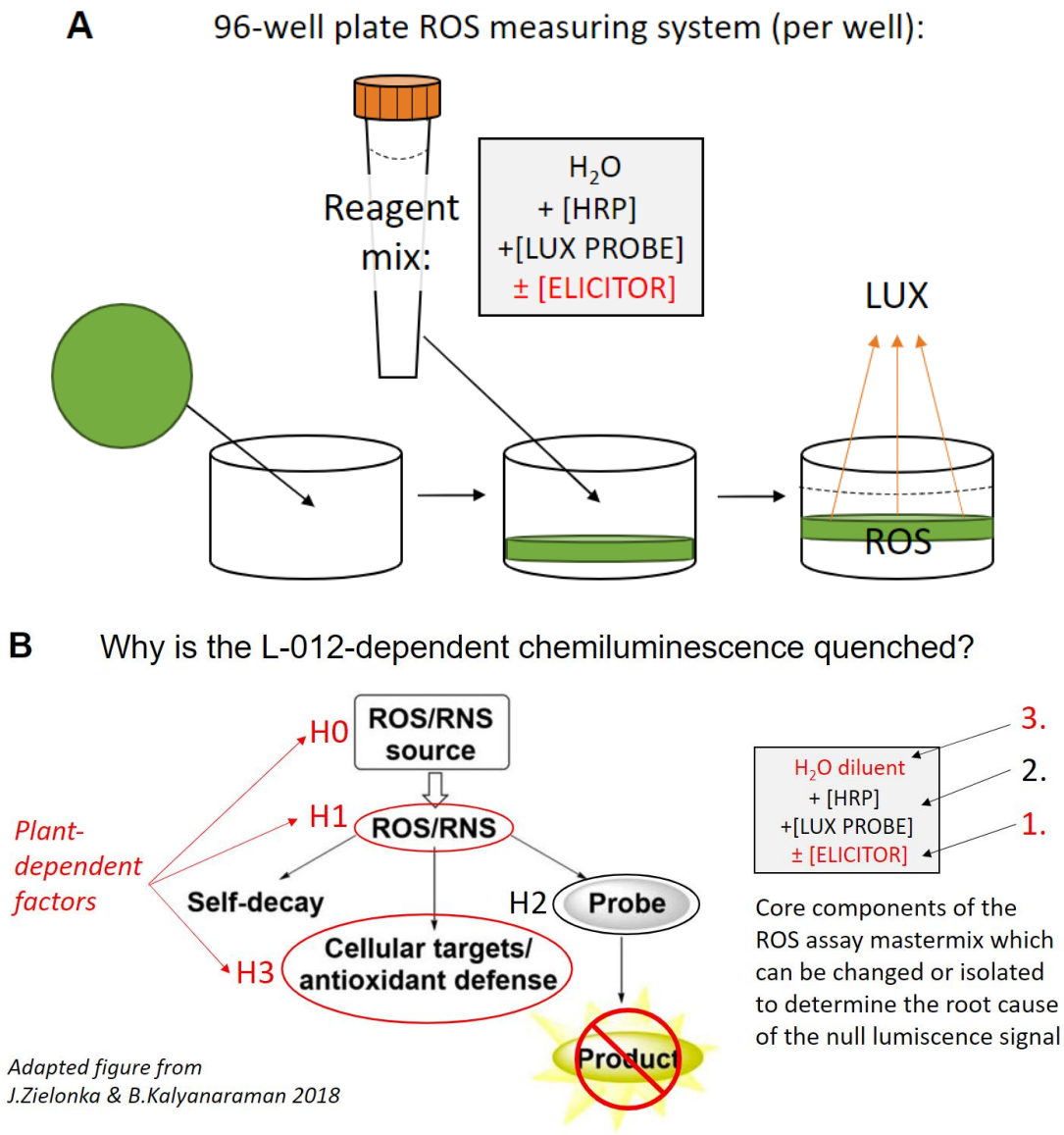


Fig. 6. Dissecting the 96-well plate probe-dependent chemiluminescence ROS assay and potential factors for a null luminescence response. A) A representation of the 96-well plate showing one leaf disc, one reaction well and the core components included in the reagent mix for ROS-induced luminescence generation. B) Flow chart showing points for assaying the cause of a null luminescence response, an annotated adaptation from J. Zielonka & B. Kalyanaraman 2018. H0 represents the earliest point for a null luminescence response where no ROS was produced in the first place. To test this hypothesis, the capacity of quinoa to produce ROS under salinity could be evaluated using gene expression analysis of the RBOH gene either by transcriptomic or Real-Time Quantitative Reverse Transcription PCR (RT-QPCR) analysis of treated leaf discs. H1 represents a measurable concentration of ROS being produced in the reaction well which cannot oxidise the chemiluminescence probe for luminescence because the probe or enzyme have been pre-inhibited by an excess of leaked salt ions H2. H3 shows how the ROS in the reaction well is preferentially consumed by oxidising cellular targets

or quenched by antioxidant activity due to endogenous plant factors which have also leaked into the reaction well solution. Text highlighted in red are plant dependent factors that can be replaced using artificial exogenous sources such as H_2O_2 as a ROS source and Vitamin C as a robust antioxidant (the latter can be added to the assay mastermix dissolved in the H_2O diluent as a proxy for endogenous antioxidants). Text highlighted in black is used to denote plant-independent factors of the ROS assay: the L-012 probe which is dependent also on the activity of the exogenously supplied HRP enzyme.

A key observation was made following the ROS assay trials with saline tissue where leaf discs taken from high salt plants showed significant leaf disc edge tissue damage and a reduced size after 3 h incubation in hypoosmotic (Milli-Q water; 0 mM NaCl) bathing solutions (Fig.7).

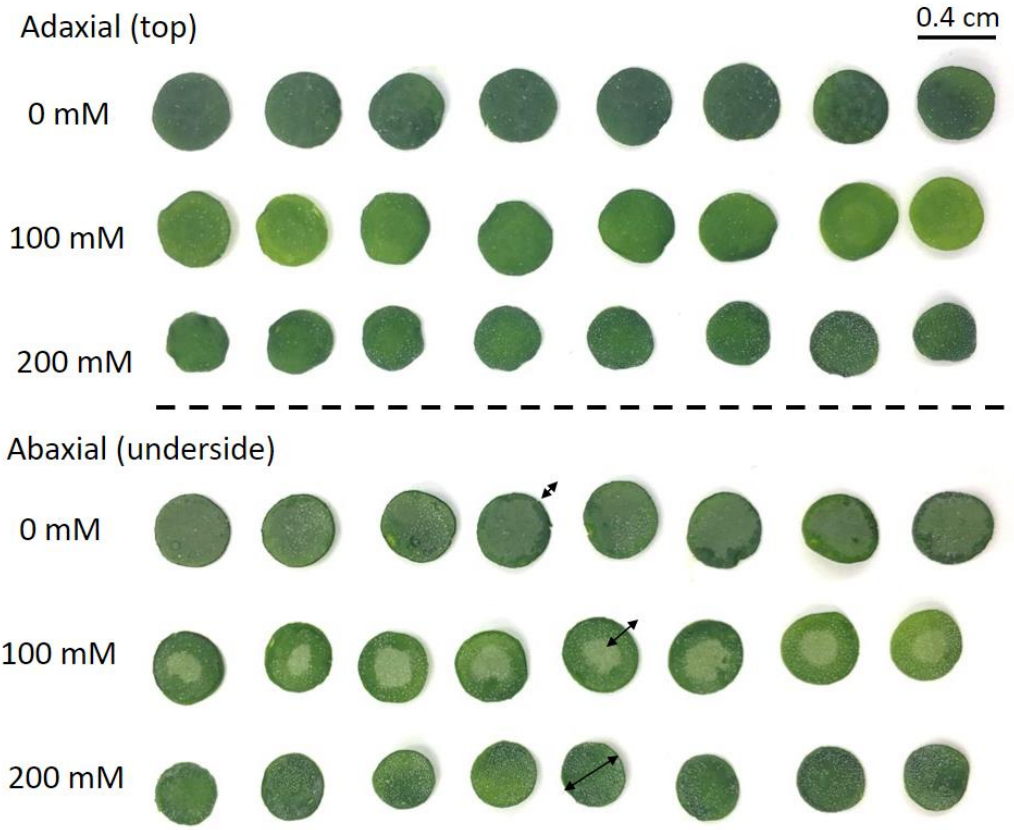


Fig.7. Hypoosmotic conditions cause tissue damage of leaf discs harvested from saline quinoa.
Leaf disc morphologies observed after a ROS assay had been run: the leaf discs had been left for a maximum of 3 h incubating in the wells of the 96-well plate which contained 150 µL of the ROS reagent mix where H_2O (0 mM NaCl) had been used as the diluent for (Methods). Prior to their use in the ROS assay the discs had been incubated for 16 h in (empirically) osmotically equilibrated solutions overnight (as is standard procedure in the ROS assay in order to acclimatise discs of leaf tissue to water and to reduce the effect of damage). Black arrows indicate the darkened tissue due to cell death

and/or water soaking due to cell lysis from hypoosmotic stress and water uptake. Photo taken on iPhone model 6S under visible light.

To calculate the true osmotic point of leaf discs from differentially saline quinoa leaf tissue, an experiment was designed whereby leaf discs had their fresh weight (FW) percentage mass change measured after 90-minutes incubation in solutions of different osmotic pressures (Fig.8). The FW of leaf discs of different salinity varied over 90-minutes when soaked in different concentrations of NaCl (0-1000 mM NaCl) (Fig.8A). The iso-osmotic point for each quinoa leaf disc types is found where the curve crosses the x-axis: 358 mM NaCl for 0 mM NaCl quinoa tissue, 505 mM for 100 mM NaCl tissue and 658 mM NaCl for 200 mM NaCl tissue (Fig.8B). Photos of correctly equilibrated leaf discs are shown in Fig.8C.

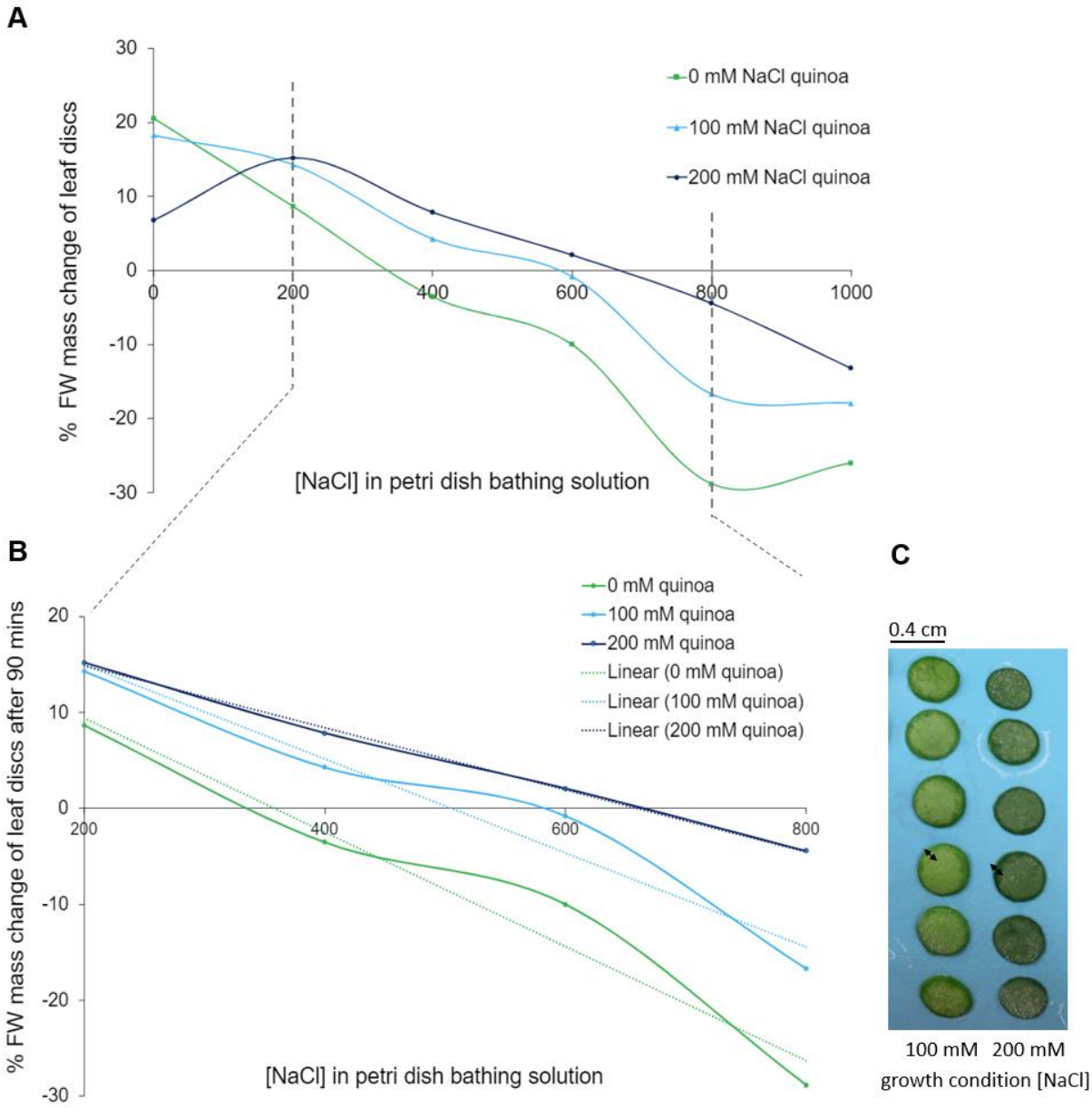


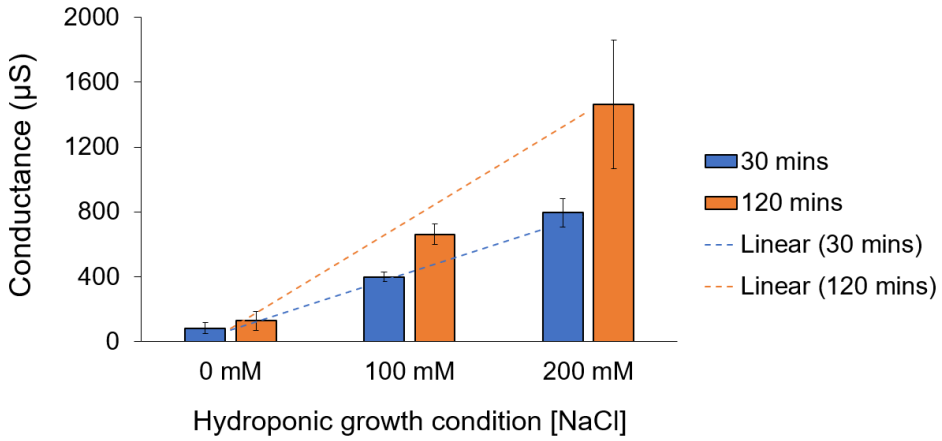
Fig.8. Quinoa leaves grown under different salinities have distinct osmotic points which can be used to guide the osmotic equilibration of *in vitro* leaf disc set-ups. A) % fresh weight (FW) change between 0 and 90 minutes of differentially saline leaf discs incubated at increasing NaCl molarities (0 -1000 mM). from plants grown hydroponically at 0 mM, 100 mM and 200 mM NaCl. Data represent the pooled mass of 10 leaf discs each taken from fully expanded leaves of three plants of each salinity type (0, 100 and 200 mM NaCl) and floated in small petri dishes containing specific NaCl concentrations. B) Trendlines showing the linearity of the relationship between % FW mass change of leaf discs and increasing salinity of the bathing solution between 200 – 800 mM NaCl. The lowest and highest limits of 0 mM and 1000 mM NaCl were not included when fitting a trendline due to excessive osmotic stress imposed on the leaf discs which resulted in excessive leaf disc damage causing a notably greater effect on the % FW change than the other salinities. C) Example of what the leaf disc tissue

looks like after a 90-minute incubation in iso-osmotic solutions where black arrows indicate a reduced leaf disc edge damage area.

5.2.2.1. Excess NaCl is not responsible for inhibiting the chemiluminescence signal of the ROS assay

To address H2, the hypothesis that salt may interfere with technical components (HRP enzyme or L-012 probe) of the ROS assay, a series of plant-independent experiments were designed. First, the concentration of leached ions in the reaction wells was approximated by taking electrical conductivity readings of leaf disc bathing solutions representative of the ROS assay at biologically relevant timepoints: 30 minutes is typically the point of peak ROS burst in quinoa, and 120 minutes is an extended time period to the 90 minutes typically used for the ROS experiment to provide a larger margin for excess salt to leach out (Fig.9A).To approximate the concentration of NaCl leaked into the wells from their conductance values, a standard curve for NaCl-conductivity was made (not shown) and results tabulated in Fig.9B.

A



B

Leaf disc Time point	0 mM (30 min)	0 mM (120 min)	100 mM (30 min)	100 mM (120 min)	200 mM (30 min)	200 mM (120 min)
Mean (µS/cm)	82.7 ± 32.4	127.2 ± 57.6	398.5 ± 30.4	662.0 ± 61.5	794.2 ± 88.1	1463.5 ± 397.5
[NaCl] (mM)	1.4	2.1	4.7	9.7	12.3	25.1

Fig.9. Na^+ & Cl^- ions leach into leaf disc bathing solutions in proportion to endogenous quinoa leaf salinity. A) NaCl leaked from leaf discs of quinoa plants grown under varying salinity is proportional to the salt concentration of the medium used, with most ions leaked during the first 30 minutes. B) The approximate concentration of Na^+ and Cl^- ions released into the bathing solutions for different quinoa salinity types after 30 mins and 120 mins incubation, calculated using a standard curve equation from a series of NaCl solutions. Electrical conductance readings were measured by Jenway 3450 Conductivity Meter. Data represent the mean of six biological replicates, where each replicate

represents six pooled leaf discs harvested from equivalent leaves of three plants per salinity type. Error bars show standard deviation. Trendlines were included in graph A to highlight the linearity between the salinity concentration of the quinoa growth medium and the electrical conductance of the bathing solution.

As expected, conductance readings of leaf disc bathing solutions increased with increasing salinity of the quinoa growth regime (and thus tissue salinity) and the relative increase between conductance at 30 and 120 minutes timepoints for each tissue type was similar, shown by the linear dotted lines (Fig.9A). This reflects the trend for leaf cell sap osmolality readings obtained in Chapter 2 and considering the direct relationship between NaCl standards and bathing solution conductivity (data not shown) it suggests the major contributing electrolytes being leaked from quinoa leaves are indeed ions of NaCl.

The fact that none of the 120-minute conductance readings were four times higher than their 30-minute readings, rather 1.5-1.8 times higher suggests that the majority if ions are leaked in the first 30 minutes and the rate slows over time. For example, the saltiest quinoa tissue type tested (200 mM NaCl) increased the salinity of the bathing solution by 11 mM and 24 mM NaCl after the 30-minute and 120-minute windows (Fig.9B). This results next enabled a test of the effect of NaCl at a relevant range of concentrations on the ROS chemiluminescence in a plant-independent manner.

The ROS reagents chemiluminescence probe L-012 and HRP enzyme were diluted in saline water and an exogenous ROS source (H_2O_2) was added to induce luminescence and the signal was tracked over time. A clear positive luminescence signal was found under a range of salinities tested (0 mM – 200 mM) (data not shown), which corroborated with other studies showing a stabilising effect of salt ions on the excited state of the L-012 derivative luminol probe (Collaudin & Blum, 1997). Therefore, it was concluded that salt was not inhibitory and rather promoted the luminescence signal at higher concentrations tested (100 – 200 mM NaCl). Concomitantly, it could also be concluded that HRP enzyme activity is not significantly affected by salt as the positive luminescence ROS signal was still able to be produced. We also found a positive signal for Arabidopsis when treated with flg22 under 50 mM and 100 mM NaCl (data not shown). The results from Collaudin & Blum (1997) also reported how salts affect the nonenzymatic steps of the luminol chemiluminescence reaction rather than a modification of the enzymatic process itself. Therefore, the null hypothesis for H2 was

accepted: excess salt ions are not responsible for chemiluminescence inhibition and so alternative hypotheses were queried next.

5.2.2.2. Endogenous antioxidants of saline quinoa leaf tissue can suppress the measurable PAMP-triggered oxidative burst

It has been proposed that the wound response of plants can override specific PTI responses and therefore invalidate assays such as the ROS leaf-disc assay (Klauser et al., 2013; Bredow et al., 2019). Through investigating the potential causes of ROS quenching in saline quinoa it was discovered that the most likely explanation for an attenuated or null ROS response when using leaf discs shortly after harvesting them (even from Arabidopsis) is instead due to the resulting fast release of antioxidants into the bathing solutions.

An assay was developed therefore to perform high-throughput comparative analyses of antioxidant activity of leaf discs by making several modifications to the 96-well plate ROS assay, full details for which are summarised in the Antioxidant Assay Methods section. Key amendments are highlighted here: either pre-prepared leaf disc bathing solutions (containing a plant leaf's endogenous antioxidants) or water (as a no plant control) or water supplemented with ascorbic acid (positive antioxidant control) were used as the assay's reagent diluent, to which H_2O_2 was added as an exogenous ROS source at a concentration of 0.01 or 0.1 mM and also the HRP enzyme, whose concentration was reduced to 2 µg/mL, a 10-fold dilution to that used in the ROS assay. This last amendment was particularly important for more reliable and quantitative comparisons to be made as shown by the steadier dynamics of the blue curve relative to higher HRP working solution concentrations in Fig.10.

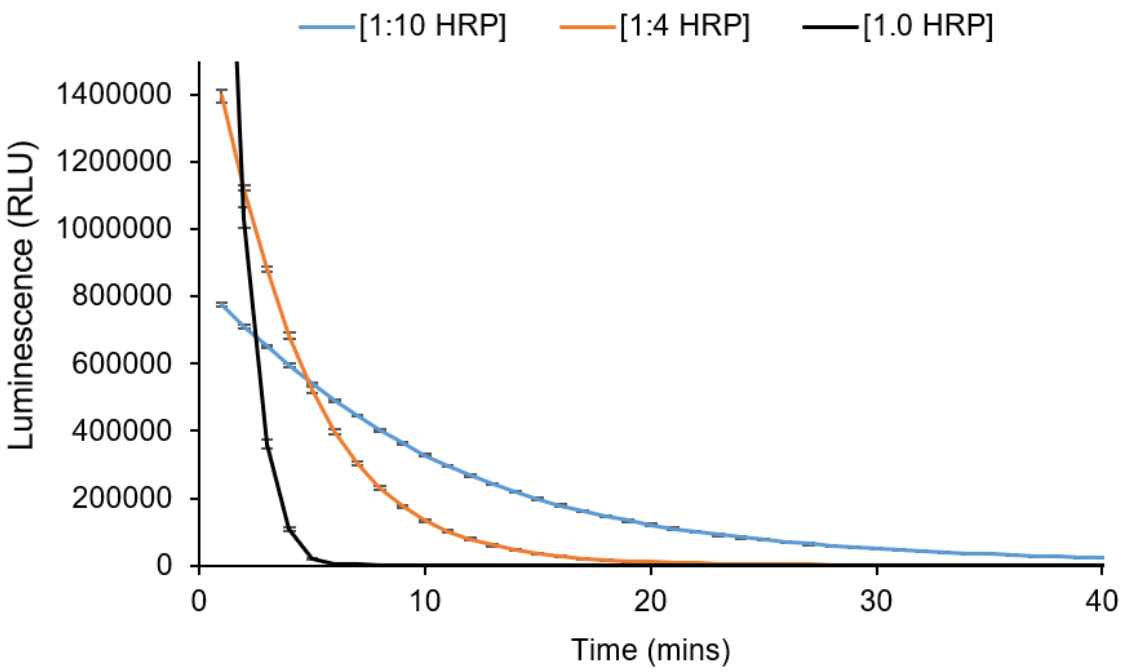


Fig.10. Diluting the HRP solution 10-fold produces a curve with an appreciably longer timeframe for evaluating luminescence kinetics relative to ROS availability. Three separate reagent mixes of L-012, HRP enzyme (at 1x, 1:4 and 1:10 concentrations: 20 µg/mL, 5 µg/mL and 2 µg/mL) were dissolved in water and supplemented with H_2O_2 at 0.01 mM in the wells of a white opaque 96-well plate of final well volume 150 µL. Luminescence was tracked over time using a TECAN plate reader using the standard ROS assay script as described in Methods.

To establish a means for quantifying antioxidant capacity of leaf disc bathing solutions and to understand the limits of sensitivity of the assay, a standard curve using a range of ascorbic acid concentrations (guided by the literature) was prepared. The range 100 – 400 µg/ml produced the clearest differences where 400 µg/ml was sufficient to quench ROS considerably with negligible differences found between 800 and 160 µg/ml concentrations (Fig.11).

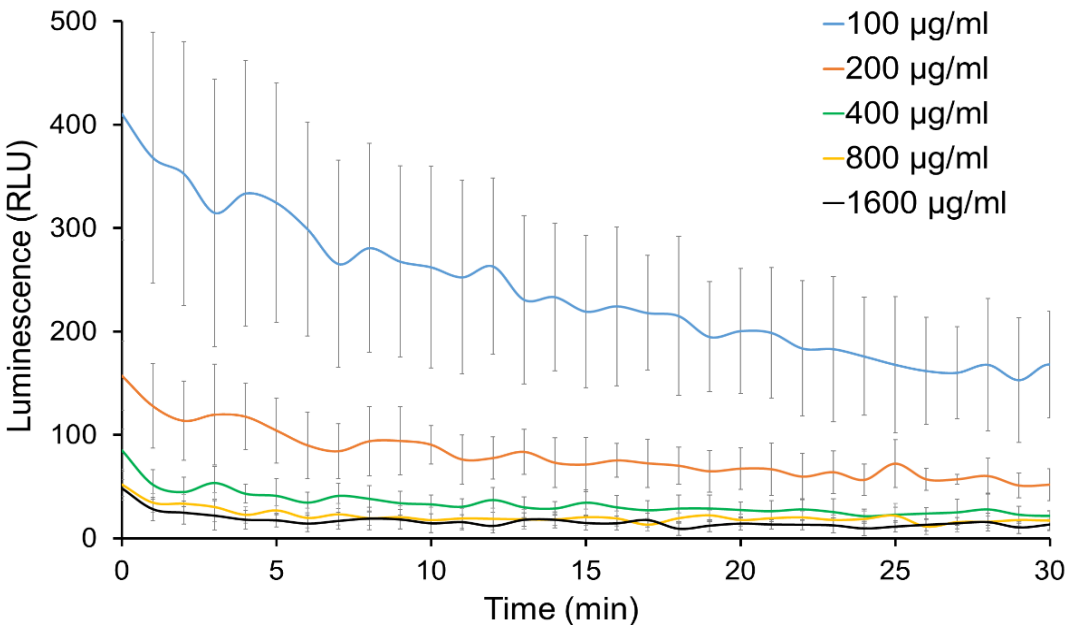


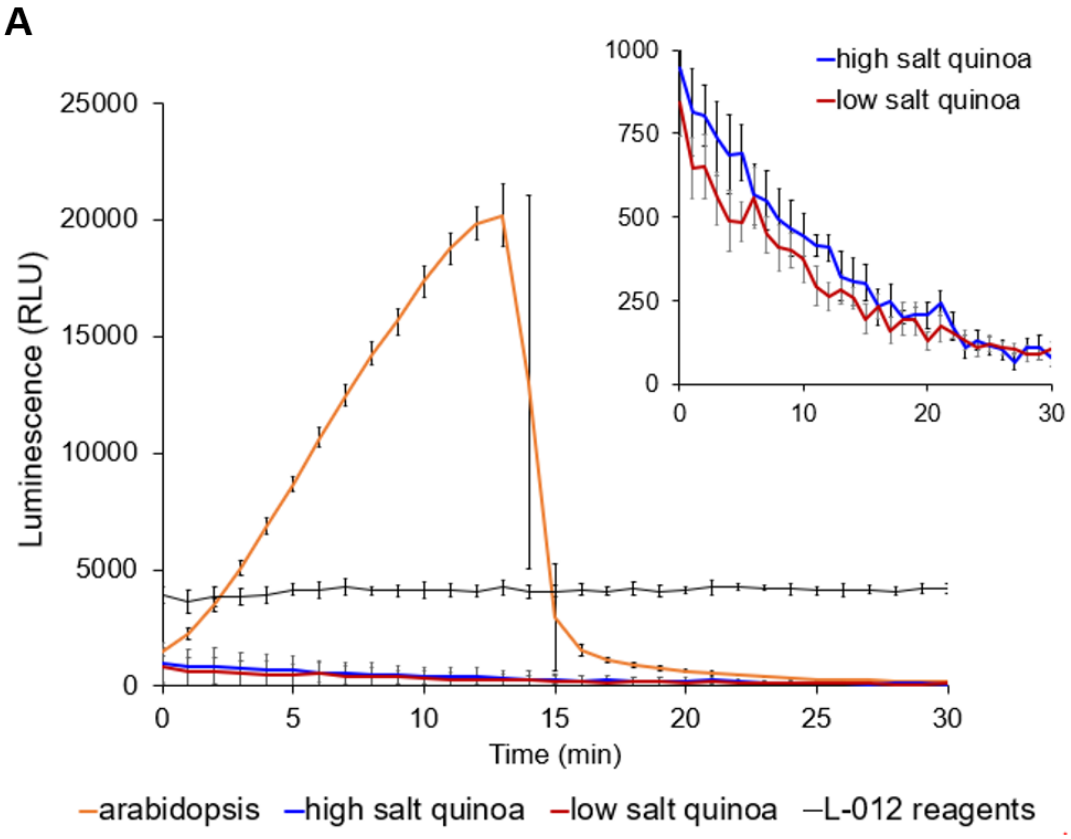
Fig.11. ROS-quenching dynamics of ascorbic acid at different concentrations over time

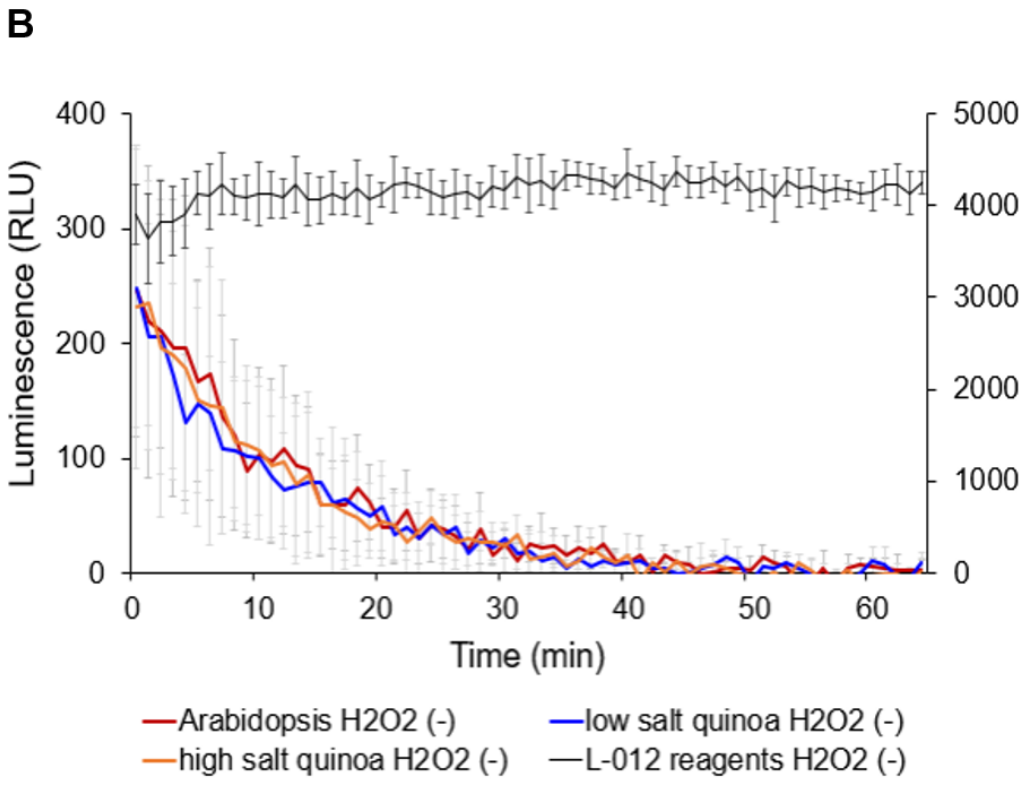
An opaque 96-well plate was set-up with six different ascorbic acid concentrations 0 – 1600 µg/ml diluted in the L-012/HRP reagent mix and 0.01 mM H_2O_2 was added just before the ROS assay plate reader script was started. All samples except for 0 µg/ml are plotted. Values are the mean of *n = 8* replicates and error bars show the standard deviation.

When the Antioxidant Assay (Methods) was applied to the leaf disc bathing solutions of differentially saline quinoa and Arabidopsis it was found that the luminescence signal was quenched very rapidly in both types of quinoa but not for Arabidopsis, which produced a trace with a very similar shape to the ROS assay, reaching a maximum peak of 20,000 RLU at 14 minutes before dropping off rapidly (Fig.12A), a dynamic that was consistently found upon several further repeats. The black line in Fig.12A shows the stable luminescence trace produced in the presence of exogenous ROS but with water as the diluent (no-plant control). A second negative control was also run to evaluate curve dynamics in the absence of exogenous ROS (Fig.12B) where background oxygen in the wells was sufficient to oxidise the L-012 probe/HRP reagents to produce a stable luminescence trace that was 10-fold lower than found in the presence of exogenous ROS (black line; right hand side axis), whereas the antioxidant activity in leaf disc bathing solutions for all three plant types was enough to quench this oxygen.

Given the very rapid quenching of luminescence for undiluted quinoa bathing solutions, dilutions of 1:2, 1:10 and 1:100 were prepared and re-sampled which revealed clearer

differences in antioxidant capacity between the two tissue types, where high salt quinoa showed stronger ROS-quenching potential than low salt quinoa (Fig.12C).





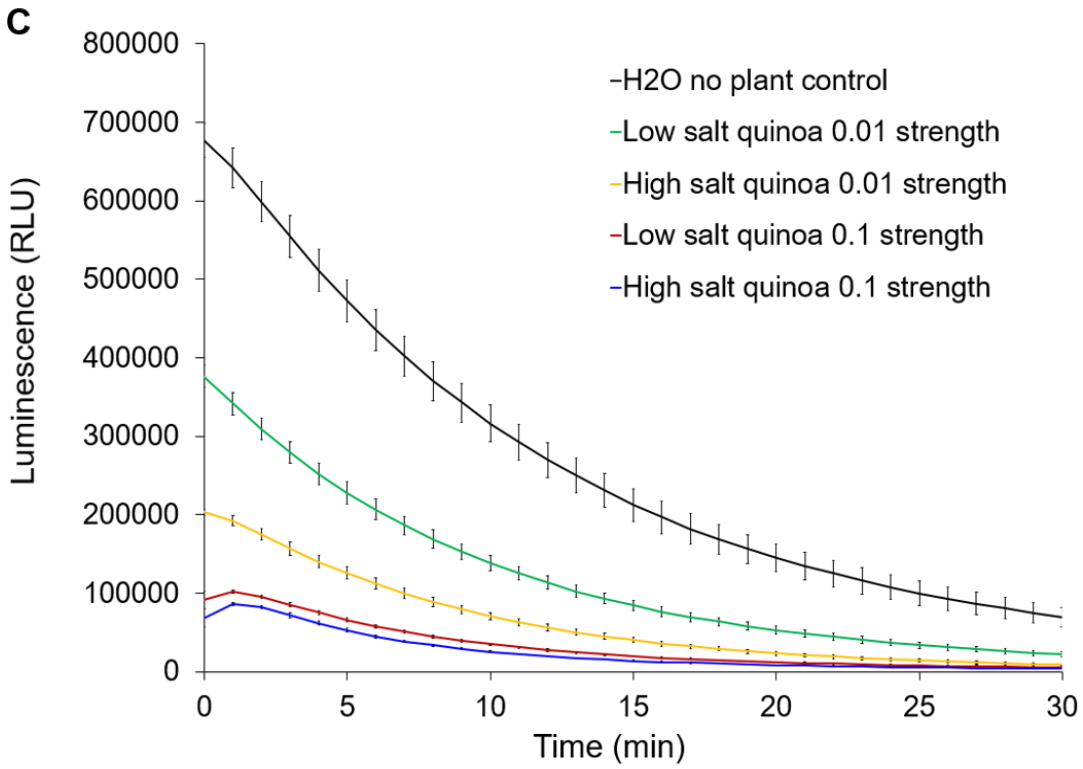


Fig. 12. ROS quenching capacity of endogenous antioxidants from leaf discs of Arabidopsis and differentially saline quinoa plants. A) Variable luminescence dynamics of leaf disc bathing solutions of quinoa, Arabidopsis and a no plant control (L-012 reagents diluted in water) following treatment with exogenous ROS (0.01 mM H_2O_2). **B) Curve dynamics of plant samples in the absence of exogenous ROS reveal a capacity to quench background ROS of the assay** (performed using stocks of the same sample types used in A). **C) Dilutions of endogenous antioxidant-containing bathing solutions reveal clearer differences between plant tissue type.** Conditions and samples used in (A) were diluted 10 and 100-fold and run against the undiluted samples. Curves for all three graphs show the mean of *n = 8* technical replicates and error bars show standard deviation between these. Each species sample type used to prepare technical replicates represents 36 leaf discs, prepared as six leaf discs floated across six wells containing sterile Milli-Q water, and harvested from the fully expanded leaves of three plants for each species type (see experimental set-up in Methods). HRP enzyme and L-012 probe were used as the catalyst and reporting system with differences to the ROS protocol highlighted in Methods.

5.2.3. A novel combinatorial abiotic x biotic transcriptomic dataset in quinoa allows an exploration of how quinoa's salt-acclimation interacts with PTI

To initiate investigations of how salt-adaptation mechanisms in halophytes may influence foliar immune responses to biotic stresses, an RNA-seq experiment was designed using hydroponically grown quinoa and the immune elicitor flg22 to profile basal and salt-influenced PTI transcriptional responses. Untreated zero-damage leaf controls were included to help understand the impact of mechanical damage induced by the leaf infiltration step mentioned previously. The experimental design is summarised below (Fig.13) with full details on treatment comparisons and bioinformatics approach used in Methods (Fig.19).

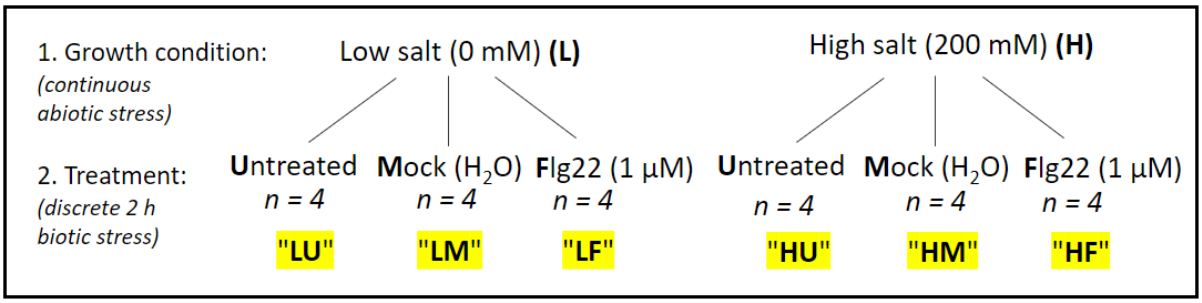


Fig.13. Experimental design scheme for the combinatorial stress RNA-seq experiment. The growth condition shows the two salt levels (low salt; L and high salt; H) used for growing the plants representing a continuous abiotic stress. These plants were then subjected to a secondary discrete biotic stress: 2h 1 µM flg22 exposure applied to fully expanded leaves of 4.5-week-old plants. No. of biological replicates are noted, and the shorthand sample names used throughout this chapter are highlighted in yellow, for example, LU = low salt untreated, LM = low salt mock treated and LF = low salt flg22 treated, which repeats for the high salt growth condition as HU, HM and HF.

The six sample types generated allowed us to produce seven key treatment comparisons, three of which are core comparisons, specifically designed to address the hypothesis that quinoa's PTI response is different between low and high salt-grown plants. Firstly, the single stress response to salt (comparison 1: HUvLU), secondly the single stress response to flg22 (comparison 2: LFvLM) and lastly the combinatorial stress of salt x flg22 (comparison 3: HFvHM). These three core datasets enable the direct comparison of the effect of salt on quinoa's PTI. The remaining four comparisons HMvHU, LMvLU, HMvLM and HFvLF were also

generated (Fig.15) but used mainly as controls to infer the transcriptional impact of the apoplast infiltration method where further analyses could be done in future work.

As an early quality control (QC) step, a principal component analysis (PCA) was performed to check for sample outliers and be sure the variance between biological replicates was smaller than the variance between treatment groups which would indicate a successful stress application and experimental design (Fig.14).

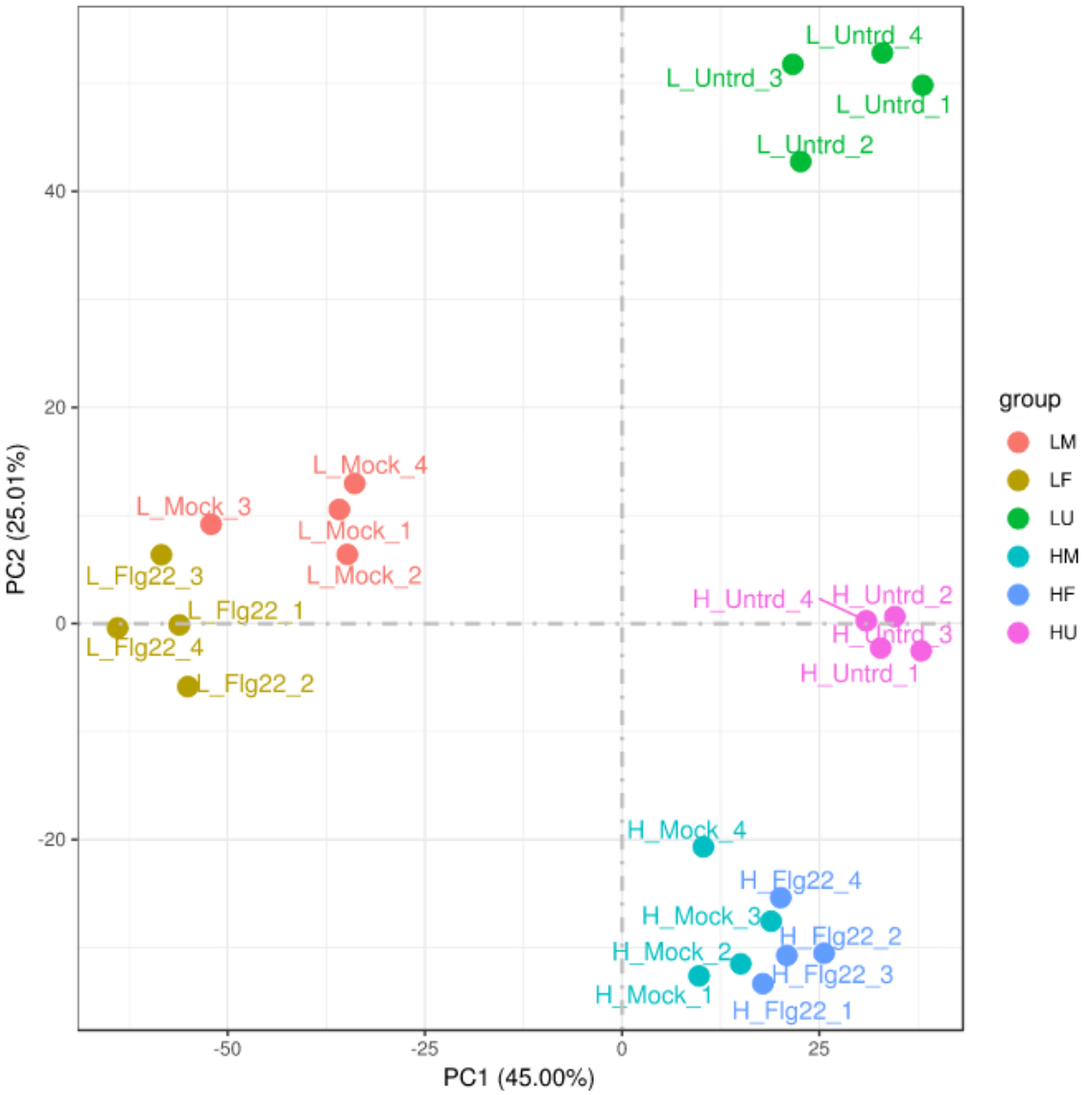


Fig.14. Principal Component Analysis conducted on the normalised transcript data for each sample type reveals small intra-group sample variability and pronounced intergroup variability. The first two principal components shown were plotted using all four biological replicates for each treatment group, colour coded as follows: red (LM; Low salt mock treated; gold (LF; Low salt flg22 treated); green

(LU; Low salt untreated); turquoise (HM; high salt mock treated); blue (HF; high salt flg22 treated); pink (HU; high salt untreated). Percentages of variation explained by each PC are indicated along the axes. R library DESeq2 with function plotPCA was used to generate this graph using normalized (by library size and transcript length) rlog transformed data (Novogene).

The two major PC axes PC1 and PC2 contribute to 45% and 25% of the total variance. Interestingly the infiltration damage appears to have a more significant transcriptome-wide effect than the flg22 treatment on both low and high salt quinoa, but especially so in low salt quinoa, whereas the salt level growth condition has the strongest effect on the transcriptome of samples, explaining 45% of the variation (PC1).

Next the total number of significantly expressed up and downregulated genes for seven key comparisons was made and plotted (Fig.15) and as expected, the largest number of differentially expressed genes (DEGs) was found for the combinatorial stress comparison of flg22-treated high salt leaves (HF) vs flg22-treated low salt leaves (LF) followed by Low-Mock (LM) vs Low-Untreated (LU), reflecting the observation in the PCA. The greater impact of combinatorial stress can also be observed by comparing the higher number of DEGs for High-Mock (HM) vs Low-Mock (LM) of 8285 vs the 5597 DEGs of the High-Untreated (HU) vs Low-Untreated (LU) datasets, the former represents the influence of salt plus the infiltration damage response (2h post-infiltration with water) and the latter represents the influence of just the saline vs non-saline hydroponics growth regime on the gene expression profile.

Interestingly, despite the macroscopic damage caused by the leaf infiltration in high salt-grown plants observed previously in Fig.3, the number of DEGs found when comparing High-Mock (HM) vs High-Untreated (HU) was proportionally small, 2810 with a surprisingly small proportion of downregulated genes, 14% (compared to the 45% downregulated genes in response to damage in low salt plants; LMvsLU) (Fig.15). Flg22 treatment of high salt plants triggered less extensive (broad) transcriptome reprograming than in low salt plants: 1061 vs 1807 DEGs respectively. Next, an analysis of DEG identities, their $\log_2$ fold changes (L2FC) and globally enriched functions will reveal a higher resolution on differences between quinoa's single stress and combinatorial stress transcriptional phenotypes.

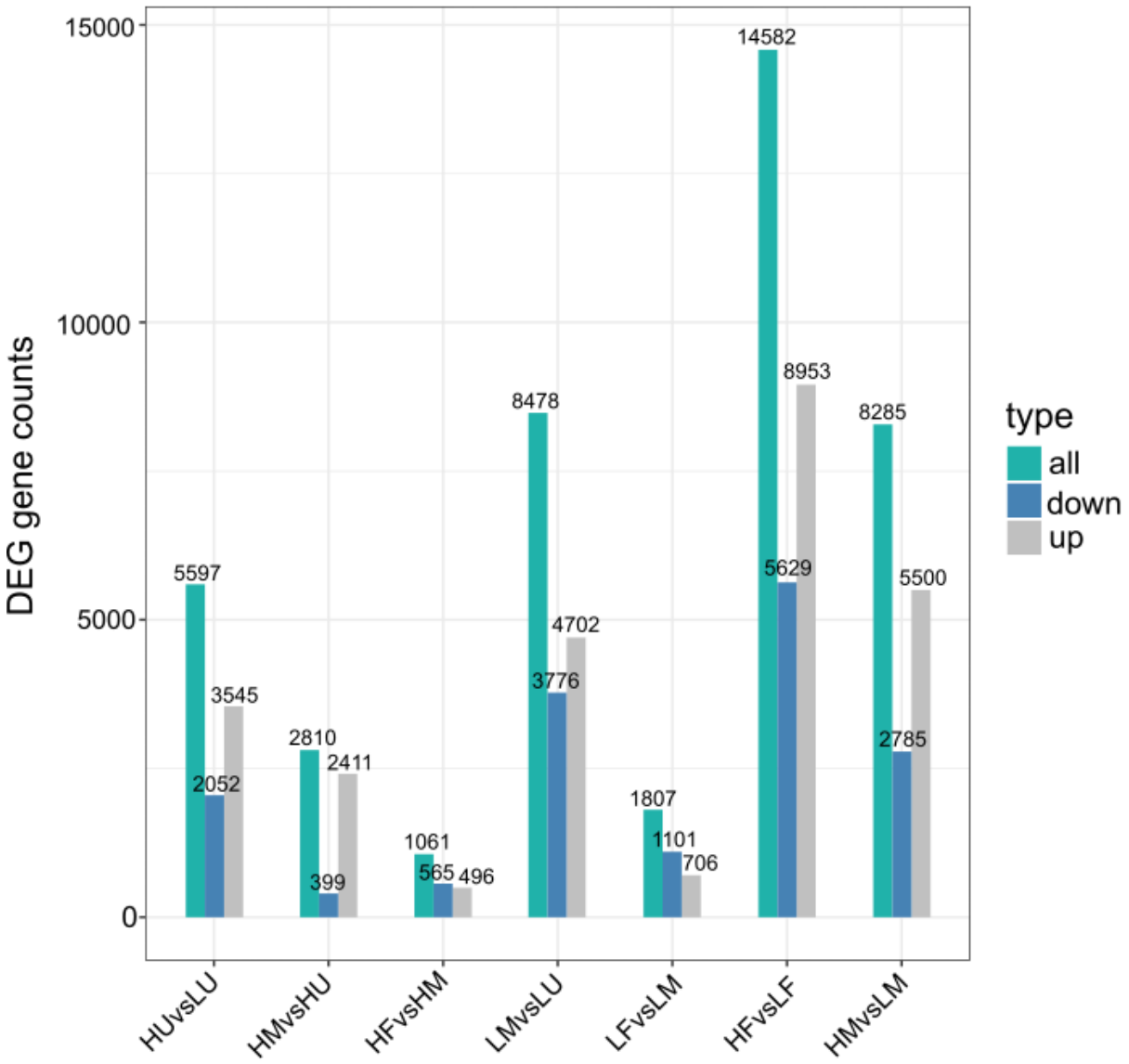
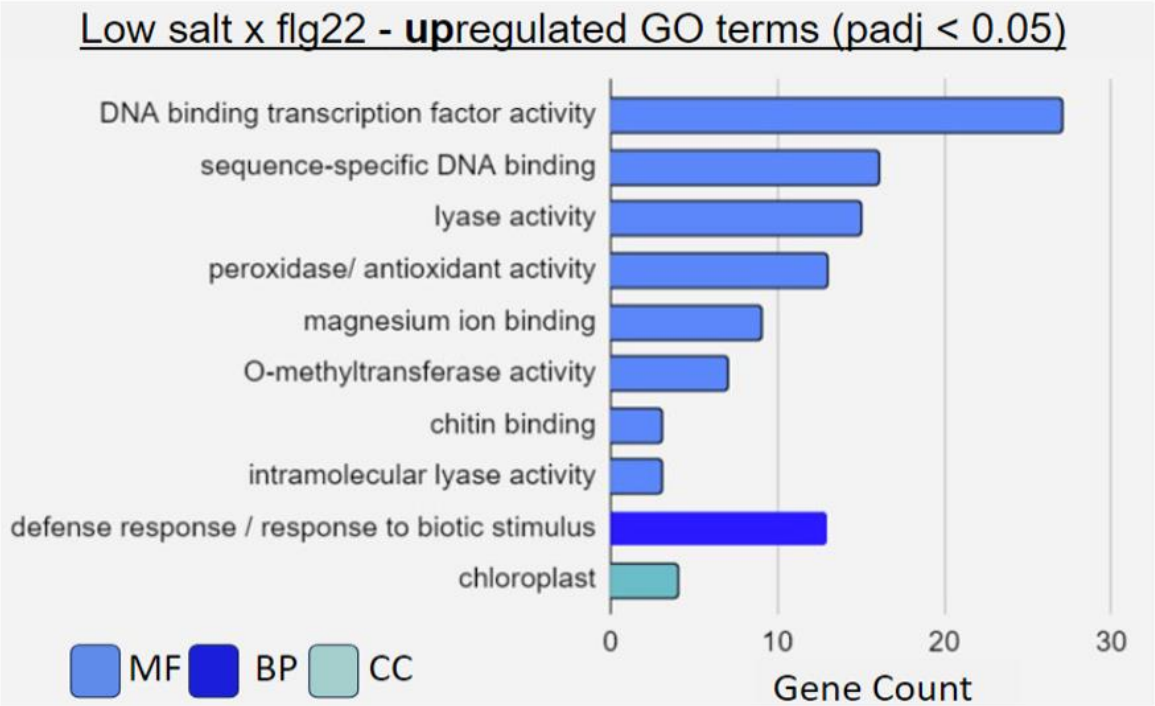


Fig.15: Total numbers of single and combinatorial stress induced DEGs found in the leaves of differentially saline hydroponically grown quinoa (*P < 0.05*). Bar charts showing total numbers and proportions of up and downregulated DEGs between seven different treatment comparisons, where H and L denote samples grown under high and low salt levels respectively, the second letter F, M and U represent 2h flg22 (1 µM) infiltrated, mock (water) infiltrated and untreated treatments respectively. Full bioinformatic analysis steps are given in Methods.

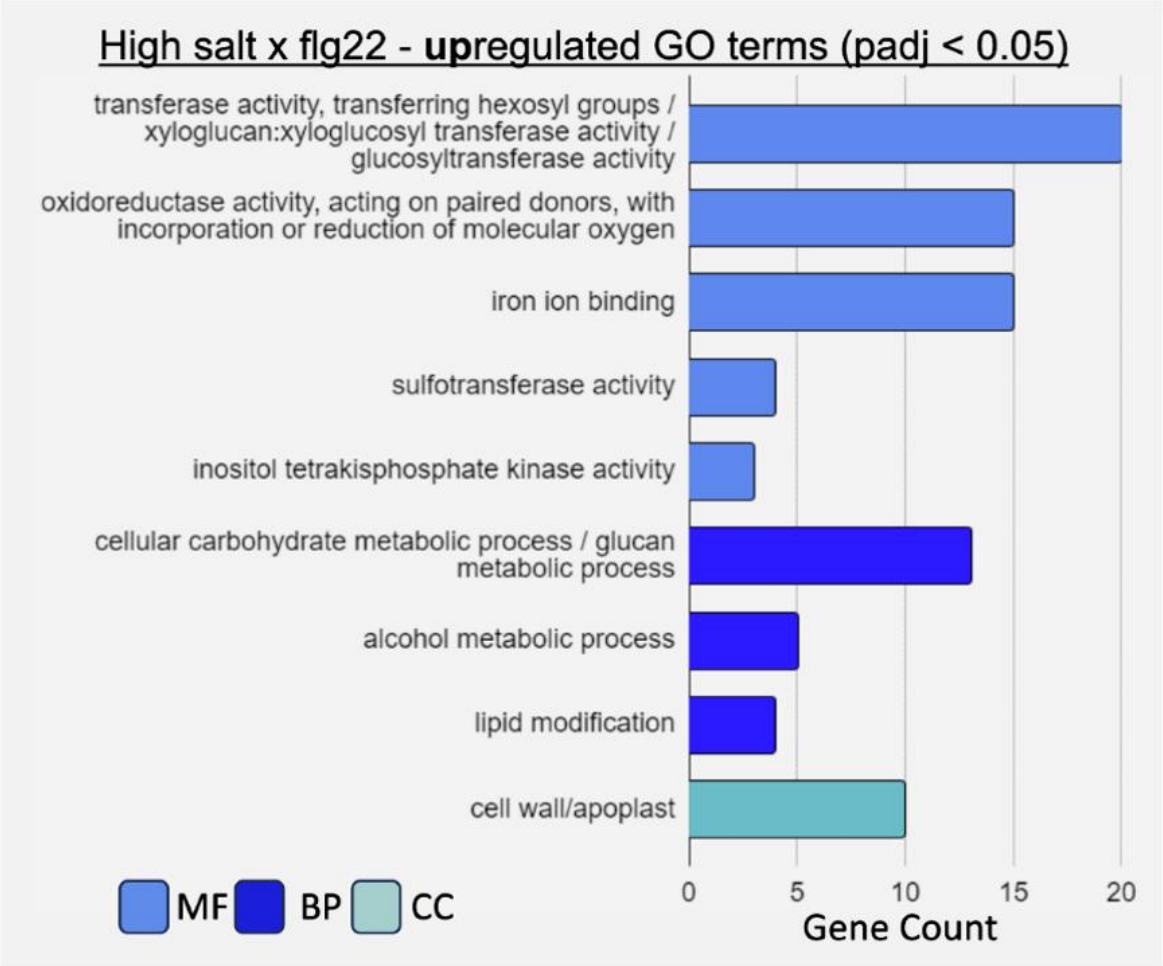
5.2.3.1. Global functional and gene-level comparisons of the low salt vs high salt PTI responses reveal strikingly opposing mechanisms in quinoa

To identify key trends in gene expression in response to flg22 the full list of DEGs (unfiltered by padj value) for the HF vs HM and LF vs LM comparisons were annotated with GO terms and gene set enrichment analysis (GSEA) was performed. The enriched terms are shown across four charts Fig.16 (A-D) split into up and downregulated term sets for each salinity phenotype, where terms are colour coded by GO categories. Surprisingly, no terms were shared between the upregulated term sets for low and high salt plants and likewise for the downregulated term sets suggesting these plants respond fundamentally differently to flg22. Furthermore, several opposing responses, marked by the black stars in the downregulated graphs (Fig.16C and Fig.16D) were found, which were the GO terms: 'glucosyltransferase activity / xyloglucan: xyloglucosyl transferase activity, 'glucan metabolic process', 'cell wall/apoplast' were downregulated in low salt plants but upregulated in high salt plants, whilst 'chloroplast' and 'lyase activity' were downregulated in high salt plants but upregulated in low salt plants.

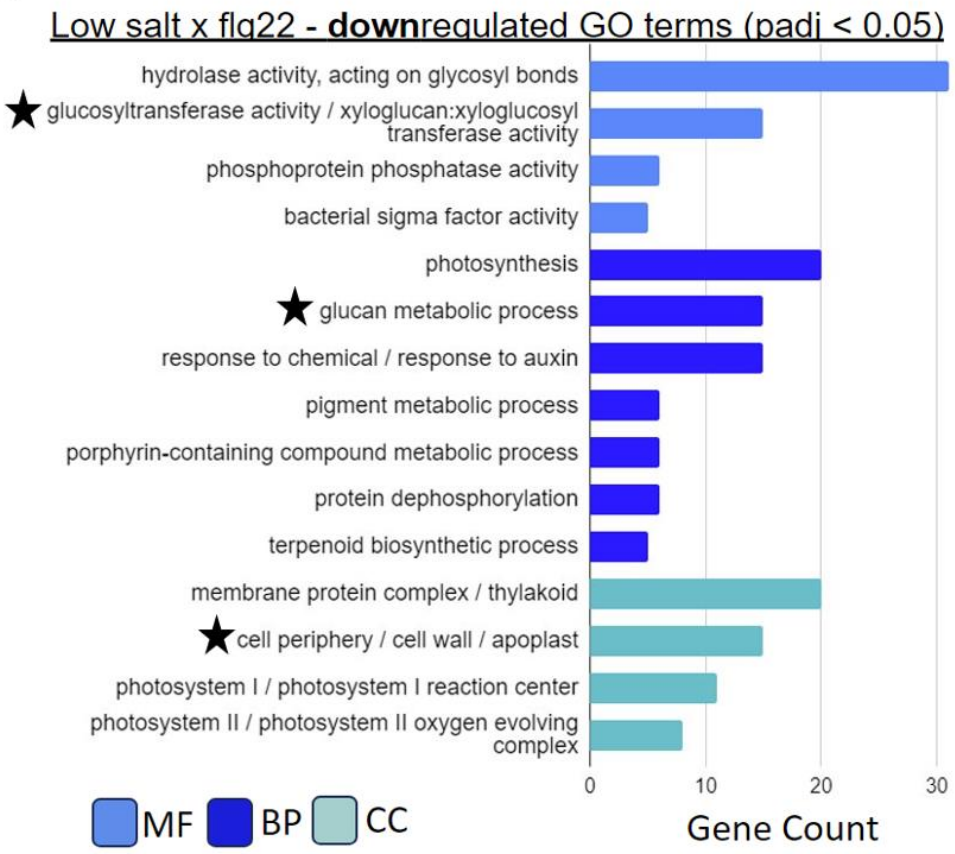
A


Low salt x flg22 - upregulated GO terms (padj < 0.05)
DNA binding transcription factor activity
sequence-specific DNA binding
lyase activity
peroxidase/ antioxidant activity
magnesium ion binding
O-methyltransferase activity
chitin binding
intramolecular lyase activity
defense response / response to biotic stimulus
chloroplast
0
10
20
30
Gene Count
MF
BP
CC

B


High salt x flg22 - upregulated GO terms (padj < 0.05)
transferase activity, transferring hexosyl groups / xyloglucan:xyloglucosyl transferase activity / glucosyltransferase activity
oxidoreductase activity, acting on paired donors, with incorporation or reduction of molecular oxygen
iron ion binding
sulfotransferase activity
inositol tetrakisphosphate kinase activity
cellular carbohydrate metabolic process / glucan metabolic process
alcohol metabolic process
lipid modification
cell wall/apoplast
0
5
10
15
20
Gene Count
MF
BP
CC

C


Low salt x flg22 - downregulated GO terms (padj < 0.05)
hydrolase activity, acting on glycosyl bonds
glucosyltransferase activity / xyloglucan:xyloglucosyl transferase activity
phosphoprotein phosphatase activity
bacterial sigma factor activity
photosynthesis
glucan metabolic process
response to chemical / response to auxin
pigment metabolic process
porphyrin-containing compound metabolic process
protein dephosphorylation
terpenoid biosynthetic process
membrane protein complex / thylakoid
cell periphery / cell wall / apoplast
photosystem I / photosystem I reaction center
photosystem II / photosystem II oxygen evolving complex
0
10
20
30
MF
BP
CC
Gene Count

D

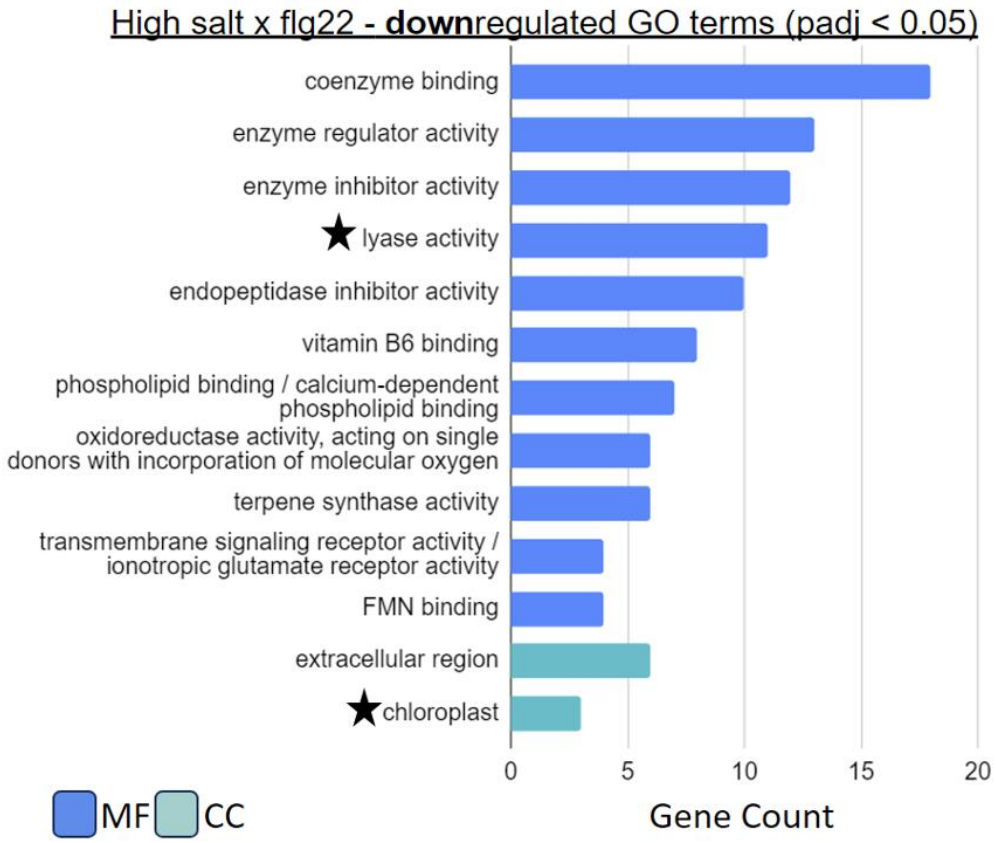

High salt x flg22 - downregulated GO terms (padj < 0.05)
coenzyme binding
enzyme regulator activity
enzyme inhibitor activity
lyase activity
endopeptidase inhibitor activity
vitamin B6 binding
phospholipid binding / calcium-dependent phospholipid binding
oxidoreductase activity, acting on single donors with incorporation of molecular oxygen
terpene synthase activity
transmembrane signaling receptor activity / ionotropic glutamate receptor activity
FMN binding
extracellular region
chloroplast
0
5
10
15
20
MF
CC
Gene Count

Fig.16. Enriched up and downregulated GO terms associated with the flg22 response in low and high salt grown quinoa leaves. GSEA was performed in the R package clusterProfiler by Novogene, and output files were analysed to remove redundant GO terms and plot graphs by GO category: MF = Molecular Function, BP = Biological Process and CC = Cellular Components. Gene Count is the number of genes annotated by the term. GO terms that are split by a "/" denotes the term to the right is a 'child' term of the 'parent' term to the left and all genes are encompassed by the parent term, however the parent term has additional genes that are not labelled with the child term. Any redundant GO terms (i.e., where all gene identities and GO term gene counts were identical) were identified and discarded manually and the most specific/information rich term was kept. A) upregulated enriched terms for LF vs LM. B) upregulated enriched terms for HF vs HM. C) downregulated enriched terms for LF vs LM. D) downregulated enriched terms for HF vs HM. Black stars in charts C and D signify terms also found in charts B and A respectively. All terms are significantly enriched to $P < 0.05$.

From the opposing responses observed at the global GO terms level, it was next hypothesised that the full DEG lists for LF vs LM and HF vs HM would also contain many different and potentially oppositely regulated genes. A similar approach used for comparing the flg22-induced transcriptional response between quinoa and Arabidopsis in Chapter 2 was taken whereby the full DEG lists were compared to each other, and the overlapping genes extracted and analysed for the direction of their L2FCs (Fig.17). Of the 1807 and 1061 PTI DEGs for low salt and high salt flg22 treated datasets, just 169 DEGs were found to be shared, representing 9% and 16% of their total flg22 responsive genes respectively. Of these 169 shared DEGs, just 19% were expressed in the same direction:10 genes were jointly upregulated and 22 jointly downregulated, whereas 81% (137 genes) were opposingly regulated (Fig.17) and examples for each are given in Table 1.

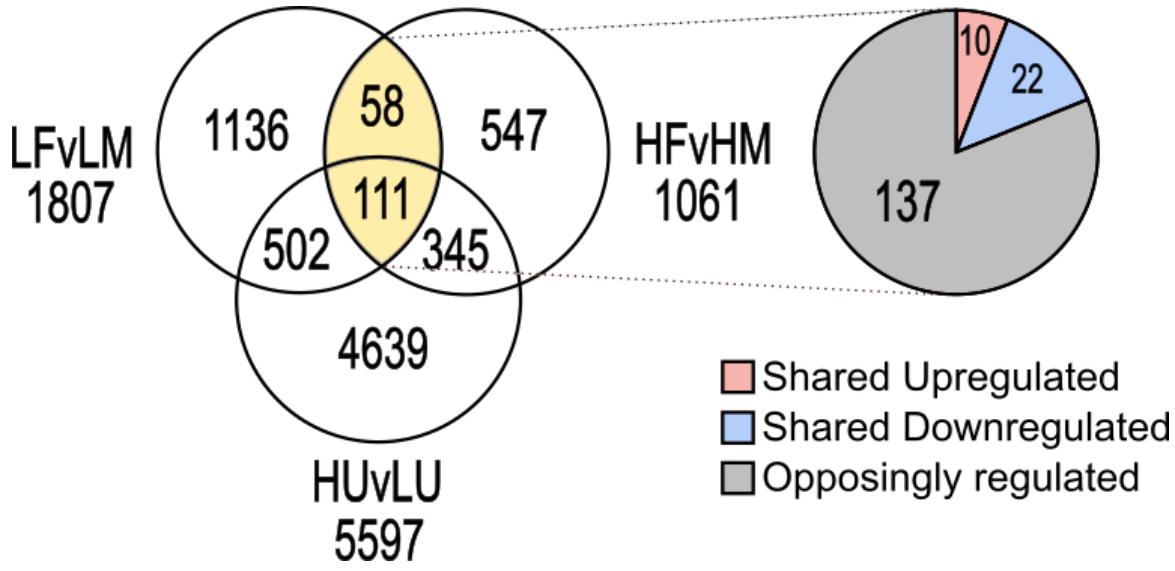


Fig.17. Interrogating the expression trends of shared DEGs between the PTI response of low and high salt quinoa and the overlap with single salt stress DEGs. Venn diagram highlights the proportion of shared or unique DEGs as specific numbers. The 169 shared DEGs between LFvLM and HFvHM are highlighted in yellow, and their composition further analysed as shown by the pie chart, showing shared upregulated (pink), downregulated (blue) and opposingly regulated (grey) DEGs. Sizes of circles and overlaps are not to scale. All DEGs used for these analyses are significant to $P < 0.05$.

Table 1 details the quinoa gene loci IDs, their gene descriptions and Arabidopsis orthologs (obtained through BLASTp and validated through OrthoFinder (Emms & Kelly 2019), where additional gene information such as GO term descriptions were retrieved from the ID mapping function for AtGeneIDs in UniProt to improve the functional understanding of these genes (Supplementary Table 6). Within the shared upregulated genes, the most highly expressed DEGs (as ordered by HFvHM) included canonical biotic stress genes such as MLO-like protein and two cytochrome P450s and two copies of EARLY STARVATION 1, chloroplastic (AtESV1) (Protein REDUCED GRAVITROPIC 1), one of which was strongly inhibited in the HUvLU single salt stress dataset. For shared downregulated genes: the photosystem stability gene and an insect defence response protein with serine-type endopeptidase inhibitor activity (miraculin-like Kunitz trypsin inhibitor 5) were strongly suppressed in both flg22 treated datasets; a glucan endo-1,3-beta-glucosidase implicated in defence responses to fungi and nematodes was strongly suppressed in all three datasets; and an uncharacterised loci (LOC110724688) and 7-deoxyloganetin glucosyltransferase-like gene were suppressed in both flg22-treated datasets but upregulated in the salt stress dataset. As for the opposingly

regulated DEGs between the two flg22 datasets, a very clear trend can be seen when observing the direction of the expression of the salt dataset: all 12 overlapping salt induced genes (out of total 20 shared candidates shown here, full list found in S.Table.7) were in the same direction as the low salt flg22 response. Important genes for the high salt flg22 response but suppressed in the low salt flg22 dataset are an auxin transporter gene, putative disease resistance protein RGA3/RPP13-like protein 1 and a sorbitol dehydrogenase gene, which was conversely the most strongly inhibited gene in the low-salt flg22-induced dataset (Table 1). Important genes for the low salt flg22 response but suppressed in the high salt flg22-induced dataset were the lysine histidine transporter 1-like/ Patatin-like protein 2 (AtPLP2), aminotransferase ALD1-like and ethylene-responsive transcription factor ERF114-like.

Table 1: Identity of shared DEGs between LFvLM and HFvHM and overlapping DEGs with HUvLU.

Quinoa ID	Arabidopsis	Gene description	HFvHM	LFvLM	HUvLU
LOC110729028	AT4G02600	MLO-like protein 1	3.10	1.91	
LOC110690623	AT1G42430	EARLY STARVATION 1, chloroplastic (AtESV1) (Protein REDUCED GRAVITROPIC 1)	2.19	1.49	
LOC110710327	AT2G30490	cytochrome P450 CYP73A100-like	1.97	1.18	
LOC110699044	AT1G42430	EARLY STARVATION 1, chloroplastic (AtESV1) (Protein REDUCED GRAVITROPIC 1)	1.93	2.42	-1.67
LOC110729650	AT2G36770	Cytochrome P450, family 715, subfamily A, polypeptide 1	1.72	1.69	3.61
LOC110691535	-	zeatin O-glucosyltransferase-like/ UDP-glycosyltransferase	1.31	1.09	3.03
LOC110682187	AT5G16760	(inositol-tetrakisphosphate 1-kinase 1-like)	1.18	1.18	3.06
LOC110700776	AT1G17860	uncharacterized LOC110700776	1.16	2.04	

LOC110717936	AT4G16260	inositol-tetrakisphosphate 1-kinase 1-like	1.13	1.34	
LOC110693036	AT5G23120	inositol-tetrakisphosphate 1-kinase 1-like	1.09	1.21	
LOC110690390	AT1G17860	miraculin-like/ Kunitz trypsin inhibitor 5 (AtKTI5)	-2.34	-1.24	
LOC110717179	AT4G16260	glucan endo-1,2C3-beta-glucosidase-like	-2.10	-1.45	-2.39
LOC110692010	AT5G23120	photosystem II stability/assembly factor HCF136,2C chloroplastic-like	-1.94	-3.27	
LOC110703614	AT5G59810	subtilisin-like protease SBT5.4	-1.91	-2.41	
LOC110729041	AT1G45616	receptor like protein 30-like/ Receptor-like protein 6 (AtRLP6)	-1.63	-1.87	
LOC110724688	-	uncharacterised LOC110724688	-1.56	-1.31	1.99
LOC110691411	AT5G06860	polygalacturonase inhibitor 1-like	-1.34	-1.26	
LOC110717778	AT2G44130	F-box/kelch-repeat protein At2g44130-like	-1.33	-1.00	
LOC110706606	AT1G22360	7-deoxyloganetin glucosyltransferase-like	-1.31	-1.41	1.77
LOC110730096	AT4G19170	probable carotenoid cleavage dioxygenase 4,2C chloroplastic	-1.27	-1.03	
LOC110717490	AT5G62360	21 kDa protein-like/ Plant invertase/pectin methylesterase inhibitor superfamily protein	-1.24	-1.27	-1.02
LOC110713329	AT2G32150	phosphate metabolism protein 8-like/ Haloacid dehalogenase-like hydrolase (HAD) superfamily protein	-1.21	-1.32	
LOC110705715	AT3G63470	serine carboxypeptidase-like 40	-1.17	-1.53	

LOC110710968	-	uncharacterised LOC110710968	-1.17	-1.06	
LOC110732628	-	uncharacterised LOC110732628	-1.14	-1.21	
LOC110699372	AT2G40435	Transcription factor SCREAM-like protein	-1.12	-2.58	
LOC110683689	-	uncharacterized LOC110683689	-1.11	-1.93	
LOC110683401	-	uncharacterized LOC110683401	-1.06	-1.40	
LOC110701376	AT1G22400	7-deoxyloganetic acid glucosyltransferase-like	-1.06	-1.22	
LOC110729136	AT2G26700	protein kinase PINOID 2-like	-1.01	-1.39	
LOC110716991	AT4G15440	fatty acid hydroperoxide lyase,2C chloroplastic-like	-1.00	-1.11	
LOC110699010	AT1G42470	Niemann-Pick C1 protein-like	-1.00	-1.00	1.27
LOC110725331	AT1G77690	auxin transporter-like protein 3	2.22	-1.31	-1.80
LOC110685661	AT3G14470	putative disease resistance protein RGA3/RPP13-like protein 1	1.78	-1.41	
LOC110724549	-	uncharacterised LOC110724549	1.77	-1.87	-1.21
LOC110736841	-	periaxin-like	1.75	-1.23	-2.10
LOC110703830	AT5G51970	sorbitol dehydrogenase-like	1.70	-5.50	
LOC110687611	AT1G53708	Small polypeptide DEVIL 22 (Small polypeptide ROTUNDIFOLIA LIKE 9) (Small polypeptide ROT-FOUR-LIKE 9)	1.52	-2.18	
LOC110727569	AT5G49230	protein DEHYDRATION-INDUCED 19 homolog 5-like, transcript variant X3	1.50	-1.11	-1.38
LOC110687231	AT1G11330	G-type lectin S-receptor-like serine/threonine-protein kinase At1g11330	1.42	-1.02	-1.00

LOC110727076	AT4G25810	probable xyloglucan endotransglucosylase/hydrolase protein 23	1.34	-1.43	
LOC110691494	AT2G41820	leucine-rich repeat receptor-like tyrosine-protein kinase PXC3	1.33	-3.17	
LOC110724228	AT2G26560	lysine histidine transporter 1-like/ Patatin-like protein 2 (AtPLP2)	-1.96	3.51	7.35
LOC110696485	AT2G13810	aminotransferase ALD1-like	-3.39	3.48	
LOC110698737	AT5G61890	ethylene-responsive transcription factor ERF114-like	-3.83	3.41	5.28
LOC110696584	AT2G26560	patatin-like protein 2,2C transcript variant X1	-1.38	3.39	4.13
LOC110733634	AT5G25250	flotillin-like protein 3	-1.23	3.14	
LOC110715038	AT4G23180	putative receptor-like protein kinase At4g00960	-1.48	3.13	
LOC110693704	AT5G42930	uncharacterized LOC110693704	-2.73	2.92	4.82
LOC110705716	AT5G13790	agamous-like MADS-box protein AGL15,2C transcript variant X2	-1.44	2.90	1.97
LOC110704238	AT1G71695	peroxidase 12-like	-1.95	2.84	1.98
LOC110705783	AT3G02230	UDP-arabinopyranose mutase 1-like	-1.34	2.70	1.72

Notes: The cells are colour coded as per Fig.17 and their gene descriptions, L2FCs and corresponding quinoa and Arabidopsis gene codes (where possible) are shown. A further column for HUvLU DEG L2FCs is also included, where white empty cells signify the gene was not differentially expressed in the dataset. The criteria for selecting the shared DEGs shown are as follows: all shared up (10) and downregulated (22) DEGs, then the top 10 opposingly regulated DEGs ordered by descending L2FC for HFvHM comparison, and the top 10 opposingly regulated ordered by descending L2FC for LFvLM. The full table can be found in Supplementary Table.7.

5.2.3.2. Further inter single stress and single vs combinatorial stress treatment comparisons shed light on core stress response functions and candidate genes in quinoa

The enriched up and downregulated terms shown for high salt quinoa challenged by flg22 represent the *'combinatorial salt x PTI stress response'* found in this experiment. However, further comparisons could be made between the single salt and flg22 stress datasets where overlapping functions could represent *'core stress responses'* in quinoa. Likewise, functions that are shared between single stress salt and combined stress datasets could represent an enhancement of pre-existing stress responses. Examples are summarised in Table 2.

Table 2: Summary of shared enriched GO terms between different single or combined stress datasets

Treatment comparison	Enriched GO terms
Shared between single stresses NaCl & flg22: upregulated in both (HU v LU) & (LF v LM) ***- 'core upregulated stress response'***	DNA binding transcription factor activity; sequence-specific DNA binding; peroxidase activity; defense response / response to biotic stimulus
Shared between single stresses NaCl & flg22: downregulated in both (HU v LU) & (LF v LM) ***- 'core downregulated stress response'***	None
Shared between opposingly regulated single stresses NaCl & flg22: downregulated in (HU v LU) & upregulated (LF v LM) ***- 'opposing stress response'***	peroxidase activity / antioxidant activity
Shared between opposingly regulated single stresses NaCl & flg22: upregulated in (HU v LU) & downregulated (LF v LM) ***- 'opposing stress response'***	hydrolase activity, hydrolysing (O) glycosyl compounds; glucosyltransferase activity / xyloglucan:xyloglucosyl transferase activity; cell wall; extracellular region/apoplast
Shared between single stress NaCl & combined stress NaCl x flg22: upregulated in both (HU v LU) & (HF v HM) ***- 'enhanced pre-existing stress response state'***	transferase activity, transferring hexosyl groups / xyloglucan:xyloglucosyl transferase activity; oxidoreductase activity, acting on paired donors, with incorporation or reduction of molecular oxygen ; cellular carbohydrate metabolic process; cell wall; extracellular region/apoplast
Shared between single stress NaCl & combined stress NaCl x flg22: downregulated in both (HU v LU) & (HF v HM) ***- 'enhanced pre-existing stress response state'***	None

Notes: Enriched GO terms shown were from GSEA mentioned in Fig.16. Boxes highlighted in blue are of particular interest and the GO terms were chosen for further analyses at the gene identity level.

There were no shared enriched downregulated GO terms between single stress salt and flg22 treatments (*'core downregulated stress response'*) and no shared enriched downregulated GO terms between single stress salt and high salt x flg22 treatments. However, four shared enriched upregulated GO terms (*'core upregulated stress response')* were found for the single stress salt and flg22 treatments along with one opposingly regulated GO term, and five shared

upregulated GO terms were found between the single stress salt and high salt x flg22 combinatorial stress treatments (*'enhanced pre-existing stress response state'*) (Table 2). Further analyses of these shared enriched GO terms were performed as follows: gene IDs for all the genes annotated by each GO term for each condition were extracted and mapped to their respective DEG lists to obtain L2FCs and gene descriptions. This enabled us to query whether similar or different genes were being induced for the shared enriched function by the different single stresses. *Core upregulated stress response* GO terms were analysed first.

Within the shared GO term 'DNA binding transcription factor activity' the main gene descriptions found were ethylene-responsive and WRKY-like transcription factors (TFs), which represented ~25% total genes of the 104 and 28 unique gene loci found for the single salt and flg22 stress datasets respectively. TFs regulate transcriptional programmes and therefore represent important signal transduction components that convert stress signals to a network of stress-responsive genes (Guo et al., 2016). The three most highly expressed TF genes for the flg22 response were: heat stress transcription factor B-3-like (+3.69 L2FC), ethylene-responsive transcription factor ERF114-like (+3.40 L2FC), and dehydration-responsive element-binding protein 1F-like (+3.23 L2FC). For the salt-acclimation response, WRKY transcription factor 22-like (+ 6.45 L2FC) was the most highly expressed gene followed by two loci for ethylene-responsive transcription factor ERF114-like (+5.28 and +5.27 L2FC). Treatment-specific but highly represented TF gene descriptions were homeobox-leucine zipper protein ATHB-12-like, represented by four different loci in the salt stress dataset, and Agamous-like MADS-box protein AGL15-2C transcript variant and GATA transcription factor 16-like which were represented as two copies each in the flg22 stress dataset.

For the shared enriched 'defence response' GO term, the most highly expressed shared gene descriptions were: pathogenesis-related protein STH-21-like represented by multiple gene loci where the highest L2FC values were +5.83 and +2.79 for the salt and flg22 induced genes equating to fold changes of 57 and 6.9; major allergen Pru ar 1-like, one gene copy for each at +4.27 (salt) and +2.22 (flg22) L2FC; MLO-like protein, represented by multiple loci, with the highest L2FC values of +4.57 (salt) and +1.91 (flg22). MLP-like protein was also highly expressed but only induced by salt (+3.86 L2FC). A pathogenesis-related protein PR-4-like gene description was also found as one and two copies for flg22 and salt stress respectively, and all loci had comparably lower L2FC values of +1.11 and +1.05 (fold change of ~two).

5.2.3.3. Peroxidase genes are differentially regulated in quinoa's response to single and combined stresses

Table 2 shows the enriched GO term 'peroxidase activity' was shared between the single stresses NaCl and flg22 as a mutually upregulated response and as an opposingly regulated response, the latter being due to the term being significantly upregulated and downregulated in response to single salt stress. A further analysis of the genes responsible for these observations was performed whereby all genes annotated with this GO term (as found by GSEA) were extracted along with an additional set of genes annotated with gene descriptions 'peroxidase' and 'respiratory burst oxidase' from the full DEG lists. This was done for LFvLM in the upregulated DEGs list and for HUvLU in both lists of up and downregulated DEGs).

From this, a very large number of genes (64) annotated with 'peroxidase' were found where L2FCs ranged from very high expression to very high suppression (+6.34 and -6.72 L2FC i.e., +81-fold and -105-fold change). Fascinatingly, only one of 64 gene loci was shared between treatments, LOC110700700, with the gene description 'respiratory burst oxidase homolog protein A-like' (an RBOH gene). LOC110700700 was upregulated in response to single flg22 stress by +1.75 L2FC but downregulated in the single salt stress (-1.93 L2FC). A second 'respiratory burst oxidase homolog protein A-like' gene loci (LOC110722611) was also upregulated in response to the single flg22 stress (+1.43 L2FC). Interestingly, a different 'respiratory burst oxidase homolog protein B-like' gene was upregulated in the single salt stress dataset, represented as two loci expressed at +1.83 (LOC110708673) and +1.57 L2FC (LOC110736865), yet neither were found in either single (LFvLM) or combined (HFvHM) flg22 stress datasets suggesting this homolog is disengaged under biotic stress.

L-ascorbate peroxidase 3-like and peroxidases 72-like, 11-like and P7-like were the four most highly expressed genes in response to single stress salt, whereas the most responsive flg22-induced genes were cationic peroxidase 1-like, peroxidase 12-like and P7-like. Peroxidases 72 and 11-like descriptions (both represented by two different gene loci) were induced in response to both single flg22 and salt stresses, which could represent core stress responsive genes. Interesting, contrasts were found for peroxidase genes shared between low and high salt flg22 treated plants: peroxidase 12 genes, (represented by two loci) were found in the 137 opposingly regulated DEGs list (Supplementary Table 7). In single stress low salt flg22-

treated plants, the two peroxidase 12 gene loci occupied the 9th and 29th most highly expressed positions respectively when the 137 DEGs were ordered by descending LFvLM L2FCs, but these loci were strongly downregulated in high salt flg22-treated plants, occupying the 3rd and 25th position when the DEGs were ordered by ascending HFvHM L2FCs). Lastly, given the dynamic role of peroxidases found in the previous comparisons, all genes with the functional descriptions 'peroxidase' and 'respiratory burst oxidase' were extracted from the LFvLM downregulated DEGs dataset, finding five more putative peroxidase genes, four of which had unique gene descriptions. Interestingly, three of these downregulated single stress flg22-induced gene identities were present in the upregulated single stress salt-induced dataset, further supporting the trend of opposing responses found by GSEA and gene-level expression analyses.

5.3. Discussion

This Chapter aimed to shed light on the impact of salt on quinoa's PTI responses, previously characterised in Chapter 2. Results from Chapter 4 had shown enhanced disease resistance in the salt-acclimated phenotype, and so it was hypothesised that quinoa's immune mechanisms may be altered due to an abiotic stress primed state. The first two specific objectives were to optimise the pre-established biochemical PTI assays in saline quinoa tissue and to evaluate any potential PTI differences between low and high salt quinoa plants. These were met to limited extent due to the technical difficulties that arose from working with the more succulent, hyperosmotic and antioxidant-rich salt-acclimated tissue, but which inspired the development of two compatible *in vitro* assays (an antioxidant activity screen and an osmotic point experiment) to improve the validity of conclusions drawn.

The last two objectives of this Chapter were to design and perform a combinatorial transcriptomics experiment with NaCl and flg22 in quinoa and to use this to characterise single and combined abiotic (salt) and biotic (flg22) stress responses in quinoa, which could provide evidence as to why saline plants are more disease resistant. These last two objectives were successfully met, the single and combinatorial transcriptomics datasets generated facilitated an interrogation of quinoa's core and salt-primed stress responses with exciting opportunities for further analyses.

5.3.1. The salt-acclimated phenotype of quinoa significantly affects flg22-inducible PTI responses

The four biochemical PTI assays (MAPK activation, ROS burst, peroxidase activity and callose deposition) previously optimised for soil grown non-saline quinoa leaves in Chapter 2 were trialled in hydroponically grown saline leaf tissue. Two of these PTI assays, the early MAPK activation response and the later callose deposition response were successfully assayed and found to be active in high salt quinoa leaves. Previously, a strong biochemical MAPK response was found in soil-grown non-saline ('low salt') plants 45 minutes after flg22 treatment (Chapter 2), but this was not evident at the later 2h time-point used in this Chapter for hydroponically grown low salt plants. Hydroponically grown high salt plants however did show a strong MAPK response at 2h which could suggest the response is sustained for longer due to a differential balance of kinase and phosphatase enzyme post-translational control (Zhang and Zhang et al., 2022). Interestingly, the 2h transcriptomic data, derived from the same tissue samples used for the MAPK western blot, could potentially support these differential biochemical MAPK results. For low salt quinoa four loci with mitogen-activated protein kinase – related annotations (three MAP kinase kinase kinase and one MAP kinase kinase) were induced but only very subtly (L2FCs ranging from +1.0 to +1.2). For high salt plants, just one MAPK-related gene loci (mitogen-activated protein kinase kinase 5-like) was found to be significantly induced, but to a L2FC of +2.3 which could suggest an enhanced MAPK signalling capacity as a central component of MAPK cascades (Chapter 2 Fig.1) upstream of the phosphorylated MAPKs observed through western blotting. Crucially, the positive signals for MAPK and callose deposition in high salt plants demonstrate that flg22 is perceived by the FLS2 pattern recognition receptor and the signal is successfully transduced to downstream PTI response genes such as callose synthase within 24 h. Due to the early time-point used for the RNA-seq experiment we were unable to find significant induction of callose synthase genes (Wang et al., 2022).

The two canonical PTI assays which measure an apoplastic ROS burst and upregulated peroxidase activity (data not shown) were not possible to adapt to saline tissue due to technical incompatibilities of the leaf-disc set-up. While appropriate for low salt plants, which showed a positive ROS response, no signal was measurable for leaf discs taken from plants

grown under medium or high salinity (100 – 200 mM NaCl). The series of exploratory experiments which followed revealed that a higher concentration of endogenous antioxidants was leaked into the reaction wells from saline tissue which appeared to quench all ROS present before it had a chance to oxidise the L-012 probe (Nishinaka, 1993). While results from the antioxidant assay were not able to conclusively determine whether apoplastic ROS *can* be produced by saline plants as a PTI response to flg22 (Hypothesis 1; Fig.6) the positive flg22-induced callose deposition response suggests it could be considering how flg22-induced callose deposition of Arabidopsis is dependent on the upstream ROS signalling pathway (Luna et al., 2010; Yi et al., 2014).

5.3.2. Endogenous antioxidants may play an important role in the PTI of naturally stress resilient plants

The identification of antioxidants as confounding factors for the *in vitro* ROS assay has highlighted an important new consideration for evaluating the PTI-ROS response in non-model species. The complimentary leaf-disc bathing solution electrical conductance experiment confirmed that excessive leaf edge damage can occur and in proportion to the *in planta* salt levels in quinoa (a differential abiotic stress acclimated phenotype). The complimentary leaf disc osmotic point experiment demonstrated how suitable concentrations of osmotica for leaf-disc osmotic equilibration can be determined, which could improve the validity of future experiments (providing the osmotica are sufficiently inert to not interfere with the assay's read-out components).

The enhanced antioxidant activity of high salt grown quinoa plants could reflect a need to more tightly control higher levels of background oxidative stress caused by excess salt ions. A salt induced differential state of ROS homeostasis could be a feature of quinoa's high salt phenotype, in a similar way to how the zinc-induced metal hyperaccumulating phenotype of *Noccaea caerulescens* is also shifted to an altered ROS homeostasis (Fones et al., 2013).

The constitutively expressed high levels of antioxidants in the leaves of *N. caerulescens* (proposed as a defence adaptation to high metal accumulation) is suggested to have driven the decoupling of ROS from its canonical role in biotic stress signalling pathways (Fones et al., 2013). Quinoa leaves are known to have high levels of antioxidants which could reflect an evolutionary adaptation to combat harsh abiotic stress conditions. The known antioxidants in

quinoa leaves include non-enzymatic sources, the secondary metabolites ascorbic acid, carotenoids, phenolic compounds, flavonoids, and anthocyanins and antioxidant enzymes superoxide dismutase (SOD), glutathione peroxidase (GPX), ascorbate peroxidase (APX), glutathione reductase and catalase (CAT), many of which have been shown to increase under salt to counteract the increase in oxidative stress (Agirresarobe et al., 2022; Hajihashemi et al., 2022; Souid et al., 2023). Our datasets revealed just one ascorbate peroxidase gene upregulated under salt, whereas many glutathione-S-transferase genes were found upregulated by salt, several by flg22 treatment and just one unique gene by the combination of salt x flg22.

The role of antioxidants in quinoa's PTI and salt x PTI stress defences could be explored further by directly evaluating their cellular origin and type. If the antioxidants were predominantly of apoplastic origin (APXs) then perhaps they would also quench (and therefore invalidate the typical role of) any PAMP-induced apoplastic ROS *in planta*. The newly developed Antioxidant Assay could easily be extended to check both the identity and origin of the antioxidants from quinoa leaf discs using different sample work ups: whole cell leaf extracts of differentially saline quinoa leaves and apoplastic fluid extracts (both of varying dilutions) could be run alongside the current leaf disc set-up and their luminescence quenching kinetics compared. From there, orthogonal antioxidant activity assays of increasing specificity could be performed on these three different sample workups to elucidate more precisely their identity (enzymatic vs non enzymatic and the subclass of enzymatic sources) which would help determine their likely cellular location. For example, activity of the Glucose-6-phosphate dehydrogenase (G6PD) enzyme is routinely used as a cytosolic contamination marker for quality control of apoplastic washing fluid extractions (O'Leary et al., 2014). A flowchart for addressing potential confounding factors (e.g., antioxidants) for the PTI-ROS assay in new species is found in Supplementary Materials (S.Fig.2) with the Antioxidant Assay in Methods.

5.3.3. A combinatorial abiotic x biotic stress RNA-seq experiment elucidates candidate genes responsible for a salt-primed enhanced disease resistance in quinoa

The single biotic stress of flg22 treatment in low salt quinoa when compared to the combinatorial abiotic x biotic stress treatment (flg22 treated high salt quinoa) revealed distinct transcriptional responses at the global functional and gene levels, suggesting that salt

acclimation causes a pronounced effect on quinoa's PTI. No enriched GO terms were found to be jointly up or downregulated while at the gene level, just 1.2% (32 genes) out of a combined total of 2699 flg22-induced DEGs across both low and high salt phenotypes were expressed in the same direction. Some of the most striking findings were at the level of canonical stress phytohormone related genes, where contrasting expression patterns occurred between single biotic and combinatorial abiotic x biotic stressed plants.

Firstly, all 17 of the shared stress related phytohormone regulated genes were opposingly regulated between flg22-treated low and high salt quinoa plants. These genes were related to jasmonic acid (JA), abscisic acid (ABA) ethylene (ET) or salicylic acid (SA) signal transduction (Table 3). Secondly, all 17 except for one ABA-related DEG (Alkaline ceramidase TOD1; LOC110691817; AT5G46220) were downregulated in the combinatorial stress plants but upregulated in the biotic stress plants. This is potentially consistent with the antagonism between ABA and other hormonal signalling pathways observed in other systems (Tamaoki et al., 2013; Gupta et al., 2020). Eleven JA related DEGs were found, with GO term annotations JA biosynthetic process or response to or regulation of JA. Six DEGs were related to ABA, annotated with response to or abscisic acid-activated signalling pathway. Two previously discussed ET-related homologs ethylene responsive factor 114-like genes (LOC110698737 and LOC110687053; AT5G61890) were found, annotated with ethylene-activated signalling pathway and defence response to fungus and lastly two SA-related gene Protein DOWNY MILDEW RESISTANCE 6 (AtDMR6) (LOC110692918; AT5G24530) and chloroplastic aminotransferase ALD1 AGD2-like defence response protein 1 (LOC110696485; AT2G13810) annotated with response to salicylic acid and salicylic acid catabolic process. The genes for these are found in Table 3 below.

Table 3: Summary of shared opposingly regulated hormone related genes between flg22 treated low and high salt quinoa.

Quinoa ID	AtGeneID	Gene description	HFvHM	LFvLM	Phytohormone GO term annotations
LOC110715921	AT2G06050	12-oxophytodienoate reductase 3-like (AtOPR3)	-1.39	1.48	jasmonic acid biosynthetic process
LOC110735423	AT2G06050	12-oxophytodienoate reductase 3-like (AtOPR3)	-1.80	2.53	jasmonic acid biosynthetic process
LOC110724846	AT1G13280	chloroplastic Allene oxide cyclase 4	-1.04	1.44	jasmonic acid biosynthetic process
LOC110728173	AT1G13280	chloroplastic Allene oxide cyclase 4	-1.60	1.04	jasmonic acid biosynthetic process
LOC110721619	AT1G20510	4-coumarate-CoA ligase isoform 9 (At4CL9)	-1.19	1.34	jasmonic acid biosynthetic process; response to jasmonic acid
LOC110719970	AT3G25780	chloroplastic Allene oxide cyclase 3, chloroplastic	-1.24	2.28	jasmonic acid biosynthetic process
LOC110718526	AT3G45140	chloroplastic Lipoxygenase 2 (AtLOX2)	-1.74	2.28	jasmonic acid biosynthetic process; response to jasmonic acid
LOC110690479	AT5G13220	Protein JASMONATE-ASSOCIATED 1 (Protein JAZ10)	-1.76	1.41	regulation of jasmonic acid mediated signaling pathway; response to jasmonic acid

LOC110712921	AT5G18860	apoplastic Nucleoside hydrolase 3 (Adenosine nucleosidase)	-2.13	1.07	response to jasmonic acid
LOC110731869	AT2G33150	peroxisomal 3-ketoacyl-CoA thiolase 2	-1.17	1.14	jasmonic acid biosynthetic process; positive regulation of abscisic acid-activated signaling pathway
LOC110728089	AT2G33150	peroxisomal 3-ketoacyl-CoA thiolase 2	-2.40	1.55	jasmonic acid biosynthetic process; positive regulation of abscisic acid-activated signaling pathway
LOC110691817	AT5G46220	Alkaline ceramidase TOD1 (Protein TURGOR REGULATION DEFECT 1)	1.23	-1.51	abscisic acid-activated signaling pathway; response to abscisic acid
LOC110718631	AT1G18390	LEAF RUST 10 DISEASE-RESISTANCE LOCUS RECEPTOR-LIKE PROTEIN KINASE-like 1.2	-1.17	1.21	cellular response to abscisic acid stimulus
LOC110735225	AT5G40010	mitochondrial AAA-ATPase ASD (AAA-ATPase 1)	-1.51	2.18	response to abscisic acid
LOC110695250	AT2G22570	Nicotinamidase 1 (AtNIC1)	-1.60	2.22	response to abscisic acid
LOC110692918	AT5G24530	Protein DOWNY MILDEW RESISTANCE 6 (AtDMR6)	-1.29	1.14	response to salicylic acid; salicylic acid catabolic process
LOC110696485	AT2G13810	chloroplastic aminotransferase ALD1 (AGD2-like defence response protein 1)	-3.39	3.48	salicylic acid mediated signaling pathway

LOC110687053	AT5G61890	Ethylene-responsive transcription factor ERF114 (ERF bud enhancer)	-3.71	2.29	ethylene-activated signaling pathway
LOC110698737	AT5G61890	ethylene-responsive transcription factor ERF114-like	-3.83	3.41	ethylene-activated signaling pathway
LOC110725331	AT1G77690	Auxin transporter-like protein 3 (AUX1-like protein 3)	2.22	-1.31	auxin polar transport; auxin-activated signaling pathway; response to auxin
LOC110684388	AT5G07990	Flavonoid 3'-monooxygenase (Cytochrome P450 75B1)	-1.03	1.66	response to auxin
LOC110682659	AT5G13750	Protein ZINC INDUCED FACILITATOR-LIKE 1 (Protein ZIF-LIKE 1)	-1.07	1.12	basipetal auxin transport
LOC110684375	AT5G54510	Indole-3-acetic acid-amido synthetase GH3.6 (Auxin-responsive GH3-like protein 6)	-1.12	1.34	auxin-activated signaling pathway; response to auxin
LOC110705716	AT5G13790	Agamous-like MADS-box protein AGL15	-1.44	2.90	cellular response to auxin stimulus

Notes: Quinoa and their candidate Arabidopsis orthologs are shown with gene descriptions and GO terms obtained from UniProt. L2FCs are shown and colour coded according to expression level, where red is up, and blue is downregulated.

SA and JA/ET-mediated signalling pathways have long been considered as integral to the immune response of plants to biotic stress (Koornneef et al., 2008), yet Rollano-Peñaloza et al. (2022) reported the surprising absence of gene induction of canonical SA-defence gene quinoa orthologs of *AtCAT2* and *AtEP3* in response to downy mildew infection and we found that another key SA signalling gene receptor AtNPR1 (AT1G64280) (TAIR; Wu et al., 2012) showed no clear orthologs in quinoa. Rollano-Peñaloza et al. (2022) did however find that canonical JA response pathway genes *AtWRKY33* and *AtHSP90* were strongly induced. Reflecting on the leaf pathosystem symptoms for infection with PG1 pathovars showing notable chlorosis, which is known to be stimulated by methyl-jasmonate mimic coronatine, our transcriptomic findings along with results from Rollano-Peñaloza et al. (2022) suggest that a JA-mediated defence response pathway is intact and an important feature of quinoa's

response to biotrophic pathogens. Traditionally it was assumed that JA signalling was more important for defence against necrotrophic pathogens but increasing studies have shown deviances (Asai et al., 2014; Guerreiro et al., 2016; Rollano-Peñaloza et al., 2022). It is therefore useful to generate and interrogate new datasets such as these to understand what role 'canonical biotic stress genes' play in halophytic crops and how the presence of an abiotic stress and acclimation process alters immune responses.

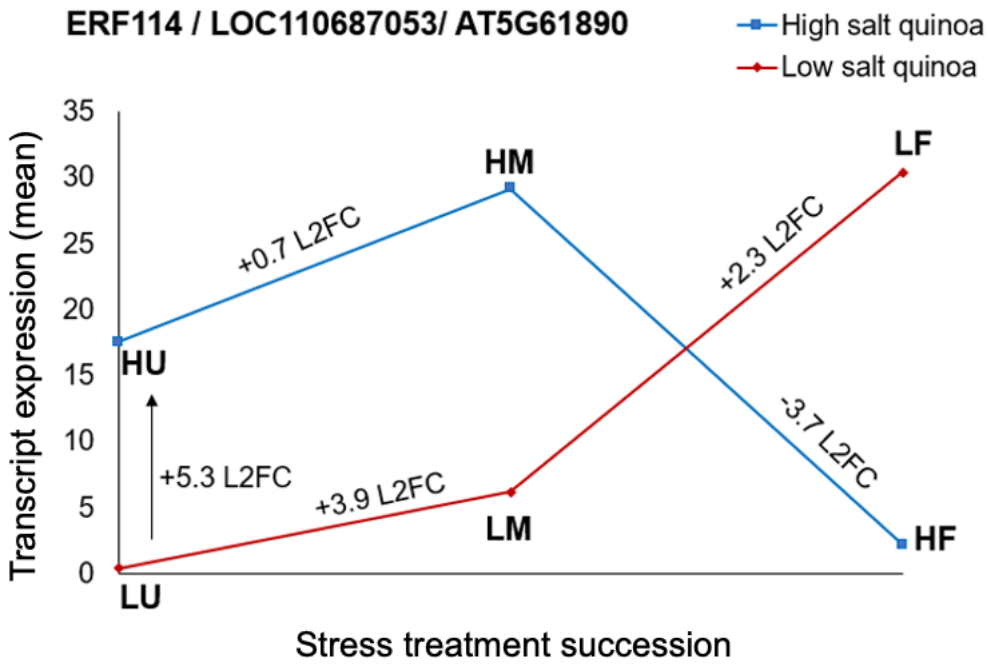
The gene most highly upregulated in high salt flg22 treated plants but which was suppressed for low salt flg22 plants was the auxin-activated signalling pathway term Auxin transporter-like protein 3 (AUX1-like protein 3; LOC110725331; AT1G77690). Auxin stimulates plant growth by promoting cell elongation in tissues, examples include initiating lateral shoot and root formation and mediating gravitropic responses, for example away from salt (halotropism) or in response to other abiotic stresses, via members of the AUX protein class in several species (Galvan-Ampudia et al., 2013; Cackett et al., 2022). However, as seen for the pattern of stress phytohormone between low and high salt quinoa the four other shared auxin-related terms were (marginally) upregulated in low salt and suppressed in high salt.

Lastly, Coolen et al. (2016) found that the sequential application of two stresses (out of infection by the necrotrophic fungus *Botrytis cinerea*, herbivory by chewing larvae of *Pieris rapae,* or drought stress) on Arabidopsis produced transcriptome profiles that were most similar to the second stress, irrespective of the combination or order of stresses. The significant first-stress signatures that were however still present in the sequential stress profiles were related to phytohormones and the authors proposed therefore that hormones must be global modulators of crosstalk between different types of stress. However, when comparing the phytohormone responses found for our combined stress treatment with those of the first (single) stress (salt) in our system, the phytohormone pattern was more similar to the second (single) stress flg22. For example, for the key ET TF ERF114 (both homeologs) showed the following trend: an increase in L2FC in response to just salt (HUvLU), or to just damage (LMvLU) or even damage upon prior salt treatment (HMvHU) (Fig.18A), yet when the biotic stress flg22 is applied to the high salt phenotype the transcript expression drops to negligible levels. Conversely in the low salt phenotype background the single flg22 stress increases ERF114 expression to a similar level found in the mock treated high salt phenotype

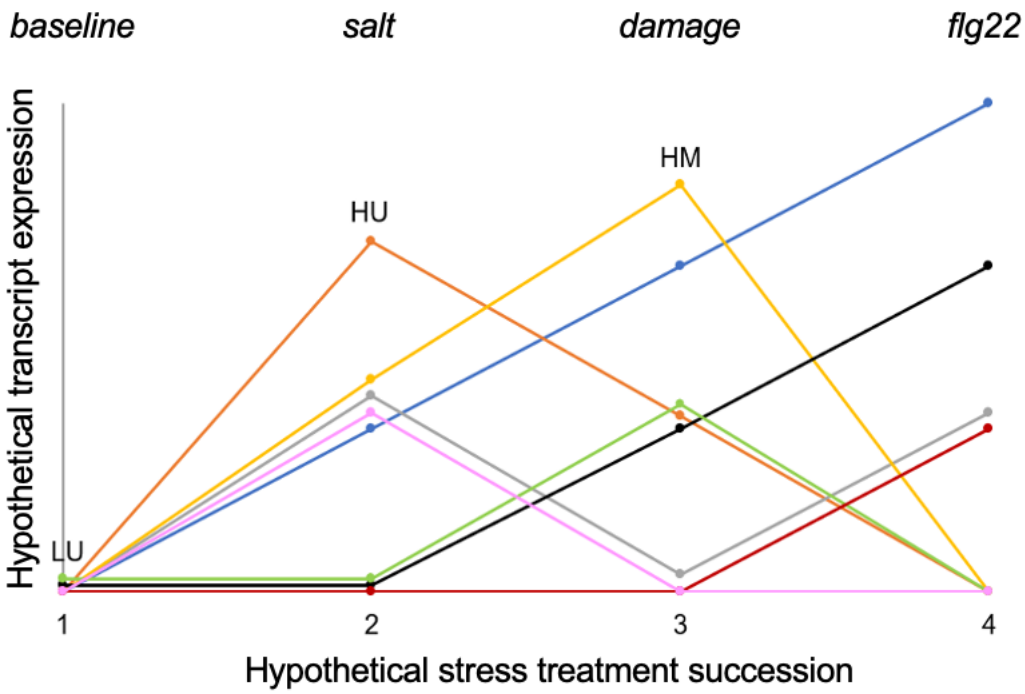
(Fig.18A). This pattern of transcript expression was described as 'combinatorial mode' by Rasmussen et al. (2013) where single stress transcripts behave similarly to each other, but a different transcript response is found when the two stresses are combined.

A clear example of stress processes being maintained or enhanced under sequential stresses in quinoa (i.e., flg22 treatment on the salt-acclimated phenotype) is given by the enriched GO terms transferase activity and oxidoreductase activity (see Table 2 for full list) suggesting these processes are core to quinoa's stress response. The upregulated genes contained within these enriched terms include many cytochrome P450 homologs such as cytochrome P450 78A3-like (which had by far the highest L2FC), and other redox homeostasis enzymes such as previously mentioned peroxidases and glutathione transferases (processes which were also found to be enriched in the soil-grown flg22-treated plants in Chapter 2).

A



B



- incrementally enhanced
- salt enhanced, damage and flg22 incrementally suppressed
- salt enhanced, damage suppressed, flg22 enhanced
- salt and damage enhanced, flg22 suppressed
- not salt responsive, damage and flg22 incrementally enhanced
- not salt responsive, damage enhanced, flg22 suppressed
- not salt or damage responsive, flg22 enhanced
- salt enhanced, damage and flg22 suppressed

Fig.18. Schematic representation of how the mean transcript expression value of ERF114 changes in response to a succession of different stresses and theorising patterns for other transcripts. A) Transcript expression values are the normalized mean read counts for the four biological replicates of each stress treatment or control. The stress treatment x-axis is not to scale and represents the additional levels of stress applied on the two quinoa phenotypes (low and high salt): firstly, damage imposed by water infiltration (mock treatment; LM or HM) and then the effect of this damage plus flg22 (i.e., LF or HF). The blue line represents the responses of high salt acclimated quinoa, and the red line represents low salt quinoa. The black vertical arrow between LU and HU represents the initial impact of long-term salt exposure. The L2FC changes are also given. **B) Eight possible theoretical patterns of expression of a stress-responsive gene with increasing succession of stress treatments:** salt (H_), damage (_M), damage + flg22 (HF) (x-axis). The two letter codes used in our experiments are maintained here for easier understanding of how these patterns of expression could be checked in practise. The Y-axis represents relative changes in expression in binary increments between each stress treatment succession, except for the orange line which shows a relative increase of two units instead of one to signify an exaggerated impact of salt and in order to facilitate an incremental decrease with increasing number of stresses.

In future work, the list of 111 intersecting differentially expressed transcripts between the two single stresses salt, flg22 and the combined stress salt x flg22, could be analysed for one of the five transcript mode patterns proposed by Rasmussen et al. (2013) to gain a higher resolution understanding of quinoa's single and sequential combinatorial stress responses. When considering the impact of the 'damage' induced by the infiltration method (mock treatment vs untreated) even more combinations of transcript behaviour would be possible. An example of eight (out of 16+) possibilities of hypothetical stress responsive transcript behaviour is summarised in Fig.18B.

Whether the relative shut down of a stress signalling pathway by 2h in high salt grown plants (as seen here for ERF114) would last is another consideration. Further analyses of hormone dynamics across additional time-points could be achieved using RT-qPCR and gene expression data could be complemented by metabolomics. This would evaluate more conclusively any antagonistic or synergistic interactions between hormonal signal-transduction pathways.

Lastly, Coolen et al. (2016) showed that irrespective of the first stress, Arabidopsis can efficiently adapt its transcriptome to respond to the second stress and over time the second

stress-induced transcriptome becomes highly similar to that of plants that did not receive a first stress. The goal of quinoa's response to an increasing number of stresses would be to utilise its resources in the most cost-efficient manner (Pieterse et al., 2012; Vos et al., 2013a, 2015, Coolen et al., 2016). It is interesting that the majority (70%) of the shared opposingly regulated flg22 responsive DEGs between low and high salt quinoa were found to be downregulated in the high salt phenotype and with stronger magnitudes of negative L2FC also. When this is compared to the higher proportion of upregulated genes found in response to both single stresses of salt (HUvLU) and damage (HMvHU) it indicates a reduced investment in transcription (and their respective gene products) in the combinatorial stressed phenotype, where other stress adaptive mechanisms such as post-translational modifications or protein turnover could be prioritised.

5.4. Conclusion

Through biochemical and transcriptomic analyses, we have demonstrated how several early PTI responses differ between low and high salt quinoa plants showing that salt acclimation cross talks with quinoa's PAMP-triggered immunity. Future work could perform Gene Duplication Analysis of expanded gene sets found here (due to polyploidization and long-term stress adaptation) such as the peroxidase genes, cytochrome P450s, glutathione transferases, ethylene responsive TFs, as has been done for the WRKY genes in quinoa before (Yue et al., 2019) or transmembrane proteins (Schmöckel et al., 2017) along with co-expression analyses to reveal connected stress response hubs. A cis-element enrichment analysis could help validate the role of the enriched TFs and phytohormone-related genes here along with new candidates that may have been missed in the transcriptomics analyses due to their transient nature before or beyond the 2h flg22 time-point. Hosseini et al. (2023) recently used co-expression analysis to construct gene interaction networks for the salt stress response of the widely studied variety Titicaca using the Cytoscape software, whereas Zhang et al., 2023 implemented this strategy to yield candidate genes associated with different phosphorus levels in quinoa seedlings. Lastly, the generation of several single and sequentially stressed datasets for quinoa has revealed the dynamic patterns of certain key stress-responsive genes such as ERF-114 (Fig.18A) which reinforces the validity of descriptive frameworks for combinatorial stress transcript response behaviours such as the 'modes' proposed by

Rasmussen et al. (2013) and provides new ideas for evaluating combinatorial stress datasets through bioinformatic analyses (Fig.18B).

5.5. Methods

Hydroponic plant growth - *as described in Chapter 3.*

MAPK, Callose and ROS assays in differentially saline leaf tissue

All were performed identically to Chapter 2's protocols. The only amendment was for the callose experiment, where chlorophyll clearing was done using a 2-3h at 50°C incubation instead of 1 h at RT in the 1:3 solution of acetic acid: ethanol solution.

Null ROS-luminescence interrogations experiments

The effect of salt on luminescence was evaluated by preparing a range of NaCl concentrations in water and using this as the reagent diluent, where the standard concentrations of L-012 and HRP used for the ROS assay (see below Table 4) and H_2O_2 concentrations of 0.1-10 mM trialled.

Leaf disc electrolyte leakage

Leaf discs were incubated in 24 well plates using the same ratio of leaf discs: water as the 96-well plate assay i.e., one leaf disc (diameter 0.4 cm) per 150 µL diluent but scaled up to six leaf discs in 900 µL to obtain sufficient solution volumes for reliable conductivity measurements. The machine x was used to measure electrical conductance.

Leaf disc osmotic point assay

A series of NaCl concentrations were used to exert linearly increasing osmotic pressure to evaluate the pooled fresh weight mass changes of 10 representative leaf discs by 90 minutes. Leaf discs were harvested using a 0.4 cm diameter borer from three equivalent leaves of plants grown under 0 mM, 100 mM and 200 mM NaCl and floated in small petri dishes containing 5 mL of saline (0-1000 mM NaCl) solution each. After 90 mins, the 10 leaf discs were carefully removed using a home-made plastic leaf-disc scoop (two plastic green inoculation loops taped together) and blotted gently on tissue paper to remove excess surface water before weighing in weighing boats. The change in fresh weight of each type of leaf disc

was then plotted against the bathing solution salinity. Trendlines were calculated using the Excel function to assess the linearity of the relationship between FW mass change of leaf discs and increasing salinity of the bathing solution between 200 – 800 mM NaCl and the resulting equations and R^2 values are shown.

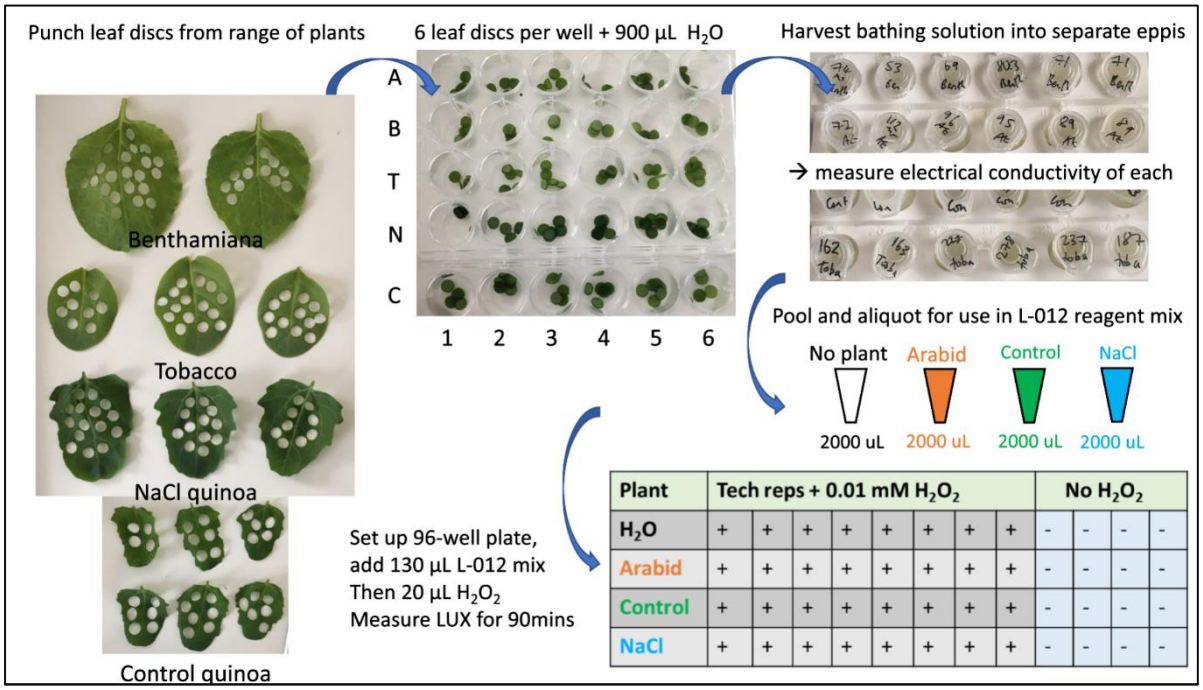
Antioxidant Assay

This antioxidant protocol is based on the 96-well plate ROS assay with several modifications as documented in Table 4. A flowchart is also provided in Supplementary Material (S.Fig.2).

Table 4: Direct comparison between the 96-well plate ROS assay and new antioxidant assay

Reagents/ details	**ROS assay**	**Antioxidant Assay**
Final reaction well volume	150 µL	75 µL
Duration	60-90 minutes	40-60 minutes
Mastermix reagents 1-3:		
1) Probe: L-012	10 µM	10 µM
2) Enzyme: HRP	20 µg/mL	2 µg/mL
3) Diluent	H_2O	Leaf disc bathing solution (neat or diluted 1:2, 1:10 or 1:100)
ROS source	Plant-endogenous: leaf disc + PTI elicitor e.g., PAMP flg22 100 nM, added into the Mastermix (i.e., probe/enzyme/diluent)	Plant exogenous: addition of 10 µL 0.1 mM (or 0.01 mM) H_2O_2, which is added last to wells already containing 65 µL Mastermix
Negative control *(no ROS source)*	Leaf disc + Mastermix using H_2O with no PTI elicitor added	Mastermix, with just H_2O added last to the wells in place of the exogenous H_2O_2 solution
Assay-specific positive control	The Arabidopsis PTI response: Use Arabidopsis leaf discs + Mastermix + the PTI elicitor flg22 100 nM	The Antioxidant ascorbic acid: Use at the concentration 800 µg/mL + Mastermix + H_2O_2 (added last to wells in the same way as the other samples)
Reagents (*no plant)* control	No plant leaf discs, just Mastermix + PTI elicitor	No leaf disc bathing solution, i.e., use H_2O as the diluent for the Mastermix, prepare two sets of wells with ± H_2O_2
Plate reader assay script	96-well white opaque plate in plate reader (e.g., Tecan) with ROS script (Buscaill et al., 2019)	96-well white opaque plate reader with the ROS script from Buscaill et al., 2019

The core steps are shown by the schematic below: punch leaf discs from different species/plant type; float leaf discs in water 'bathing solution' in wells of a 24-well plate using the same ratio of leaf disc to typical volume of ROS mastermix per reaction well i.e. 1 leaf disc per 150 µL, hence 6 leaf discs in 900 µL; harvest leaf-disc bathing solution after 2h (or at later timepoints as a time series having refreshed the bathing solution if looking at the dynamics of cell death/electrolyte leakage over time); measure electrical conductivity of bathing solutions; pool equivalent replicate samples; take aliquots for making different types of diluents (1:10 or 1:100 dilution, boiled, un-boiled - neat); use these diluents for preparing the reagent mix (Table 4) and pipette into 96-well plate with appropriate controls and run the ROS script used in the typical ROS assay (Chapter 2; Buscaill et al., 2019)



Plant	Tech reps + 0.01 mM H_2O_2								No H_2O_2			
H_2O	+	+	+	+	+	+	+	+	-	-	-	-
Arabid	+	+	+	+	+	+	+	+	-	-	-	-
Control	+	+	+	+	+	+	+	+	-	-	-	-
NaCl	+	+	+	+	+	+	+	+	-	-	-	-

Combinatorial stress RNA-seq experiment

<u>RNA-sequencing experimental design, sample preparation and sequencing (via Novogene)</u>

Experimental design is depicted by Fig.19. and sample preparation was performed identically to the protocol in Chapter 2. For this experiment the early RNA-sequencing steps were performed by Novogene's robust pipeline. This was due to several key factors: firstly, help wasn't available for carrying out the more complex multifactorial experimental design, the local R programme and past scripts were no longer working due to package vs software

incompatibilities, significant time limitations for completing the thesis and lastly the lack of know-how for mapping to the quinoa genome instead of transcriptome and working with quinoa proteins instead of Arabidopsis-mapped proteins). The two major differences to the protocol described in Chapter 2 therefore was the mapping of reads step and use of Arabidopsis was only used for the final gene-level analyses. Mapping reads: paired-end clean reads were mapped to the *C. quinoa* reference transcriptome ASM168347v1 for cultivar QQ74 (Jarvis et al.,2017) using the HISAT2 software, all samples had total mapping rate >93% with unique mapping rate >84%, mapped reads were >94% exogenic. Gene model annotation files were downloaded from the genome website browser (NCBI/UCSC/Ensembl) directly. *Quantification:* Featurecounts was used to count read numbers of each mapped gene, including known and novel genes and FPKM (Fragments Per Kilobase of exon model per Million mapped reads) were calculated to account for confounding effects of sequencing depth and gene length method when estimating gene expression levels.

RNA-seq data bioinformatic analysis

Differential expression analysis: DESeq2 R package was used which uses a model based on the negative binomial distribution. The resulting P values were adjusted using the Benjamini and Hochberg's approach for controlling the False Discovery Rate (FDR). Genes with an adjusted *P value* < 0.05 and |fold change| >2 i.e., a |L2FC| > 1 found by DESeq2 were assigned as significantly differentially expressed. *Enrichment analysis:* biological ontologies (biological processes, molecular functions, and cellular component) were assigned to genes using Gene Ontology (GO) and pathway enrichment information (e.g., metabolic or signal transduction involvement) was assigned using Kyoto Encyclopaedia of Genes and Genomes (KEGG). The clusterProfiler R package tested for significant statistical enrichment (P < 0.05) for DEG ontologies. Excel was used to visualise GO term enrichment results obtained from Novogene's GSEA data outputs in order to manually inspect and remove GO term redundancies found. *Gene level analyses:* genes in the core enrichment column from the GSEA outputs were extracted and further gene description information was called from the full DEG lists in R. DEG list comparisons between different stress treatments were done in R and data generated were visualised and explored further using R or Excel. The quinoa transcript gene loci were mapped to the TAIR Arabidopsis reference transcriptome using BLAST and further gene level descriptions were then called using UniProt's web browser ID mapping function, and the

protein with the highest percentage identity to the quinoa loci was selected and redundancy of protein isoforms removed.

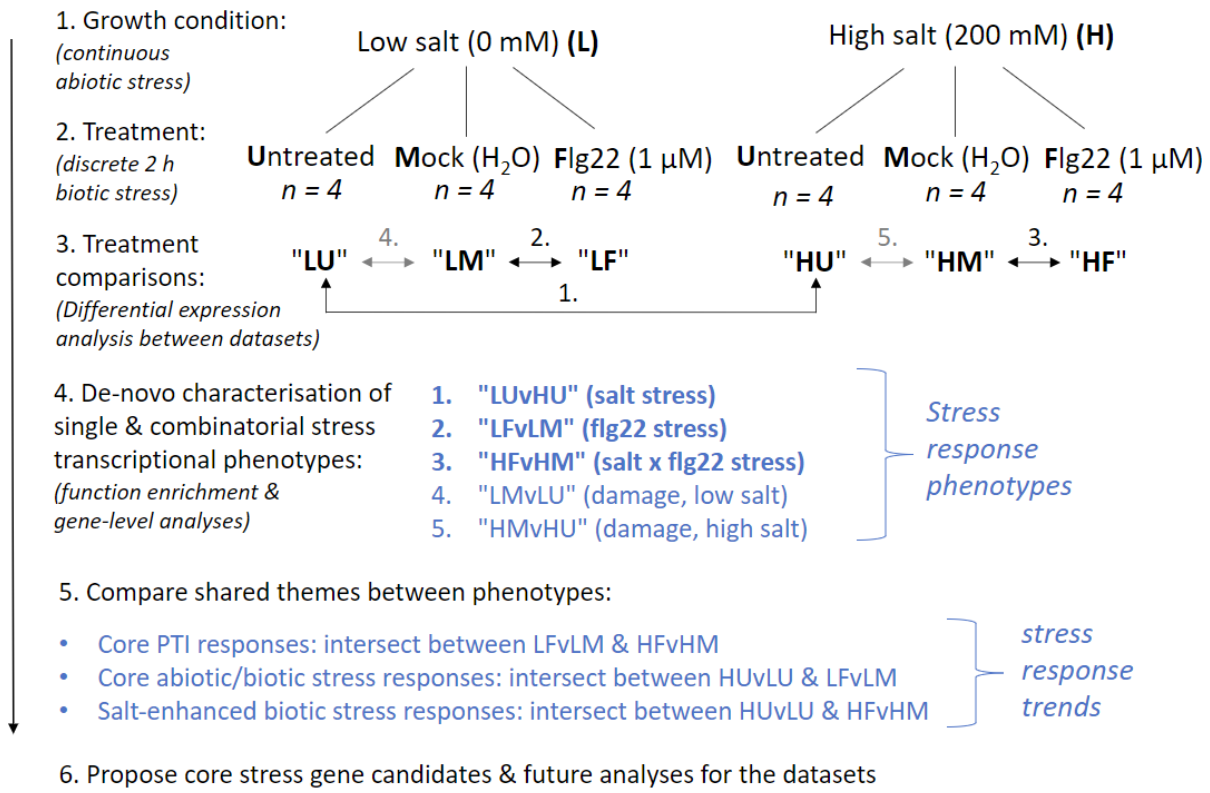


Fig.19. Full experimental design for the combinatorial RNA-seq experiment and core bioinformatics analysis strategy

Chapter 6.0: General Discussion

Before starting this project considerable knowledge of quinoa's salt tolerance mechanisms was known. This provided a springboard for making early hypotheses, for testing the salt tolerance of the European-bred commercial variety Atlas (by adapting pre-existing protocols), and for interpreting results. The first experimental chapter, Chapter 2, shed light on several mechanisms of quinoa's basal PTI using a panel of PAMPs representative of a range of biotic stresses. Quinoa's biochemical PTI responses MAPK activation, ROS burst, callose deposition and the upregulation of peroxidase (POX) activity were active but at notably reduced intensities or at time delays (in the case of the apoplastic ROS burst and POX activity) relative to the responses of Arabidopsis (studies performed in parallel). The reason for differential ROS and potentially also POX activity was later explained by the higher baseline constitutively produced and salt-induced antioxidant levels of quinoa leaves (Chapter 5). The flg22-induced 2h transcriptomic (RNA-seq) and proteomic (ptRIC) responses were also subsequently analysed and compared to parallel datasets in Arabidopsis produced by Bach-Pages et al., (2020 & unpublished) which revealed many more species-specific differences. This further highlights the need to extend our understanding of - and techniques for validly evaluating – the PTI mechanisms of non-model plant species such as the halophyte quinoa.

In Chapter 3, the salt acclimation strategies of quinoa cv. Atlas were analysed at various levels from transcriptional and biochemical to morphological and ultrastructural responses and pronounced phenotypic differences were found between control and saline conditions. Most notably these included tissue and cellular reorganisation, fortification of cell walls for enhanced turgor and enhanced water use efficiency (and retention) by accumulating and/or synthesising high levels of osmolytes. These findings indicate that despite being bred primarily for photoperiod insensitivity in European latitudes, and with less concern for its salt tolerance traits, the Atlas cultivar has retained many of the previously identified halophytic adaptions of native quinoa varieties (Stephen Jones, personal comms 2018; Ruiz et al., 2016). Breeding for certain yield-related agronomic traits in other species has often resulted in significant trade-offs with the plants' stress tolerance, where the pressure of climate change is now demanding breeders to introgress genes back in from hardier crop wild relatives (Hajjar & Hodgkin 2007; Kapazoglou et al., 2023). In contrast, for quinoa, improvement of yield traits

would constitute comparably new genetic changes which may be less likely to disrupt its valuable abiotic stress tolerance which evolved over thousands of years due to the high soil salinity in quinoa's traditional growing regions. Therefore, this may present an easier and exciting opportunity for producing high yielding, climate resilient, highly nutritious crops.

Prior to this project starting, the available information on quinoa's biotic stress tolerance was comparably limited, however most examples suggested high susceptibility to viral infection, insect infestation and crop losses due to fungal and oomycete diseases such as downy mildew (Bonifacio et al., 2001; Danielsen et al., 2003; Li et al., 2017). Chapter 4 therefore sought to establish a model pathosystem with the model bacterial pathogen *Pseudomonas syringae* for understanding host-pathogen interactions. The outcome of these interactions was found to be phylogroup and pathovar dependent, where pathovar strains belonging to pv. *aptata* and pv. *spinaciae* from related species sugar beet and spinach and the environmentally sourced isolate CC1557 grew most aggressively and caused highest disease severity in quinoa. Quinoa successfully suppressed the growth of the T3SS deficient mutant *P. syringae* pv. *tomato* DC3000 hrpA- which demonstrated the effectiveness of its PTI defences. The hydroponic growth system established in Chapter 3 was then used to test how salt acclimated plants respond to direct apoplast infection of *P. syringae*. The saline 'halophytic' phenotype of quinoa was found to be significantly more disease resistant to the model disease strain *P. syringae* pv. *aptata* than the non-saline control phenotype and salt (NaCl) was also shown to directly inhibit the pathogen at the level of growth and virulence gene expression *in vitro*.

The experimental work of the final chapter, Chapter 5, was designed to address the hypothesis that salt acclimation primes quinoa's immune-specific defences for more effective suppression of pathogenesis of *P. syringae* pv. *aptata*. The biochemical PTI assays were thus repeated in salt acclimated plants where the pronounced tissue salinity, higher osmolarity and antioxidant activity were found to negate the feasibility of leaf-disc based assays. This could have given the false interpretation that salt acclimation of quinoa decouples the oxidative inducible responses from basal PTI signalling as was seen in another abiotic stress resilient species *Noccaea caerulescens* (Fones et al., 2013). Instead, through the development of a new leaf-disc based antioxidant assay and adaptations of existing osmotic point and electrolyte leakage leaf-disc assays, we demonstrated (what we believe to be) a previously

unconsidered confounding technical factor for *in vitro* ROS assays: high levels of endogenous activities can quench and invalidate a measurable ROS signal. This is especially problematic when working with plants with high tissue osmolarities as significant osmotic stress can induce tissue damage when leaf discs are not osmotically equilibrated in the assay's reagents, resulting in further cell death and further release of endogenous antioxidants into the solution. These findings were summarised in a flowchart of technical considerations for assaying the PTI-ROS response of novel or non-model halophytic or abiotic stress resilient (or stress acclimated) plants (S.Fig.2). Lastly, a combinatorial stress RNA-seq experiment was designed using the robust saline hydroponic growth system and PTI-inducing flg22 elicitor to produce several single stress and combined stress transcriptomic datasets to provide further molecular evidence on how quinoa's salt adaptations may influence its immunity. It is hoped these datasets will provide a valuable resource for future analyses and follow up work.

6.1. Quinoa, a model system for evaluating combinatorial stress responses of plants

Through the establishment of a combinatorial stress research system in quinoa cv. Atlas, several valuable fundamental insights were obtained, which can be understood using the disease triangle framework. On the plant side, quinoa's salt adaptive mechanisms were found to strongly influence the transcriptional responses of PTI producing contrasting gene expression patterns as well as enhancing the antioxidant capacity of the leaves. The higher salt and osmolyte concentration of the leaf cell sap and apoplast fraction (with preliminary data showing striking changes in metal composition) were shown to also play an inhibitory role on pathogen proliferation and virulence. Therefore, the term 'halophytic disease triangle' was coined to conceptualise the specific interactions between the components or 'vertices' of our disease triangle framework (Fig.1). The control/baseline condition is quinoa vs *P. syringae* in the absence of salt, and the salt acclimated condition is the quinoa vs *P. syringae* disease outcome following long-term exposure of plants to 100 or 200 mM NaCl. Further details are explained in Fig.1.

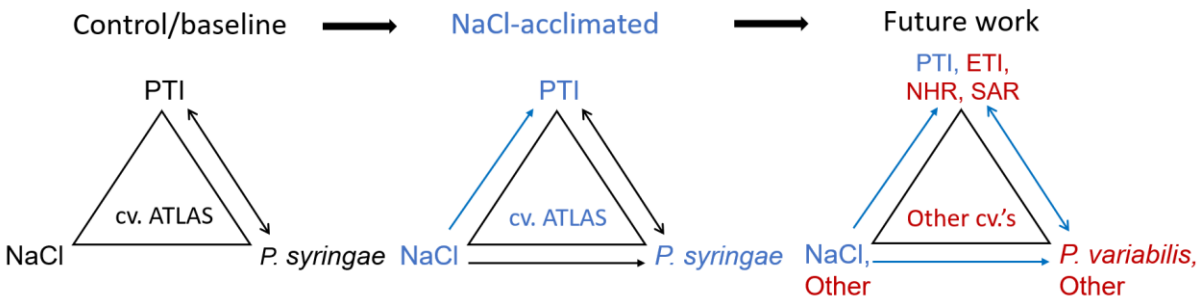


Fig.1. Researching within the Halophytic Disease Triangle of *Chenopodium quinoa* and *Pseudomonas syringae.* In the control (baseline) phenotype (left triangle), quinoa's basal immunity (in this study, just PTI) and its apoplast microenvironment were analysed and found to suppress *P. syringae* pv. *aptata's* pathogenesis to a limited extent, whereas in the saline phenotype (middle triangle), salt acclimation (whether administered hydroponically or via soil irrigation) was found to alter quinoa's PTI immunity and apoplast microenvironment composition significantly, which resulted in a more successful suppression of pv. *aptata* pathogenesis. The underlying mechanisms of these outcomes were assessed by isolating the effect of salt (left vertex) on the pathogen's viability and virulence (right vertex) in Chapter 4 and on quinoa's PTI (top vertex) in Chapter 5. Many more aspects could be researched using this framework with suggestions highlighted in red in the third triangle (furthest right). For example, other aspects of quinoa's immune system could be evaluated, or other pathogens screened, or the vast genotypic diversity within quinoa could be screened to uncover additional combinatorial stress tolerance strategies. Agirresarobe et al. (2022) used this approach to uncover genetic differences within quinoa's salt tolerance traits by using nine varieties from different latitudes.

Since the sequencing of the quinoa genome and the subsequent increase in molecular level studies, quinoa has been widely accepted as a valuable model halophyte, especially considering its potential as a nutritious food crop for stressful and varied climates (Adolf et al., 2013; Ruiz et al., 2016; Jarvis et al., 2017). Studies have already looked at the interaction between different abiotic stresses in quinoa, particularly high temperature in combination with drought and high salinity (Yang et al., 2016; Becker et al., 2017), but we believe our study is one of the first to specifically address the abiotic vs biotic stress interaction in quinoa.

The practical advantages and disadvantages of the quinoa plant and the quinoa leaf as model systems for combinatorial stress experiments will be evaluated first. The quinoa plant's fast growth rate, adaptability and remarkable range of abiotic stress tolerance has already been highlighted by various groups (Adolf et al., 2013; Ruiz et al., 2016; Mizuno et al., 2020) and is

a product of its evolution in stressful environments and typical of the Amaranthaceae plant family (Morales-Briones et al., 2021*;* Estrada et al. 2021). The plasticity of quinoa, as well as being of agronomical practical value for adapting to contrasting climates, is incredibly useful for controlled condition laboratory studies whereby a range of clear, tightly controlled phenotypic gradients can be produced in response to abiotic, biotic or combinatorial stresses (Mizuno et al., 2020; Colque-Little et al., 2021; this thesis). Our hydroponic set-up produced plants with identical foliar phenotypes to soil grown plants and similar cell sap osmolalities were obtained for soil-grown (0 mM NaCl) plants vs hydroponic 0 mM NaCl plants. Furthermore, our saline water irrigated soil trials successfully guided the attainment of reproducible results in hydroponics whereas for other species this is less straightforward: Tavakkoli et al. (2012) found that for the model salt tolerant monocot species barley, salt tolerance in saline hydroponics was not a reliable indicator of soil-based comparisons.

Our studies have shown clear gradients of salt acclimation across a range of development ages and particularly for quinoa's leaves, which became our focus for establishing a differentially saline pathosystem for performing biotic and combinatorial abiotic x biotic stress assays. Extending the hydroponically grown leaf system to additional quinoa accessions, different pathogens, or different modes of infection with the same pathogen such as spray or dip inoculation appears feasible when considering the following successes in: adapting other quinoa accessions to other hydroponics systems (Turcio et al., 2021; Schmöckel et al., 2017); adapting 20 diverse native Bolivian accessions to our hydroponic system (Scrafton & Preston unpublished); the establishment of a robust foliar pathosystem with *Peronospora variabilis* (Colque-Little et al., 2021); and lastly the success of preliminary work done establishing a hydroponics compatible dip inoculation system with cv. Atlas (data not shown) with the use of the Silwet wetting agent and routine commercially available humidity covers. Furthermore, the hydroponics set-up can also be used for trialling the impact of additional salts, metals, or differential micro or macronutrient compositions where preliminary trials depleting three key macronutrients by 100% produced viable plants with clear differential leaf phenotypes (size, shape, colour, pigment content; data not shown), work which is now being continued by collaborators Ing. Marcelo Gonzales Torrico at the Technical University of Oruro (UTO) in Bolivia.

As a pseudocereal crop, quinoa's pre-panicle initiation phenological stage (also termed 'inflorescence emergence') was chosen for its more stable vegetative biological state. This is equivalent to the use of the pre-flowering stage in other plant systems (Liu et al, 2015; Bach-Pages et al, 2020) which for Atlas grown under our conditions equated to 5-week-old plants with 8+ true leaves. This early vegetative phenological stage has been considered more stress-sensitive especially under field conditions (Bolivian collaborators, various: Bonifacio, Gonzales Torrico, Huanca Alanoca, personal comms 2018-2022) and age-related resistance (ARR) has been observed in several different plant species under controlled conditions (Kus et al., 2002; reviewed in Whalen, 2005). Therefore, the applicability of our pathosystem's findings would need to be tested in older and younger plants and specifically between young, middle and old leaves on the same plant to see the robustness of age-related immunity in quinoa (Zeier 2005; Berens et al., 2019). It is widely known that quinoa's young leaves have a much higher density and turgidity of EBCs which could be responsible for the constitutively higher total levels (two-fold) of osmolytes under control conditions and which are thought to protect the plant from UV radiation (Bonifacio personal comms; Shabala et al., 2012; Imamura et al., 2020). Shabala et al. (2012) observed a 2.3-fold increase in the leaf sap osmolality in young and intermediate leaves in response to salt treatment whereas a 3.8-fold increase was found in old leaves. The proportion of inorganic to organic osmolytes also changed, where all three leaf ages shifted to the more prominent use of cheap (inorganic; salt ions) osmotica, which was especially pronounced in older leaves. This suggests a marked differential physiological and morphological status which is likely to impact local immunity and plant disease resistance.

Under our controlled growth conditions (Methods) by 4.5 weeks the Atlas plant has 3-5 equivalent mature and fully expanded leaves which are sufficiently succulent and spacious to facilitate easy abaxial infiltration. However, the saline phenotype makes infiltration more challenging due to reduced ease of water flow within the tissue structure and also because the notably higher succulency and high salt levels result in greater (macroscopically observed) damage with excess salt being released around the infiltration zone. The size of the leaves can be altered substantially by simply providing more growing space to Atlas: leaf diameters across the top half of the leaf are plant density dependent (1.5 cm to 5 cm for 18 vs 6 plants per tub respectively) for the hydroponic system, and can be up to 7 cm in 1 L soil pots, whereas certain quinoa accessions native to Bolivia such Kellu (Salinas) and J'acha Grano (which means

'big grain' in the indigenous language Aymara, developed by Dr Alejandro Bonifacio, PROINPA, Bolivia) were found to reach leaf diameters of 10 and 12 cm in the field (Scrafton & Williams unpublished). Indeed, the field size of quinoa plants, especially according to the traditional low density spacing on the southern Altiplano can be substantial (>2 m tall). This led D. Visintainer (University of Copenhagen, unpublished/personal comms 2023) to directly evaluate the applicability of using the comparably root-restricted growth systems of (1 L or 2 L) pots in greenhouses to quinoa plants grown in the field. The 1 L pots, which he used to produce what he calls 'mini plants' are equivalent to those we used for our initial soil-grown experiments, which validates our use of them as plant maximal fitness references when establishing our hydroponics system. Several key agronomic traits including seed size and time till flowering correlated highly between mini plants and field grown plants ($R > 70$, $P < 0.01$) which provides promise for the applicability of findings from our research system.

The model plant immunity and molecular pharming species *Nicotiana benthamiana* is well suited to leaf infiltration inoculation methods (whether for pathogen studies or agroinfiltration for recombinant protein expression or virus-induced gene silencing) due to their large sized suitably planar leaves for unhindered and precise abaxial infiltrations (Jutras et al., 2019). Their large size also permits parallel studies of ETI within one leaf (Qi et al., 2018; Ouyang et al., 2023). Beyond the utility for comparative infection assays, larger leaves can be beneficial when needing to harvest a higher number of leaf discs from the same leaf, or, when needing to collect higher amounts of apoplastic fluid extracts for downstream analyses (*in vitro* pathogen growth studies or other apoplast compositional analyses). Switching to the use of the bigger leaf yielding six-plants-per-tub density under hydroponics greatly improved the ease of harvesting sufficient apoplastic washing fluid from saline leaves.

Next, the practicalities and potential for drawing fundamental stress response insights from various levels of plant organization in quinoa (morphological, physiological, biochemical, and molecular) will be evaluated. Quinoa's halophytic adaptations to salinity can influence pathogenesis at varying levels. Starting from the morphological aspects of the quinoa leaf, its local topological structure is unusual whereby epidermal hairs (trichomes) are replaced by enormous constitutively expressed osmolyte-sequestering epidermal bladder cells (EBCs) which make up c. 35% of the fresh leaf biomass (Moog et al., 2022). Quinoa's cuticle is also

appreciably hydrophobic which suggests a significant proportion of cutin polyesters and waxes, while stomatal density and aperture appear to be controlled by ABA (Jacobsen et al., 2009; Alandia et al., 2016). While this project focused on inducible 'active' PTI responses with an apoplast-centred approach due to its relevance for our pathosystem with *P. syringae*, the first mechanism of disease resistance of plants is through their pre-formed 'passive' defences. These are physical barriers such leaf surfaces and cell walls or antimicrobial compounds which could be hypothesised to become more prominent and stress protective in salt-acclimated leaves. It would therefore be interesting to next test epiphytic pathogens and cell wall penetrating microbes such as hyphae-producing oomycetes under the hypothesis that the reduced number of natural leaf openings due to salt induced ABA-regulated stomatal density (and aperture), or that salt induced thickening (lignification) of cell walls could reduce the first step of pathogenesis: colonization. Further work investigating the spatiotemporal dynamics of *P. syringae* populations colonising the quinoa leaf is under way using the bioluminescence-fluorescence construct tools developed by Soldan et al. (2021).

Moog et al. (2022) showed that an EBC-free mutant was equally as salt tolerant as WT quinoa and that Na^+ ions were accumulated to a comparably lesser degree than K^+ and Cl^- and other metabolites in the EBCs of WT plants. Given the high osmolarity of EBCs, they are instead hypothesised to act as water or metabolite sinks which can be returned to the leaf lamina when necessary (Moog et al., 2022). The EBC metabolites stored comprise sugars, organic acids, amino acids, phenolic compounds, betanin, saponins and lipids (Otterbach et al., 2021). Unexpectedly, few changes in the metabolic composition of EBCs were found in response to abiotic stresses and they were mainly related to heat, cold and high-light treatments but not to salt stress (Otterbach et al., 2021) which raises the question, under what conditions could this rich store of primary and secondary metabolites and water be used? Perhaps instead they are used for biotic stress interactions.

The physiological changes in water status (transpiration, respiration and osmotic pressure), photochemistry, redox and pH homeostasis are focal points for abiotic stress studies (Singh et al., 2018; Paes de Melo et al., 2022) and could be further explored to assess their potential implications for plant immunity and pathogen susceptibility. An increasing number of studies have shown differential disease interactions under differing first stress exposure intensities

(Janda et al., 2019; Li et al., 2018; Gao et al., 2019), yet due to the systemic effects of these stresses it is practically more difficult to isolate the direct effect on the pathogen and so relationships are more correlative rather than causative. The biochemical impact of salinity on the specific leaf microenvironment of quinoa however could be explored more precisely, for example by using metabolomics or proteomics to identify potential antimicrobial factors. Kiani-Pouya et al. (2017) have shown already striking differences in the metabolite compositions of salt-treated vs non-treated and brushed vs non-brushed leaves which could be impactful on pathogens e.g., phenolic compounds (Lelario et al., 2018; Al-Qabba et al., 2020). More recently, 'integrative multi-omics' analysis comprising metabolome, transcriptome, proteome, ubiquitome and acetylome data was used to uncover converging and diverging responses of rice to the two distinct PAMPs chitin and flg22 at multiple regulatory layers. Molecular transcriptome and proteome level responses were similar but biochemical responses of the metabolome were divergent, which they explained could be due to post-translational regulation via ubiquitination and acetylation to modulate enzymatic activities. In this project, the antioxidant defences of quinoa were queried briefly at the biochemical and molecular level through the Antioxidant Assay and RNA-seq experiments and further experiments were suggested in Chapter 5/S.Fig.2 for characterising these further. Lastly, the molecular transcriptomic and proteomic halophytic adaptations and how these interact with pathogenesis and general stress resistance can be evaluated with further bioinformatic analyses and follow-on experimental designs.

6.1.1 Limitations of this quinoa research system

Beyond the technical challenges of working with salt-acclimated high osmolarity tissue (Chapter 5), two further general limitations have been noted for using quinoa as a model system: 1) the prematurity of genetic modification technology and 2) specifically for this project, the lack of a true quinoa-specialised pathogen for use in our halophytic pathosystem.

1) The novelty of the crop along with its complex allotetraploid genome has limited the advance of molecular knowledge as functional gene studies of quinoa have not benefitted from an earlier availability of robust genetic modification systems. Rather, quinoa stress tolerance research has exploited the rich genetic diversity of the germplasm instead to

provide the ranges in function of certain stress mechanisms. However, utilising available germplasm has also been challenging due to (original) limitations of seed access and then a lack of genetic homogeneity found within the seed (Michael Way, Kew Gardens, personal comms 2018). The availability of genome sequences for an increasing number of quinoa lines (Patiranage et al., 2022) paired with the development of gene editing, gene silencing or overexpression technologies will allow causal relationships to be understood more quickly and with greater precision. The facility to study quinoa gene function *in situ* would greatly improve the understanding of quinoa's stress defences as well as other key agronomical traits. Obtaining untargeted/randomly generated loss of function mutants in quinoa was initiated using ethyl methanesulfonate (EMS)-mediated mutagenesis, where successful mutant populations have been made in several quinoa lines including in the principal reference genome QQ74 PI 614886 accession, with 5030 single gene mutant families available at the Jarvis Lab genetic resource at Brigham Young University (Jarvis personal comms 2023). Via EMS, groups have isolated mutants defective in EBC formation (two reduced number EBC mutants by Imamura et al., 2022 and the EBC-free mutant by Moog et al., 2022), betalain synthesis (green hypocotyl mutant by Imamura et al., 2018 and Cox et al., unpublished thesis 2020), the regulation of chlorophyll biosynthesis and chloroplast development (Liet al., 2022).

To improve the efficiency of screening mutant populations a new highly sensitive screening method called FIND-IT (Fast Identification of Nucleotide variants by droplet DigITal PCR) has been developed (Knudsen et al., 2022) and recently applied to quinoa to identify two mutants deficient in saponin biosynthesis without any agronomic trait trade-offs relative to WT (Trinh et al., unpublished, personal comms 2023), a genetic resource with huge promise for the quinoa food industry.

Lastly, targeted genetic modification and transformation protocols in quinoa are soon to be widely available (López-Marqués et al., 2020; various personal comms 2023). This promise has been inspired by efficient CRISPR-mediated protocols developed for hexaploid wheat (Zhang et al., 2019) and the continued optimisation of agrobacterium-mediated transformation protocols via tissue culture and the regeneration of transformed plants from callus (Komari 1990; Eisa et al., 2005; Telahigue and Toumi, 2017; Shahin, 2019).

2) The research limitation for evaluating more precise disease susceptibility and resistance mechanisms in quinoa stems from the fact *P. syringae* is a newer, lesser known and currently comparably minor pathogen of quinoa, and so none of the *P. syringae* pathovars used in this project were isolates of quinoa plants in the field. No systemic infection or sign of an ability to spread beyond the inoculation area was observed for any of the pathovars which could be addressed further by using lower inoculum densities to avoid premature necrosis/leaf collapse from excessive bacterial loads. Even the pathovars which caused the most notable disease symptoms and positive early growth *in planta* pv. *aptata* and pv. *spinaciae* could not reach magnitudes of titres seen in other systems, nor could they maintain a high level of growth beyond two-three days post initial infection.

However, given how a range of disease and resistant phenotypes were still able to be produced by distinct *P. syringae* pathovars isolated from a range of crop hosts including those from the same botanic family as quinoa, and the recent observations of quinoa - *P. syringae* infections in the field, it should not be too difficult for future projects to obtain true specialised isolates from the crop (Fonseca-Guerra et al., 2021). Additionally, it is important to note that this research system only focused on quinoa's PTI mechanisms of immunity and additional key branches of immunity such as effector triggered immunity (ETI), systemic acquired resistance (SAR) and non-host resistance (NHR) would need to be tested next. No obvious phenotypic evidence of ETI was found for the *P. syringae* strains that were unable to grow in quinoa, however the use of assays for observing microscopic signs of programmed cell death alongside testing a wider range of strains or effectors or field isolates could help.

Lastly, a key point of a model system is to yield understandings that can be applied to crops in the field. Quinoa being a crop species itself ensures the application of fundamental science derived from quinoa research systems to field scenarios is dependent on technological rather than biological compatibilities. Most quinoa research has traditionally been of the applied type, either for food science or agronomy, especially in its countries of origin Bolivia, Peru and Chile (Ahamed et al., 1998; Graf et al., 2015; Pathan et al., 2022; Alandia et al., 2020; Angeli et al., 2020). Quinoa's global agronomic performance is benefitting from increasing numbers of field-based studies (Alandia et al., 2020; Pulvento and Bazile 2023; Lozano-Isla et al., 2023; Tester personal comms, 2023) and recently large multinational field studies are underway as

part of the 2022-2025 'Quinoa4Med' PRIMA project led by Schmöckel (University of Hohenheim). The project partners are researching fundamental aspects of quinoa's germination under salt and heat stress in parallel to the applied science field trials for translational efficiency (Iglesias-Fernandez and Schmöckel personal comms, 2023). Quinoa's rich primary genetic diversity comprises ecotypes adapted to five diverse agroecological regions in the Andes: Inter-Andean Valley (Ecuador–Colombia); Yungas (Bolivia); Highlands (Peru–Bolivia–Argentina); Salares (northern Chile–southern Bolivia); and Coastal/lowland (southern Chile) (Bazile et al., 2013). This germplasm diversity plus naturally diverse field sites highly suits the well-known strategy for achieving multi stress field tolerance via candidate variety screens in multi-environment trials i.e., trials at multiple locations during several years (Malosetti et al., 2013). Indeed, as a side project to this thesis I trialled the potential for this in Bolivia through a BSPP Junior Fellowship: alongside Bolivian quinoa collaborators at UTO and MBiol (Master's) student Ellen Williams we coordinated a preliminary multi-environment field experiment using three key climatically distinct experimental sites in the northern, central and southern Altiplano and tested eight different quinoa ecotypes of highest local importance (Gonzales Torrico, personal comms 2021). The objective of my fellowship was to evaluate the foliar disease incidence and resulting yield penalties of environmental stresses between plants grown on different soil types (and which faced different climate pressures) to draw potential correlations between disease incidence, yield, environment and genotype x environment adaptations. An objective was to isolate endophytic bacterial pathogens, but only non-pathogenic strains were found (S.Fig.1).

In summary, there is fundamental science and applied value for using quinoa as a model plant for interrogating the impact of changing environmental conditions on the immune system and disease susceptibility. Studying the interaction of prolonged abiotic stress acclimation followed by biotic stress precisely is certainly possible and should be explored further. Lastly, it is important to reiterate quinoa's immense genetic diversity here to demonstrate the current potential of this crop for identifying stress tolerance genes within its primary and secondary germplasm. Quinoa is still a novel crop outside of the Andes and represents a more nascent state of domestication relative to staple crops which presents a rare opportunity for studying the evolution of its stress resilience traits (Patiranage et al., 2022). Selection for

agronomically valuable traits can now occur with a clearer understanding of trade-offs between stress tolerance and growth and how to secure high yields under a changing climate.

6.2. The halophytic salt-acclimation of quinoa interacts with basal PTI responses, challenging the robustness of canonical PTI under changing environments

Our understanding of the plant immune system and how to assay it has been derived largely from glycophytic model species, with limited insight from Amaranthaceae species or other abiotic stress tolerant plants. This has meant limited knowledge exists on how abiotic stress tolerance traits and their induced state interacts with biotic stress perception and response; what trade-offs have occurred? Are certain genes and mechanisms responsible for combinatorial stress tolerance? And if so, how robust are they and can they be harnessed? The first two questions were directly addressed in this thesis where a review of the major findings could yield suggestions for addressing the third question.

The three RNA-seq experiments performed in this project were fundamental to broadening our understanding of quinoa cv. Atlas's PTI (Chapter 2), salt acclimation responses (Chapter 3), and the interaction between these representative abiotic and biotic stress signalling pathways (Chapter 5) (Fig.2). The transcriptomics results obtained along with our biochemical (MAPK activation, ROS burst, callose deposition, POX activity, osmolality assessments) and proteomic RBP data has allowed us to start populating candidate components in the combinatorial stress framework introduced in Chapter 1 Fig.13, now updated here in Fig.2.

The components are colour-coded to highlight their prominence in certain stress conditions under our experimental conditions: purple denotes a role in all three stress-perception - signalling – response axes, thus representing putative general stress response genes which could represent the most promising candidates for combinatorial abiotic x biotic stress tolerance. Examples of these include expected features such as detoxifying cytochrome P450s and enzymatic and/or non-enzymatic antioxidants for redox homeostasis and glutathione S-transferase (GSTU) genes.

GSTUs were extensively upregulated in salt-acclimated plants totalling 22 with four additional glutathione-related genes. The majority either lacked orthologs in Arabidopsis or did not offer further functional information (TAIR), however, orthologs were found for two highly expressed loci: GLUTATHIONE S-TRANSFERASE TAU 8 (GSTU8) and GSTU25, the latter (AT1G17180), remarkably mapped as one to many (13) homologs in quinoa. The importance of this class of enzymes in quinoa's generic stress response is suggested by the following two findings: two novel GSTU T3-like genes were found as the only upregulated representatives in the salt x flg22 treated plants (and which have no orthologs in Arabidopsis) whilst six GSTU genes were also found to be strongly induced in quinoa's basal PTI (low salt flg22 treated plants). Orthologs for quinoa's GSTU genes might instead be found in more closely related and/or salt tolerant species such as *Spinacia oleracea*, *Beta vulgaris* and *Amaranthus* spp. as found by Schmöckel et al. (2017) when investigating transmembrane protein orthologs across Arabidopsis and these three species.

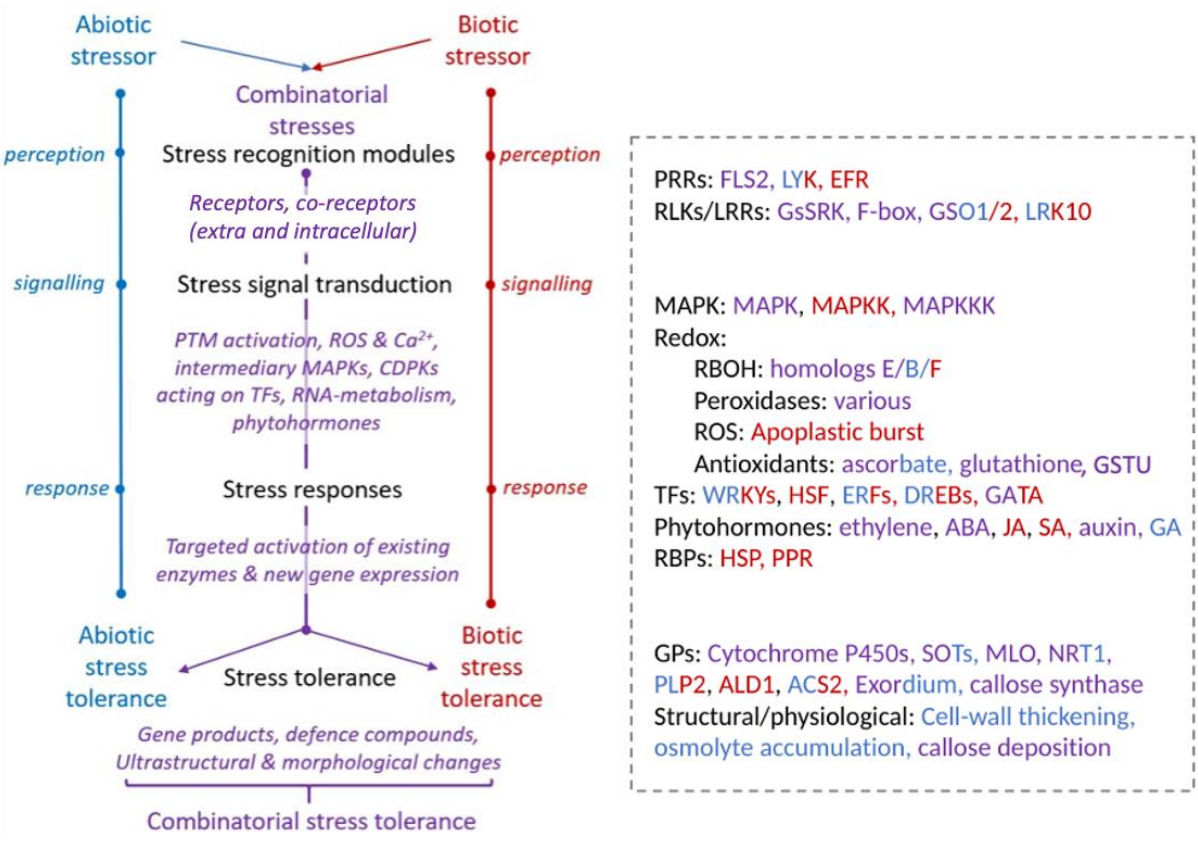


Fig.2. Candidate components involved in quinoa cv. Atlas's abiotic, biotic and combinatorial stress signalling pathways. Several notable components were hypothesised to be involved summarised within the three stress signalling axes on the left (Fig. 13 from Chapter 1) which are organised into

stress recognition modules, signal transduction and stress response components, levels at which candidate stress tolerance genes and mechanisms could be targeted for engineering improved tolerances (Vuong et al., 2022). The grey dotted box contains specific components identified through our transcriptomic analyses and/or biochemical results which could underpin the halophytic and disease outcome phenotypes in Atlas. Their individual or collective contribution to the enhanced stress tolerance observed against *P. syringae* in salt-acclimated plants would need to be targeted using GM/functional studies in future experiments. Specific high confidence gene identities are given and colour-coded according to their positive measurement/upregulation as a salt-acclimation response (blue), PTI response (red) or a combinatorial response (purple). Words coloured in just red or blue represent features found to be uniquely upregulated in response to the single biotic or abiotic stress respectively. Full words in purple signify their involvement/upregulation in all three stress conditions: abiotic (two weeks 200 mM NaCl), biotic (2h 1 µM flg22) and abiotic x biotic (NaCl x flg22) responses tested here. Where genes were upregulated in just two out of three of the stress conditions the words are coloured half by each, or in the instance of RBOH the distinct homologs engaged (denoted by their letters) are coloured accordingly. Note that for RBPs only the flg22 response was analysed. PRRs (pattern recognition receptors), FLS2 (flagellin-sensitive 2 receptor to flg22), LYK (lysin motif receptor to chitin), EFR (elongation factor-Tu receptor to elf18), CERK1 (chitin elicitor receptor kinase 1), RLK (receptor like kinase), LRR (leucine-rich repeat receptor), GsSRK (G-type lectin S-receptor-like serine/threonine-protein kinase SD2-5), F-box (F-box/LRR-repeat protein), GSO1/2 (GSO1 and GSO2), LRK10 (LEAF RUST 10 DISEASE-RESISTANCE LOCUS RECEPTOR), GATA (GATA zinc finger domain), Dehydration-Responsive Element-Binding protein (DREB), GA (gibberellic acid), SOTs (sulfotransferases), NRT1 (HIGH AFFINITY NITRATE TRANSPORTER), PLP2 (PATATIN-LIKE PROTEIN 2). No specific indication of the spatio-temporal dynamics of these components are conveyed by this figure but responses ranged from constitutive levels of expression for components of the salt-acclimated phenotype, to a snapshot transient expression at 2h following flg22 exposure. Further spatio-temporal details revealed through our biochemical assays include minute-scale apoplastic responses (ROS burst) and subcellular signalling (MAPK cascades) to hour-scale apoplastic POX gene induction/ upregulated activity, and callose deposition at the cell-wall.

In contrast, only ascorbate-related terms were found in salt acclimated plants: L-ascorbate peroxidase 3 and monodehydroascorbate reductase were uniquely found in single and combinatorial stress datasets respectively. Other components beyond the previously discussed differentially regulated RBOH and peroxidase homologs (Chapter 5) are gene products sulfotransferases (SOTs), identified in both combinatorial and single salt stress

datasets (hence the purple and blue colour code), and which have been noted for their roles in abiotic and biotic stress responses in other studies (Baek et al., 2010; Hirschmann et al., 2014; Jin et al., 2017). Of particular relevance to our research system is the Arabidopsis SOT12 gene (AT2G03760) which was found to be strongly induced by salt and osmotic stresses and exogenous hormones auxin, cytokinin, MeJA and SA (but not ET) which through sulfonating SA positively regulates SA production for enhanced resistance to *P. syringae* pv. DC3000 (Baek et al., 2010).

A final comparative analysis between the three stress response transcriptomic datasets will next be discussed with the aim of suggesting further gene candidate/ leads for future work.

Perhaps most surprising of all was the high similarities in the direction of gene expression found between quinoa's single abiotic (salt) and biotic (flg22) stress-induced transcripts within the 111 shared DEGs (between all three datasets; Chapter 5 Fig.17). For example, approximately 50% of all induced TFs in each single stress scenario were represented by ethylene-responsive transcription factors and WRKY-like TFs. The order of importance of specific differentially expressed TFs varied however, with unique features such as heat stress transcription factor B-3-like (HSFB3) for flg22 treatment and WRKY transcription factor 22-like for salt-grown plants representing the most highly expressed TFs. The gene locus for quinoa's HSFB3 gene has an ortholog in Arabidopsis for which no additional functional studies have been conducted. Heat shock proteins are known to play pivotal roles in abiotic and biotic responses however (Ul Haq et al., 2019; Khan et al., 2021), including in the quinoa - downy mildew interaction found by Rollano-Peñaloza et al. (2022) and HSP18 has been proposed as a promising candidate for enhancing plant immunity through its positive regulatory role on SA and resistance to bacterial pathogens of rice (*Xanthamonas oryzae* pv. *oryzae* and pv. *oryzicola*) (Ju et al., 2017; Kuang et al., 2017; Vuong et al., 2023). Interestingly, WRKY22 is often used as a PTI-biomarker gene in other species (Asai et al., 2002; Kloth et al., 2016; Hsu et al., 2013) and so it was surprising to not see it significantly engaged in the hydroponically grown flg22-treated low salt dataset. Homologs of several canonical abiotic stress response TFs such as Heat Shock Factor protein (HSF24-like), heat stress response and ethylene responsive DREB TFs were also upregulated in both single flg22 or salt treated conditions genes (Nover et al., 2001; Sakuma et al., 2002; Guo et al. 2016).

Given the expansion of the WRKY gene family in plants and their diverse roles in plant growth, metabolism, and abiotic and biotic stress signalling (Winkelmüller et al., 2021), Yue et al., 2019 performed a genome-wide analysis of quinoa's WRKY genes. 92 WRKY genes were identified in quinoa, where the expression level of over half of these showed significant variation under salt or drought stress. In other species, the ectopic overexpression of WRKY42 TF from diploid woodland strawberry species *Fragaria vesca* has been found to enhance both biotic and abiotic tolerance in Arabidopsis (resistance to powdery mildew, osmotic stress, and salt stress) by increasing ABA sensitivity (Wei et al., 2018). WRKY TFs have also been shown to be important fast acting combinatorial stress modulators by Hsu et al. (2013) in Arabidopsis whereby their rapid upregulation in response to submergence induced hypoxia stress correlated with the induction of innate immunity genes conferring higher resistance to *P. syringae* pv. DC3000 and WRKY22 was found to be the most highly induced gene. We therefore next examined the expression of WRKYs in our single and combined stress transcriptomic datasets and found contrasting results.

In the DEG list for low salt quinoa's 2h PTI response eight differentially expressed WRKY genes were found, all of which were upregulated, whereas no WRKY DEGs were found in the PTI response of high salt quinoa. Given how a similarly large number of WRKY genes were differentially expressed in both quinoa's untreated and mock-treated salt acclimated phenotype (HUvLU and HMvLM) i.e., in response to salt irrespective of whether an additional damage stress is applied or not, there is strong evidence flg22 treatment must negate the role of WRKY TFs in salt-acclimated plants, suggesting other TFs such as GATA zinc finger TFs are important. To explore this further, the full list of 133 unique TF loci obtained through the GSEA GO term 'DNA-binding transcription factor' of single stress transcriptome datasets (HUvLU and LFvLM) obtained in Chapter 5 was compared to the full list of upregulated DEGs for the combined stress flg22-treated salt acclimated dataset (HFvHM). Surprisingly, only four of the 133 TFs were found, all of which were ethylene-responsive TFs and just one gene description ERF017-like (present as two copies) had appreciable L2FCs (+2.1 and +2.0 L2FC), interestingly these gene loci were different to the ERF017-like genes in the other datasets.

It is important to note however, that a more comprehensive comparative analysis of TFs would need to be performed whereby more TF-related search terms are used along with a de-novo sequence-based search for DNA-binding domain containing transcripts to draw out further putatively important genes. Certain TFs may also have been missed entirely by their transient role before the 2h flg22 treatment sample harvesting time-point, for which an analysis of specific TF binding elements within the DEGs could help elucidate. Example TF binding domain candidates based on results of our single stress datasets and the literature include: heat shock promoter elements (HSE) for HSFs, the W-box [(T)TGAC(C/T)] for WRKYs, the GCC-box for ERFs (Ohme-Takagi & Shinshi, 1995) and the A/GCCGAC element for DREBs, especially associated with ABA, drought and cold responsive genes (Stockinger et al., 1997) or NAC-domain or HLH-binding motives known to be expanded in quinoa or involved in the salt adaptation of sugar beet leaves (Li et al., 2019; Skorupa et al., 2019).

Alternatively, it must be noted that perhaps salt-acclimated flg22-treated plants rely more on post-translational regulation i.e., through modifications of pre-existing proteins (PTMs) or through other proteome-level responses such as the action of RBPs (Bach-pages et al., 2020). Further proteomics followed by PTM site enrichment analyses of flg22-treated salt-acclimated plants could be done similarly to Bach-Pages et al. (2020) approach in Arabidopsis.

A final interesting observation was the opposing patterns of photosynthesis-related transcriptome reprograming found between quinoa's PTI and salt acclimation responses and the absence of global functional representation in quinoa's salt x PTI response. Photosynthesis efficiency is a standard read out for plant fitness, especially for plants under abiotic stresses, yet has been shown in many plant species, including quinoa grown in low salt conditions (this thesis), to be suppressed during PTI (Bjornson et al., 2021; Su et al., 2018; Amrine et al., 2015). The antagonistic 'growth—immunity trade-off' is explained by a diversion of photosynthesis-derived energy and metabolites to defence-related pathways and away from growth (Kuźniak and Kopczewski 2020). With our single stress and combinatorial stress transcriptome datasets we found that photosynthesis related terms dominated the enriched upregulated Biological Process (BP) and Cellular Component (CC) GO terms and KEGG terms in the high salt vs low salt single stress comparison (Chapter 3), whereas for quinoa's PTI response in low salt soil-grown (Chapter 2) and hydroponically- grown (Chapter

5) several photosynthesis related terms were downregulated. Moving onto the high salt flg22 vs high salt mock comparison, no photosynthetic GO terms featured in either significantly enriched upregulated or suppressed datasets. The chloroplast CC term was upregulated in low salt quinoa's PTI response but suppressed in high salt quinoa's PTI, however the genes annotated with this term (contributing to the term's significant enrichment) were all homologous genes for allene oxide cyclase, an enzyme which catalyses an essential step in jasmonic acid biosynthesis. Four gene homologs exist in Arabidopsis whereas six orthologs were found in quinoa, four of which were found to be induced in low salt PTI and three of these four genes were inhibited in high salt quinoa's PTI. This corroborates with the pattern of shared but opposingly regulated DEGs found between low and high salt quinoa.

Lastly, it is important to highlight the limitations of our transcriptome experiments, which were all prepared using total RNA extracted from quinoa leaves which underwent a polyA selection. The transcripts thus represent only mRNA (gene product) responses and gene functional information was retrieved by calling annotations from the pre-existing nuclear reference genome and transcriptome of quinoa (Jarvis et al., 2017), with further functional depth retrieved using Arabidopsis protein orthologs (OrthoFinder; Emms and Kelly 2019; TAIR; UniProt; Supplementary Table 8). This means other RNA types and organellar stress responses e.g., chloroplastic specific stress responses cannot be easily explored within our dataset. However, our raw reads could be mapped to the available quinoa chloroplast genomes (Hong et al., 2017; Maughan et al., 2019) and processed using the ChloroSeq bioinformatic pipeline developed by Castandet et al. (2016) which facilitates parallel analyses of the chloroplast and nuclear expression levels along with splicing and RNA editing efficiencies to understand nucleus-organelle crosstalk. If interesting results are found, then a future experiment could be guided by the elegant design and sample preparation methodology of Woo et al. (2016) who performed a multidimensional transcriptome analysis across age, RNA-type, and organelle type in Arabidopsis.

6.3. Could the salt acclimation of quinoa be used as a disease mitigation strategy?

Continuous long-term exposure of plants to abiotic stresses is commonly imposed by the plant's immediate soil conditions. Whether as excessive salts or metal contamination or

through a nutrient deficiency such as the lack of nitrogen and phosphate in the soils of the Southern Altiplano of Bolivia (Barrientos and Gonzales Torrico personal comms, 2021; Cárdenas-Castillo et al., 2021), marginal soil conditions will induce relevant abiotic stress adaptations. For example, during my BSPP Fellowship project striking phenotypic differences were observed in the native Bolivian ecotype 'Kellu' grown in different field conditions: when grown on the impoverished 90% sandy soils on the edge of the Salar de Uyuni the plants produced much thicker and tougher leaves than when grown in the comparably richer soils of the central Altiplano, presumably as a drought, salt and/or mineral tolerance adaptation. Under controlled experimental conditions using the European-bred cultivar Atlas we found that prolonged salt treatment produces quinoa plants with leaves that are structurally different, thicker and more succulent, and which have a much higher osmolarity, antioxidant activity and higher disease resistance. Furthermore, and in corroboration with other quinoa cultivars, salt-acclimation of a final concentration of 100-200 mM NaCl produced plants with no significant leaf growth penalties but which had shorter, potentially more robust (lignified) stems and which became more water use efficient and thus more drought-resilient. Most remarkable was the finding that saline quinoa leaves were also significantly more disease resistant to *P. syringae*. All these properties are of high agronomic and commercial value beyond the already invaluable trait of high adaptive capacity to saline soils and thus represent the wider potential applied value for exploiting quinoa's halophytic adaptations. The potential application of these salt-acclimation phenotypic observations is summarised below in Fig.3.

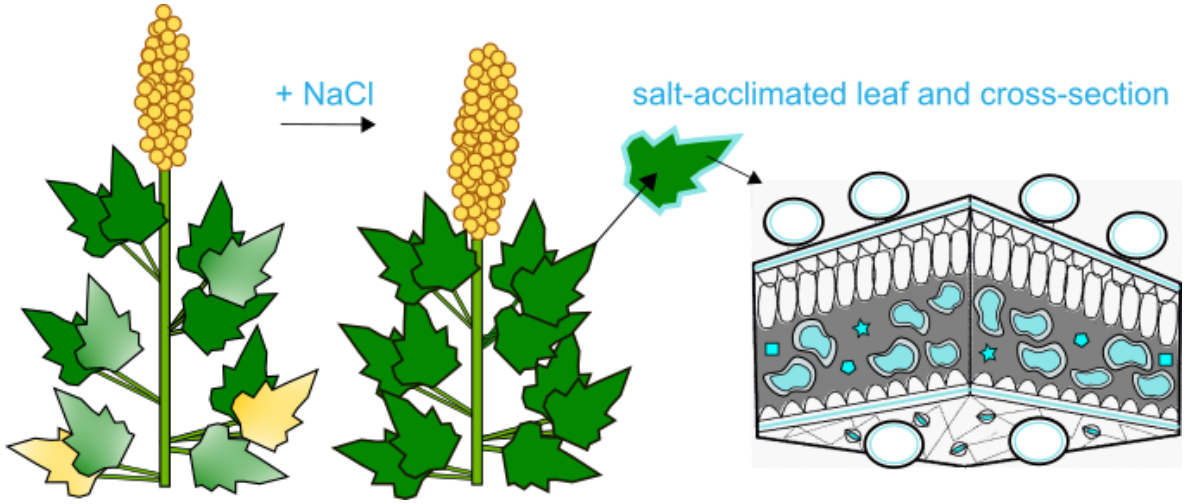


Fig.3. Schematic representation of the salt-acclimation strategy for improving several key agronomic properties of quinoa observed in this project. The plant on the left is suffering a yield penalty due to

a pathogen infection, which while not lethal, is limiting the capacity of the plant, similar to what was observed at The British Quinoa Company fields in 2019 (Chapter 1; Fig.8). The plant on the right has been agronomically improved through salt-acclimation, where effects at multiple scales of the plant are further highlighted with the help of a simplified drawing of a leaf cross-section. At the whole plant level, a reduction in stem height, enhanced disease resistance (shown by all leaves coloured healthy green) and higher energy investment into seed yield is shown. At the leaf organ level and beyond at the morphological, ultrastructural and biochemical level the salt-acclimated phenotypes are denoted by the light blue border or colour fill: an increased leaf thickness; putative changes to external features such as the waxy cuticle; EBCs with enhanced structural turgidity and differential vacuolar content storing salt-induced osmolytes; and stomata, which although not studied in our system are highlighted to show salt-induced morphological changes such as a reduced stomatal density, or physiologically regulated changes such as aperture closure (Shabala et al., 2012). Within the leaf lamina salt sequestration into the vacuoles of cells of the spongy mesophyll layer are shown (uniquely so for simplicity) which populate the grey-coloured apoplast containing stars, squares and pentagons to represent salt-induced antioxidant compounds, secreted antimicrobial compounds and other activated stress response components (which apoplast-colonising bacteria may encounter). These factors could all play some role in contributing to the salt-induced enhanced foliar resistance to *P. syringae* and may be valuable for improving the resistance to other pathogens. For example, salt-induced thicker cells walls and differential leaf topologies could create more robust physical barriers to the appressorium penetration of fungi and oomycetes (filamentous pathogens) (Li et al., 2020).

Beyond the potential for salt acclimation to confer improved foliar disease protection broader resistance to several abiotic stresses (salt, drought, UV, high wind) could be achieved and be partly responsible for quinoa's impressive tolerance to these stresses on the Bolivian altiplano. When considering the secondary potentially advantageous salt-acclimation effect of a reduced vertical stem height alongside a more efficient stress responsive state and potentially improved photosynthetic capacity (through higher chloroplast density of thickened leaves; Tester and Munns, 2008; Terletskaya et al., 2022), one can imagine how the plant could 'unlock' additional energy for diverting towards seed panicle development for higher yields (Fig.3). This concept is akin to the shorter 'dwarfed' wheat plants of the green revolution (Norman Borlaug 1963; Van de Velde et al., 2021), and along with sturdier crops stems has already been identified as a priority trait for quinoa breeding programmes (RADICLE; Tester, World Quinoa Congress, personal comms 2023).

The major practical limitation of this hypothetical strategy is the mode of inducing salt acclimation; how could we control the salt treatment of quinoa in a field setting to induce the desired salt acclimated phenotypic traits without further adding to the salinization of soils? How dependent is the expression of these traits on accumulating salt ions through saline water absorbed through the soil? Could foliar applications, akin to Omex Saltex which has previously been used as an herbicide in UK quinoa fields to reduce the pressure of comparably salt-sensitive weeds (Stephen Jones, BQC, personal comms), be developed? What is the minimum amount of salt needed to be sensed and accumulated by the plants to induce desirable salt-acclimated phenotypes, and which quinoa genotypes are most efficient at this? Or could superior salt sensing, uptake and transport genes of quinoa be exploited for a phytoremediatory salt 'hyperaccumulating' trait to improve the quality of salinized soil, whilst at the same time conferring a disease resilient crop for food production? The salt acclimation strategy and associated principles could also be more safely used in controlled environment agriculture settings to prevent the leaching of excess sodium and chloride ions whilst producing food with reduced costs for pathogen management. Future work could also explore whether key salt stress-signalling phytohormones identified in quinoa such as ABA and ET could be used to exogenously induce salt-acclimation defences independent of salt being present.

As speculated in Chapter 1, quinoa and other naturally stress resilient nutritious crops could be the best placed candidates for achieving food security. This is because of their evolved comparably efficient stress tolerance mechanisms (owing to different genes or gene isoforms, or expansion of gene copy numbers for example) which may require less energy investment from the plant's side, freeing up energy for higher yields, and eventually, a reduced time and money investment for farmers on stress-mitigation strategies. Indeed, at the start of this project we hypothesised that the naturally stress resilient crop quinoa may have evolved molecular and morphological trade-offs and beneficial synergies within its stress defences which could be targeted and harnessed through priming phenomena.

Lastly, following results from this project, what would happen if we doubly primed through salt acclimation and flg22-PTI induction preceding pathogen infection? Priming, the pre-

exposure of plant to stress elicitors, induces 'stress memory' to enable a quicker or more effective activation of defence systems upon exposure to a subsequent stress (Aranega-Bou et al., 2014; Xiao et al., 2017) and PAMP-priming has been widely documented for enhancing disease resistance to pathogens (Sarowar et al., 2019; Zipfel et al., 2010; Wang et al., 2023). The use of disease enhancing endophytes (bioinoculants) in quinoa work on the same principal and examples were given in Chapter 4. A final point to consider however is the potential of exploiting quinoa's endophytes to support the abiotic stress tolerance of other crops: rhizobacterial strains isolated from the roots of plants grown on the Peruvian or Bolivian altiplano could be used as novel biofertilizers to support the salt or cold temperature-acclimation (Torrico Gonzales personal comms; Chumpitaz-Segovia et al., 2020).

6.3.1. Could salt acclimation crosstalk principles be extended to other crops?

Comparative transcriptome studies in plants have revealed that variation in gene expression between or within species was greatest for stress-responsive genes (Winkelmüller et al., 2021). From our comparisons of quinoa's basal PTI responses to Arabidopsis in Chapter 2 little overlap was found, and when the shared core stress dataset from Chapter 5 was checked against the ~1000 core upregulated PTI DEGs from Arabidopsis found by Bjornson et al. (2021) <2% genes overlapped, and all of which were in the opposingly regulated shared genes found between low and high salt PTI. Similarly, just one gene (AT5G62360; pectin methylesterase inhibitor superfamily protein) overlapped with the ~100 core downregulated genes from Bjornson et al. (2021) where full details can be found in Supplementary Table 7. Whether the findings from our studies may resonate more closely with abiotic, biotic and combinatorial stress tolerance trends found in other species remains to be evaluated. Obvious starting points would be related members of the Amaranthaceae family.

By comparing our results with transcriptome data available for the commercially important species *Beta vulgaris* (sugar beet), which evolved from its halophytic wild ancestor, *Beta maritima* (sea beet) and which has maintained appreciable, but not halophilic levels of salt-tolerance, termed a 'salt-tolerant glycophyte' (Skorupa et al., 2019), the potential applicability of findings could be speculated. An example of shared responses include: the upregulation of nitrate transporters (NRTs) in sugar beet's salt stress acclimation response; an enhanced

capacity to change the expression levels of ion channels and aquaporins depending on salt stress intensity (salt shock or salt stress) for inorganic osmolyte accumulation; and the synthesis of organic osmolytes such as proline for osmotic adjustment. The researchers also noted how sugar beet leaves became more succulent which was suggested to counteract the potential loss in photosynthetic capacity from smaller leaves, and Tester and Munns 2008 suggested that net photosynthesis was maintained through increased leaf thickness, cell density and therefore enhanced chloroplast density. Members of the EXORDIUM protein family, which have cell wall expansion regulatory functions were downregulated in response to salt stress or non-responsive to salt shock in sugar beet (Skorupa et al., 2019) whereas in our single salt stress and combined salt x flg22 datasets three loci in each were upregulated. Potassium levels were also decreased in the salt-treated leaves of both sugar beet and sea beet which is not true for quinoa (Adolf et al., 2013; Turcios et al., 2021) and thus also provides an area which could be explored for improving the salt tolerance of sugar beet. Furthermore, the recent finding that neither Na^+ nor K^+ uptake were altered in the epidermal bladder cell free quinoa mutant adds further promise to the translatability of salt tolerance mechanisms considering how neither beets have EBCs (Moog et al., 2022).

6.4. Conclusion

This project has established a framework for administering controlled combinatorial salt and immune stress in quinoa using the European-bred commercial variety Atlas. Similarly to results in other plant systems, it was found that quinoa's combinatorial stress response was complex and unique relative to its responses to individually applied stresses, shown by oppositely regulated and uniquely activated genes. Therefore, combinatorial stress responses of cv. Atlas could not have been extrapolated from previously known abiotic stress mechanisms of quinoa. With an increasing molecular understanding of quinoa's stress responses, clearer and more robust methods for phenotyping highly valuable multi-stress tolerance traits could be developed. Quinoa's rich germplasm could then be exploited and paired with the increasing feasibility for obtaining functional gene level information (through genetic modification technology) to support the breeding of multi-stress tolerant quinoa varieties suitable for a range of environments (Chapter 1 Fig.1 & Fig.4).

Typical genetic modification strategies for improved disease tolerance traits have relied on transgenes which boost ETI e.g., by stacking resistance genes (Zhang et al., 2017). It is critical however to consider the robustness of transgenic immune mechanisms under new climate pressures, where the core stress response genes of naturally stress resilient crops like quinoa could represent promising resistance gene candidates.

Future work should next evaluate whether our findings can be applied to other quinoa cultivars or related species and how robust Atlas's halophytic immunity is when challenged with other pathogens such as *Peronospora variabilis* (downy mildew; DM), or when under additional stresses relevant to specific field sites. It could be that other underutilised nutritious and stress resilient crops such as less domesticated wild relatives of quinoa, *Chenopodium pallidicaule and C. petiolare or C. hircinum,* may also show abiotic stress inducible immunity. These crops could further support the diversification and safeguarding of our food system under climate change. It would be interesting to develop findings from this project alongside other notable quinoa pathology findings which were published towards the end of this project, such as the work done on major pathogen DM by Colque-little et al. (2021). For example, exploring whether salinity enhanced disease resistance holds true for DM, especially when considering the potential protective impact of salt-induced fortification of cell walls to limit the penetration of pathogen appressoria or insects, and whether any change in mechanosensory properties of EBCs could lead to more sensitive perception (Matsumura et al., 2022). The extent (if any) to which the observed genetic trends of quinoa's resistance to the oomycete *P. variabilis* are similar to resistance against bacterial pathogens like *P. syringae* could shed light on the existence of core downstream immune mechanisms. Features to look at include stomatal aperture (which was shown to weakly correlate with DM resistance by Colque-Little et al., 2021), the plant and leaf age-dependency of infections, and lastly, as initiated in this project, how disease resistance correlates with the salt, antimicrobial and antioxidant contents of (basal or salt-acclimated) infected leaf tissue.

Finally, coming back to the third non-experimental aim of this project, to engage with applied aspects of quinoa research and especially in one of quinoa's countries of origin Bolivia, a developing country, an opportunity for collaborative follow-on work was successfully created. We secured a material transfer agreement with Bolivia's National germplasm bank INIAF and obtained a core panel of diversity of 30 native quinoa accessions, along with four accessions

of the ancestral species *Chenopodium pallidicaule.* These accessions were carefully selected by local experts for their varying (field-based) biotic and abiotic stress tolerances, and it is hoped therefore that we can extend our halophytic pathosystem to screen locally important accessions to Bolivia as well as new varieties being developed in Europe. This is an example of how both collaborating countries can benefit through an exchange of resources: a genetically rich quinoa panel could provide high levels of variation in core stress traits to further our understanding of quinoa's single and combinatorial stress responses, which in turn could stimulate grant funding to support important applied science goals such as the conservation of local germplasm and the development of improved quinoa varieties for food security.

References

Acosta-Motos, J. R., Ortuño, M. F., Bernal-Vicente, A., Diaz-Vivancos, P., Sanchez-Blanco, M. J., & Hernandez, J. A. (2017). Plant responses to salt stress: Adaptive mechanisms. Agronomy, 7(1), 1–38. https://doi.org/10.3390/agronomy7010018

Adolf, V. I., Jacobsen, S. E., & Shabala, S. (2013). Salt tolerance mechanisms in quinoa (*Chenopodium quinoa* Willd.). Environmental and Experimental Botany, 92, 43–54. https://doi.org/10.1016/j.envexpbot.2012.07.004

Agirresarobe, A., Miranda-Apodaca, J., Odriozola, I., Muñoz-Rueda, A., & Pérez-López, U. (2022). Photosynthesis is not the unique useful trait for discriminating salt tolerance capacity between sensitive and tolerant quinoa varieties. Planta, 256(2), 1–17. https://doi.org/10.1007/s00425-022-03928-w

Agudelo, A., Carvajal, M., & Martinez-Ballesta, M. D. C. (2021). Halophytes of the Mediterranean basin—underutilized species with the potential to be nutritious crops in the scenario of the climate change. Foods, 10(1). https://doi.org/10.3390/foods10010119

Alandia, G., Jacobsen, S. E., Kyvsgaard, N. C., Condori, B., & Liu, F. (2016). Nitrogen Sustains Seed Yield of Quinoa Under Intermediate Drought. Journal of Agronomy and Crop Science, 202(4), 281–291. https://doi.org/10.1111/jac.12155

Alandia, G., Rodriguez, J. P., Jacobsen, S. E., Bazile, D., & Condori, B. (2020). Global expansion of quinoa and challenges for the Andean region. Global Food Security, 26(March), 100429. https://doi.org/10.1016/j.gfs.2020.100429

Al-Qabba, M. M., El-Mowafy, M. A., Althwab, S. A., Alfheeaid, H. A., Aljutaily, T., & Barakat, H. (2020). Phenolic profile, antioxidant activity, and ameliorating efficacy of *Chenopodium quinoa* sprouts against ccl4-induced oxidative stress in rats. Nutrients, 12(10), 1–15. https://doi.org/10.3390/nu12102904

Amrine, K. C. H., Blanco-Ulate, B., & Cantu, D. (2015). Discovery of core biotic stress responsive genes in Arabidopsis by weighted gene co-expression network analysis. PLoS ONE, 10(3). https://doi.org/10.1371/journal.pone.0118731

Anderson, J. P., Badruzsaufari, E., Schenk, P. M., Manners, J. M., Desmond, O. J., Ehlert, C., Maclean, D. J., Ebert, P. R., & Kazan, K. (2004). Antagonistic interaction between abscisic acid and jasmonate-ethylene signaling pathways modulates defence gene expression and disease resistance in Arabidopsis. Plant Cell, 16(12), 3460–3479. https://doi.org/10.1105/tpc.104.025833

Arnold, D. L., & Preston, G. M. (2019). *Pseudomonas syringae*: Enterprising epiphyte and stealthy parasite. Microbiology (United Kingdom), 165(3), 251–253. https://doi.org/10.1099/mic.0.000715

Asai, S., Ohta, K., & Yoshioka, H. (2008). MAPK signaling regulates nitric oxide and nadph oxidase-dependent oxidative bursts in *Nicotiana benthamiana*. The Plant Cell Online, 20(5), 1390–1406. https://doi.org/10.1105/tpc.107.055855

Aswath, C. R., Kim, S. H., Mo, S. Y., & Kim, D. H. (2005). Transgenic plants of creeping bent grass harboring the stress inducible gene, 9-cis-epoxycarotenoid dioxygenase, are

highly tolerant to drought and NaCl stress. Plant Growth Regulation, 47(2–3), 129–139. https://doi.org/10.1007/s10725-005-3380-6

Anwar, K., Joshi, R., Dhankher, O. P., Singla-Pareek, S. L., & Pareek, A. (2021). Elucidating the response of crop plants towards individual, combined and sequentially occurring abiotic stresses. International Journal of Molecular Sciences, 22(11), 1-26. https://doi.org/10.3390/ijms22116119

Aranega-Bou, P., de la O Leyva, M., Finiti, I., Garcfa-Agustfn, P., & Gonzalez-Bosch, C. (2014). Priming of plant resistance by natural compounds. Hexanoic acid as a model. Frontiers in Plant Science, 5(October), 1–12. https://doi.org/10.3389/fpls.2014.00488

Asai, T., Tena, G., Plotnikova, J., Willmann, M. R., Chiu, W. L., Gomez-Gomez, L., Boller, T., Ausubel, F. M., & Sheen, J. (2002). MAP kinase signalling cascade in Arabidopsis innate immunity. Nature, 415(6875), 977–983. https://doi.org/10.1038/415977a

Audenaert, K., de Meyer, G. B., & Höfte, M. M. (2002). Abscisic acid determines basal susceptibility of tomato to *Botrytis cinerea* and suppresses salicylic acid-dependent signaling mechanisms. Plant Physiology, 128(2), 491–501. https://doi.org/10.1104/pp.010605

Bach-Pages, M., Chen, H., Sanguankiattichai, N., Soldan, R., Kaschani, F., Kaiser, M., Mohammed, S., Van Der Hoorn, R. A. L., Castello, A., & Preston, G. M. (2020). Preprint: Proteome-wide profiling of RNA-binding protein responses to flg22 reveals novel components of plant immunity. BioRxiv, 2020.09.16.299701. https://www.biorxiv.org/content/10.1101/2020.09.16.299701v1%0Ahttps://www.biorxiv.org/content/10.1101/2020.09.16.299701v1.abstract

Bach-Pages, M., Homma, F., Kourelis, J., Kaschani, F., Mohammed, S., Kaiser, M., van der Hoorn, R. A. L., Castello, A., & Preston, G. M. (2020). Discovering the RNA-binding proteome of plant leaves with an improved RNA interactome capture method. Biomolecules, 10(4), 1–21. https://doi.org/10.3390/biom10040661

Bach-Pages, M., & Preston, G. M. (2018). Methods to quantify biotic-induced stress in plants. In Methods in Molecular Biology, 1734, 241–255. Humana Press Inc. https://doi.org/10.1007/978-1-4939-7604-1_19

Badran, A., Eid, N. A., Hassan, A. R., & Mahmoudi, H. (2023). Differential responses in some quinoa genotypes of a consortium of beneficial endophytic bacteria against bacterial leaf spot disease. Frontiers in Microbiology, 14. https://doi.org/10.3389/fmicb.2023.1167250

Baek, D., Pathange, P., Chung, J. S., Jiang, J., Gao, L., Oikawa, A., Hirai, M. Y., Saito, K., Pare, P., & Shi, H. (2010). A stress-inducible sulphotransferase sulphonates salicylic acid and confers pathogen resistance in Arabidopsis. Plant, Cell and Environment, 33(8), 1383–1392. https://doi.org/10.1111/j.1365-3040.2010.02156.x

Bai, Y., Kissoudis, C., Yan, Z., Visser, R. G. F., & van der Linden, G. (2018). Plant behaviour under combined stress: tomato responses to combined salinity and pathogen stress. Plant Journal, 93(4), 781–793. https://doi.org/10.1111/tpj.13800

Baltrus, D. A., McCann, H. C., & Guttman, D. S. (2017). Evolution, genomics and epidemiology of *Pseudomonas syringae*: Challenges in Bacterial Molecular Plant Pathology. Molecular Plant Pathology, 18(1), 152–168. https://doi.org/10.1111/mpp.12506

Bamunusinghe, D., Chaturvedi, S., Seo, J.-K., & Rao, A. L. N. (2013). Mutations in the capsid protein of brome mosaic virus affecting encapsidation eliminate vesicle induction in planta: implications for virus cell-to-cell spread. Journal of Virology, 87(16), 8982–8992. https://doi.org/10.1128/jvi.01253-13

Barrientos-Pérez, E., Carevic-Vergara, F. S., Rodriguez, J. P., Arenas-Charlín, J., & Delatorre-Herrera, J. (2023). effect of native vegetative barriers to prevent wind erosion: a sustainable alternative for quinoa (*Chenopodium quinoa* Willd.) production. Agriculture, 13(7), 1432. https://doi.org/10.3390/agriculture13071432

Bass, J. J., Wilkinson, D. J., Rankin, D., Phillips, B. E., Szewczyk, N. J., Smith, K., & Atherton, P. J. (2017). An overview of technical considerations for Western blotting applications to physiological research. Scandinavian Journal of Medicine and Science in Sports, 27(1), 4–25. Blackwell Munksgaard. https://doi.org/10.1111/sms.12702

Bazihizina, N., Vita, F., Balestrini, R., Kiferle, C., Caparrotta, S., Ghignone, S., Atzori, G., Mancuso, S., & Shabala, S. (2022). Early signalling processes in roots play a crucial role in the differential salt tolerance in contrasting *Chenopodium quinoa* accessions. Journal of Experimental Botany, 73(1), 292–306. https://doi.org/10.1093/jxb/erab388

Bazile, D., Fuentes, F., & Mujica, Á. (2013). Historical perspectives and domestication. Quinoa: Botany, Production and Uses, September, 16–35. https://doi.org/10.1079/9781780642260.0016

Bazile, D., Pulvento, C., Verniau, A., Al-Nusairi, M. S., Ba, D., Breidy, J., Hassan, L., Mohammed, M. I., Mambetov, O., Otambekova, M., Sepahvand, N. A., Shams, A., Souici, D., Miri, K., & Padulosi, S. (2016). Worldwide evaluations of quinoa: Preliminary results from post international year of quinoa FAO projects in nine countries. Frontiers in Plant Science, 7(850), 1-18. https://doi.org/10.3389/fpls.2016.00850

Bazin, J., Mariappan, K., Jiang, Y., Blein, T., Voelz, R., Crespi, M., & Hirt, H. (2020). Role of MPK4 in pathogen-associated molecular pattern-triggered alternative splicing in Arabidopsis. PLoS Pathogens, 16(4), 1-21. https://doi.org/10.1371/journal.ppat.1008401

Becker Verena I., Goessling Johannes W., Duarte Bernardo, Caçador Isabel, Liu Fulai, Rosenqvist Eva, Jacobsen Sven-Erik (2017). Combined effects of soil salinity and high temperature on photosynthesis and growth of quinoa plants (*Chenopodium quinoa*). Functional Plant Biology 44, 665-678. https://doi.org/10.1071/FP16370

Bigeard, J., Colcombet, J., & Hirt, H. (2015). Signaling mechanisms in pattern-triggered immunity (PTI). In Molecular Plant, 8(4), 521–539. Cell Press. https://doi.org/10.1016/j.molp.2014.12.022

Bjornson, M., Pimprikar, P., Nürnberger, T., & Zipfel, C. (2021). The transcriptional landscape of *Arabidopsis thaliana* pattern- triggered immunity. Nature Plants, 7(5), 579–586. https://doi.org/10.1038/s41477-021-00874-5.

Blighe, K, S Rana, and M Lewis. 2018. "EnhancedVolcano: Publication-ready volcano plots with enhanced colouring and labeling." https://bioconductor.org/packages/devel/bioc/vignettes/EnhancedVolcano/inst/doc/EnhancedVolcano.html

Boller, T., & Felix, G. (2009). A renaissance of elicitors: Perception of microbe-associated molecular patterns and danger signals by pattern-recognition receptors. Annual Review of Plant Biology, 60, 379–407. https://doi.org/10.1146/annurev.arplant.57.032905.105346

Bonifacio, A., Alcon, M., Vargas, A., & Apaza, R. (2001). Evaluación de la resistencia de quinua frente a la enfermedad del mildiu (Issue Bonifacio, pp. 26–28).

Bredow, M., Sementchoukova, I., Siegel, K., & Monaghan, J. (2019). Pattern-triggered oxidative burst and seedling growth inhibition assays in *Arabidopsis thaliana*. Journal of Visualized Experiments, 2019(147). https://doi.org/10.3791/59437

Brutus, A., Sicilia, F., Macone, A., Cervone, F., & de Lorenzo, G. (2010). A domain swap approach reveals a role of the plant wall-associated kinase 1 (WAK1) as a receptor of oligogalacturonides. Proceedings of the National Academy of Sciences of the United States of America, 107(20), 9452–9457. https://doi.org/10.1073/pnas.1000675107

Buchfink, B., Xie, C., & Huson, D. H. (2014). Fast and sensitive protein alignment using DIAMOND. In Nature Methods, 12(1), 59–60. Nature Publishing Group. https://doi.org/10.1038/nmeth.3176

Buscaill, P., Chandrasekar, B., Sanguankiattichai, N., Kourelis, J., Kaschani, F., Thomas, E. L., Morimoto, K., Kaiser, M., Preston, G. M., Ichinose, Y., & van der Hoorn, R. A. L. (2019). Glycosidase and glycan polymorphism control hydrolytic release of immunogenic flagellin peptides. Science, 364(6436). https://doi.org/10.1126/science.aav0748

Cackett, L., Cannistraci, C. V., Meier, S., Ferrandi, P., Pěnčík, A., Gehring, C., Novák, O., Ingle, R. A., & Donaldson, L. (2022). salt-specific gene expression reveals elevated auxin levels in *Arabidopsis thaliana* plants grown under saline conditions. Frontiers in Plant Science, 13(February), 1-20. https://doi.org/10.3389/fpls.2022.804716

Cai, Z. Q., & Gao, Q. (2020). Comparative physiological and biochemical mechanisms of salt tolerance in five contrasting highland quinoa cultivars. BMC Plant Biology, 20(70), 1-15 https://doi.org/10.1186/s12870-020-2279-8

Camacho, C., Coulouris, G., Avagyan, V., Ma, N., Papadopoulos, J., Bealer, K., & Madden, T. L. (2009). BLAST+: Architecture and applications. BMC Bioinformatics, 10, 1-9. https://doi.org/10.1186/1471-2105-10-421

Cárdenas-Castillo, J. E., Delatorre-Herrera, J., Bascuñán-Godoy, L., & Rodriguez, J. P. (2021). Quinoa (*Chenopodium quinoa* Willd.) seed yield and efficiency in soils deficient of nitrogen in the bolivian altiplano: An analytical review. Plants, 10(11), 1-20. https://doi.org/10.3390/plants10112479

Chele, K. H., Tinte, M. M., Piater, L. A., Dubery, I. A., & Tugizimana, F. (2021). Soil salinity, a serious environmental issue and plant responses: A metabolomics perspective. Metabolites, 11(11), 1-19. https://doi.org/10.3390/metabo11110724

Cheng, C., Gao, X., Feng, B., Sheen, J., Shan, L., & He, P. (2013). Plant immune response to pathogens differs with changing temperatures. Nature Communications, 4(May), 1–9. https://doi.org/10.1038/ncomms3530

Chojak-Koźniewska, J., Linkiewicz, A., Sowa, S., Radzioch, M. A., & Kuźniak, E. (2017). Interactive effects of salt stress and *Pseudomonas syringae* pv. *lachrymans* infection in cucumber: Involvement of antioxidant enzymes, abscisic acid and salicylic acid. Environmental and Experimental Botany, 136, 9–20. https://doi.org/10.1016/j.envexpbot.2017.01.004

Chojak-Koźniewska, J., Kuźniak, E., & Zimny, J. (2018). The effects of combined abiotic and pathogen stress in plants: Insights from salinity and *Pseudomonas syringae* pv

lachrymans interaction in cucumber. Frontiers in Plant Science, 871(November), 1–9. https://doi.org/10.3389/fpls.2018.01691

Chojak, J., Kuźniak, E., Świercz, U., Sekulska-Nalewajko, J., & Gocławski, J. (2012). interaction between salt stress and angular leaf spot (*Pseudomonas syringae* pv *lachrymans*) in cucumber. Vegetable Crops Research Bulletin, 77, 5–16. https://doi.org/10.2478/v10032-012-0011-4

Chou, W. C., Lin, S. S., Yeh, S. D., Li, S. L., Peng, Y. C., Fan, Y. H., & Chen, T. C. (2017). Characterization of the genome of a phylogenetically distinct tospovirus and its interactions with the local lesion-induced host *Chenopodium quinoa* by whole-transcriptome analyses. PLoS ONE, 12(8). https://doi.org/10.1371/journal.pone.0182425

Chu, C. C., Chen, S. Y., Chyau, C. C., Wang, S. C., Chu, H. L., & Duh, P. der. (2022). Djulis (*Chenopodium formosanum*) and Its Bioactive Compounds Protect Human Lung Epithelial A549 Cells from Oxidative Injury Induced by Particulate Matter via Nrf2 Signaling Pathway. Molecules, 27(1). https://doi.org/10.3390/molecules27010253

Chumpitaz-Segovia, C., Alvarado, D., Ogata-Gutiérrez, K. and Zúñiga-Dávila, D. (2020). Bioprospection of native psychrotolerant plant-growth-promoting rhizobacteria from Peruvian Andean Plateau soils associated with *Chenopodium quinoa*. Canadian Journal of Microbiology. 66(11): 641-652. https://doi.org/10.1139/cjm-2020-0036

Colque-Little, C., Amby, D. B., & Andreasen, C. (2021). A review of *Chenopodium quinoa* (Willd.) diseases—an updated perspective. Plants, 10(6), 1-39. https://doi.org/10.3390/plants10061228

Colque-Little, C., Abondano, M. C., Lund, O. S., Amby, D. B., Piepho, H. P., Andreasen, C., Schmöckel, S., & Schmid, K. (2021). Genetic variation for tolerance to the downy mildew pathogen *Peronospora variabilis* in genetic resources of quinoa (*Chenopodium quinoa*). BMC Plant Biology, 21(1), 1–19. https://doi.org/10.1186/s12870-020-02804-7

Colque-Little, C., Lund, O.C., Andreasen, C., Amby, D.B., (2023). *Chenopodium quinoa*, a new host for *Alternariasection alternata* and *Alternaria section* Infectoriae causing yellow leaf blotch disease. Plant Disease, First Look. 1-6. https://doi.org/10.1094/PDIS-10-22-2320-SC

Collaudin, A. B., & Blum, L. J. (1997). Investigations of the enhancer effect of a high-salt concentration medium on the luminol chemiluminescent reaction. Photochemistry and Photobiology, 65(2), 303–308. https://doi.org/10.1111/j.1751-1097.1997.tb08562.x

Coolen, S., Proietti, S., Hickman, R., Davila Olivas, N. H., Huang, P. P., Van Verk, M. C., Van Pelt, J. A., Wittenberg, A. H. J., De Vos, M., Prins, M., Van Loon, J. J. A., Aarts, M. G. M., Dicke, M., Pieterse, C. M. J., & Van Wees, S. C. M. (2016). Transcriptome dynamics of Arabidopsis during sequential biotic and abiotic stresses. The Plant Journal: For Cell and Molecular Biology, 86(3), 249–267. https://doi.org/10.1111/tpj.13167

Crutzen, F., Kreit, M., & Bragard, C. (2009). The beet virus Q coat protein readthrough domain is longer than previously reported, with two transmembrane domains. Journal of General Virology, 90(3), 754–758. https://doi.org/10.1099/vir.0.008029-0

Cunnac, S., Chakravarthy, S., Kvitko, B. H., Russell, A. B., Martin, G. B., & Collmer, A. (2011). Genetic disassembly and combinatorial reassembly identify a minimal functional repertoire of type III effectors in *Pseudomonas syringae*. Proceedings of the National Academy of Sciences of the United States of America, 108(7), 2975–2980. https://doi.org/10.1073/pnas.1013031108

Danielsen, S., Bonifacio, A., & Ames, T. (2003). Diseases of quinoa (*Chenopodium quinoa*). Food Reviews International, 19(1–2), 43–59. https://doi.org/10.1081/FRI-120018867

Daudi, A., Cheng, Z., O'Brien, J. A., Mammarella, N., Khan, S., Ausubel, F. M., & Bolwell, G. P. (2012). The apoplastic oxidative burst peroxidase in Arabidopsis is a major component of Pattern-Triggered Immunity. The Plant Cell, 24(1), 275–287. https://doi.org/10.1105/tpc.111.093039

Davila Olivas, N. H., Coolen, S., Huang, P., Severing, E., van Verk, M. C., Hickman, R., Wittenberg, A. H. J., de Vos, M., Prins, M., van Loon, J. J. A., Aarts, M. G. M., van Wees, S. C. M., Pieterse, C. M. J., & Dicke, M. (2016). Effect of prior drought and pathogen stress on Arabidopsis transcriptome changes to caterpillar herbivory. New Phytologist, 210(4), 1344–1356. https://doi.org/10.1111/nph.13847

De La Riva, E. G., Olmo, M., Poorter, H., Ubera, J. L., & Villar, R. (2016). Leaf mass per area (LMA) and its relationship with leaf structure and anatomy in Mediterranean woody species along a water availability gradient. PLoS ONE, 11(2). https://doi.org/10.1371/journal.pone.0148788

Dettmer, J., Hong-Hermesdorf, A., Stierhof, Y. D., & Schumacher, K. (2006). Vacuolar H+-ATPase activity is required for endocytic and secretory trafficking in Arabidopsis. Plant Cell, 18(3), 715–730. https://doi.org/10.1105/tpc.105.037978

De Vleesschauwer, D., Xu, J., & Höfte, M. (2014). Making sense of hormone-mediated defence networking: From rice to Arabidopsis. In Frontiers in Plant Science, 5 (November), 1–15. doi: 10.3389/fpls.2014.00611

Dillon, M. M., Almeida, R. N. D., Laflamme, B., Martel, A., Weir, B. S., Desveaux, D., & Guttman, D. S. (2019). Molecular evolution of *Pseudomonas syringae* type III secreted effector proteins. Frontiers in Plant Science, 10. https://doi.org/10.3389/fpls.2019.00418

Dodds, P. N., & Rathjen, J. P. (2010). Plant immunity: Towards an integrated view of plant pathogen interactions. In Nature Reviews Genetics, 11(8), 539–548. https://doi.org/10.1038/nrg2812

Dong, X., Mindrinos, M., D, K. R., & Ausubel, F. M. (1991). lnduction of Arabidopsis defence genes by virulent and avirulent *Pseudomonas syringae* strains and by a cloned avirulence gene. The Plant Cell, 61–72. https://academic.oup.com/plcell/article/3/1/61/5984290

Egea, I., Estrada, Y., Faura, C., Egea-Fernández, J. M., Bolarin, M. C., & Flores, F. B. (2023). Salt-tolerant alternative crops as sources of quality food to mitigate the negative impact of salinity on agricultural production. In Frontiers in Plant Science, 14. Frontiers Media S.A. https://doi.org/10.3389/fpls.2023.1092885

Eisa, S., Koyro, H. W., Kogel, K. H., & Imani, J. (2005). Induction of somatic embryogenesis in cultured cells of *Chenopodium quinoa*. Plant Cell, Tissue and Organ Culture (2005), 81, 243–246. https://doi.org/10.1007/s11240-004-4793-z

El-Iklil, Y., Karrou, M., Benichou, M., & El-iklil, Y. (2000). Salt stress effect on epinasty in relation to ethylene production and water relations in tomato. Agronomie, 20(4), 399–406. https://doi.org/10.1051/agro:2000136ï

El Hadrami, A., Adam, L. R., el Hadrami, I., & Daayf, F. (2010). Chitosan in plant protection. In Marine Drugs, 8(4), 968–987. https://doi.org/10.3390/md8040968

Ellinger, D., Naumann, M., Falter, C., Zwikowics, C., Jamrow, T., Manisseri, C., Somerville, S. C., & Voigt, C. A. (2013). Elevated early callose deposition results in complete penetration resistance to powdery mildew in Arabidopsis. Plant Physiology, 161(3), 1433–1444. https://doi.org/10.1104/pp.112.211011

Emms, D. M., & Kelly, S. (2019). OrthoFinder: Phylogenetic orthology inference for comparative genomics. Genome Biology, 20(1), 1–14. https://doi.org/10.1186/s13059-019-1832-y

Estrada, Y., Fernández-Ojeda, A., Morales, B., Egea-Fernández, J. M., Flores, F. B., Bolarín, M. C., & Egea, I. (2021). Unravelling the strategies used by the underexploited amaranth species to confront salt stress: similarities and differences with quinoa species. Frontiers in Plant Science, 12(February), 1–18. https://doi.org/10.3389/fpls.2021.604481

Fischer, I., Diévart, A., Droc, G., Dufayard, J. F., & Chantret, N. (2016). Evolutionary dynamics of the leucine-rich repeat receptor-like kinase (LRR-RLK) subfamily in angiosperms. Plant Physiology, 170(3), 1595–1610. https://doi.org/10.1104/pp.15.01470

Fliegmann, J., & Felix, G. (2016). Immunity: Flagellin seen from all sides. In Nature Plants, 2(9). Palgrave Macmillan Ltd. https://doi.org/10.1038/nplants.2016.136

Flowers, T. J., & Colmer, T. D. (2015). Plant salt tolerance: Adaptations in halophytes. In Annals of Botany, 115(3), 327–331. Oxford University Press. https://doi.org/10.1093/aob/mcu267

Fones, H. N., Eyles, C. J., Bennett, M. H., Smith, J. A. C., & Preston, G. M. (2013). Uncoupling of reactive oxygen species accumulation and defence signalling in the metal hyperaccumulator plant *Noccaea caerulescens*. New Phytologist, 199(4), 916–924. https://doi.org/10.1111/nph.12354

Fonseca-Guerra, I., Chiquillo, C., Padilla, M. J., and Benavides-Rozo, M. (2021). First report of bacterial leaf spot on Chenopodium quinoa caused by pseudomonas syringae in Colombia. J. Plant Dis. Protec. 128, 871–874. doi: 10.1007/s41348-021-00435-0

Freeman, B. C., Chen, C., Yu, X., Nielsen, L., Peterson, K., & Beattie, G. A. (2013). Physiological and transcriptional responses to osmotic stress of two *Pseudomonas syringae* strains that differ in epiphytic fitness and osmotolerance. Journal of Bacteriology, 195(20), 4742–4752. https://doi.org/10.1128/JB.00787-13

Fujita, M., Fujita, Y., Noutoshi, Y., Takahashi, F., Narusaka, Y., Yamaguchi-Shinozaki, K., & Shinozaki, K. (2006). Crosstalk between abiotic and biotic stress responses: a current view from the points of convergence in the stress signaling networks. Current Opinion in Plant Biology, 9(4), 436–442. https://doi.org/10.1016/j.pbi.2006.05.014

Galvan-Ampudia, C. S., Julkowska, M. M., Darwish, E., Gandullo, J., Korver, R. A., Brunoud, G., Haring, M. A., Munnik, T., Vernoux, T., & Testerink, C. (2013). Halotropism is a response of plant roots to avoid a saline environment. Current Biology, 23(20), 2044–2050. https://doi.org/10.1016/j.cub.2013.08.042

Gao, M. Z., Dong, Y. H., Valcárcel, V., Ren, Z. M., & Li, Y. L. (2021). Complete chloroplast genome of the grain *Chenopodium quinoa* Willd., an important economical and dietary

plant. Mitochondrial DNA Part B: Resources, 6(1), 40–42. https://doi.org/10.1080/23802359.2020.1845107

Garcia, M. L., Grau, O., & Sarachu, A. N. (1991). *Citrus psorosis* is probably caused by a bipartite ssRNA virus. Res. Virol. LVVl, 142, 303–311. https://doi.org/10.1016/0923-2516(91)90017-W

Garcia-Moreno, M., Noerenberg, M., Ni, S., Järvelin, A. I., González-Almela, E., Lenz, C. E., Bach-Pages, M., Cox, V., Avolio, R., Davis, T., Hester, S., Sohier, T. J. M., Li, B., Heikel, G., Michlewski, G., Sanz, M. A., Carrasco, L., Ricci, E. P., Pelechano, V., … Castello, A. (2019). System-wide profiling of RNA-binding proteins uncovers key regulators of virus infection. Molecular Cell, 74(1), 196-211.e11. https://doi.org/10.1016/J.MOLCEL.2019.01.017

García-Parra, M., Zurita-Silva, A., Stechauner-Rohringer, R., Roa-Acosta, D., & Jacobsen, S. E. (2020). Quinoa (*Chenopodium quinoa* Willd.) and its relationship with agroclimatic characteristics: A Colombian perspective. In Chilean Journal of Agricultural Research, 80(2), 290–302. Instituto de Investigaciones Agropecuarias, INIA. https://doi.org/10.4067/S0718-58392020000200290

Gharat, S. A., Parmar, S., Tambat, S., Vasudevan, M., & Shaw, B. P. (2016). Transcriptome analysis of the response to NaCl in *Suaeda maritima* provides an insight into salt tolerance mechanisms in halophytes. PLoS ONE, 11(9). https://doi.org/10.1371/journal.pone.0163485

Gharbi, E., Martínez, J. P., Benahmed, H., Lepoint, G., Vanpee, B., Quinet, M., & Lutts, S. (2017). Inhibition of ethylene synthesis reduces salt-tolerance in tomato wild relative species *Solanum chilense*. Journal of Plant Physiology, 210, 24–37. https://doi.org/10.1016/j.jplph.2016.12.001

Godson, A., & van der Hoorn, R. A. L. (2021). The front line of defence: A meta-analysis of apoplastic proteases in plant immunity. In Journal of Experimental Botany, 72(9), 3381–3394. Oxford University Press. https://doi.org/10.1093/jxb/eraa602

Goel, A. K., Lundberg, D., Torres, M. A., Matthews, R., Akimoto-Tomiyama, C., Farmer, L., Dangl, J. L., & Grant, S. R. (2008). The *Pseudomonas syringae* Type III Effector HopAM1 enhances virulence on water-stressed plants. MPMI, 21(3), 361–370. https://doi.org/10.1094/MPMI

Gong, Q., Li, P., Ma, S., Indu Rupassara, S., & Bohnert, H. J. (2005). Salinity stress adaptation competence in the extremophile *Thellungiella halophila* in comparison with its relative *Arabidopsis thaliana*. Plant Journal, 44(5), 826–839. https://doi.org/10.1111/j.1365-313X.2005.02587.x

Gonzalez-Guzman, M., Rodriguez, L., Lorenzo-Orts, L., Pons, C., Sarrion-Perdigones, A., Fernandez, M. A., Peirats-Llobet, M., Forment, J., Moreno-Alvero, M., Cutler, S. R., Albert, A., Granell, A., & Rodriguez, P. L. (2014). Tomato PYR/PYL/RCAR abscisic acid receptors show high expression in root, differential sensitivity to the abscisic acid agonist quinabactin, and the capability to enhance plant drought resistance. Journal of Experimental Botany, 65(15), 4451–4464. https://doi.org/10.1093/jxb/eru219

Goodin, M. M., Zaitlin, D., Naidu, R. A., & Lommel, S. A. (2008). *Nicotiana benthamiana*: Its history and future as a model for plant-pathogen interactions. MPMI, 21(8), 1015–1026. https://doi.org/10.1094/MPMI

Graf, L., Rojas-Silva, P., Rojo, L., Delatorre-Herrera, J., Baldeon, M., & Raskin, I. (2015). Innovations in health value and functional food development of quinoa (*Chenopodium quinoa* Willd.) Brittany. Compre Rev Food Sci Food Safety, 14(4), 431–445. https://doi.org/10.1111/1541-4337.12135.Innovations

Grenfell-Shaw, L., & Tester, M. (2021). Abiotic Stress Tolerance in Quinoa, 139–167. https://doi.org/10.1007/978-3-030-65237-1_9

Grigore, M. N., & Vicente, O. (2023). Wild halophytes: tools for understanding salt tolerance mechanisms of plants and for adapting agriculture to climate change. In Plants, 12(2). https://doi.org/10.3390/plants12020221

Großkinsky, D. K., Albacete, A., Jammer, A., Krbez, P., van der Graaff, E., Pfeifhofer, H., & Roitsch, T. (2014). A rapid phytohormone and phytoalexin screening method for physiological phenotyping. In Molecular Plant, (7, 6), 1053–1056. Oxford University Press. https://doi.org/10.1093/mp/ssu015

Guerreiro, A., Figueiredo, J., Sousa Silva, M., & Figueiredo, A. (2016). Linking jasmonic acid to grapevine resistance against the biotrophic oomycete *Plasmopara viticola*. Frontiers in Plant Science, 7(April), 1–7. https://doi.org/10.3389/fpls.2016.00565

Guo, B., Wei, Y., Xu, R., Lin, S., Luan, H., Lv, C., Zhang, X., Song, X., & Xu, R. (2016). Genome-wide analysis of APETALA2/ethylene-responsive factor (AP2/ERF) Gene family in barley (*Hordeum vulgare L.).* PLoS ONE, 11(9), 1–17. https://doi.org/10.1371/journal.pone.0161322

Guo, S., & Wong, S. M. (2018). Disruption of a stem-loop structure located upstream of pseudoknot domain in Tobacco mosaic virus enhanced its infectivity and viral RNA accumulation. Virology, 519, 170–179. https://doi.org/10.1016/j.virol.2018.04.009

Gupta, A., Hisano, H., Hojo, Y., Matsuura, T., Ikeda, Y., Mori, I. C., & Senthil-Kumar, M. (2017). Global profiling of phytohormone dynamics during combined drought and pathogen stress in *Arabidopsis thaliana* reveals ABA and JA as major regulators. Scientific Reports, 7(1), 1–13. https://doi.org/10.1038/s41598-017-03907-2

Gupta, A., Bhardwaj, M., & Tran, L. S. P. (2020). Jasmonic acid at the crossroads of plant immunity and *Pseudomonas syringae* virulence. In International Journal of Molecular Sciences, 21(20), 1–19. https://doi.org/10.3390/ijms21207482

Gust, A. A., Biswas, R., Lenz, H. D., Rauhut, T., Ranf, S., Kemmerling, B., Götz, F., Glawischnig, E., Lee, J., Felix, G., & Nürnberger, T. (2007). Bacteria-derived peptidoglycans constitute pathogen-associated molecular patterns triggering innate immunity in Arabidopsis. Journal of Biological Chemistry, 282(44), 32338–32348. https://doi.org/10.1074/jbc.M704886200

Gutiérrez-Luna, F. M., Hernández-Domínguez, E. E., Valencia-Turcotte, L. G., & Rodríguez-Sotres, R. (2018). Review: "Pyrophosphate and pyrophosphatases in plants, their involvement in stress responses and their possible relationship to secondary metabolism." Plant Science, 267, 11–19. https://doi.org/10.1016/J.PLANTSCI.2017.10.016

Hajihashemi, S., Jahantigh, O., & Alboghobeish, S. (2022). The redox status of salinity-stressed *Chenopodium quinoa* under salicylic acid and sodium nitroprusside treatments. Frontiers in Plant Science, 13(November), 1–12. https://doi.org/10.3389/fpls.2022.1030938

Hajjar, R., & Hodgkin, T. (2007). The use of wild relatives in crop improvement: A survey of developments over the last 20 years. Euphytica, 156(1–2), 1–13. https://doi.org/10.1007/s10681-007-9363-0

Han, G. Z. (2019). Origin and evolution of the plant immune system. In New Phytologist, 222(1), 70–83. Blackwell Publishing Ltd. https://doi.org/10.1111/nph.15596

Hariadi, Y., Marandon, K., Tian, Y., Jacobsen, S. E., & Shabala, S. (2011). Ionic and osmotic relations in quinoa (*Chenopodium quinoa* Willd.) plants grown at various salinity levels. Journal of Experimental Botany, 62(1), 185–193. https://doi.org/10.1093/jxb/erq257

Hasiów-Jaroszewska, B., & Zarzyńska-Nowak, A. (2022). Tomato black ring virus (ring spot of beet). https://www.cabidigitallibrary.org/doi/epdf/10.1079/cabicompendium.54060

Hassani, A., Azapagic, A., & Shokri, N. (2021). Global predictions of primary soil salinization under changing climate in the 21st century. Nature Communications, 12(1). https://doi.org/10.1038/s41467-021-26907-3

Hettenhausen, C., Baldwin, I. T., & Wu, J. (2012). Silencing MPK4 in *Nicotiana attenuata* enhances photosynthesis and seed production but compromises abscisic acid-induced stomatal closure and guard cell-mediated resistance to *Pseudomonas syringae* pv. tomato DC3000. Plant Physiology, 158(2), 759–776. https://doi.org/10.1104/pp.111.190074

Hinojosa, L., González, J. A., Barrios-Masias, F. H., Fuentes, F., & Murphy, K. M. (2018). Quinoa abiotic stress responses: A review. In Plants, 7(4). https://doi.org/10.3390/plants7040106

Hirschmann, F., Krause, F., & Papenbrock, J. (2014). The multi-protein family of sulfotransferases in plants: Composition, occurrence, substrate specificity, and functions. Frontiers in Plant Science, 5(October), 1–13. https://doi.org/10.3389/fpls.2014.00556

Hoagland, D., Arnon, D., Hoagland, D. R., Arnon, D. I., & Hutchison, C. B. (1950). The water-culture method for growing plants without soil. http://hdl.handle.net/2027/uc2.ark:/13960/t51g1sb8j

Hong, S. Y., Cheon, K. S., Yoo, K. O., Lee, H. O., Cho, K. S., Suh, J. T., Kim, S. J., Nam, J. H., Sohn, H. B., & Kim, Y. H. (2017). Complete chloroplast genome sequences and comparative analysis of *Chenopodium quinoa* and *C. album*. Frontiers in Plant Science, 8(October), 1–12. https://doi.org/10.3389/fpls.2017.01696

Hosseini, S. S., Ramezanpour, S. S., Soltanloo, H., & Seifati, S. E. (2023). RNA-seq analysis and reconstruction of gene networks involved in response to salinity stress in quinoa (cv. Titicaca). Scientific Reports, 13(1). https://doi.org/10.1038/s41598-023-34534-9

Hou, S., Shen, H., & Shao, H. (2019). PAMP-induced peptide 1 cooperates with salicylic acid to regulate stomatal immunity in *Arabidopsis thaliana*. Plant Signaling and Behaviour, 14(11). https://doi.org/10.1080/15592324.2019.1666657

Huang, P. Y., & Zimmerli, L. (2014). Enhancing crop innate immunity: New promising trends. In Frontiers in Plant Science, 5, 1-7. Frontiers Media S.A. https://doi.org/10.3389/fpls.2014.00624

Hunt, S. P., Jarvis, D. E., Larsen, D. J., Mosyakin, S. L., Kolano, B. A., Jackson, E. W., Martin, S. L., Jellen, E. N., & Maughan, P. J. (2020). A chromosome-scale assembly of the Garden Orach (*Atriplex hortensis L.*) genome using Oxford Nanopore Sequencing. Frontiers in Plant Science, 11, 1-20. https://doi.org/10.3389/fpls.2020.00624

Huot, B., Yao, J., Montgomery, B. L., & He, S. Y. (2014). Growth-defence tradeoffs in plants: A balancing act to optimize fitness. Molecular Plant, 7(8), 1267–1287. https://doi.org/10.1093/mp/ssu049

Hsu, F. C., Chou, M. Y., Chou, S. J., Li, Y. R., Peng, H. P., & Shih, M. C. (2013). Submergence confers immunity mediated by the WRKY22 transcription factor in Arabidopsis. Plant Cell, 25(7), 2699–2713. https://doi.org/10.1105/tpc.113.114447

Hupp, S., Rosenkranz, M., Bonfig, K., Pandey, C., & Roitsch, T. (2019). Non-invasive phenotyping of plant–pathogen interaction: consecutive in situ imaging of fluorescing *Pseudomonas syringae*, plant phenolic fluorescence, and chlorophyll fluorescence in Arabidopsis leaves. Frontiers in Plant Science, 10, 1-10. https://doi.org/10.3389/fpls.2019.01239

Hwang, M. S. H., Morgan, R. L., Sarkar, S. F., Wang, P. W., & Guttman, D. S. (2005). Phylogenetic characterization of virulence and resistance phenotypes of *Pseudomonas syringae.* Applied and Environmental Microbiology, 71(9), 5182–5191. https://doi.org/10.1128/AEM.71.9.5182-5191.2005

Imamura, T., Yasui, Y., Koga, H., Takagi, H., Abe, A., Nishizawa, K., Mizuno, N., Ohki, S., Mizukoshi, H., & Mori, M. (2020). A novel WD40-repeat protein involved in formation of epidermal bladder cells in the halophyte quinoa. Communications Biology, 3(1). https://doi.org/10.1038/s42003-020-01249-w

Iriti, M., & Vitalini, S. (2021). Plant immunity and crop yield: A sustainable approach in agri-food systems. In Vaccines, 9(2), 1–3. MDPI AG. https://doi.org/10.3390/vaccines9020121

Ishihara, A., Hashimoto, Y., Tanaka, C., Dubouzet, J. G., Nakao, T., Matsuda, F., Nishioka, T., Miyagawa, H., & Wakasa, K. (2008). The tryptophan pathway is involved in the defence responses of rice against pathogenic infection via serotonin production. Plant Journal, 54(3), 481–495. https://doi.org/10.1111/j.1365-313X.2008.03441.x

Jacobsen, S. E. (2003). The worldwide potential for quinoa (*Chenopodium quinoa* Willd.). Food Reviews International, 19(1–2), 167–177. https://doi.org/10.1081/FRI-120018883

Jacobsen, S. E., Liu, F., & Jensen, C. R. (2009). Does root-sourced ABA play a role for regulation of stomata under drought in quinoa (*Chenopodium quinoa* Willd.). Scientia Horticulturae, 122(2), 281–287. https://doi.org/10.1016/j.scienta.2009.05.019

Jacobsen, S. E. (2017). The scope for adaptation of quinoa in Northern Latitudes of Europe. Journal of Agronomy and Crop Science, 203(6), 603–613. https://doi.org/10.1111/jac.12228

Janda, M., Lamparová, L., Zubíková, A., Burketová, L., Martinec, J., & Krčková, Z. (2019). Temporary heat stress suppresses PAMP-triggered immunity and resistance to bacteria in *Arabidopsis thaliana*. Molecular Plant Pathology, 20(7), 1005–1012. https://doi.org/10.1111/mpp.12799

Jarvis, D. E., Sproul, J. S., Navarro-Domínguez, B., Krak, K., Jaggi, K., Huang, Y. F., Huang, T. Y., Lin, T. C., Jellen, E. N., & Maughan, P. J. (2022). Chromosome-Scale Genome Assembly of the Hexaploid Taiwanese Goosefoot "Djulis" (*Chenopodium formosanum*). Genome Biology and Evolution, 14(8), 1–7. https://doi.org/10.1093/gbe/evac120

Jarvis, D. E., Sproul, J. S., Navarro-Domínguez, B., Krak, K., Jaggi, K., Huang, Y. F., Huang, T. Y., Lin, T. C., Jellen, E. N., & Maughan, P. J. (2022). Chromosome-scale genome assembly of the hexaploid Taiwanese goosefoot "Djulis" (*Chenopodium formosanum*). Genome Biology and Evolution, 14(8). https://doi.org/10.1093/gbe/evac120

Jellen, E. N., Jarvis, D. E., Hunt, S. P., Mangelsen, H. H., & Maughan, P. J. (2019). New seed collections of north american pitseed goosefoot (*Chenopodium berlandieri*) and efforts to identify its diploid ancestors through whole-genome sequencing. Ciencia e Investigacion Agraria, 46(2), 187–196. https://doi.org/10.7764/rcia.v46i2.2150

Jiang, C., Belfield, E. J., Cao, Y., Smith, J. A. C., & Harberd, N. P. (2013). An Arabidopsis Soil-Salinity-tolerance mutation confers ethylene-mediated enhancement of

sodium/potassium homeostasis. The Plant Cell, 25(9), 3535–3552. https://doi.org/10.1105/tpc.113.115659

Jiang, C., Belfield, E. J., Mithani, A., Visscher, A., Ragoussis, J., Mott, R., Smith, J. A. C., & Harberd, N. P. (2012). ROS-mediated vascular homeostatic control of root-to-shoot soil Na delivery in Arabidopsis. EMBO Journal, 31(22), 4359–4370. https://doi.org/10.1038/emboj.2012.273

Jin, L., Ouyang, N., Huang, Y., Liu, C., & Ruan, Y. (2019). Genome-wide analysis of sulfotransferase genes and their responses to abiotic stresses in Chinese cabbage (*Brassica rapa L.).* PloS ONE, 14(8), 1–17. https://doi.org/10.1371/journal.pone.0221422

Ju, Y., Tian, H., Zhang, R., Zuo, L., Jin, G., Xu, Q., Ding, X., Li, X., & Chu, Z. (2017). Overexpression of OsHSP18.0-CI enhances resistance to bacterial leaf streak in rice. Rice, 10(1), 1–11. https://doi.org/10.1186/s12284-017-0153-6

Jutras, P. V., Dodds, I., & van der Hoorn, R. AL. (2020). Proteases of *Nicotiana benthamiana*: an emerging battle for molecular farming. Current Opinion in Biotechnology, 61, 60–65. https://doi.org/10.1016/j.copbio.2019.10.006

Kámán-Tóth, E., Dankó, T., Gullner, G., Bozsó, Z., Palkovics, L., & Pogány, M. (2019). Contribution of cell wall peroxidase- and NADPH oxidase-derived reactive oxygen species to *Alternaria brassicicola*-induced oxidative burst in Arabidopsis. Molecular Plant Pathology, 20(4), 485–499. https://doi.org/10.1111/mpp.12769

Kanyuka, K., & Rudd, J. J. (2019). Cell surface immune receptors: the guardians of the plant's extracellular spaces. Current Opinion in Plant Biology, 50, 1–8. https://doi.org/10.1016/J.PBI.2019.02.005

Kapazoglou, A., Gerakari, M., Lazaridi, E., Kleftogianni, K., Sarri, E., Tani, E., & Bebeli, P. J. (2023). Crop wild relatives: a valuable source of tolerance to various abiotic stresses. Plants, 12(2), 1–20. https://doi.org/10.3390/plants12020328

Katagiri, F., Thilmony, R., & He, S. Y. (2002). The *Arabidopsis thaliana-Pseudomonas syringae* Interaction. The Arabidopsis Book, 1, e0039. https://doi.org/10.1199/tab.0039

Katoh, K., & Standley, D. M. (2013). MAFFT multiple sequence alignment software version 7: Improvements in performance and usability. Molecular Biology and Evolution, 30(4), 772–780. https://doi.org/10.1093/molbev/mst010

Kazachkova, Y., Eshel, G., Pantha, P., Cheeseman, J. M., Dassanayake, M., & Barak, S. (2018). Halophytism: What have we learnt from *Arabidopsis thaliana relative* model systems? In Plant Physiology, 178(3), 972–988. American Society of Plant Biologists. https://doi.org/10.1104/pp.18.00863

Khan, S., Jabeen, R., Deeba, F., Waheed, U., Khanum, P., & Iqbal, N. (2021). Heat shock proteins: classification, functions and expressions in plants during environmental stresses. Journal of Bioresource Management, 8(2), 85–97. https://doi.org/10.35691/jbm.1202.0183

Kiani-Pouya, A., Rasouli, F., Bazihizina, N., Zhang, H., Hedrich, R., & Shabala, S. (2019). A large-scale screening of quinoa accessions reveals an important role of epidermal bladder cells and stomatal patterning in salinity tolerance. Environmental and Experimental Botany, 168. https://doi.org/10.1016/j.envexpbot.2019.103885

Kissoudis, C., Chowdhury, R., van Heusden, S., van de Wiel, C., Finkers, R., Visser, R. G. F., Bai, Y., & van der Linden, G. (2015). Combined biotic and abiotic stress resistance in tomato. Euphytica, 202(2), 317–332. https://doi.org/10.1007/s10681-015-1363-x

Kissoudis, C., Sunarti, S., van de Wiel, C., Visser, R. G. F., van der Linden, C. G., & Bai, Y. (2016). Responses to combined abiotic and biotic stress in tomato are governed by stress intensity and resistance mechanism. Journal of Experimental Botany, 67(17), 5119–5132. https://doi.org/10.1093/jxb/erw285

Klauser, D., Flury, P., Boller, T., & Bartels, S. (2013). Several MAMPs, including chitin fragments, enhance AtPep-triggered oxidative burst independently of wounding. Plant Signaling and Behavior, 8(9), 20–23. https://doi.org/10.4161/psb.25346

Kloth, K. J., Wiegers, G. L., Busscher-Lange, J., Van Haarst, J. C., Kruijer, W., Bouwmeester, H. J., Dicke, M., & Jongsma, M. A. (2016). AtWRKY22 promotes susceptibility to aphids and modulates salicylic acid and jasmonic acid signalling. Journal of Experimental Botany, 67(11), 3383–3396. https://doi.org/10.1093/jxb/erw159

Knudsen, S., Wendt, T., Dockter, C., Thomsen, H. C., Rasmussen, M., Jørgensen, M. E., Lu, Q., Voss, C., Murozuka, E., Østerberg, J. T., Harholt, J., Braumann, I., Cuesta-Seijo, J. A., Kale, S. M., Bodevin, S., Petersen, L. T., Carciofi, M., Pedas, P. R., Husum, J. O., Skadhauge, B. (2022). FIND-IT: Accelerated trait development for a green evolution. Science Advances, 8(34). https://doi.org/10.1126/sciadv.abq2266

Komari, T. (1990). Transformation of cultured cells of *Chenopodium quinoa* by binary vectors that carry a fragment of DNA from the virulence region of pTiBo542. Plant Cell Reports, 9(6), 303–306. https://doi.org/10.1007/BF00232856

Koornneef, A., Leon-Reyes, A., Ritsema, T., Verhage, A., Den Otter, F. C., Van Loon, L. C., & Pieterse, C. M. J. (2008). Kinetics of salicylate-mediated suppression of jasmonate signaling reveal a role for redox modulation. Plant Physiology, 147(3), 1358–1368. https://doi.org/10.1104/pp.108.121392

Kuang, J., Liu, J., Mei, J., Wang, C., Hu, H., Zhang, Y., Sun, M., Ning, X., Xiao, L., & Yang, L. (2017). A Class II small heat shock protein OsHsp18.0 plays positive roles in both biotic and abiotic defence responses in rice. Scientific Reports, 7(1), 1–14. https://doi.org/10.1038/s41598-017-11882-x

Kumar, H., Bhardwaj, K., Cruz-Martins, N., Nepovimova, E., Oleksak, P., Dhanjal, D. S., Bhardwaj, S., Singh, R., Chopra, C., Verma, R., Chauhan, P. P., Kumar, D., & Kuča, K. (2021). Applications of fruit polyphenols and their functionalized nanoparticles against foodborne bacteria: A mini review. In Molecules, 26(11). https://doi.org/10.3390/molecules26113447

Kumar, A., Bhargava, A., Shukla, S., Singh, H. B., & Ohri, D. (2006). Screening of exotic *Chenopodium quinoa* accessions for downy mildew resistance under mid-eastern

conditions of India. Crop Protection, 25(8), 879–889. https://doi.org/10.1016/j.cropro.2005.11.012

Kumari, A., Das, P., Parida, A. K., & Agarwal, P. K. (2015). Proteomics, metabolomics, and ionomics perspectives of salinity tolerance in halophytes. Frontiers in Plant Science, 6(July). https://doi.org/10.3389/fpls.2015.00537

Kundu, S., & Gantait, S. (2017). Abscisic acid signal crosstalk during abiotic stress response. Plant Gene, 11(May), 61–69. https://doi.org/10.1016/j.plgene.2017.04.007

Kus, J. V., Zaton, K., Sarkar, R., & Cameron, R. K. (2002). Age-related resistance in Arabidopsis is a developmentally regulated defence response to *Pseudomonas syringae.* Plant Cell, 14(2), 479–490. https://doi.org/10.1105/tpc.010481

Kuźniak, E., & Kopczewski, T. (2020). The chloroplast reactive oxygen species-redox system in plant immunity and disease. Frontiers in Plant Science, 11(November), 1–8. https://doi.org/10.3389/fpls.2020.572686

Lamprecht, S., & Jelkmann, W. (1997). Infectious cDNA clone used to identify strawberry mild yellow edge-associated potexvirus as causal agent of the disease. In Journal of General Virology (Vol. 78). doi: 10.1099/0022-1317-78-9-2347

Lelario, F., Scrano, L., De Franchi, S., Bonomo, M. G., Salzano, G., Milan, S., Milella, L., & Bufo, S. A. (2018). Identification and antimicrobial activity of most representative secondary metabolites from different plant species. Chemical and Biological Technologies in Agriculture, 5(1), 1–12. https://doi.org/10.1186/s40538-018-0125-0

Letunic, I., & Bork, P. (2019). Interactive Tree of Life (iTOL) v4: Recent updates and new developments. Nucleic Acids Research, 47(W1), 256–259. https://doi.org/10.1093/nar/gkz239

Li, B., Meng, X., Shan, L., & He, P. (2016). Transcriptional regulation of Pattern-Triggered Immunity in plants. In Cell Host and Microbe, 19(5), 641–650. Cell Press. https://doi.org/10.1016/j.chom.2016.04.011

Li, C., Ran, M., Liu, J., Wang, X., Wu, Q., Zhang, Q., Yang, J., Yi, F., Zhang, H., Zhu, J. K., & Zhao, C. (2022). Functional analysis of CqPORB in the regulation of chlorophyll biosynthesis in *Chenopodium quinoa*. Frontiers in Plant Science, 13(December), 1–14. https://doi.org/10.3389/fpls.2022.1083438

Li, P., Lu, Y. J., Chen, H., & Day, B. (2020). The Lifecycle of the Plant Immune System. Critical Reviews in Plant Sciences, 39(1), 72–100. https://doi.org/10.1080/07352689.2020.1757829

Li, J., Zhou, X., Huang, H., & Li, G. (2017). Diseases characteristic and control measurements for *Chenopodium quinoa* Willd. Advances in Engineering Research (AER), 143, 1-4. doi: 10.2991/iceep-17.2017.53

Li, W., Zhang, C., Lu, Q., Wen, X., & Lu, C. (2011). The combined effect of salt stress and heat shock on proteome profiling in Suaeda salsa. Journal of Plant Physiology, 168(15), 1743–1752. https://doi.org/10.1016/j.jplph.2011.03.018

Li, Z., Zhang, L., Yu, Y., Quan, R., Zhang, Z., Zhang, H., & Huang, R. (2011). The ethylene response factor AtERF11 that is transcriptionally modulated by the bZIP transcription factor HY5 is a crucial repressor for ethylene biosynthesis in Arabidopsis. Plant Journal, 68(1), 88–99. https://doi.org/10.1111/j.1365-313X.2011.04670.x

Lindeberg, M., Cunnac, S., & Collmer, A. (2012). *Pseudomonas syringae* type III effector repertoires: Last words in endless arguments. In Trends in Microbiology. 20(4), 199–208. https://doi.org/10.1016/j.tim.2012.01.003

Liu, W., & Wang, G. L. (2016). Plant innate immunity in rice: A defence against pathogen infection. In National Science Review, 3(3), 295–308. Oxford University Press. https://doi.org/10.1093/nsr/nww015

Lombardi, T., Bertacchi, A., Pistelli, L., Pardossi, A., Pecchia, S., Toffanin, A., & Sanmartin, C. (2022). biological and agronomic traits of the main halophytes widespread in the Mediterranean region as potential new vegetable crops. In Horticulturae, 8(3). https://doi.org/10.3390/horticulturae8030195

López-Marqués, R. L., Nørrevang, A. F., Ache, P., Moog, M., Visintainer, D., Wendt, T., Østerberg, J. T., Dockter, C., Jørgensen, M. E., Salvador, A. T., Hedrich, R., Gao, C., Jacobsen, S. E., Shabala, S., & Palmgren, M. (2020). Prospects for the accelerated improvement of the resilient crop quinoa. Journal of Experimental Botany, 71(18), 5333–5347. https://doi.org/10.1093/jxb/eraa285

López-Portillo, J., Ewers, F. W., Méndez-Alonzo, R., López, C. L. P., Angeles, G., Jiménez, A. L. A., Lara-Domínguez, A. L., & Barrera, M. del C. T. (2014). Dynamic control of osmolality and ionic composition of the xylem sap in two mangrove species. American Journal of Botany, 101(6), 1013–1022. https://doi.org/10.3732/ajb.1300435

Love, M. I., Huber, W., & Anders, S. (2014). Moderated estimation of fold change and dispersion for RNA-seq data with DESeq2. Genome Biology, 15(12). https://doi.org/10.1186/s13059-014-0550-8

Lozano-Isla, F., Apaza, J. D., Mujica Sanchez, A., Blas Sevillano, R., Haussmann, B. I. G., & Schmid, K. (2023). Enhancing quinoa cultivation in the Andean highlands of Peru: a breeding strategy for improved yield and early maturity adaptation to climate change using traditional cultivars. Euphytica, 219(2), 1–17. https://doi.org/10.1007/s10681-023-03155-8

Ma, J., Wang, L. yue, Dai, J. xi, Wang, Y., & Lin, D. (2021). The NAC-type transcription factor CaNAC46 regulates the salt and drought tolerance of transgenic *Arabidopsis thaliana*. BMC Plant Biology, 21(1). https://doi.org/10.1186/s12870-020-02764-y

Mahjoor, F., Ghaemi, A. A., & Golabi, M. H. (2016). Interaction effects of water salinity and hydroponic growth medium on eggplant yield, water-use efficiency, and evapotranspiration. International Soil and Water Conservation Research, 4(2), 99–107. https://doi.org/10.1016/J.ISWCR.2016.04.001

Maier, B. A., Kiefer, P., Field, C. M., Hemmerle, L., Bortfeld-Miller, M., Emmenegger, B., Schäfer, M., Pfeilmeier, S., Sunagawa, S., Vogel, C. M., & Vorholt, J. A. (2021). A general

non-self response as part of plant immunity. Nature Plants, 7(5), 696–705. https://doi.org/10.1038/s41477-021-00913-1

Malosetti, M., Ribaut, J. M., & van Eeuwijk, F. A. (2013). The statistical analysis of multi-environment data: Modeling genotype-by-environment interaction and its genetic basis. Frontiers in Physiology, 4(March), 1–17. https://doi.org/10.3389/fphys.2013.00044

Manna, M., Rengasamy, B., & Sinha, A. K. (2023). Revisiting the role of MAPK signalling pathway in plants and its manipulation for crop improvement. Plant Cell and Environment, 46, 2277–2295. https://doi.org/10.1111/pce.14606

Mansfield, J., Genin, S., Magori, S., Citovsky, V., Sriariyanum, M., Ronald, P., Dow, M., Verdier, V., Beer, S. v., Machado, M. A., Toth, I., Salmond, G., & Foster, G. D. (2012). Top 10 plant pathogenic bacteria in molecular plant pathology. In Molecular Plant Pathology, 13(6), 614–629. https://doi.org/10.1111/j.1364-3703.2012.00804.x

Maraite, H. M. M. (1997). *Pseudomonas syringae* pathovars and related pathogens. 9(January 1997). https://doi.org/10.1007/978-94-011-5472-7

Martel, A., Lo, T., Desveaux, D., & Guttman, D. S. (2020). A high-throughput, seedling screen for plant immunity. Molecular Plant-Microbe Interactions, 33(3), 394–401. https://doi.org/10.1094/MPMI-10-19-0295-TA

Matsumura, M., Nomoto, M., Itaya, T., Aratani, Y., Iwamoto, M., Matsuura, T., Hayashi, Y., Mori, T., Skelly, M. J., Yamamoto, Y. Y., Kinoshita, T., Mori, I. C., Suzuki, T., Betsuyaku, S., Spoel, S. H., Toyota, M., & Tada, Y. (2022). Mechanosensory trichome cells evoke a mechanical stimuli–induced immune response in Arabidopsis thaliana. Nature Communications, 13(1), 1–15. https://doi.org/10.1038/s41467-022-28813-8

Maughan, P. J., Chaney, L., Lightfoot, D. J., Cox, B. J., Tester, M., Jellen, E. N., & Jarvis, D. E. (2019). Mitochondrial and chloroplast genomes provide insights into the evolutionary origins of quinoa (*Chenopodium quinoa* Willd.). Scientific Reports, 9(1). https://doi.org/10.1038/s41598-018-36693-6

May, A., Berger, S., Hertel, T., & Köck, M. (2011). The *Arabidopsis thaliana* phosphate starvation responsive gene AtPPsPase1 encodes a novel type of inorganic pyrophosphatase. Biochimica et Biophysica Acta – General Subjects, 1810(2), 178–185. https://doi.org/10.1016/j.bbagen.2010.11.006

McClerklin, S. A., Lee, S. G., Harper, C. P., Nwumeh, R., Jez, J. M., & Kunkel, B. N. (2018). Indole-3-acetaldehyde dehydrogenase-dependent auxin synthesis contributes to virulence of *Pseudomonas syringae* strain DC3000. PloS Pathogens, 14(1). https://doi.org/10.1371/journal.ppat.1006811

McDonald, B. A., & Stukenbrock, E. H. (2016). Rapid emergence of pathogens in agro-ecosystems: Global threats to agricultural sustainability and food security. In Philosophical Transactions of the Royal Society B: Biological Sciences, 371(1709). Royal Society of London. https://doi.org/10.1098/rstb.2016.0026

Mcdonald, K. L., & Cahill, D. M. (1999). Influence of abscisic acid and the abscisic acid biosynthesis inhibitor, norflurazon, on interactions between *Phytophthora sojae* and soybean (*Glycine max*). In European Journal of Plant Pathology,105, 651–658. https://link.springer.com/article/10.1023/A:1008705321113

McDonell, E. (2018). The Quinoa Boom Goes Bust in the Andes, https://nacla.org/news/2018/03/12/quinoa-boom-goes-bust-andes (accessed August 2023)

McNew, G.L. (1960) The nature, origin, and evolution of parasitism. In: Plant Pathology: An Advanced Treatise (Horsfall, J.G. and Dimond, A.E., eds), pp. 19–69. New York: Academic Press.

Melcher, R. L. J., & Moerschbacher, B. M. (2016). An improved microtiter plate assay to monitor the oxidative burst in monocot and dicot plant cell suspension cultures. Plant Methods, 12(5), 1-11. https://doi.org/10.1186/s13007-016-0110-1

Mickelbart, M. v., Hasegawa, P. M., & Bailey-Serres, J. (2015). Genetic mechanisms of abiotic stress tolerance that translate to crop yield stability. In Nature Reviews Genetics, 16(4), 237–251. Nature Publishing Group. https://doi.org/10.1038/nrg3901

Minh, B. Q., Schmidt, H. A., Chernomor, O., Schrempf, D., Woodhams, M. D., Von Haeseler, A., Lanfear, R., & Teeling, E. (2020). IQ-TREE 2: New models and efficient methods for phylogenetic inference in the genomic era. Molecular Biology and Evolution, 37(5), 1530–1534. https://doi.org/10.1093/molbev/msaa015

Mittler, R., Vanderauwera, S., Suzuki, N., Miller, G., Tognetti, V. B., Vandepoele, K., Gollery, M., Shulaev, V., & van Breusegem, F. (2011). ROS signaling: the new wave? Trends in Plant Science, 16(6), 300–309. https://doi.org/10.1016/J.TPLANTS.2011.03.007

Mizuno, N., Toyoshima, M., Fujita, M., Fukuda, S., Kobayashi, Y., Ueno, M., Tanaka, K., Tanaka, T., Nishihara, E., Mizukoshi, H., Yasui, Y., & Fujita, Y. (2020). The genotype-dependent phenotypic landscape of quinoa in salt tolerance and key growth traits. DNA Research, 27(4), 1–12. https://doi.org/10.1093/dnares/dsaa022

Mohr, G., Cahill, D.M. (2003). Abscisic acid influences the susceptibility of *Arabidopsis thaliana* to *Pseudomonas syringae* pv. tomato and *Peronospora parasitica*. Functional Plant Biology, 30(4) 461 – 469. https://doi.org/10.1071/FP02231

Moog, M. W., Trinh, M. D. L., Nørrevang, A. F., Bendtsen, A. K., Wang, C., Østerberg, J. T., Shabala, S., Hedrich, R., Wendt, T., & Palmgren, M. (2022). The epidermal bladder cell-free mutant of the salt-tolerant quinoa challenges our understanding of halophyte crop salinity tolerance. 236, 1409–1421 New Phytologist. https://doi.org/10.1111/nph.18420

Morales-Briones, D. F., Kadereit, G., Tefarikis, D. T., Moore, M. J., Smith, S. A., Brockington, S. F., Timoneda, A., Yim, W. C., Cushman, J. C., & Yang, Y. (2021). Disentangling sources of gene tree discordance in phylogenomic data sets: testing ancient hybridizations in *Amaranthaceae s.l.* Systematic Biology, 70(2), 219–235. https://doi.org/10.1093/sysbio/syaa066

Morris, C. E., Lamichhane, J. R., Nikolić, I., Stanković, S., & Moury, B. (2019). The overlapping continuum of host range among strains in the *Pseudomonas syringae* complex. Phytopathology Research, 1(4). https://doi.org/10.1186/s42483-018-0010-6

Mott, A. G., Desveaux, D., & Guttman, D. S. (2018). A high-sensitivity, microtiter-based plate assay for plant pattern-triggered immunity. Molecular Plant-Microbe Interactions, 31(5), 499–504. https://doi.org/10.1094/MPMI-11-17-0279-TA

Mur, L. A. J., Kenton, P., Atzorn, R., Miersch, O., & Wasternack, C. (2006). The outcomes of concentration-specific interactions between salicylate and jasmonate signaling include synergy, antagonism, and oxidative stress leading to cell death. Plant Physiology, 140(1), 249–262. https://doi.org/10.1104/pp.105.072348

Munns, R. (2002). Comparative physiology of salt and water stress. Plant, Cell and Environment, 25(2), 239–250. https://doi.org/10.1046/j.0016-8025.2001.00808.x

Munns, R. (2005). Genes and salt tolerance: Bringing them together. In New Phytologist, 167(3), 645–663. https://doi.org/10.1111/j.1469-8137.2005.01487.x

Munns, R., & Tester, M. (2008). Mechanisms of Salinity Tolerance. Annual Review of Plant Biology, 59(1), 651–681. https://doi.org/10.1146/annurev.arplant.59.032607.092911

Nguyen, N. T., McInturf, S. A., & Mendoza-Cózatl, D. G. (2016). Hydroponics: A versatile system to study nutrient allocation and plant responses to nutrient availability and exposure to toxic elements. Journal of Visualized Experiments, 2016(113). https://doi.org/10.3791/54317

Nawrath, C. (1999). Salicylic acid induction–deficient mutants of Arabidopsis. express PR-2 and PR-5 and accumulate high levels of camalexin after pathogen inoculation. Society, 11(August), 1393–1404. https://doi.org/10.1105/tpc.11.8.1393

Nerva, L., Vigani, G., Silvestre, D. di, Ciuffo, M., Forgia, M., Chitarra, W., & Turina, M. (2019). Biological and molecular characterization of *Chenopodium quinoa* Mitovirus 1 reveals a distinct small RNA response compared to those of cytoplasmic RNA viruses. J Virol., 93(7). doi: 10.1128/JVI.01998-18

Ngou, B. P. M., Ahn, H. K., Ding, P., & Jones, J. D. G. (2021). Mutual potentiation of plant immunity by cell-surface and intracellular receptors. Nature, 592(7852), 110–115. https://doi.org/10.1038/s41586-021-03315-7

Nikolić, I., Stanković, S., Dimkić, I., Berić, T., Stojšin, V., Janse, J., & Popović, T. (2018). Genetic diversity and pathogenicity of *Pseudomonas syringae* pv. *aptata* isolated from sugar beet Plant Pathology, 67(5), 1194–1207. https://doi.org/10.1111/ppa.12831

Nishinaka, Y., Aramaki, Y., Yoshida, H., Masuya, H., Sugawara, T., & Ichimori, Y. (1993). A New sensitive chemiluminescence probe, L-012, for measuring the production of superoxide anion by cells. Biochemical and Biophysical Research Communications, 193(2), 554–559. https://doi.org/https://doi.org/10.1006/bbrc.1993.1659

Nobori, T., & Tsuda, K. (2019). The plant immune system in heterogeneous environments. Current Opinion in Plant Biology, 50, 58–66. https://doi.org/10.1016/J.PBI.2019.02.003

Nover, L., Bharti, K., Döring, P., Mishra, S. K., Ganguli, A., & Scharf, K. D. (2001). Arabidopsis and the heat stress transcription factor world: How many heat stress transcription factors do we need? Cell Stress and Chaperones, 6(3), 177–189. https://www.ncbi.nlm.nih.gov/pmc/articles/PMC434399/

O'Brien, J. A., Daudi, A., Finch, P., Butt, V. S., Whitelegge, J. P., Souda, P., Ausubel, F. M., & Bolwell, G. P. (2012). A peroxidase-dependent apoplastic oxidative burst in cultured Arabidopsis cells functions in MAMP-elicited defence. Plant Physiology, 158(4), 2013–2027. https://doi.org/10.1104/pp.111.190140

O'Leary, B. M., Rico, A., McCraw, S., Fones, H. N., & Preston, G. M. (2014). The infiltration-centrifugation technique for extraction of apoplastic fluid from plant leaves using Phaseolus vulgaris as an example. Journal of Visualized Experiments, 94. https://doi.org/10.3791/52113

Ohme-takagi, M., & Shinshi, H. (1995). Ethylene-lnducible DNA binding proteins that lnteract with an ethylene-responsive element Masaru. The Plant Cell, 7(February), 173–182.

Orsini, F., Accorsi, M., Gianquinto, G., Dinelli, G., Antognoni, F., Carrasco, K. B. R., Martinez, E. A., Alnayef, M., Marotti, I., Bosi, S., & Biondi, S. (2011). Beyond the ionic and osmotic response to salinity in *Chenopodium quinoa*: Functional elements of successful halophytism. Functional Plant Biology, 38(10), 818–831. https://doi.org/10.1071/FP11088

Ortuño, N., Claros, M., Gutiérrez, C., Angulo, M., & Castillo, J. (2014). Bacteria associated with the cultivation of quinoa in the Bolivian Altiplano and their biotechnological potential. July, 53–61. https://www.researchgate.net/publication/283152814_

Osman, K.T. Saline and Sodic Soils. 2018, 255–298, https://doi.org/10.1007/978-3-319-75527-4_10.

Otterbach, S. L., Khoury, H., Rupasinghe, T., Mendis, H., Kwan, K. H., Lui, V., Natera, S. H. A., Klaiber, I., Allen, N. M., Jarvis, D. E., Tester, M., Roessner, U., & Schmöckel, S. M. (2021). Characterization of epidermal bladder cells in *Chenopodium quinoa*. Plant Cell and Environment, 44(12), 3606–3622. https://doi.org/10.1111/pce.14181

Ouyang, X., Chen, J., Sun, Z., Wang, R., Wu, X., Li, B., Song, C., Liu, P., & Zhang, M. (2023). Ubiquitin E3 ligase activity of *Ralstonia solanacearum* effector RipAW is not essential for induction of plant defence in *Nicotiana benthamiana*. Frontiers in Microbiology, 14(May). https://doi.org/10.3389/fmicb.2023.1201444

Panchal, S., Roy, D., Chitrakar, R., Price, L., Breitbach, Z. S., Armstrong, D. W., & Melotto, M. (2016). Coronatine facilitates P*seudomonas syringae* infection of Arabidopsis leaves at night. Frontiers in Plant Science, 7(June), 1–11. https://doi.org/10.3389/fpls.2016.00880

Pathan, S., & Siddiqui, R. A. (2022). Nutritional Composition and Bioactive Components in Quinoa (*Chenopodium quinoa* Willd*.)* Greens: A Review. Nutrients, 14(3), 1–12. https://doi.org/10.3390/un14030558

Patiranage, D. S. R., Rey, E., Emrani, N., Wellman, G., Schmid, K., Schmöckel, S. M., Tester, M., & Jung, C. (2022). Genome-wide association study in quinoa reveals selection

pattern typical for crops with a short breeding history. ELife, 11. https://doi.org/10.7554/elife.66873

Paes de Melo, B. P., Carpinetti, P. de A., Fraga, O. T., Rodrigues-Silva, P. L., Fioresi, V. S., de Camargos, L. F., & da Silva Ferreira, M. F. (2022). Abiotic stresses in plants and their markers: a practice view of plant stress responses and programmed cell death mechanisms. Plants, 11(9). https://doi.org/10.3390/plants11091100

Peng, P., Li, R., Chen, Z. H., & Wang, Y. (2022). Stomata at the crossroad of molecular interaction between biotic and abiotic stress responses in plants. In Frontiers in Plant Science, 13. Frontiers Media S.A. https://doi.org/10.3389/fpls.2022.1031891

Petropoulos, S. A., Karkanis, A., Martins, N., & Ferreira, I. C. F. R. (2018). Edible halophytes of the Mediterranean basin: Potential candidates for novel food products. Trends in Food Science & Technology, 74, 69–84. https://doi.org/10.1016/J.TIFS.2018.02.006

Pitzschke, A. (2018). Molecular dynamics in germinating, endophyte-colonized quinoa seeds. Plant and Soil, 422(1–2), 135–154. https://doi.org/10.1007/s11104-017-3184-2

Pizzio, G. A. (2022). Abscisic acid perception and signaling in *Chenopodium quinoa*. Stresses, 3(1), 22–32. https://doi.org/10.3390/stresses3010003

Poonia, A., & Upadhayay, A. (2015). *Chenopodium album* Linn: review of nutritive value and biological properties. Journal of Food Science and Technology, 52(7), 3977–3985. https://doi.org/10.1007/s13197-014-1553-x

Preston, G. M. (2017). Profiling the extended phenotype of plant pathogens: Challenges in Bacterial Molecular Plant Pathology. Molecular Plant Pathology, 18(3), 443–456. https://doi.org/10.1111/mpp.12530

Preston, G. M. (2000). *Pseudomonas syringae* pv. tomato: the right pathogen, of the right plant, at the right time. Molecular Plant Pathology, 1(5), 263–275. https://doi.org/10.1046/j.1364-3703.2000.00036.x

Pulvento, C., & Bazile, D. (2023). Worldwide evaluations of Quinoa—biodiversity and food security under climate change pressures: advances and perspectives. Plants, 12(4), 10–13. https://doi.org/10.3390/plants12040868

Puniran-Hartley, N., Hartley, J., Shabala, L., & Shabala, S. (2014). Salinity-induced accumulation of organic osmolytes in barley and wheat leaves correlates with increased oxidative stress tolerance: In planta evidence for cross-tolerance. Plant Physiology and Biochemistry, 83, 32–39. https://doi.org/10.1016/j.plaphy.2014.07.005

Qi, T., Seong, K., Thomazella, D. P. T., Kim, J. R., Pham, J., Seo, E., Cho, M. J., Schultink, A., & Staskawicz, B. J. (2018). NRG1 functions downstream of EDS1 to regulate TIR-NLR-mediated plant immunity in *Nicotiana benthamiana*. Proceedings of the National Academy of Sciences of the United States of America, 115(46), 10979–10987. https://doi.org/10.1073/pnas.1814856115

Qureshi, A. S., & Daba, A. W. (2020). Evaluating growth and yield parameters of five quinoa (*Chenopodium quinoa* Willd*.)* genotypes under different salt stress conditions. Journal of Agricultural Science, 12(3), 128–140. https://doi.org/10.5539/jas.v12n3p128

Rabbani, M. A., Maruyama, K., Abe, H., Khan, M. A., Katsura, K., Ito, Y., Yoshiwara, K., Seki, M., Shinozaki, K., & Yamaguchi-Shinozaki, K. (2003). Monitoring expression profiles of rice genes under cold, drought, and high-salinity stresses and abscisic acid application using cDNA microarray and RNA gel-blot analyses. Plant Physiology, 133(4), 1755–1767. https://doi.org/10.1104/pp.103.025742

Rahme, L. G., Mindrinos, M. N., & Panopoulos, N. J. (1992). Plant and environmental sensory signals control the expression of hip genes in *Pseudomonas syringae* pv. *phaseolicola*. Journal of Bacteriology, 174(11), 3499–3507.

Raines, C. A. (2011). Increasing photosynthetic carbon assimilation in C3 plants to improve crop yield: Current and future strategies. Plant Physiology, 155(1), 36–42. https://doi.org/10.1104/p

Raja, V., Majeed, U., Kang, H., Andrabi, K. I., & John, R. (2017). Abiotic stress: Interplay between ROS, hormones and MAPKs. Environmental and Experimental Botany, 137, 142–157. https://doi.org/10.1016/J.ENVEXPBOT.2017.02.010

Ramachandran, M., Arulbalachandran, D., Dilipan, E., & Ramya, S. (2021). Comparative analysis of abscisic acid recovery on two varieties of rice (*Oryza sativa L*.) under drought condition. Biocatalysis and Agricultural Biotechnology, 33(102006), 1-11. https://doi.org/10.1016/J.BCAB.2021.102006

Ramakrishna, A., & Ravishankar, G. A. (2011). Influence of abiotic stress signals on secondary metabolites in plants. In Plant Signaling and Behaviour, 6(11), 1720–1731. https://doi.org/10.4161/psb.6.11.17613

Raney, J. a, Reynolds, D. J., Elzinga, D. B., Page, J., Udall, J. a, Jellen, E. N., Bonfacio, A., Fairbanks, D. J., & Maughan, P. J. (2014). Transcriptome analysis of drought induced stress in *Chenopodium quinoa*. American Journal of Plant Sciences, 5(February), 338–357. https://doi.org/10.4236/ajps.2014.53047

Rankenberg, T., Geldhof, B., van Veen, H., Holsteens, K., van de Poel, B., & Sasidharan, R. (2021). Age-dependent abiotic stress resilience in plants. Trends in Plant Science, 26(7), 692–705. https://doi.org/10.1016/J.TPLANTS.2020.12.016

Ranković, T., Nikolić, I., Berić, T., Popović, T., Lozo, J., Medić, O., & Stanković, S. (2023). Genome analysis of two *Pseudomonas syringae* pv. *aptata* strains with different virulence capacity isolated from sugar beet: features of successful pathogenicity in the phyllosphere microbiome. Microbiology Spectrum, 11(2). https://doi.org/10.1128/spectrum.03598-22

Rao, W., Wan, L., & Wang, E. (2023). Plant immunity in soybean: progress, strategies, and perspectives. Molecular Breeding, 43(6). https://doi.org/10.1007/s11032-023-01398-w

Rasmussen, S., Barah, P., Suarez-Rodriguez, M. C., Bressendorff, S., Friis, P., Costantino, P., Bones, A. M., Nielsen, H. B., & Mundy, J. (2013). Transcriptome responses to

combinations of stresses in Arabidopsis. Plant Physiology, 161(4), 1783–1794. https://doi.org/10.1104/pp.112.210773

Rasouli, F., Kiani-Pouya, A., Movahedi, A., Wang, Y., Li, L., Yu, M., Pourkheirandish, M., Zhou, M., Chen, Z., Zhang, H., & Shabala, S. (2023). Guard cell transcriptome reveals membrane transport, stomatal development and cell wall modifications as key traits involved in salinity tolerance in halophytic *Chenopodium quinoa*. Plant and Cell Physiology, 64(2), 204–220. https://doi.org/10.1093/pcp/pcac158

Rengasamy, P. (2006). World salinization with emphasis on Australia. Journal of Experimental Botany, 57(5), 1017–1023. https://doi.org/10.1093/jxb/erj108

Rezzonico, E., Flury, N., Meins, F., & Beffa, R. (1998). Transcriptional down-regulation by abscisic acid of pathogenesis-related β-1,3-glucanase genes in tobacco cell cultures. Plant Physiology, 117(2), 585–592. https://doi.org/10.1104/pp.117.2.585

Rollano-Peñaloza, O. M., Palma-Encinas, V., Widell, S., Mollinedo, P., & Rasmusson, A. G. (2022). The disease progression and molecular defence response in *Chenopodium quinoa* infected with *Peronospora variabilis*, the causal agent of quinoa downy mildew. Plants, 11(21). https:/doi.org/10.3390/plants11212946

Roman, V. J., den Toom, L. A., Castro Gamiz, C., van der Pijl, N., Visser, R. G. F., van Loo, E. N., & van der Linden, C. G. (2020). Differential responses to salt stress in ion dynamics, growth and seed yield of European quinoa varieties. Environmental and Experimental Botany, 177, 104146. https://doi.org/10.1016/J.ENVEXPBOT.2020.104146

Rong, W., Qi, L., Wang, A., Ye, X., Du, L., Liang, H., Xin, Z., & Zhang, Z. (2014). The ERF transcription factor TaERF3 promotes tolerance to salt and drought stresses in wheat. Plant Biotechnology Journal, 12(4), 468–479. https://doi.org/10.1111/pbi.12153

Ruiz, K. B., Biondi, S., Martínez, E. A., Orsini, F., Antognoni, F., & Jacobsen, S. E. (2016). Quinoa – a model crop for understanding salt-tolerance mechanisms in halophytes. Plant Biosystems, 150(2), 357–371. https://doi.org/10.1080/11263504.2015.1027317

Ruiz, K. B., Rapparini, F., Bertazza, G., Silva, H., Torrigiani, P., & Biondi, S. (2017). Comparing salt-induced responses at the transcript level in a salares and coastal-lowlands landrace of quinoa (*Chenopodium quinoa* Willd.). Environmental and Experimental Botany, 139, 127–142. https://doi.org/10.1016/J.ENVEXPBOT.2017.05.003

Ruiz, K. B., Maldonado, J., Biondi, S., & Silva, H. (2019). RNA-seq analysis of salt-stressed versus non salt-stressed transcriptomes of 285*Chenopodium quinoa* landrace R49. Genes, 10(12). https://doi.org/10.3390/genes10121042

Ruiz-Carrasco, K., Antognoni, F., Coulibaly, A. K., Lizardi, S., Covarrubias, A., Martínez, E. A., Molina-Montenegro, M. A., Biondi, S., & Zurita-Silva, A. (2011). Variation in salinity tolerance of four lowland genotypes of quinoa (*Chenopodium quinoa* Willd.) as assessed by growth, physiological traits, and sodium transporter gene expression. Plant Physiology and Biochemistry, 49(11), 1333–1341. https://doi.org/10.1016/j.plaphy.2011.08.005

Ruiz-Carrasco, K., Antognoni, F., Coulibaly, A. K., Lizardi, S., Covarrubias, A., Martínez, E. A., Molina-Montenegro, M. A., Biondi, S., & Zurita-Silva, A. (2011). Variation in salinity tolerance of four lowland genotypes of quinoa (*Chenopodium quinoa* Willd.) as assessed by growth, physiological traits, and sodium transporter gene expression. Plant Physiology and Biochemistry, 49(11), 1333–1341. https://doi.org/10.1016/j.plaphy.2011.08.005

Ruto, E., Tzemi, D., Gould, I., & Bosworth, G. (2021). Economic impact of soil salinization and the potential for saline agriculture. in future of sustainable agriculture in saline environments,93–114. CRC Press. https://doi.org/10.1201/9781003112327-6

Saijo, Y., & Loo, E. P. iian. (2020). Plant immunity in signal integration between biotic and abiotic stress responses. New Phytologist, 225(1), 87–104. https://doi.org/10.1111/nph.15989

Sakuma, Y., Liu, Q., Dubouzet, J. G., Abe, H., Yamaguchi-Shinozaki, K., & Shinozaki, K. (2002). DNA-binding specificity of the ERF/AP2 domain of Arabidopsis DREBs, transcription

factors involved in dehydration- and cold-inducible gene expression. Biochemical and Biophysical Research Communications, 290(3), 998–1009. https://doi.org/10.1006/bbrc.2001.6299

Sarowar, S., Alam, S. T., Makandar, R., Lee, H., Trick, H. N., Dong, Y., & Shah, J. (2019). Targeting the Pattern-Triggered Immunity pathway to enhance resistance to *Fusarium graminearum*. Molecular Plant Pathology, 20(5), 626–640. https://doi.org/10.1111/mpp.12781

Schellenberger, R., Touchard, M., Clément, C., Baillieul, F., Cordelier, S., Crouzet, J., & Dorey, S. (2019). Apoplastic invasion patterns triggering plant immunity: plasma membrane sensing at the frontline. In Molecular Plant Pathology, 20(11), 1602–1616. Blackwell Publishing Ltd. https://doi.org/10.1111/mpp.12857

Schenk, S., & Schikora, A. (2015). Staining of callose depositions in root and leaf tissues. BIO-PROTOCOL, 5(6). https://doi.org/10.21769/bioprotoc.1429

Schlick, NASA (1993). Technical Publication (TP) https://ntrs.nasa.gov/citations/19940015664 (accessed August 2018)

Schmöckel, S. M., Lightfoot, D. J., Razali, R., Tester, M., & Jarvis, D. E. (2017). Identification of putative transmembrane proteins involved in salinity tolerance in *Chenopodium quinoa* by integrating physiological data, RNAseq, and SNP Analyses. Frontiers in Plant Science, 8(June), 1–12. https://doi.org/10.3389/fpls.2017.01023

Sedelnikova, O. v, Hughes, T. E., & Langdale, J. A. (2018). Understanding the genetic basis of C4 Kranz Anatomy with a view to engineering C3 crops. Annual Review of Genetics, 52(1), 249–270. https://doi.org/10.1146/annurev-genet-120417-031217

Seki, M., Ishida, J., Narusaka, M., Fujita, M., Nanjo, T., Umezawa, T., Kamiya, A., Nakajima, M., Enju, A., Sakurai, T., Satou, M., Akiyama, K., Yamaguchi-Shinozaki, K., Carninci, P., Kawai, J., Hayashizaki, Y., & Shinozaki, K. (2002). Monitoring the expression pattern of around 7,000 Arabidopsis genes under ABA treatments using a full-length cDNA

microarray. Functional and Integrative Genomics, 2(6), 282–291. https://doi.org/10.1007/s10142-002-0070-6

Shabala, L., Mackay, A., Tian, Y., Jacobsen, S. E., Zhou, D., & Shabala, S. (2012). Oxidative stress protection and stomatal patterning as components of salinity tolerance mechanism in quinoa (*Chenopodium quinoa*). Physiologia Plantarum, 146(1), 26–38. https://doi.org/10.1111/j.1399-3054.2012.01599.x

Shabala, S. & Mackay, A. (2011). Ion transport in halophytes. Advances in Botanical. Research, 57, 151-199, https://doi.org/10.1016/B978-0-12-387692-8.00005-9.

Shabala, S., Bose, J., & Hedrich, R. (2014). Salt bladders: do they matter? Trends in Plant Science, 19(11), 687–691. https://doi.org/10.1016/J.TPLANTS.2014.09.001

Shabala, S. (2013). Learning from halophytes: Physiological basis and strategies to improve abiotic stress tolerance in crops. In Annals of Botany, 112(7), 1209–1221. https://doi.org/10.1093/aob/mct205

Shahin, H. (2019). Callus formation and production of secondary metabolites by seedling explants of *Chenopodium quinoa*. Egyptian Journal of Botany, 59(2), 451–460. https://doi.org/10.21608/ejbo.2019.6323.1251

Shapiguzov, A., Vainonen, J. P., Wrzaczek, M., & Kangasjärvi, J. (2012). ROS-talk- how the apoplast, the chloroplast, and the nucleus get the message through. In Frontiers in Plant Science, 3, (December), 1-9. Frontiers Research Foundation. https://doi.org/10.3389/fpls.2012.00292

Sharma, A., Shahzad, B., Rehman, A., Bhardwaj, R., Landi, M., & Zheng, B. (2019). Response of phenylpropanoid pathway and the role of polyphenols in plants under abiotic stress. Molecules, 24(13), 2452. https://doi.org/10.3390/molecules24132452

Shen, S., Li, N., Wang, Y., Zhou, R., Sun, P., Lin, H., Chen, W., Yu, T., Liu, Z., Wang, Z., Tan, X., Zhu, C., Feng, S., Zhang, Y., & Song, X. (2022). High-quality ice plant reference genome

analysis provides insights into genome evolution and allows exploration of genes involved in the transition from C3 to CAM pathways. Plant Biotechnology Journal, 20(11), 2107–2122. https://doi.org/10.1111/pbi.13892

Silva, P. M., Massuela, D. C., Khan, M. W., Hamar, A., Khajehei, F., Grae, S., & Piatti, C. (2020). Quinoa (*Chenopodium quinoa* Willd.): An overview of the potentials of the "golden grain" and socio-economic and environmental aspects of its cultivation and marketization. Foods, 9(216), 31.

Singh, B., Kukreja, S., & Goutam, U. (2018). Milestones achieved in response to drought stress through reverse genetic approaches. F1000 Research, 7, 1–10. https://doi.org/10.12688/f1000research.15606.1

Skorupa, M., Gołębiewski, M., Kurnik, K., Niedojadło, J., Kęsy, J., Klamkowski, K., Wójcik, K., Treder, W., Tretyn, A., & Tyburski, J. (2019). Salt stress vs. salt shock- The case of sugar beet and its halophytic ancestor. BMC Plant Biology, 19(1). https://doi.org/10.1186/s12870-019-1661-x

Soldan, R., Sanguankiattichai, N., Bach-Pages, M., Bervoets, I., Huang, W. E., & Preston, G. M. (2021). From macro to micro: a combined bioluminescence-fluorescence approach to monitor bacterial localization. Environmental Microbiology, 23(4), 2070–2085. https://doi.org/10.1111/1462-2920.15296

Soudek, P., Katrušáková, A., Sedláček, L., Petrová, Š., Kočí, V., Maršík, P., Griga, M., & Vaněk, T. (2010). Effect of heavy metals on inhibition of root elongation in 23 cultivars of flax (*Linum usitatissimum L.).* Archives of Environmental Contamination and Toxicology, 59(2), 194–203. https://doi.org/10.1007/s00244-010-9480-y

Spoel, S. H., Johnson, J. S., & Dong, X. (2007). Regulation of tradeoffs between plant defences against pathogens with different lifestyles. Proceedings of the National Academy of Sciences of the United States of America, 104(47), 18842–18847. https://doi.org/10.1073/pnas.0708139104

Srivarathan, S., Addepalli, R., Adiamo, O. Q., Kodagoda, G. K., Phan, A. D. T., Wright, O. R. L., Sultanbawa, Y., Osborne, S., & Netzel, M. E. (2023). Edible halophytes with functional properties: in vitro protein digestibility and bioaccessibility and intestinal absorption of minerals and trace elements from Australian indigenous halophytes. Molecules, 28(10). https://doi.org/10.3390/molecules28104004

Subramanian, A., Tamayo, P., Mootha, V. K., Mukherjee, S., Ebert, B. L., Gillette, M. A., Paulovich, A., Pomeroy, S. L., Golub, T. R., Lander, E. S., & Mesirov, J. P. (2005). Gene set enrichment analysis: A knowledge-based approach for interpreting genome-wide expression profiles. 102(43), 5545–15550. www.pnas.orgcgidoi10.1073pnas.0506580102

Su, J., Yang, L., Zhu, Q., Wu, H., He, Y., Liu, Y., Xu, J., Jiang, D., & Zhang, S. (2018). Active photosynthetic inhibition mediated by MPK3/MPK6 is critical to effector-triggered immunity. PLoS Biology, 16(5), 1–29. https://doi.org/10.1371/journal.pbio.2004122

Sun, T., & Zhang, Y. (2022). MAP kinase cascades in plant development and immune signaling. EMBO Reports, 23(2). https://doi.org/10.15252/embr.202153817

Suzuki, N., Rivero, R. M., Shulaev, V., Blumwald, E., & Mittler, R. (2014). Abiotic and biotic stress combinations. New Phytologist, 203(1), 32–43. https://doi.org/10.1111/nph.12797

Sysoev, V. O., Fischer, B., Frese, C. K., Gupta, I., Krijgsveld, J., Hentze, M. W., Castello, A., & Ephrussi, A. (2016). Global changes of the RNA-bound proteome during the maternal-to-zygotic transition in Drosophila. Nature Communications, 7. https://doi.org/10.1038/ncomms12128

Taji, T., Seki, M., Satou, M., Sakurai, T., Kobayashi, M., Ishiyama, K., Narusaka, Y., Narusaka, M., Zhu, J. K., & Shinozaki, K. (2004). Comparative genomics in salt tolerance between Arabidopsis and Arabidopsis-related halophyte salt cress using Arabidopsis microarray. Plant Physiology, 135(3), 1697–1709. https://doi.org/10.1104/pp.104.039909

Takaku, Y., Suzuki, H., Ohta, I., Ishii, D., Muranaka, Y., Shimomura, M., & Hariyama, T. (2013). A thin polymer membrane, nano-suit, enhancing survival across the continuum between air and high vacuum. Proceedings of the National Academy of Sciences of the United States of America, 110(19), 7631–7635. https://doi.org/10.1073/pnas.1221341110

Takken, F., & Rep, M. (2010). The arms race between tomato and *Fusarium oxysporum*. In Molecular Plant Pathology, 11(2), 309–314. https://doi.org/10.1111/j.1364-3703.2009.00605.x

Tamaoki, D., Seo, S., Yamada, S., Kano, A., Miyamoto, A., Shishido, H., Miyoshi, S., Taniguch, S., Akimitsu, K., & Gomi, K. (2013). Jasmonic acid and salicylic acid activate a common defence system in rice. Plant Signaling and Behavior, 8(6). https://doi.org/10.4161/psb.24260

Tanaka, Y., Sano, T., Tamaoki, M., Nakajima, N., Kondo, N., & Hasezawa, S. (2005). Ethylene inhibits abscisic acid-induced stomatal closure in Arabidopsis. Plant Physiology, 138(4), 2337–2343. https://doi.org/10.1104/pp.105.063503

Tavakkoli, E., Fatehi, F., Rengasamy, P., & McDonald, G. (2012). A comparison of hydroponic and soil-based screening In *Posidonia oceanic*a cadmium induces changes in DNA methods to identify salt tolerance in the field in barley. Journal of Experimental Botany, 63(10), 3853–3868.

Telahigue, D., & Toumi, L. (2017). Influence of medium and growth regulators on callogenesis of quinoa (*Chenopodium quinoa* Willd.) and effect of hydrous stress induced by P.E.G 6000 on the callus. Horticultural Biotechnology Research, 1(9). https://doi.org/10.25081/hbr.2017.v3.337

Tian, H., Guo, H., Dai, X., Cheng, Y., Zheng, K., Wang, X., & Wang, S. (2015). An ABA down-regulated bHLH transcription repressor gene, bHLH129 regulates root elongation and ABA response when overexpressed in Arabidopsis. Scientific Reports, 5. https://doi.org/10.1038/srep17587

Tsai, P. J., Chen, Y. S., Sheu, C. H., & Chen, C. Y. (2011). Effect of nanogrinding on the pigment and bioactivity of djulis (*Chenopodium formosanum Koidz*.). Journal of Agricultural and Food Chemistry, 59(5), 1814–1820. https://doi.org/10.1021/jf1041273

Tur, J. A., & Bibiloni, M. M. (2016). Functional foods. Encyclopaedia of Food and Health, 157–161. https://doi.org/10.1016/B978-0-12-384947-2.00340-8

Turcios, A. E., Papenbrock, J., &Tränkner, M. (2021). Potassium, an important element to improve water use efficiency and growth parameters in quinoa (*Chenopodium quinoa*) under saline conditions. Journal of Agronomy and Crop Science, 207(4), 618–630. https://doi.org/10.1111/jac.12477

Tuteja, N., & Sopory, S. K. (2008). Chemical signaling under abiotic stress environment in plants. In Plant Signaling and Behavior, 3(8), 525–536. Landes Bioscience. https://doi.org/10.4161/psb.3.8.6186

Ul Haq, S., Khan, A., Ali, M., Khattak, A. M., Gai, W. X., Zhang, H. X., Wei, A. M., & Gong, Z. H. (2019). Heat shock proteins: Dynamic biomolecules to counter plant biotic and abiotic stresses. International Journal of Molecular Sciences, 20(21), 1–31. https://doi.org/10.3390/ijms20215321

Ullah, C., Schmidt, A., Reichelt, M., Tsai, C. J., & Gershenzon, J. (2022). Lack of antagonism between salicylic acid and jasmonate signalling pathways in poplar. New Phytologist, 235(2), 701–717. https://doi.org/10.1111/nph.18148

Urcelay, C., Acho, J., & Joffre, R. (2011). Fungal root symbionts and their relationship with fine root proportion in native plants from the Bolivian Andean highlands above 3,700 m elevation. Mycorrhiza, 21(5), 323–330. https://doi.org/10.1007/s00572-010-0339-x

Van De Velde, K., Thomas, S. G., Heyse, F., Kaspar, R., Van Der Straeten, D., & Rohde, A. (2021). N-terminal truncated RHT-1 proteins generated by translational reinitiation cause semi-dwarfing of wheat Green Revolution alleles. Molecular Plant, 14(4), 679–687. https://doi.org/10.1016/j.molp.2021.01.002

Vaseva, I. I., Mishev, K., Depaepe, T., Vassileva, V., & van der Straeten, D. (2021). The diverse salt-stress response of Arabidopsis ctr1-1 and ein2-1ethylene signaling mutants is linked to altered root auxin homeostasis. Plants, 10(3), 1–19. https://doi.org/10.3390/plants10030452

Velásquez, A. C., Castroverde, C. D. M., & He, S. Y. (2018). Plant–pathogen warfare under changing climate conditions. In Current Biology, 28(10), 619–634). Cell Press. https://doi.org/10.1016/j.cub.2018.03.054

Verma, V., Ravindran, P., & Kumar, P. P. (2016). Plant hormone-mediated regulation of stress responses. BMC Plant Biology, 16(1). https://doi.org/10.1186/s12870-016-0771-y

Villacrés, E., Quelal, M., Galarza, S., Iza, D., & Silva, E. (2022). Nutritional value and bioactive compounds of leaves and grains from quinoa (*Chenopodium quinoa* Willd.). Plants, 11(2), 1–11. https://doi.org/10.3390/plants11020213

Volkov, V. (2015). Salinity tolerance in plants. Quantitative approach to ion transport starting from halophytes and stepping to genetic and protein engineering for manipulating ion fluxes. In Frontiers in Plant Science, 6(October). Frontiers Research Foundation. https://doi.org/10.3389/fpls.2015.00873

Vuong, U. T., Iswanto, A. B. B., Nguyen, Q. M., Kang, H., Lee, J., Moon, J., & Kim, S. H. (2023). Engineering plant immune circuit: walking to the bright future with a novel toolbox. Plant Biotechnology Journal, 21(1), 17–45. https://doi.org/10.1111/pbi.13916

Wan, J., Zhang, X. C., & Stacey, G. (2008). Chitin signaling and plant disease resistance. Plant Signaling and Behavior, 3(10), 831–833. https://doi.org/10.4161/psb.3.10.5916

Wang, B., Andargie, M., & Fang, R. (2022). The function and biosynthesis of callose in high plants. Heliyon, 8(4), e09248. https://doi.org/10.1016/j.heliyon.2022.e09248

Wang, D., Wei, L., Liu, T., Ma, J., Huang, K., Guo, H., Huang, Y., Zhang, L., Zhao, J., Tsuda, K., & Wang, Y. (2023). Suppression of ETI by PTI priming to balance plant growth and

defence through an MPK3/MPK6-WRKYs-PP2Cs module. Molecular Plant, 16(5), 903–918. https://doi.org/10.1016/j.molp.2023.04.004

Wang, X., Liu, F. Lai, & Jiang, D. (2017). Priming: A promising strategy for crop production in response to future climate. Journal of Integrative Agriculture, 16(12), 2709–2716. https://doi.org/10.1016/S2095-3119(17)61786-6

Wang, Y., Zhang, Y., Dai, C., Ma, J., Zhou, Y., Jaikishun, S., Yan, J., Yang, Z., Xu, T., & Song, S. (n.d.). The establishment of two eficient transformation systems in quinoa. Preprint. https://doi.org/10.21203/rs.3.rs-364280/v1

Wasternack, C., & Strnad, M. (2018). Jasmonates: News on occurrence, biosynthesis, metabolism and action of an ancient group of signaling compounds. In International Journal of Molecular Sciences, 19(9). MDPI AG. https://doi.org/10.3390/ijms19092539

Wege, S., Gilliham, M., & Henderson, S. W. (2017). Chloride: Not simply a “cheap osmoticum”, but a beneficial plant macronutrient. In Journal of Experimental Botany, 68(12), 3057–3069. Oxford University Press. https://doi.org/10.1093/jxb/erx050

Wei, H.-L., & Collmer, A. (2018). Defining essential processes in plant pathogenesis with *Pseudomonas syringae* pv. tomato DC3000 disarmed polymutants and a subset of key type III effectors. Molecular Plant Pathology, 1(16). https://doi.org/10.1111/mpp.12655

Wei, W., Cui, M. Y., Hu, Y., Gao, K., Xie, Y. G., Jiang, Y., & Feng, J. Y. (2018). Ectopic expression of FvWRKY42, a WRKY transcription factor from the diploid woodland strawberry *(Fragaria vesca*), enhances resistance to powdery mildew, improves osmotic stress resistance, and increases abscisic acid sensitivity in Arabidopsis. Plant Science, 275(February), 60–74. https://doi.org/10.1016/j.plantsci.2018.07.010

Whalen, M. C. (2005). Host defence in a developmental context. In Molecular Plant Pathology, 6(3), 347–360. https://doi.org/10.1111/J.1364-3703.2005.00286.X

Wichmann, F., Vorhölter, F. J., Hersemann, L., Widmer, F., Blom, J., Niehaus, K., Reinhard, S., Conradin, C., & Kölliker, R. (2013). The noncanonical type III secretion system of *Xanthomonas translucens* pv. *graminis* is essential for forage grass infection. Molecular Plant Pathology, 14(6), 576–588. https://doi.org/10.1111/mpp.12030

Wilson, C., Read, J. J., & Abo-Kassem, E. (2002). Effect of mixed-salt salinity on growth and ion relations of a quinoa and a wheat variety. Journal of Plant Nutrition, 25(12), 2689–2704. https://doi.org/10.1081/PLN-120015532

Winkelmüller, T. M., Entila, F., Anver, S., Piasecka, A., Song, B., Dahms, E., Sakakibara, H., Gan, X., Kułak, K., Sawikowska, A., Krajewski, P., Tsiantis, M., Garrido-Oter, R., Fukushima, K., Schulze-Lefert, P., Laurent, S., Bednarek, P., & Tsuda, K. (2021). Gene expression evolution in Pattern-Triggered Immunity within *Arabidopsis thaliana* and across Brassicaceae species. Plant Cell, 33(6), 1863–1887. https://doi.org/10.1093/plcell/koab073

Xiao-lin, Z., Bao-qiang, W., & Xiao-hong, W. (2022). Identification and expression analysis of the CqSnRK2 gene family and a functional study of the CqSnRK2.12 gene in quinoa (*Chenopodium quinoa* Willd.). BMC Genomics, 23(1). https://doi.org/10.1186/s12864-022-08626-1

Xin, X. F., Kvitko, B., & He, S. Y. (2018). *Pseudomonas syringae*: What it takes to be a pathogen. In Nature Reviews Microbiology, 16(5),316–328. Nature Publishing Group. https://d

Xiong, L., & Yang, Y. (2003). Disease resistance and abiotic stress tolerance in rice are inversely modulated by an abscisic acid-inducible mitogen-activated protein kinase. Plant Cell, 15(3), 745–759. https://doi.org/10.1105/tpc.008714

Yang, A., Akhtar, S. S., Amjad, M., Iqbal, S., & Jacobsen, S. E. (2016). Growth and physiological responses of quinoa to drought and temperature stress. Journal of Agronomy and Crop Science, 202(6), 445–453. https://doi.org/10.1111/jac.12167

Yang, D. L., Yang, Y., & He, Z. (2013). Roles of plant hormones and their interplay in rice immunity. In Molecular Plant, 6(3), 675–685. Oxford University Press. https://doi.org/10

Yao, X. C., Meng, L. F., Zhao, W. L., & Mao, G. L. (2023). Changes in the morphology traits, anatomical structure of the leaves and transcriptome in *Lycium barbarum L*. under salt stress. Frontiers in Plant Science, 14. https://doi.org/10.3389/fpls.2023.1090366

Yasuda, M., Ishikawa, A., Jikumaru, Y., Seki, M., Umezawa, T., Asami, T., Maruyama-Nakashita, A., Kudo, T., Shinozaki, K., Yoshida, S., & Nakashita, H. (2008). Antagonistic interaction between systemic acquired resistance and the abscisic acid-mediated abiotic stress response in Arabidopsis. Plant Cell, 20(6), 1678–1692. https://doi.org/10.1105/tpc.107.054296

Yeo, A. R., & Flowers, T. J. (1983). Varietal differences in the toxicity of sodium ions in rice leaves. Physiologia Plantarum, 59(2), 189–195. https://doi.org/10.1111/j.1399-3054.1983.tb00756.x

Yu, G., Wang, L. G., Yan, G. R., & He, Q. Y. (2015). DOSE: An R/Bioconductor package for disease ontology semantic and enrichment analysis. Bioinformatics, 31(4), 608–609. https://doi.org/10.1093/bioinformatics/btu684

Yuan, X., Wang, H., Cai, J., Li, D., & Song, F. (2019). NAC transcription factors in plant immunity. Phytopathology Research, 1(1). https://doi.org/10.1186/s42483-018-0008-0

Yuan, M., Jiang, Z., Bi, G., Nomura, K., Liu, M., Wang, Y., Cai, B., Zhou, J. M., He, S. Y., & Xin, X. F. (2021). Pattern-Recognition Receptors are required for NLR-mediated plant immunity. Nature, 592(7852), 105–109. https://doi.org/10.1038/s41586-021-03316-6

Yue, H., Chang, X., Zhi, Y., Wang, L., Xing, G., Song, W., & Nie, X. (2019). Evolution and identification of the WRKY gene family in Quinoa (*Chenopodium quinoa*). Genes, 10(2). https://doi.org/10.3390/genes10020131

Zandalinas, S. I., & Mittler, R. (2022). Plant responses to multifactorial stress combination. New Phytologist, 234(4), 1161–1167. https://doi.org/10.1111/nph.18087

Zandalinas, S. I., Sengupta, S., Fritschi, F. B., Azad, R. K., Nechushtai, R., & Mittler, R. (2021). The impact of multifactorial stress combination on plant growth and survival. New Phytologist, 230(3), 1034–1048. https://doi.org/10.1111/nph.17232

Zeier, J. (2005). Age-dependent variations of local and systemic defence responses in Arabidopsis leaves towards an avirulent strain of *Pseudomonas syringae*. Physiological and Molecular Plant Pathology, 66(1–2), 30–39. https://doi.org/10.1016/j.pmpp.2005.03.007

Zeng, F., Shabala, S., Maksimović, J. D., Maksimović, V., Bonales-Alatorre, E., Shabala, L., Yu, M., Zhang, G., & Živanović, B. D. (2018). Revealing mechanisms of salinity tissue tolerance in succulent halophytes: A case study for *Carpobrotus rossi.* Plant Cell and Environment, 41(11), 2654–2667. https://doi.org/10.1111/pce.13391

Zhang, Y., Tan, J., Guo, Z., Lu, S., He, S., Shu, W., & Zhou, B. (2009). Increased abscisic acid levels in transgenic tobacco over-expressing 9 cis-epoxycarotenoid dioxygenase influence H_2O_2 and NO production and antioxidant defences. Plant, Cell and Environment, 32(5), 509–519. https://doi.org/10.1111/j.1365-3040.2009.01945.x

Zhang, S., Liu, J., Shi, L., Wang, Q., Zhang, P., Wang, H., Liu, J., Li, H., Li, L., Li, X., Huang, L., & Qin, P. (2023). Identification of core genes associated with different phosphorus levels in quinoa seedlings by weighted gene co-expression network analysis. BMC Genomics, 24(1). https://doi.org/10.1186/s12864-023-09507-x

Zhang, M., & Zhang, S. (2022). Mitogen-activated protein kinase cascades in plant signaling. Journal of Integrative Plant Biology, 64(2), 301–341. https://doi.org/10.1111/jipb.13215

Zhao, Y., Thilmony, R., Bender, C. L., Schaller, A., He, S. Y., & Howe, G. A. (2003). Virulence systems of *Pseudomonas syringae* pv. tomato promote bacterial speck disease in

tomato by targeting the jasmonate signaling pathway. Plant Journal, 36(4), 485–499. https://doi.org/10.1046/j.1365-313X.2003.01895.x

Zhou, N., Tootle, T. L., & Glazebrook, J. (1999). Arabidopsis PAD3, a gene required for camalexin biosynthesis, encodes a putative cytochrome p450 monooxygenase. The Plant Cell, 11(12), 2419–2428. https://doi.org/10.2307/3870965

Zhu, A., Ibrahim, J. G., & Love, M. I. (2019). Heavy-Tailed prior distributions for sequence count data: Removing the noise and preserving large differences. Bioinformatics, 35(12), 2084–2092. https://doi.org/10.1093/bioinformatics/bty895

Zhu, J. K. (2002). Salt and drought stress signal transduction in plants. In Annual Review of Plant Biology, 53(1), 247–273. https://doi.org/10.1146/annurev.arplant.53.091401.143329

Zipfel, C., Kunze, G., Chinchilla, D., Caniard, A., Jones, J. D. G., Boller, T., & Felix, G. (2006). Perception of the bacterial PAMP EF-Tu by the receptor EFR restricts Agrobacterium-mediated transformation. Cell, 125(4), 749–760. https://doi.org/10.1016/j.cell.2006.03.037

Zipfel, C., & Robatzek, S. (2010). Pathogen-Associated Molecular Pattern-Triggered Immunity: Veni, vidi...? Plant Physiology, 154(2), 551–554. https://doi.org/10.1104/pp.110.161547

Supplementary Material

Supplementary Tables as Excel files *(uploaded for sharing via the Oxford Research Archive)*

Supplementary Tables 1-3 are contained as sheets in file “Supplementary_Tables_1-3.xlsx”:

- **Supplementary Table 1**: Longlist of enriched abiotic and biotic stress – related GO and KEGG terms for flg22-treated quinoa
- **Supplementary Table 2**: Candidate flg22-treated stress response DEGs in quinoa obtained through GSEA analyses

- **Supplementary Table 3**: Shortlist of enriched abiotic and biotic stress – related enriched GO and KEGG terms for flg22-treated quinoa

Supplementary Table 4: Full flg22-induced DEGs lists for quinoa and Arabidopsis

Supplementary Table 5: Shared flg22-induced DEGs between quinoa and Arabidopsis

Supplementary Table 6: Core PTI quinoa genes

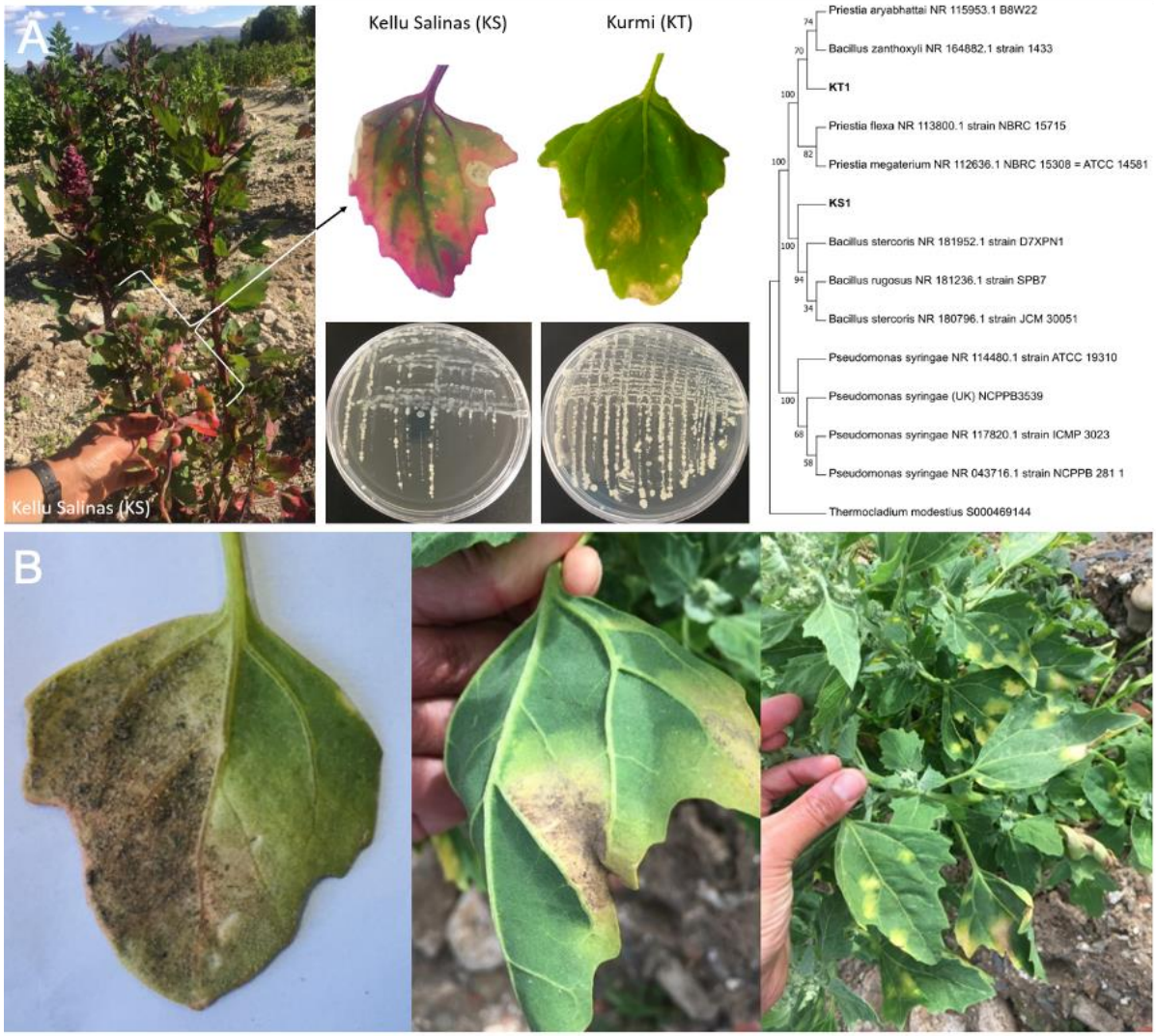
Supplementary Table 7: Comparing quinoa's core PTI quinoa genes with those identified for Arabidopsis in Bjornson et al., 2021.

Supplementary Table 8: Quinoa vs Arabidopsis orthologs

In January 2022 Scrafton and Williams (through a BSPP Junior Fellowship and BSPP Travel Award/Mbiol project respectively) screened eight Bolivian quinoa ecotypes Kurmi, Chucapaca, Blanca (adapted to Caracollo), Blanca (adapted to Salinas), Blanquita, Kellu-Caracollo, Kellu-Salinas and J'acha Grano being grown in two different field locations (Caracollo and Salinas de Garci Mendoza) by UTO collaborators (Ing Marcelo Gonzales Torrico and Ing Roberto Carlos Quispe Macedo) for bacterial leaf spot symptoms (or any disease symptoms atypical of downy mildew; S.Fig.1B). Symptoms were guided by the phenotypes of *P. syringae* infected leaves from (Fonseca-Guerra et al., 2021; Chapter 1; Fig. 10). Upon isolating the bacterial endophytes using bacteria-selective media no *P. syringae* isolates were found and Koch's postulates criteria were not convincingly met: leaves of cv. Atlas (which was *not* the original quinoa ecotype) and three other related chenopods were asymptomatic indicating these isolates might not be the causative agent for the original disease symptoms, and may instead have been of fungal origin (S.Fig.1) (Colque-Little personal comms, 2022). Given the growing conditions and plant material were different to the plants originally harvested (due to the pathology assessments being done in the UK), the bacteria DNA was isolated and sent for sequencing, finding their identity to be *Bacillus* spp. (S.Fig.1A).

This method had also been tested previously in British grown quinoa cv. Atlas in Shropshire 2019 following a field walk with the Preston Lab group and Stephen Jones of the British Quinoa Company (Chapter 1; Fig.8) where non-pathogenic bacterial endophytes were also isolated and did not reproduce yellowing or speck symptoms when tested in glasshouse

grown Atlas. Later the causal agent of the original field symptoms was suggested to be viral (Adrian Fox, personal comms, 2021). Colque-Little et al. (2023) have since shown that quinoa is a host to Alternaria which has been found to be mistaken for the downy mildew in diseased plants in Peru (Colque-Little, personal comms 2023).



S.Fig. 1. Quinoa diseased leaf symptoms and attempts at isolation bacterial pathogen species from Salinas de Garci Mendoza diseased plants. A) Stunted plant Kellu with example leaf and morphologies of bacterial endophytic isolates obtained from diseased Kellu Caracollo (first; left) and Kurmi (second; right) and their phylogenetic position relative to *P. syringae* as *Bacillus* spp. B) Example diseased quinoa leaves with typical down mildew symptoms for reference (which were not analysed further).

S.Fig.2. Flowchart for investigating PTI-ROS of new species with the Antioxidant Assay

